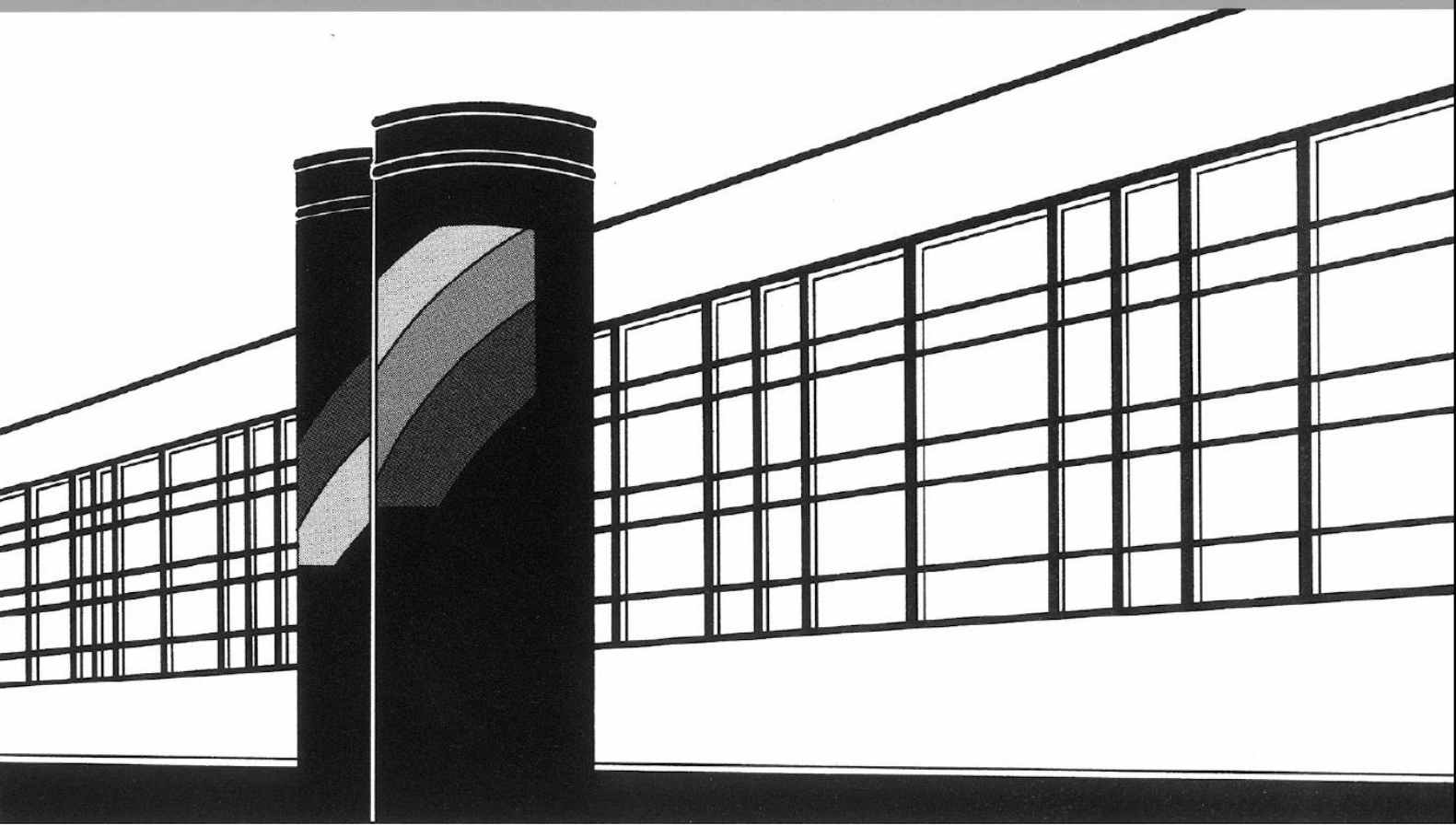


Universität Stuttgart



Institut für Wasser- und Umweltsystemmodellierung

Mitteilungen



Heft 298 Najibullah Sadid

Bedload Transport Estimation in Mountainous
Intermittent Rivers and Streams

Bedload Transport Estimation in Mountainous Intermittent Rivers and Streams

von der Fakultät Bau- und Umweltingenieurwissenschaften
der Universität Stuttgart zur Erlangung der Würde eines
Doktor-Ingenieurs (Dr.-Ing.) genehmigte Abhandlung

vorgelegt von
Najibullah Sadid
aus Logar, Afghanistan

Hauptberichter: Prof. Dr.-Ing. Silke Wieprecht
Mitberichter: Prof. Ing. Aronne Armanini

Tag der mündlichen Prüfung: 11. Januar 2023

Institut für Wasser- und Umweltsystemmodellierung
der Universität Stuttgart
2023

Heft 298 **Bedload Transport Estimation
in Mountainous Intermittent
Rivers and Streams**

von
Dr.-Ing.
Najibullah Sadid

Eigenverlag des Instituts für Wasser- und Umweltsystemmodellierung
der Universität Stuttgart

D93 Bedload Transport Estimation in Mountainous Intermittent Rivers and Streams

Bibliografische Information der Deutschen Nationalbibliothek

Die Deutsche Nationalbibliothek verzeichnet diese Publikation in der Deutschen Nationalbibliografie; detaillierte bibliografische Daten sind im Internet über <http://www.d-nb.de> abrufbar

Najibullah Sadid:
Bedload Transport Estimation in Mountainous Intermittent Rivers and Streams,
Universität Stuttgart. - Stuttgart: Institut für Wasser- und
Umweltsystemmodellierung, 2023

(Mitteilungen Institut für Wasser- und Umweltsystemmodellierung, Universität
Stuttgart: H. 298)
Zugl.: Stuttgart, Univ., Diss., 2023
ISBN 978-3-910293-02-1
NE: Institut für Wasser- und Umweltsystemmodellierung <Stuttgart>: Mitteilungen

Gegen Vervielfältigung und Übersetzung bestehen keine Einwände, es wird lediglich um Quellenangabe gebeten.

Herausgegeben 2023 vom Eigenverlag des Instituts für Wasser- und Umweltsystemmodellierung

Druck: DCC Kästl e.K., Ostfildern

Disclaimer

Erklärung über die Eigenständigkeit der Dissertation

Ich versichere, dass ich die vorliegende Arbeit mit dem Titel Bedload Transport Estimation in Mountainous Intermittent Rivers and Stream selbständig verfasst und keine anderen als die angegebenen Quellen und Hilfsmittel benutzt habe; aus fremden Quellen entnommene Passagen und Gedanken sind als solche kenntlich gemacht. Diese Dissertation wurde zu keiner Zeit in derselben oder substantiell ähnlichen Version bei einem anderen Prüfungsamt eingereicht.

Declaration of Authorship

I hereby certify that the dissertation entitled Bedload Transport Estimation in Mountainous Intermittent Rivers and Stream is entirely my own work except where otherwise indicated. Passages and ideas from other sources have been clearly indicated. This thesis has never been submitted in the same or substantially similar version to any other examination office.

Name/Name: _____

Unterschrift/Signed: _____

Datum/Date: _____

Acknowledgement

I would like to express my gratitude to Prof. Dr.-Ing. Silke Wieprecht for her kind support and advises throughout my research work at the University of Stuttgart. Thank you for her unlimited help and motivation for making it possible to finish another milestone of my life. I am very grateful to Prof. Ing. Aronne Armanini for his very constructive advises and recommendations that added more value to this research work.

Especial thanks to all colleagues In Institute for Modelling Hydraulic and Environmental Systems (IWS) for being very cooperative and supportive all the time. Thank you all for making IWS a very pleasant and friendly working environment. Thank to Dr. Gabriele Hartmann for helping me overcome the formal paper works. Thanks to all colleagues in Kabul River Basin Department, Ministry of Water and Energy of Islamic Republic of Afghanistan for their help in conducting the field studies under very difficult security and logistic conditions.

Above all, I would like to thank my Parents and my siblings for their unending love, support and encouragment that have always enlighten my ways forward. Last but not least, I would like to thank my wife and my doughter for their love and support and for being tolerant with me in during ups and downs of my life-situations.

I would like to acknowledge and sincerely thank the German Academic Exchange Services (DAAD) for providing the financial support for this research work.

Najibullah Sadid

Abstract

Rivers and streams with the flow, sediment, and habitat seasonality are termed as intermittent rivers and streams (IRS). IRS are the main water bodies in arid and semi-arid regions of the world but are also found in the temperate and humid environment, where they are particularly draining headwater streams. Thus, a large part of headwater streams in the mountainous regions behave as intermittent water bodies, where the steep channel slope and a wide variety of sediment sizes add to their hydrosedimentological complexity. Bedload transport as an important sedimentological characteristic of mountainous IRS and essential for planning sediment management strategies, is far from being well understood. Often the knowledge of lowland perennial rivers is adapted to steep IRS, which may lead to an overestimation of bedload transport mainly due to the overestimation of near-bed flow characteristics. Despite the development of numerous methods for modifying near-bed flow parameters for steep IRS such as Double-averaging of Navier-Stokes equation and flow resistance methods modifications for steep IRS, their application is limited to small domains and laboratory conditions.

In this research, the flow resistance, main determinant of near-bed flow characteristic is estimated using a regime channel approach. In this approach, the flow resistance is estimated on reach-scale based on the channel's regime dimension, slope and bankfull discharge assuming an IRS is in regime state (equilibrium condition). A channel's regime state represents a long-term average characteristic of a river and does not significantly change over time. A channel reach of a constant slope develops a certain flow resistance during its regime state development to resist the change imposed by bankfull discharge and maintain a specific regime geometry, slope, and sediment grain size.

2D- hydromorphological computer simulations are employed to simulate the development of channel regime state for several cases of initial geometries, slopes, and grain sizes by steering the flow resistance. This modifies the riverbed shear stress by the ratio of total flow resistance to grain resistance also known as relative flow resistance μ in order to account for flow energy dissipation on resistance sources such as macro-roughness elements (MRE), and bedforms.

Alternatively, two cases of MRE as a main flow resistance inducer is built as non-erodible trapezoidal shapes (i) randomly distributed over the channel bed, and (ii) arranged in cascade bedforms are used in regime channel simulations. MRE protects the channel by reducing the exposed riverbed to erosion and changing the flow characteristics in their vicinity.

Regime channel simulations are performed on artificial channels of initial slopes between 0.0% to 10% and initial dimensions of 5.5 m x 200 m and 16.5 m x 200 m resembling a fixed (laboratory) and an extended-width (natural wide channel) condition. Three channel

slope combination cases representing a natural channel reach which can be composed of one or more constant slope stretch are also studied beside single slope channels. Steady state simulations are performed for six sediment grain size (GSD) sets, which cover a wide spectrum of naturally occurring sediment sizes.

The simulation results show a power-law relationship between μ and regime channel slopes for all channel dimensions, reach combinations, GSD, initial slopes and with (R1) and without sediment feeding (R). The increase in relative flow resistance (μ) with regime channel slope is well reproduced in form of bedforms. Regime channels developed step-pool to cascade bedforms for steep slopes and plane- to riffle bed for gentle slopes channels. The relationship between μ and regime slope derived using regime channel simulation approach exhibits good agreement with some field measurement of flow resistance for mountainous rivers and streams. The approach is applied on two IRS case studies with observed data in Kabul River basin, Afghanistan to estimate bedload transport. The relative flow resistance resulted from models calibration showed good agreement with those derived from test channels regime development simulation.

The outcome of channel regime simulation with presence of MRE as geometrical shapes produced a logarithmic-law with a horizontal asymptote relationship between MRE concentrations and channel regime slopes. Similar results are also reported from flume experiments that the ratio of drag to total shear stress increases rapidly when the MRE are sufficiently distant. Regime channels develop micro-channels around MRE, where the bulk of bedload transport occur. For MRE arrangements as cascades, the results show a power-law relationship between channel regime slope and step-pool dimensions $\lambda = L_D/D_B$. The results obtained are in good agreement with field measurement of naturally occurring and artificially built λ relationship with S_R .

Future studies can further enrich the validation of this approach by applying it to other study sites. Present modelling tools have their limitations when dealing with strong geometries which is often the case for mountain rivers, therefore, improvement in modelling techniques is required to flexibly deal with abrupt changes in riverbed geometry for instance when implementing MRE as main flow resistance inducer.

Kurzfassung

Flüsse und Bäche mit saisonaler Abfluss-, Sediment- und Habitatdynamik werden als intermittierende Flüsse und Bäche bezeichnet (IFB). IFB sind die vorherrschenden Fließgewässer in trockenen und halbtrockenen Regionen der Welt. Sie kommen jedoch auch in gemäßigten und feuchten Klimaten vor, dort hauptsächlich in Quellgebieten. Entsprechend zählen die meisten der Fließgewässer in Gebirgsregionen zu den IFB, wo steile Geländeneigungen und große Spektren der Sedimentgrößen zu hydro-sedimentologischer Komplexität führen. Der charakteristische Geschiebetransport der IFB in Gebirgsregionen, auf dessen Grundlage Sedimentmanagementstrategien geplant werden, ist bei weitem nicht gut verstanden. Nicht selten werden aufgrund dieser Wissenslücke die Erkenntnisse über den Geschiebetransport in perennierenden Flüssen tieferer Lage auf intermittierende Fließgewässer übertragen. Dies kann zu einer Überschätzung der transportierten Geschiebemengen führen, nicht zuletzt aufgrund einer ungenauen Schätzung der sohnahen Strömungseigenschaften, welche für den Geschiebetransport verantwortlich sind. Trotz der Entwicklung zahlreicher Methoden zur Anpassung sohnaher Strömungsparameter für steile IFB, wie z. B. der Doppelmittlung der Navier-Stokes-Gleichung und die Strömungswiderstandsberechnungen für geringe Fließtiefen, ist die Anwendung dieser angepassten Parameter auf kontrollierte Laborbedingungen beschränkt.

Die vorliegende Arbeit leistet einen Beitrag zum Schließen der genannten Wissenslücke zum charakteristischen Geschiebetransport in IFB in Gebirgsregionen. In den hier vorgestellten Untersuchungen wird der Strömungswiderstand auf Maßstabsebene von Flussabschnitten unter Verwendung eines Regime-Kanal-Ansatzes als Hauptfaktor der Strömungseigenschaften bestimmt. Dieser Ansatz beschreibt die im zeitlichen Mittel konstanten Verhältnisse eines IFB, also einen dynamischen Gleichgewichtszustand. Die Grundannahme ist dabei, dass ein Flussabschnitt mit konstanter Neigung einen bestimmten Strömungswiderstand entwickelt, um der durch den bordvollen Abfluss verursachten Änderung (Kanalbettersosion) zu widerstehen und eine bestimmte Gerinnegeometrie, Neigung und Korngrößenverteilung (KGV) beizubehalten.

Um den Regime-Zustand von Kanälen mit variierender Anfangsgeometrie, KGV und Neigung zu bestimmen, werden 2D-Feststofftransportsimulationen verwendet. Basierend auf dem Ansatz der Aufteilung des Strömungswiderstands werden die Sohl Schubspannungen durch das Verhältnis des Gesamtströmungswiderstands zum Kornwiderstand, auch als relativer Strömungswiderstand μ bezeichnet, modifiziert, um die Verlustleistung der Fließenergie auf unbeweglichen Sedimenten wie Makrorauheitselementen (MRE) und Bettformen zu berücksichtigen.

In einem alternativen Ansatz werden Szenarien mit MRE als dominierender Strömungswider-

standsursache untersucht. Die MRE sind dabei in der Regimekanalsimulation als nicht erodierbare geometrische Formen aufgebaut, die einerseits zufällig über das Kanalbett verteilt oder andererseits in Kaskadenbettformen angeordnet sind. Die MRE führen hauptsächlich zu zwei stark ausgeprägten Effekten: (i) sie verändern stark das sie lokal umgebende Strömungsmuster und (ii) sie verringern die von Erosion angegriffene Fläche im Flussbett.

Regime-Kanalsimulationen werden für akademische Beispielkanäle mit initialen Neigungen zwischen 0,0% und 10,0% sowie Startwerten für Breite \times Länge von 5,5 m \times 200,0 m bis 16,5 m \times 200,0 m durchgeführt. Sie repräsentieren jeweils Laborrinnen und natürliches Gewässer. Neben einer konstanten Neigung werden drei Neigungskombinationen untersucht, um naturähnliche Rahmenbedingungen darzustellen. Es wird ein stationäres zweischichtiges Feststofftransportmodell mit sechs KGV verwendet, was ein breites Spektrum natürlich vorkommender KGV abdeckt.

Die Simulationsergebnisse deuten auf einen Potenzgesetz-Zusammenhang zwischen μ und Regimekanal-Neigung ($S_R; S_{R1}$) hin. Dieser Zusammenhang gilt für alle Kanaldimensionen, KGV, Anfangsneigungen sowie mit $R1$ und ohne Geschiebezugabe R . Die Variation von μ mit der Neigung des Kanalregimes wird gut in den resultierenden Bettformen abgebildet: Für stark geneigte Regimekanäle entwickelten sich Bettformen von Stufen-Becken-Sequenz bis hin zu Kaskaden, für gering geneigte Regimekanäle entwickelten sich ebene Bettformen oder Riffelbettkanäle. Die Beziehung zwischen μ und der ($S_R; S_{R1}$), die unter Verwendung des Regime-Kanal-Simulationsansatzes abgeleitet wurde, stimmt gut mit Feldmessungen des Strömungswiderstands für Gebirgsflüsse überein. Der Ansatz wurde auch an zwei IFB (Shakar-Dara und Maidan) im Einzugsgebiet des Kabul-Flusses in Afghanistan verwendet und zeigt ebenfalls gute Übereinstimmung mit den Ergebnissen aus den akademischen Beispielen.

Die Simulationen der Regime-Kanal-Entwicklung mit verschiedenen quasi-zufälligen MRE-Anordnungen zeigen, dass die Beziehung zwischen MRE-Dichte und $S_R; S_{R1}$ einer logarithmischen Funktion mit einer horizontalen Asymptote folgt. Experimente in Versuchsrinnen führen zu vergleichbaren Ergebnissen, bei denen das Verhältnis von Fließwiderstand zur gesamten Schubspannung stark ansteigt, wenn ein gewisser Abstand zwischen den MRE unterschritten wird. In Regime-Kanälen entwickeln sich kleinste Rinnen um die MRE, in denen der Großteil des Sedimenttransportes stattfindet. Die Ergebnisse für MRE-Anordnung in Stufen-Becken-Abfolge- oder Kaskadenbettformen zeigen eine exponentielle Beziehung zwischen der $S_R; S_{R1}$ und dem Quotienten aus Länge L_D und Tiefe D_B der sich entwickelnden Stufen, welcher auch als Stufen-Beckenmaßzahl $\lambda = L_D/D_B$ bekannt ist. Diese Ergebnisse stimmen gut mit im Gelände erhobenen Daten zu natürlich vorkommenden und künstlich induziert Stufen-Beckens überein.

Insgesamt erweitern die hier vorgestellten Erkenntnisse das Verständnis zum charakteristischen Geschiebetransport in IFB. Folgestudien können die Anwendbarkeit und Übertragbarkeit des Regime-Kanal-Ansatzes anhand weiterer Fallbeispiele validieren. Zusätzlich wird Bedarf gesehen, eine Verbesserung in Modellierungsverfahren zu erreichen, um MRE-Formen und komplexe Flussgeometrien abbilden zu können.

Contents

Disclaimer	iii
Acknowledgement	v
Abstract	vii
Kurzfassung	ix
List of Figures	xv
List of Tables	xxi
List of Symbols	xxiii
1. Motivation and objectives	1
1.1. Motivation	1
1.2. Research objectives	4
1.3. Thesis structure	5
2. Introduction	1
2.1. Definitions of intermittent rivers and streams	1
2.1.1. Definition in terms of surface water and groundwater interaction	1
2.1.2. Definitions in terms of occurrence of zero flows (flow intermittency)	2
2.1.3. Tools other than flow records for defining IRS	3
2.2. Worldwide distribution and contribution of IRS	4
2.3. Drying and rewetting patterns in IRS	5
2.4. Causes of flow intermittency	8
2.5. Importance and challenges of IRS management	8
2.5.1. Increasing demand and decreasing water availability	8
2.5.2. Challenges in water storage and sediment management	9
2.5.3. Water right issues and water conflicts	10
2.5.4. Climate change and increase in flow variability	11
2.6. Hydro-morphological characteristics of IRS	11
2.6.1. Geomorphological characteristics and sediment transport regimes	11
2.6.2. Upland zone	12
2.6.3. Piedmont zone	12
2.6.4. Lowland zone	12
2.6.5. Floodout zone	13

2.7. Hydrological characteristics of IRS	15
2.7.1. Hydrological connectivity	15
2.8. Summary	20
3. Hydrodynamic and sediment transport in steep IRS	21
3.1. Sediment transport in rivers	21
3.1.1. Bedload transport	22
3.1.2. Sediment incipient motion	24
3.1.3. Slope dependency of critical shear stress	26
3.2. Sedimentological characteristics of IRS	29
3.2.1. Riverbed sediment characteristics in IRS	29
3.2.2. Bedload transport in IRS	31
3.2.3. Riverbed clogging and its implication on bedload transport in IRS	32
3.3. Hydraulics of mountainous IRS	36
3.3.1. Flow regions and their characteristics	36
3.3.2. Near-bed flow characteristics	38
3.3.3. Role of macro-roughness elements in changing the hydrodynamic forces on sediment particles	43
3.3.3.1. Effects on the hydraulic of the near bed regions	43
3.3.3.2. Hiding effect of MRE	44
3.3.3.3. MRE effects on the bed roughness and flow resistance	45
3.3.4. Methods for adjusting near-bed flow hydraulics for steep slopes	46
3.4. Summary	50
4. Methods	53
4.1. Channel regime concept	53
4.1.1. Description of gravel-bed rivers regime theory	55
4.1.2. Computation of regime channel R	57
4.1.3. Gravel-like regime channel formation	60
4.1.4. Regime channel R1 (with a constant bedload transport)	61
4.1.5. Channel slope and roughness development at regime conditions	63
4.2. Determination of flow resistance using gravel-like regime approach	64
4.2.1. Determination of regime relative resistance μ_c using simulations	66
4.2.2. Channel slope combinations	68
4.3. MRE as geometry (immobile boulders and step-pool bedforms)	71
4.3.1. MRE as geometry	71
4.3.2. MRE as step-pool or cascade bedforms	75
4.4. Hydro-morphological simulations	78
4.4.1. Mesh conditioning	78
4.4.2. Boundary conditions	78
4.4.3. Riverbed sediment grain size distribution (GSD)	81
4.4.4. Model Hydro_FT-2D description	83
4.5. Summary	93

5. Regime channel simulation results	95
5.1. Simulation results for flow resistance as numerical values	95
5.1.1. Channel regime dimensions development	95
5.1.2. Relationship between regime slope and relative flow resistance . . .	101
5.1.3. Comparison of simulation results with field observations	114
5.1.4. Bedload transport	117
5.1.5. Grain size distribution (GSD) at regime state	121
5.1.6. Channel regime morphology development	123
5.2. Simulations results for MRE as geometry	130
5.2.1. Relationship between MRE concentration and channel regime slope	130
5.2.2. Comparison of MRE as geometry results with field observations . .	135
5.2.3. Bedload transport in MRE as geometry channel	135
5.2.4. GSD in MRE as geometry channels at regime state	137
5.3. Simulations results for MRE as step-pool bedforms	138
5.3.1. Relationship between channel-regime slope and step-pool dimensions	138
5.3.2. Regime channel profiles for MRE as Step-pool	140
5.3.3. Comparison of simulated step-pool dimension with field observations	143
5.3.4. Bedload transport and GSD in MRE as step-pool channels	145
5.4. Summary of the regime channel simulation results	149
6. Application	153
6.1. Case study of Shakar-Dara and Maidan rivers	153
6.1.1. Shakar-Dara River	153
6.1.2. Maidan River	154
6.1.3. Field campaigns	155
6.1.4. Hydromorphological modelling results	159
7. Conclusion and outlook	169
7.1. Conclusion	169
7.2. Outlook	173
Bibliography	175
A. Appendix A	204
A.1. Initial and boundary conditions in Hydro_FT-2D	204
A.1.1. Model parameters	205
B. Appendix B	209
C. Appendix C	213
D. Appendix D	216
E. Appendix E	220

List of Figures

1.1. Examples of flow resistance development at two stretches of an IRS with different reach slopes (a) Steep stretch with step-pool bedforms and (b) gentle-slope stretch with cobble-bed	3
2.1. Definitions of perennial (p), intermittent (i) and ephemeral (e) rivers and streams in terms of surface water groundwater interactions	2
2.2. Locations of world's dryland regions and their categories	5
2.3. Drying pattern of isolated pools at (a) Dori (b) Harirud rivers (c) upstream drying extending downstream in Nahreen River and Farahrud River during (d) dry period and (e) resumption of flow	7
2.4. Conceptual model showing hydro-geomorphological zones after Schumm (1977) and (b) their longitudinal material distribution. (c) Cross-sectional view of upland zone, (d) piedmont, and (e) lowland and floodout zones. The arrows indicate the lateral and vertical exchange of surface water and groundwater showing the hydrologic connectivity in different zones	19
3.1. Schematic of different modes of sediment transport	22
3.2. Critical shear stress for incipient motion of sediment grains by (Yalin and Karahan 1979)	25
3.3. Field and flume data showing the slope dependency of critical Shields stress (a), (b) The critical shear stress variation with grain sizes and relative submergence and (c) reference shear stress τ_r^* for different slope with data stratified by bank-full flow h/D_{50} derived from measurements of 159 gravel-bed streams in North America and the United Kingdom.	28
3.4. Graphical representation of bed building in IRS with respect to the sediment supply and hydrograph shape Modified after Cooke et al. (1993)	31
3.5. Comparison of unit bedload transport as a function of bed shear stress in the ephemeral Nahal Yatir and Nahal Eshtemoa, seasonal Goodwin Creek, perennial rivers Oak Creek, Jacoby and East-fork rivers	32
3.6. Clogging of the riverbed by fine sediments deposition soon after flash flood recession at (a) upstream reach of Maidan River in Kabul River basin (b) closer view of the freshly clogged riverbed (c) and (d) clogged riverbed after it is dried. Note: The equal-distance markings (red and white strips) on the staff are 10 cm each.	34

3.7.	(a) Regions in boundary layer flow (Coleman and Alonso 1983; Graf 1991), (b) measured mean flow velocity distribution normalised by mean flow velocity for mountain rivers in Colorado (Jarret 1990) and (c) measured Reynolds stress normalised by shear velocity for flow with small submergence over a flume bed composed of glass beads using Laser Doppler Anemometer (LDA) (Nakagawa et al. 1991)	37
3.8.	Schematic view of permeable bed (a) average flow characteristics in the roughness layer normalised by shear velocity (b) velocity distribution (c) Reynolds stress (d) form induced stress and (e) turbulence intensity for three different flow submergences	42
3.9.	MRE on a natural IRS riverbed (a) and (b) their impact on the flow conditions under high (HFS) and low flow submergence (LFS)	46
4.1.	Five river reaches in north-east Afghanistan showing variable flow resistance in (a to e)	54
4.2.	Longitudinal profiles for river reaches in figure 4.1. For each reach two distinct slope can be recognised as listed in the legend	55
4.3.	Schematic view of geometric nature of $F_r; \eta_*$ -curve family for regime channel R	59
4.4.	Schematic view of geometric nature of $F_r; \eta_*$ -curve family for $R1$ - channel regime	63
4.5.	(a) Relationship between Chezy resistance factor c with tractive force η_* and (b) relationship between S and η_* for different grain size D and N values	64
4.6.	Fixed and extended-width meshes for a 4.5% slope channel (a) 2D view and (b) 3D view of the inflow region	70
4.7.	Channel slopes and slope combination cases used in the simulations (a) constant slopes from 0.5% to 10% (b) slope combination case 1 (c) slope combination case 2 and (d) slope combination case 3	71
4.8.	MRE as geometry and their influence on (a) velocity field (b) bed shear stress and (c) longitudinal profile of bed shear stress as a function of MRE concentrations for an example of 4.5% constant channel slope	73
4.9.	Example of channel-bed evolution development for initial channel slope of 8.5% with MRE concentration of 4.6% (a) initial and time-development of channel bed longitudinal profile (b) sediment extraction volume from MRE for different extraction zones and at different simulation time (c) sediment extraction zones and (d) initial and time-development of MRE trapezoidal shapes deformation	75
4.10.	Step-pool channel regime development and their effects on the flow characteristics for an example of 4.5% initial channel slope (a) 2D bed shear stress and velocity distribution and (b) longitudinal profile of shear stress for flatbed and step-pool bed channel and (c) channel bed evolution with time for step-pool bed channel	77

4.11. Schematic diagram of boundary conditions for initial, intermediate and regime phase of simulations	80
4.12. Measured (shown by stars) and generated GSD curves for (a) surface layer (AS) and (b) subsurface (US), base layer (GS) and sediment feeding.	82
4.13. Schematic illustration of flow in a river bend (a) Flow and bedload transport in river bend (b) profiles of main flow and secondary currents and the resultant near-bed shear stress components and their direction modified after Hafner (2008)	87
4.14. Flow and bedload transport directions in a Cartesian coordinate system. Modified after Klar (2016)	88
4.15. Layering management in Hydro-FT-2D for both erosion and deposition cases	93
5.1. Determination of regime channel width and depth at cross-sections shown on two examples of regime channels (a) and a_1 extended-width channel and its cross-sections and (b) and b_1 fixed-width channel and its cross-sections	97
5.2. Maximum and minimum regime channel width variations with channel regime slope (a) and (a_1) $D_{mo} = 19.0 \text{ mm}$, (b) and (b_1) $D_{mo} = 38.0 \text{ mm}$, (c) and (c_1) $D_{mo} = 57.0 \text{ mm}$ for fixed-width channels and extended-width channels respectively.	98
5.3. Maximum, minimum and average regime channel depth variations with channel regime slope (a) and (a_1) for $D_{mo} = 19.0 \text{ mm}$, (b) and (b_1) for $D_{mo} = 38.0 \text{ mm}$, (c) and (c_1) for $D_{mo} = 57.0 \text{ mm}$ for fixed-width channels and extended-width channels respectively.	101
5.4. Relationship between relative resistance μ and fixed-width channel regime slope $S_R; S_{R1}$ for regime channels R and R1 with a feeding rate of $Q_b = 5 \text{ kg/s}$ for D_{mo} values of (a) 19.0 mm (b) 28.4 mm (c) 38.0 mm (d) 47.3 mm (e) 57.0 mm and (f) 66.3 mm	105
5.5. Relationship between relative resistance μ and fixed-width channel regime slope S_R for D_{mo} values of (a) 19.0 mm (b) 38.0 mm and (c) 57.0 mm for both scenario A and B	107
5.6. Relationship between total roughness k_{st} , additional roughness k_{add} and grain roughness $k_{st'}$ with channel regime slopes for scenario A and B	108
5.7. Relationship between relative resistance μ and extended-width channel regime slope $S_R; S_{R1}$ for regime channels R and R1 with a feeding rate of $Q_b = 5 \text{ kg/s}$ for (a), (a_1) $D_{mo} = 19.0 \text{ mm}$ (b), (b_1) $D_{mo} = 38.0 \text{ mm}$ (c), (c_1) $D_{mo} = 57.0 \text{ mm}$ for flow discharge of $2.0 \text{ m}^3/\text{s}$ and $1.0 \text{ m}^3/\text{s}$ respectively	111
5.8. Channel regime profiles and their initial values for examples of channel slope combinations (a) case1 (b) case 2 and (c) case 3	113
5.9. Relationship between relative resistance and channel regime slope for single slope channels (circles), single slope with sediment feeding (filled circle) and combined slope cases (triangles)	114
5.10. Comparison of relative resistance relationship with channel regime slope acquired through regime channel simulations (stars) and field observations	117

5.11. Bedload transport rates and their cumulative total transport at model's outflow for R regime channels of GSD D_{mo} value of 38.0 mm (a) and (a ₁) for fixed-width channel (b) and (b ₁) extended-width channel	119
5.12. Bedload transport rates and their cumulative total transport at model's outflow for $R1$ regime channels of constant feeding rate $Q_b = 5.0$ kg/s for GSD with D_{mo} value of 38.0 mm (a) and (a ₁) for fixed-width channel (b) and (b ₁) extended-width channel	121
5.13. Difference between GSD of channel bed sediments at regime state and their initial values for (a) $\Delta S = 2.65\%$ (b) $\Delta S = 1.5\%$ (c) $\Delta S = 2.59\%$ (d) $\Delta S = 1.5\%$ and their associated longitudinal distribution in (a ₁) (b ₁), (c ₁) and (d ₁) respectively	123
5.14. 3D view of channel plan-forms for some selected regime slopes using $D_{mo} = 38.0$ mm (a) fixed-width channels (b) extended-width channels . . .	125
5.15. Plan-form development for fixed-width channels for channel regime slopes (a) 0.0-1.5% (b) 1.5-3.0% (c) 3.0-4.5% (d) 4.5-6.0% (e) 6.0-8.0% and (f) 8.0-10.0%	128
5.16. Plan-form development for extended-width channels for channel regime slopes (a) 0.0-1.5% (b) 1.5-3.0% (c) 3.0-4.5% (d) 4.5-6.0% (e) 6.0-8.0% and (f) 8.0-10.0%	129
5.17. Relationship between regime channel slope S_R and MRE concentrations in percentage of total area coverage for GSD subsurface layer sediments (a) $D_{mo} = 19.0$ mm (b) $D_{mo} = 38.0$ mm and (c) $D_{mo} = 57.0$ mm	131
5.18. Bed shear stress distribution along the longitudinal distance of regime channel for MRE-free bed (solid lines) and different MRE concentrations (colored lines) as a function of channel slopes (a), (a ₁) 2.5% (b), (b ₁) 4.5% (c), (c ₁) 6.5% (d), (d ₁) 8.5% and (e), (e ₁) 10% for protruding and submerged MRE cases respectively	134
5.19. Bedload transport rates at model's outflow with and without presence of MRE for (a) R regime channel and (b) $R1$ regime channel with a sediment feeding rate of $Q_b = 5.0$ kg/s	137
5.20. The effect of MRE on the GSD of bed surface layer sediments in terms of difference between regime $D_{msR/R1}$ and initial D_{ms} values and their longitudinal bed profiles in (a) (a ₁) and (b), (b ₁) for R and $R1$ regime channels respectively	138
5.21. Relationship between step-pool dimensions λ and channel regime slopes $S_R; S_{R1}$ for (a) $D_{mo} = 19.0$ mm, (b) $D_{mo} = 38.0$ mm, and (c) $D_{mo} = 57.0$ mm .	140
5.22. Regime channel profiles for the MRE as step-pool for regime channel slopes (a) $S_R < 4.5\%$ and (b) $4.5\% < S_R < 10\%$	142
5.23. 3D-view of MRE as step-pool channel plan-form development for different regime channel slopes from simulations results with $D_{mo} = 19.0$ mm	143
5.24. Relationship between step-pool dimension and channel regime slopes for nine datasets from field observations and regime channel simulations using MRE as non-erodible steps (stars)	145

5.25. Bedload transport rates at model's outflow for R and R1 regime channels with sediment feeding rate of $Q_b = 5.0 \text{ kg/s}$ for six channels of MRE as step-pools and MRE-free channels respectively for GSD (a), (a ₁) $D_{mo} = 19.0 \text{ mm}$ (b), (b ₁) $D_{mo} = 38.0 \text{ mm}$ and (c), (c ₁) $D_{mo} = 57.0 \text{ mm}$	147
5.26. The difference in mean grain diameter for surface layer between regime state D_{msR} and initial condition D_{ms} for inflow section of regime channels R and R1 in (a) (b) respectively. (a ₁) longitudinal profiles of channel bed, D_{msR} and D_{ms} at initial and regime state for R and (b ₁) longitudinal profiles of channel bed, D_{ms} , D_{msR} at initial and regime state, sediment feeding D_{mo} and transported bedload D_{mTr} for regime channel R1	149
6.1. Shakar-Dara River at downstream of hydrometeorological station	154
6.2. Maidan River section at upstream of Tangi-Sayedan hydrometeorological station	155
6.3. Surface and subsurface layers' sediment GSD determined by Basegrain and sieve analysis respectively for the study reaches (a) Shakar-Dara River (b) Maidan River	157
6.4. Shakar-Dara River reaches and their associated slopes for assigning initial k'_{st} and μ values	158
6.5. Riverbed evolution of Shakar-Dara River occurred between 2013 to 2016 (a) observed evolution (b) simulated evolution and (c) their longitudinal profiles	160
6.6. Observation and simulation of riverbed evolution for Maidan River for 2013 to 2016 (a) observation (b) simulation (c) sediment extraction areas at 200 m upstream (d) 400 m (e) 720 m and (f) 920 m downstream of Tangi-Sayedan hydrometeorological station	162
6.7. Longitudinal profiles of observed and simulated riverbed evolution for Maidan River	163
6.8. Bedload transport from calibrated model obtained at different sections (a) 560 m upstream (b) 0 m (c) 800 m and (d) 2057 m downstream of Shakar-Dara River hydrometeorological station	164
6.9. Bedload transport from calibrated model obtained by using control sections at different locations Maidan River (a) 0 m (b) 535 m (c) 1335 m (d) 2055 m (e) 2600 m and (f) 3289 m downstream of Tangi-Sayedan hydrometeorological station	166
6.10. Relative flow resistance relationship as a function of channel reach slope for an average regime channel R1 simulations and (a) Shakar-Dara River (b) Maidan River	167
B.1. Maximum and minimum regime channel width and depth variations with channel regime slope repectively for (a) and a1) $D_{mo} = 28.4 \text{ mm}$, (b) and (b1) $D_{mo} = 47.3 \text{ mm}$, (c) and (c1) $D_{mo} = 66.3 \text{ mm}$ for fixed-width channels	209

B.2.	Maximum and minimum regime channel width to depth variations with channel regime slope for D_{mo} values of (a) 19.0 mm (b) 28.4 mm (c) 38.0 mm (d) 47.3 mm (e) 57.0 mm and (f) 66.3 mm for fixed-width channels	210
B.3.	Maximum and minimum regime channel width to depth variations with channel regime slope for D_{mo} values of (a) 19.0 mm (b) 38.0 mm (c) 57.0 mm for fixed-width channels	211
B.4.	Difference in the bed shear stress arising from total roughness with respect to a reference roughness for channel regime slopes (a) 0.7% (b) 2.5% (c) 4.5% (d) 6.6% (e) 8.3% (f) 9.35%	212
C.1.	Bedload transport and their cumulative total transport variation over time at models' outflow for D_{mo} values 19.0 mm and 57.0 mm respectively in (a) (b) (c) (d) and (e) (f) (g) (h) for fixed-width channels	213
C.2.	Bedload transport and their cumulative total transport variation over time at models' outflow for D_{mo} values 19.0 mm and 57.0 mm respectively in (a) (b) (c) (d) and (e) (f) (g) (h) for extended-width channels	214
C.3.	GSD at initial and regime state respectively fo R and R1 regime channels for for D_{mo} values (a1), (b1) 19.0 mm (c1), (d1) 28.4 mm (e1), (f1) 47.3 mm (g1), (h1) 57.0 mm and (i1), (j1) 66.3 mm	215
D.1.	Regime channel sinuosity for all tested GSD in (a) R regime channel (b) R1 regime channel	216
D.2.	Plan-form development for R1 channels are shown for some selected channel regime slopes	217
D.3.	Plan-form development for three examples of slope combination cases 1, 2 and 3 respectively in (a), (b), and (c)	217
D.4.	Longitudinal profiles for R1 fixed-width channels for regime slopes (a) 0.0-1.5% (b) 1.5-3.0% (c) 3.0-4.5% (d) 4.5-6.0% (e) 6.0-8.0% (f) 8.0-10.0%	218
D.5.	Longitudinal profiles for R1 extended-width channels for regime slopes (a) 0.0-1.5% (b) 1.5-3.0% (c) 3.0-4.5% (d) 4.5-6.0% (e) 6.0-8.0%	219
E.1.	Photogrammetric analysis tool (Basegrain) of samples from (a) Shakar-Dara River (b) Maidan River	220
E.2.	Plan-form development for R1 channels are shown for some selected channel regime slopes	221
E.3.	Longitudinal profiles for R1 fixed-width channels for regime slopes (a) 0.0-1.5% (b) 1.5-3.0% (c) 3.0-4.5% (d) 4.5-6.0% (e) 6.0-8.0% (f) 8.0-10.0%	222
E.4.	Longitudinal profiles for R1 extended-width channels for regime slopes (a) 0.0-1.5% (b) 1.5-3.0% (c) 3.0-4.5% (d) 4.5-6.0% (e) 6.0-8.0%	223

List of Tables

2.1. Main distinctions in IRS longitudinal trends. Modified after Jaeger et al. (2017)	13
3.1. Main bedload transport approaches	23
3.2. Approaches for adjusting the near-bed flow hydraulics for steep IRS	50
4.1. Main sediment GSD characteristics and calculated grain roughness for measured and generated sets of GSD used for surface (AS), subsurface (US) and base layer (GS)	82
4.2. List of simulations performed for various sets of GSD	83
A.1. Some selected parameters for hydraulic calculations by Hydro_FT-2D	206
A.2. Some selected parameters used for morphologic simulations by Hydro_FT-2D207	

List of Symbols

Symbols	Description	Unit
Latin Symbols		
a	Coefficient in power-law flow resistance equation	[-]
a_1	Coefficient in power-law relationship between relative flow resistance μ and channel regime slope S_R and S_{R1}	[-]
A_*	Energy-related characteristics of regime channels based on the principles of thermodynamics Yalin and da Silva (2001) expressed $dA_* = F_r$	[-]
A_{Sec}	Secondary current factor in Hydro_FT-2D that varies between 7 and 12	[-]
A_w	Wetted area between two cross-sections	[m^2]
b	Exponent in power-law relationship between relative flow resistance μ and channel regime slope S_R and S_{R1}	[-]
b_1	Exponent in power-law flow resistance equation	[-]
B_r	Constant in the Keulegan (1938) type logarithmic-law flow resistance equation	[-]
c	Chezy resistance factor for total roughness	[-]
c_{Add}	Chezy resistance factor for additional roughness due to macro-roughness elements (MRE) or bedforms	[-]
c_f	Chezy resistance factor for grain roughness	[-]
$(c_f)_R$	Chezy grain resistance factor of a channel at regime state	[-]
$c_{f\Theta}$	Global parameter in Hydro_FT-2D model for account for the effect of channel slope on the bedload transport direction	[-]
c_g	Flow resistance development with tractive force η_* for gravel-like regime channel development	[-]
c_R	Chezy total resistance factor of a channel at regime state	[-]

Symbols	Description	Unit
c_s	Flow resistance development with tractive force η_* for sand-like regime channel development	[-]
C	Empirical coefficient in estimating velocity from unit discharge	[-]
C_D	Drag coefficient	[-]
C_L	Lift coefficient	[-]
d_p	Zero-plane displacement height d_p is defined as the distance from roughness crest into the roughness layer where the flow velocity is zero	[m]
D_b	Diameter of moving particle	[m]
D	Mean sediment grain diameter	[m]
D_s	A representative grain diameter	[m]
D_B	Depth of steps right at downstream of steps for step-pool or cascading river	[m]
D_{mo}	Mean grain diameters for subsurface layer sediments	[m]
D_{ms}	Mean grain diameters for surface layer sediments	[m]
D_{msR}	Mean grain diameters for surface layer sediments at regime state for R-channels	[m]
D_{mTr}	Mean grain diameters for bedload transport for R1-channels	[m]
D_{msR1}	Mean grain diameters for surface layer sediments at regime state for R1-channels	[m]
D_{max}	Maximum grain diameter of the surface layer sediments	[m]
D_{30}	Particle diameter representing the 30% cumulative percentile value (30% of the particles in the sediment sample are finer than the D_{30} grain size)	[m]
D_{50}	Particle diameter representing the 50% cumulative percentile value (50% of the particles in the sediment sample are finer than the D_{50} grain size)	[m]
D_{84}	Particle diameter representing the 84% cumulative percentile value (84% of the particles in the sediment sample are finer than the D_{84} grain size)	[m]
D_{90}	Particle diameter representing the 90% cumulative percentile value (90% of the particles in the sediment sample are finer than the D_{90} grain size)	[m]

List of Symbols

Symbols	Description	Unit
e	Natural logarithm ($\cong 2.718$)	[-]
e	Exponent e is used as calibration parameter and is accounting for energy loss due to macro-roughness in rough flumes and channels	[-]
E	Energy gradient	[-]
f	Darcy-Weisbach friction factor	[-]
f_{Add}	Darcy-Weisbach friction factor for additional roughness (e.g. macro-roughness elements MRE, bedforms, and large woody debris)	[-]
f_{tot}	Darcy-Weisbach friction factor for total roughness (grain roughness plus additional roughness)	[-]
f_0	Darcy-Weisbach friction factor for base level or grain roughness	[-]
F_i	Fraction of a sediment grain class in a grain size distribution	[-]
F_L	Lift forces	[N]
F_r	Froude number, $F_r = \frac{\bar{u}}{\sqrt{gh}}$ a dimensionless number proportional to the square root of the ratio of the inertial forces over the weight of fluid	[-]
$(F_r)_R$	Froude number value at channel regime state for R -regime channels	[-]
$(F_r)_{R1}$	Froude number value at channel regime state for $R1$ -regime channels	[-]
g	Standard gravitational acceleration	$[m/s^2]$
h	Water depth	$[m]$
h_R	Channel regime depth	$[m]$
$h_{R_{ave}}$	Average depth for R -regime channels	$[m]$
$h_{R_{min}}$	Minimum depth for R -regime channels	$[m]$
$h_{R_{max}}$	Maximum depth for R -regime channels	$[m]$
h_{R1}	Channel regime depth for $R1$ -regime channels	$[m]$
$h_{R1_{ave}}$	Average depth for $R1$ -regime channels	$[m]$
$h_{R1_{min}}$	Minimum depth for $R1$ -regime channels	$[m]$
$h_{R1_{max}}$	Maximum depth for $R1$ -regime channels	$[m]$

Symbols	Description	Unit
k	Von Karman value, takes a value of 0.4 for logarithmic velocity distribution	[-]
k_f	A pre-factor modifier that provides the option to adjust the bed-load transport rate to achieve a target calibration	[-]
k_s	Equivalent Nikuradse roughness height	[m]
k_{st}	Total roughness in Hydro_FT-2D in Manning-Strickler values	$[m^{1/3}/s]$
k'_{st}	Grain roughness in Hydro_FT-2D in Manning-Strickler values	$[m^{1/3}/s]$
k_ψ	Factor considers influence of the transverse slope on the sediment incipient motion in Hydro_FT-2D	[-]
k_Θ	Factor considers influence of the longitudinal slope on the sediment incipient motion in Hydro_FT-2D	[-]
K	Dimensionless parameter	[-]
K_*	Dimensionless parameter	[-]
K_{**}	Dimensionless parameter	[-]
L	Unit stream length between two cross-sections or length of a river reach	[m]
L_D	Clear distance between adjacent steps also known as step-length	[m]
L_s	Characteristic energetic eddy size (i.e., mixing length) typically generated at $z = k_s$	[m]
L_p	The average distance travelled by sediment particle during a unit time	[m]
m_1	Empirical coefficient in estimating velocity from unit discharge	[-]
m	Shows the movement path of regime channel toward achieving regime status in the so called $F_r; \eta_*$ -plane	[-]
$M_{f,i}$	Source term to describe the vertical material flow between exchange and subsurface layer of the grain class i	[m/s]
M_f	Source term to describe the vertical material flow between exchange and subsurface layer	[m/s]
$M_{f,G}$	Source term to describe the vertical material flow between subsurface layer and base layer	[m/s]
n_0	Grain roughness in Manning-Strickler values estimated from sediment grain size (i.e. D_{90})	$[m^{1/3}/s]$

List of Symbols

Symbols	Description	Unit
n_{tot}	Total roughness in Manning-Strickler values	$[m^{1/3}/s]$
N	Dimensionless specific flow rate refers to unit flow discharge over channel width at a given grain size and critical shear velocity expressed by $N = \frac{Q}{wDu_{*c}}$	[-]
N_*	Dimensionless specific flow rate for boundary curve between sand- and gravel-like regime channel	[-]
pal	A variable in Hydro_FT-2D to control the thickness of bed surface layer AS	[-]
$p_{i,al}$	Fraction of grain class i of bedload material from surface layer	[-]
$p_{i,AS}$	Fraction of grain class i in the surface layer	[-]
$p_{i,GS}$	Fraction of grain class i in the base layer	[-]
$p_{i,Tr}$	Fraction of grain class i of bedload material	[-]
$p_{i,ul}$	Fraction of grain class i of bedload material from subsurface layer	[-]
$p_{i,US}$	Fraction of grain class i in the subsurface layer	[-]
p_n	Probability of a sediment particle being eroded in a unit time	[-]
pul	A variable in Hydro_FT-2D to control the thickness of bed subsurface layer US	[-]
P	Wetted primeter of a cross-section assumed as $\frac{A_w}{h}$	$[m]$
P_g	Regime point for gravel-like regime channels in the so-called $F_r; \eta_*$ -plane	[-]
P_R	Regime point in $F_r; \eta_*$ -plane for R channels	[-]
P_{R1}	Regime point in $F_r; \eta_*$ -plane for R1 channels	[-]
P_s	Regime point for sand-like regime channels in the so-called $F_r; \eta_*$ -plane	[-]
P_0	An initial point on the channel regime development path as shown in $F_r; \eta_*$ -plane	[-]
P_0^\wedge	A point on the channel regime development path at $t = T_0^\wedge$ as shown in $F_r; \eta_*$ -plane	[-]
q	Flow discharge per unit channel width	$[m^2/s]$
q_b	Volumetric bedload transport per unit channel width $q_b = \Phi \sqrt{(s-1)gD^3}$	$[m^2/s]$

Symbols	Description	Unit
$q_{b,i}$	Volumetric bedload transport per unit channel width for a grain class i	$[m^2/s]$
$q_{b,x}$	Volumetric bedload transport per unit channel width x-direction	$[m^2/s]$
$q_{b,y}$	Volumetric bedload transport per unit channel width in y-direction	$[m^2/s]$
q_c	Critical discharge per unit channel width for sediment incipient motion	$[m^2/s]$
Q	Flow discharge	$[m^3/s]$
Q_b	Bedload transport mass discharge	$[kg/s]$
Q_{b^*}	Bedload transport capacity of a channel	$[kg/s]$
$Q_{b_{in}}$	Bedload feeding rate at model's inflow	$[kg/s]$
$Q_{b_{out}}$	Simulated bedload transport rate at model's outflow	$[kg/s]$
Q_{max}	Maximum flow discharge of a channel	$[m^3/s]$
Q_{min}	Minimum flow discharge of a channel	$[m^3/s]$
R	Regime channel R is designated to a channel with no sediment feeding from the upstream (Yalin and da Silva 2001)	[-]
Re	Flow Reynolds number representing the ratio of inertial to viscous forces	[-]
Re^*	Sediment grain Reynolds number given by $\frac{u_* D}{\nu}$	[-]
$R1$	Regime channel $R1$ is designated to a channel with a constant sediment feeding from the upstream (Yalin and da Silva 2001)	[-]
s	Relative density $\frac{\rho_s}{\rho}$	[-]
S	Channel slope or energy gradient	[-]
S_0	Initial channel slope before start of regime channel development	[-]
S_1	Channel slope at intermediate stage of regime development	[-]
S_R	Regime channel slope for R- regime channels	[-]
S_{R1}	Regime channel slope for R1- regime channels	[-]
S_{red}	Reduced energy gradient determined using flow resistance partitioning $S_{red} = S \left(\frac{n_{tot}}{n} \right)^e = S \left(\frac{f_0}{f_{tot}} \right)^e$	[-]
t	time	[sec]

List of Symbols

Symbols	Description	Unit
T_p	Unit time	[sec]
T_R	Time duration for regime channel development	[sec]
T_R	Time duration for regime channel development	[sec]
T_0^\wedge	A point in time during the regime channel development as shown in $F_r; \eta_*$ -plane	[sec]
u	Flow velocity	[m/s]
u_0	Mean reference velocity right at the roughness top $z = k_s$	[m/s]
u_{max}	Maximum flow velocity in a power-law velocity distribution	[m/s]
u_{min}	Minimum stream velocity at regime state	[m/s]
u_x	Velocity component in x-direction in a Cartesian coordinate system	[m/s]
u_y	Velocity component in y-direction in a Cartesian coordinate system	[m/s]
u_z	Effective flow velocity acting on the particle assuming a logarithmic velocity distribution	[m/s]
\bar{u}	Average cross-sectional flow velocity	[m/s]
\bar{u}_0	Initial average stream velocity at channel regime development	[m/s]
\bar{u}_c	Average cross-sectional critical velocity for sediment transport	[m/s]
u_*	Shear velocity $u_* = \sqrt{\frac{\tau}{\rho}}$	[m/s]
u_{*c}	Critical shear velocity for sediment incipient motion	[m/s]
\dot{u}	Instantaneous velocity in the flow direction	[m/s]
\tilde{u}	Time-averaged velocity in the flow direction	[m/s]
\vec{u}	Represents the depth-averaged velocity in the direction of the connected pair of nodes in the simulation mesh	[m/s]
w	Width of a channel	[m]
w_0	Channel width at the beginning of channel regime development	[m]
w_R	Channel regime width for R-regime channels	[m]
$w_{R_{max}}$	Maximum width for R1-regime channels	[m]
$w_{R_{min}}$	Minimum width for R-regime channels	[m]
w_{R1}	Channel regime width for R1-regime channels	[m]

Symbols	Description	Unit
w_{R1max}	Maximum width for R1-regime channels	[m]
w_{R1min}	Minimum width for R1-regime channels	[m]
\tilde{w}	Instantaneous velocity in the vertical direction	[m/s]
\bar{w}	Time-averaged velocity in the vertical direction	[m/s]
W	Weight of a sediment particle	[kg]
W^*	A dimensionless bedload transport rate $W^* = \frac{(s-1)g q_b}{\rho_s(\tau/\rho)^{1.5}}$	[-]
z_b	Initial bed level	[m]
z_o	Height taken from $0.3D_S$ to $0.4D_S$	[m]
z_*	The average level of the bottom of moving grain from zero bed level taken as $z_* = -0.02$	[m]
Greek Symbols		
α	Empirical component or pre-factor in the equation of Meyer-Peter and Müller varies between 2 and 8	[-]
α_A	Sediment hiding/exposure function exponent: $\alpha_A = 0.011 \cdot \tau_{dms}^*{}^{-1.5} - 0.3$ for $\alpha_A \leq 2.3$	[-]
α_b	Angle of bedload transport direction derived from $\tan \alpha_b = \frac{q_{b,y}}{q_{b,x}} \approx \frac{\sin \delta - f(\tau_{dms}^*) \cos^2 \epsilon \frac{\partial Z_b}{\partial y}}{\cos \delta - f(\tau_{dms}^*) \cos^2 \epsilon \frac{\partial Z_b}{\partial x}}$	[-]
α_1	Coefficient describing the volume of sediment grain	[-]
α_2	Coefficient describing the cross-sectional area of sediment grain	[-]
β	Empirical exponent in the equation of Meyer-Peter and Müller (1948) typically takes a value of larger than 1	[-]
β'	Dimensionless coefficient	[-]
γ	Constant that varies between 1.5 and 2 in (Schoklitsch 1962) bedload transport equation $q_b = \mu S^\gamma (q - q_c)$	[-]
δ	Flow direction or shear stress direction angle δ in Hydro_FT-2D is calculated from the tangent of depth-averaged flow velocity components in x and y directions $\tan \delta = \frac{u_y}{u_x}$	[°]
δ_{al}	Thickness of channel surface or exchange layer in Hydro_FT-2D	[m]

Symbols	Description	Unit
δ_{Sec}	Angle of the deviation between nearbed flow direction and main flow direction due to the effect of secondary currents $\tan \delta_{Sec} = \frac{\tau_{Sec}}{\tau_r} \cong \frac{\tau_{Sec}}{\tau_0} = -A_{Sec} \frac{h}{R_{Sec}}$	[°]
δ_{ul}	Thickness of channel subsurface layer in Hydro_FT-2D	[m]
$\delta_{ul,max}$	Maximum thickness of channel subsurface layer in Hydro_FT-2D	[m]
$\delta_{ul,min}$	Minimum thickness of channel subsurface layer in Hydro_FT-2D	[m]
$\delta_{ul,0}$	Initial thickness of channel subsurface layer in Hydro_FT-2D	[m]
ΔL	Characteristic length between the connected pair of nodes and \vec{u} represents the depth-averaged velocity in the direction of the connected pair of nodes in the simulation mesh	[m]
ΔS	Difference between initial and regime channel slope	[-]
ΔS_R	Difference between initial and regime slope for R regime channels	[-]
ΔS_{R1}	Difference between initial and regime slope for R1 regime channels	[-]
Δt	Simulation time-step	[sec]
$\Delta \mu$	Difference in relative flow resistance	[-]
ϵ	Angle between inclined plane and horizontal plane	[°]
ζ	Shear stress fluctuations as the ratio of the critical shear stress for a sediment mixture τ_{cm}^* to the average critical shear stress $\overline{\tau_{cm}^*}$ as $\zeta = \frac{\tau_{cm}^*}{\overline{\tau_{cm}^*}}$	[°]
η_*	Relative flow intensity also known as relative tractive force is referred to the ratio of acting shear stress to critical shear stress $\eta_* = \frac{\tau}{\tau_c} = \frac{gSh}{u_{*c}^2}$	[-]
η_p	Porosity of sediment	[-]
$(\eta_*)_R$	Relative flow intensity also known as relative tractive force is referred to the ratio of acting shear stress to critical shear stress at channel regime state	[-]
$(\eta_*)_0$	Relative flow intensity also known as relative tractive force is referred to the ratio of acting shear stress to critical shear stress at channel initial state	[-]
θ	Any instantaneous flow variable in Double-averaging of Navier-Stokes equation DANS (Nikora et al. 2001)	[-]

Symbols	Description	Unit
$\bar{\theta}$	Time-averaged value of flow variable	[-]
θ'	Fluctuating or instantaneous part of flow variable	[-]
$\bar{\theta}$	Time-averaged value of flow variable	[-]
$\tilde{\theta}$	Spatially fluctuating part of time-averaged flow variable	[-]
$\tilde{\theta}'$	Timely fluctuating part of spatially-averaged flow variables	[-]
$\langle \theta' \rangle$	Spatially averaged value of fluctuating or instantaneous part of flow variable	[-]
$\langle \bar{\theta} \rangle$	Spatially averaged value of time-averaged flow variable $\bar{\theta}$	[-]
Θ	Channel bed longitudinal slope	[-]
λ	Channel step-pool dimension given as $\lambda = L_D/D_B$	[-]
μ	Relative flow resistance defined in terms the ratio of total roughness to grain roughness $\mu = k_{st}/k_{st'}$ in Manning-Strickler values	[-]
μ_c	Ratio of total resistance to grain resistance in Chezy resistance factor	[-]
$(\mu_c)_R$	Ratio between total resistance (total dimensionless Chezy resistance factor) to grain resistance (pure grain friction component at regime state $(\mu_c)_R = c_R/(c_f)_R$)	[-]
ν	Kinematic viscosity of water	$[m^2/s]$
Ξ	Material number calculated $\Xi^3 = \frac{\rho_s g D^3}{\rho v^2}$	[-]
π	The ratio of the circumference of a circle to its diameter ($\cong 3.14$)	[-]
ρ	Water density	$[kg/m^3]$
ρ_s	density of sediments	$[kg/m^3]$
Σ	Refers to curves in the $F_r; \eta_*$ -plane for given value of μ_c , which becomes similar to 3/1-declining straight line for $\eta_* \gg 1$	[-]
τ	Effective boundary shear stress	$[N/m^2]$
τ_c	Critical shear stress required for grain initiation of motion	$[N/m^2]$
τ_d	Drag shear stress due to macro-roughness elements	$[N/m^2]$
τ_g	Total shear stress	$[N/m^2]$
τ_{Sec}	Shear stresses in secondary current directions in Hydro_FT-2D	$[N/m^2]$
τ_α	Shear stress in the direction of bedload transport	$[N/m^2]$

Symbols	Description	Unit
τ_T	Shear stress in the flow current directions in Hydro_FT-2D	$[N/m^2]$
τ^*	Ratio of bed shear stress and grain resisting stress is termed as dimensionless shear stress: $\tau^* = \frac{\tau}{(s-1)\rho g D}$	[-]
τ_c^*	Dimensionless critical shear stress for sediment incipient motion	[-]
τ_{c0}^*	Dimensionless critical shear stress for sediment incipient motion for a flatbed condition	[-]
τ_{ce}^*	Dimensionless critical shear stress for incipient motion of uniform size sediments	[-]
τ_{cm}^*	Dimensionless critical shear stress for sediment incipient motion of s sediment-mixture	[-]
$\overline{\tau_{cm}^*}$	Dimensionless mean critical shear stress	[-]
τ_{dms}^*	Dimensionless effective shear stress relevant to mean grain diameter of surface layer D_{ms}	[-]
τ_m^*	Dimensionless local shear stress of sediment-mixture	[-]
$\overline{\tau_m^*}$	Time-averaged of mean dimensionless shear stress	[-]
τ_r^*	Critical reference shear stress for a dimensionless transport rate of $W^* = 0.002$	[-]
τ_{red}^*	Reduced dimensionless shear stress as a result of flow resistance partitioning	[-]
τ_{50}^*	Dimensionless shear stress for median grain size	[-]
Y	Factor for adjusting the bedload transport in excess discharge approach	[-]
ϕ	Sediment mixture angle of repose calculated by $\phi = \cos^{-1} \left[\frac{D_b/k_s + z_*}{D_b/k_s + 1} \right]$	$[^\circ]$
ϕ_1	Dimensionless factor reflecting the effect of material number Ξ used for estimating the dimensionless flow width ∂_w	[-]
ϕ_2	Dimensionless factor reflecting the effect of friction factors used for estimating the dimensionless flow width ∂_w	[-]
Φ	Dimensionless bedload transport parameter $\Phi = \alpha(\tau^* - \tau_c^*)^\beta$	[-]
$\Phi_{dms,i}$	Dimensionless transport parameters for each sediment fraction: $\sum_{i=1}^n \Phi_{dms,i} = k_F \cdot 8 \cdot (\tau_{dms}^* - \tau_{cm}^*)^{3/2} \cdot \sum_{i=1}^n (F_i \cdot \phi_i^{3/2})$	[-]

Symbols	Description	Unit
$\Phi_{dms,i, weak}$	Dimensionless transport parameters due to bed shear stress fluctuations also known as weak transport: $\Phi_{dms,i, weak} = F_i \cdot \varphi_i^{3/2} \cdot k_F \cdot 8 \cdot \left(1.764410^{-5} \tau_{cm}^* \right)^{3/2} \left[\left(\frac{\tau_{dms}^*}{\tau_{cm}^*} \right)^{8.15} - 0.0287 \right]$	[-]
$\Psi (\Xi)$	A dimensionless parameter reflecting the effect of materil number on the critical shear stress in R1 regime channel	[-]
ψ	Channel bed transverse slope	[-]
ω	Stream power per unit channel width defined as $\omega = \tau \bar{u}$	[Watt/m]
ω_c	Critical stream power per unit channel width for sediment incipient motion given by $\omega_c = \tau_c \bar{u}_c$	[Watt/m]

1. Motivation and objectives

1.1. Motivation

Rivers and streams in arid and semi-arid regions have strong flow, sediment transport and habitat seasonality or intermittency that has made the already overstressed water resources management very complex. The intermittent rivers and streams (IRS) cease to flow and may run dry for some extended period at some reaches or completely along their course. IRS are likely to make at least half of the global fluvial network (Datry et al. 2014; Stanley et al. 1997) and recent estimates show that IRS account for 69% of total stream length (Schneider et al. 2017). Low order streams in mountainous arid, semi-arid regions and even in tempered regions in particular are prone to flow intermittency, thus the contribution of IRS to the total global fluvial network are likely higher than those estimated (Lowe and Likens 2005). While the demand for water in such severe water scarcity regions is increasing, IRS are largely poorly understood. Despite their higher contribution, IRS have received less attention in the past, largely due to the assumed higher socio-economic importance of perennial rivers and streams.

The knowledge gap in particularly in understanding the flow regime and sediment transport has led to mismanagement of IRS such as underestimation of sediment transport to dams built on IRS which leads to premature reservoir sedimentation. The problem of sediment transport estimation is even more complicated in steep IRS due to the varying flow resistance as a result of different flow submergences, grain size distributions (GSD), existing of large bedforms, and macro-roughness elements (MRE) such as immobile boulders and exposed bedrocks. Sediment transport in lowland perennial rivers has been investigated extensively and sufficient knowledge and experience of successful applications exists. The problem arises when the knowledge of lowland perennial rivers and streams are adapted to IRS. To address the sedimentation problem in arid and semiarid regions, knowledge of sediment transport processes in IRS is essential. The sediment transport process is strongly controlled by the flow magnitude, channel slope, GSD and structure of bed sediments, existing of bedforms and MRE.

The flow in IRS occurs as a response to precipitation or snowmelt producing a sharp discharge peak and often lacks base flows compared to a perennial river flow of moderate peak discharge with base flows. The IRS flow regime has important implications on the sediment transport processes. First, IRS undergo a flow decrease downstream as a result of seepage loss due to the strong gradient between surface and groundwater levels, which in turn reduces the sediment transport capacity downstream. Secondly, absence of base flows disrupts the processes of riverbed sediments sorting, which occurs during the low flow periods, thus riverbed in IRS often lacks a layering. The riverbed sorting process and

resultant bed sediment layering are strongly controlled by the flow intermittency, namely the longer the base flows are absent, the weaker the bed sediment sorting is resulted. The lack of riverbed sediment layering provides abundant of sediment availability for the next flow season, which leads to higher rates of sediment transport event at the rising limb of flow discharge. In contrast, in perennial rivers, base flows lead to a complete sorting of riverbed leading to armouring of riverbed during the low flows and as the next season peak discharge arrives, the flow force first has to destroy the armouring layer and then sediment transport starts to increase.

The sediment characteristics driven problem is more significant in steep IRS with presence of MRE. MRE such as immobile cobbles and boulders are abundant in mountainous IRS affecting the sediment transport and riverbed erosion in three distinct ways. First, MRE on the riverbed alters the flow hydrodynamic in their vicinity depending on being submerged or protruding. Secondly, they reduce the total bed surface exposed to erosion. Third, presence of MRE together with diverse GSD of bed sediments leads to the formation of step-pool and cascading bedforms, which in turn imposes an increased resistance to flow. Thus, MRE can immensely influence the sediment transport processes in mountainous IRS. If the effect of MRE on the riverbed is ignored or the MRE are assumed as mobile sediments, the rate of sediment transport can be significantly overestimated. Collectively, coarse GSD, large bedforms, MRE on the riverbed with small relative flow submergence h/D_{84} causes the flow resistance to drastically increase. This increase leads to large portion of flow energy to overcome this resistance and only small portion of total flow energy actually effectively take part in transporting the sediment particles. Therefore, to estimate bedload transport, one requires to know the flow resistance in addition to GSD, flow magnitude and river geometry. In a controlled system like flume experiments, determining the abovementioned parameters are straightforward but in nature, it is far more complex.

Rough turbulent flow in steep IRS with low flow submergence h/D_{84} shows distinct characteristics. Certain bedload transport related flow parameters such as shear stress, flow velocity, Reynolds stress, turbulence intensity, and form-induced stress strongly deviate from the flow with sufficient flow submergence h/D_{84} . Therefore, flow submergence h/D_{84} has a strong control on the flow resistance.

Several methods and approaches have been developed to adjust the near-bed flow characteristics for the effect of increased flow resistance such as Double-Averaging of Navier-Stokes equations (DANS), modified flow resistance approaches, empirical approaches (i.e. estimating flow velocity from unit discharge), flow resistance partitioning and others. Despite the modifications to adjust for the increased flow resistance in low submergence flow conditions, they have their shortcomings. First, they do not include the effect of bed forms (i.e. cascade, step-pool), grain interlocking and roughness elements arrangements due to various friction angles in mountainous rivers. Secondly, the data required to modify for increased flow resistance is seldom available for mountainous IRS and can only be applied for well-controlled laboratory condition. DANS for instance, requires information about roughness geometry of riverbed surface from high-resolution riverbed geometry of

particle size scale for approximating flow variables in the near-bed regions. In flow resistance approaches, often the flow submergence h/D_{84} is modified empirically for different roughness scale values to account for additional flow resistance. Thus, the knowledge of flow submergence is required for approximating the flow resistance. While determining h/D_{84} in a flume condition with known GSD and water depth is straightforward, in nature has high spatial variations because of varying water depth and diverse GSD.

Total flow resistances k_{st} in natural rivers are comprised of grain resistance k'_{st} and an additional resistance due to the bedforms and existing of MRE. Based on the concept of flow resistance partitioning, additional flow resistance may consume a significant of proportion of flow energy otherwise available for bedload transport. Therefore, the energy slope is reduced by multiplying with ratio of total resistance to grain resistance μ to account for the increased flow resistance. Flume and field investigations show that applying flow resistance partitioning approach, a much-improved agreement between observed and calculated bedload transport can be achieved. While k'_{st} can be relatively accurately approximated from GSD of bed surface layer sediments, k_{st} can be back calculated from bedload transport data, which is hardly available even for most of the well-researched perennial rivers.

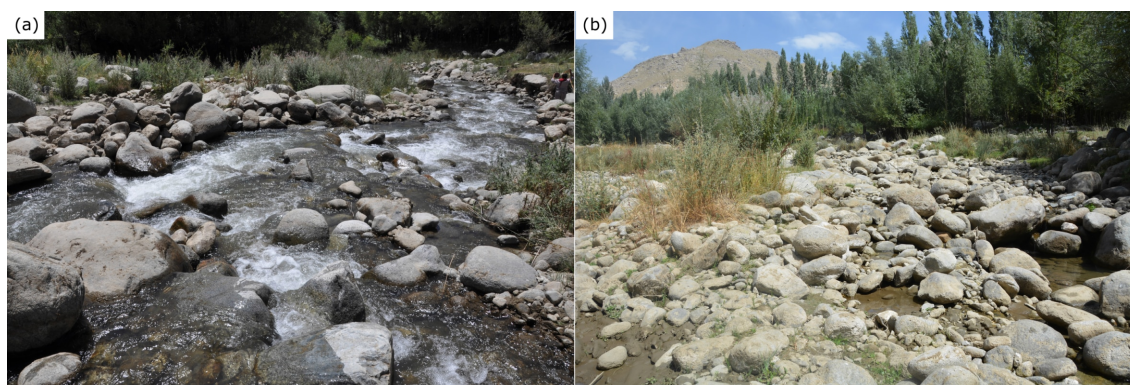


Figure 1.1.: Examples of flow resistance development at two stretches of an IRS with different reach slopes (a) Steep stretch with step-pool bedforms and (b) gentle-slope stretch with cobble-bed

Therefore, in this research, the flow resistance is considered on a macro-scale (i.e. reach scale) with regime dimensions (width and depth), slope and total regime flow resistance. The mountainous natural IRS are assumed to be in regime (equilibrium) condition, thus with known flow discharge Q , bedload transport Q_b , GSD, the rivers and streams alter its slope S , geometry and effective roughness (flow resistance) to minimise its energy-related characteristics A_* (Yalin and da Silva 2001). The A_* has been approached by different authors with different hypothesis such as minimum stream power, minimum unit stream power, maximum transport rate, maximum friction factor, minimum energy dissipation and minimum Froude number. The last hypothesis is derived based on the principles of thermodynamics, which reveals that the A_* regime value is achieved when the average

flow velocity \bar{u} is minimum (Yalin and da Silva 2001). Since a decrement of \bar{u} coincides with that of (F_r) and they achieve their minimum values together, thus the dimensionless counterpart of A_* is considered to be F_r (Yalin and da Silva 2001).

Figure 1.1 a and b shows respectively two reaches of an intermittent river in wet and dry seasons in Kabul River basin, Afghanistan. River reach a has larger regime slope than reach b and as shown, the earlier has developed cascade bedforms, while the latter has a plane bedform. While the bankfull discharge, sediment supply from upstream, GSD of riverbed, reach dimensions remain more or less the same, larger flow resistance in reach a can be merely attached to higher reach slope.

Computer simulations are employed to simulate the regime development of channels with known initial geometry, initial slope, GSD, bedload rate Q_b and bankfull discharge for a given grain resistance k'_{st} and total resistance k_{st} . The long-time hydromorphological simulations results in channel regime dimensions, regime slope and bedforms. The total flow resistance as main steering parameter is varied to determine the relationship between flow resistance and channel slope at the end of regime state.

With the description of the main idea behind this dissertation, the main hypotheses to verify and objectives to achieve are outlined below:

1.2. Research objectives

The two central hypotheses examined in this dissertation are:

1. Based on the bankfull discharge, sediment supply from upstream, GSD of bed sediments, and channel regime slope, the channel reach develops a certain resistance predominantly in form of bedforms to fulfill the increased flow resistance of steep channel regime condition. Are larger bedforms develops with increasing channel regime slope in the regime channel development simulations?
2. Large bedforms like cascades of MRE or MRE themselves on the steep channels can no longer be expressed by roughness values. If the individual MRE or their arrangements in cascades are regarded as specific bed geometrical features in their regime simulations, do they increase the flow resistance in the channel bed?

The objectives of this dissertation are formulated based on the abovementioned hypotheses. The first part is mainly outlining the research objectives set for the relative resistance relationship with channel regime slope as:

- Determining the relationship between flow resistance and regime channel slope by fulfilling channel regime condition for a certain bankfull discharge, bedload supply rate from upstream, initial channel slope and initial bed sediment GSD.
- Determining the effect of GSD of surface, subsurface and sediment supply from upstream and its magnitude on the relationship between flow resistance and regime channel slope to investigate the sensitivity of the channel bed sediment GSD.

- Determining the effect of the initial channel widths such as fixed-width resembling flume condition and extended-width representing natural streams on the relationship between flow resistance and regime channel slope, regime plan-forms and bedforms development. In this investigation, the sensitivity of rigid and erodible boundary conditions on the channel regime development is analysed.
- Analysing the sensitivity of bankfull discharge rates on the channel regime geometry, relationship between flow resistance and regime channel slope, channel regime planforms and channel regime bedforms.
- Investigating the relationship between flow resistance and regime channel slopes on channel systems composed of several reaches of distinct slopes to analyse the effect of boundary conditions developed within the combined reaches resembling a natural river system of several constant slope reaches.
- Examining the transferability of flow resistance and regime channel slopes on two mountainous IRS (i) Maidan and (ii) Shakar-Dara rivers in Kabul River basin

In the second part, the research objectives are predominantly outlining the effect of MRE on the regime channel development using computer simulations.

- Determining the relationship between quasi-randomly distributed MRE concentration on the channel bed and channel regime slope for known flow discharge, GSD of channel bed sediment, sediment supply from upstream, and initial channel slope.
- Determining the relationship between MRE cascade or step-pool dimensions L_D/D_B and channel regime slope when the MRE are artificially arranged in series of rigid cascades on steep IRS, as it occurs in steep natural streams.
- Analysing the effect of the MRE as individual elements and as cascade or step-pool bedforms on the bedload transport and channel bed erosion.

1.3. Thesis structure

This dissertation is structured into seven chapters:

1. Chapter 1 introduces the motivation, the research necessity, the main objectives and the structure of this dissertation.
2. Chapter 2 provides detailed definitions, patterns of drying and rewetting, global distribution, causes of drying of IRS. It further outlines the significant differences between perennial and IRS as well as importance of IRS as sensitive water sources in arid and semi-arid regions on examples from a mountainous region in Afghanistan.
3. Chapter 3 provides detailed information on hydrodynamic and sediment transport processes in steep IRS. It gives state of art knowledge about the forces and processes initiating bedload transport in mountainous rivers to find the answers for their

distinct behaviours. It further outlines the specific sedimentological characteristics of IRS and how their distinct characteristics compared to perennial rivers may influence the bedload transport in IRS.

4. Chapter 4 first gives a description of regime channel concept. It describes the procedure on how the flow resistance can be determined using regime channel approach. Further, it provides information about channels mesh, boundary condition and regime conditions. In the second part, it focuses on how the MRE are implemented in the model as individual trapezoidal shapes as well as their arrangement in cascade or step-pool bedforms. The chapter concludes with outlines of total numbers of simulations and description of Hydro_FT-2D modelling tool.
5. In chapter 5, the results of the regime channel simulations, analysis of the results, comparisons with flume and field data are presented. In the first part, the simulations results such as regime dimensions development, relationship between flow resistance and channel regime slope, channel regime plan-form and bedforms development for different GSD, flow discharge, and channel initial dimensions are thoroughly described. Second part is dedicated to the results of MRE regime simulations. It presents the results of MRE concentration variation with channel regime slope, as well as the effect of MRE on the bedload transport. The last part deals with the results of MRE artificial arrangement in cascades or step-pool bedforms. It shows the step-pool dimensions change with channel regime slope and the effect of MRE cascades on the bedload transport.
6. In chapter 6, two case studies of IRS, namely Maidan and Shakar-Dara rivers are studied and discussed. The relationship between flow resistance and channel regime slope acquired from regime simulations of artificial channels are implemented on two natural intermittent rivers. Moreover, the difference in flow resistance and channel regime slope relationship for these two case studies are discussed with respect to the site specific controlling parameters to determine the sensitive site-related parameters.
7. Chapter 7 concludes the dissertation with summary of the results, a detailed discussions of results and formulates new research questions for future investigations.

The appendices contain figures providing additional information referred to them in the text.

2. Introduction

2.1. Definitions of intermittent rivers and streams

Rivers and streams with the high seasonality of flow, sediment transport, and habitat are defined by different terms such as temporary, intermittent, ephemeral, episodic and dryland rivers and streams. These terms are often used interchangeably to define natural water bodies that are exposed to recurrent dry phases of varying durations. Temporary rivers and streams are often also called as intermittent and are defined as rivers that dry up partially or fully at their entire or at parts of their course at some period of time (Steward et al. 2012). Arthington et al. (2014) define temporary or intermittent rivers as those with temporal loss of flow and hydrological continuity, which results in high variability in the availability of water and habitat on a more or less predictable basis and ephemeral rivers as those with short hydrological continuity that flow and maintain water on a largely unpredictable basis.

In literature, often one distinction is made based on the predictability of flow occurrence. Ephemeral and episodic water bodies are those, which flow as a result of unpredictable rainfall in their catchment. The flow is often flash floods of short periods (Day 1990; Stringer and Perkins 2001; Williams 2005). The terms temporary, intermittent and seasonal are often referred to relatively regular flow and drying occurrence in rivers and streams (Matthews 1988; Williams 2005; Boulton et al. 2014). A second distinction is made based on the dimensions of the water body with flow seasonality. The water bodies with seasonality are mostly rivers and streams. Rivers are considered to be larger and deeper compared to streams. The similar understanding is also given to flow patterns, as ephemeral is assigned to streams with short flow duration and lower predictability of flow occurrence and intermittent is given to rivers with longer flow duration and higher predictability of flow (Jaeger et al. 2017).

2.1.1. Definition in terms of surface water and groundwater interaction

Another approach in defining the seasonal water bodies is based on the surface water and groundwater interactions (e.g. McDonough et al. 2011). Ephemeral rivers and streams are always located above groundwater table and are feeding the groundwater through seepage loss, whereas intermittent rivers or streams are only feeding the groundwater at low groundwater table and are gaining water from groundwater during high groundwater table. On the other hand, the perennial rivers and streams are always acting as gaining water bodies from the groundwater except during high water periods when they may feed groundwater.

McDonough et al. (2011) classified temporary rivers as either intermittent or ephemeral and defined intermittent river as those that flow seasonally in response to snowmelt and, or elevated groundwater tables resulting from increased periods of precipitation and, or decreased evapotranspiration. Ephemeral rivers are those that flow only during and in immediate response to precipitation events. Figure 2.1 illustrates the definitions of perennial, intermittent and ephemeral rivers in terms of surface water and groundwater interactions.

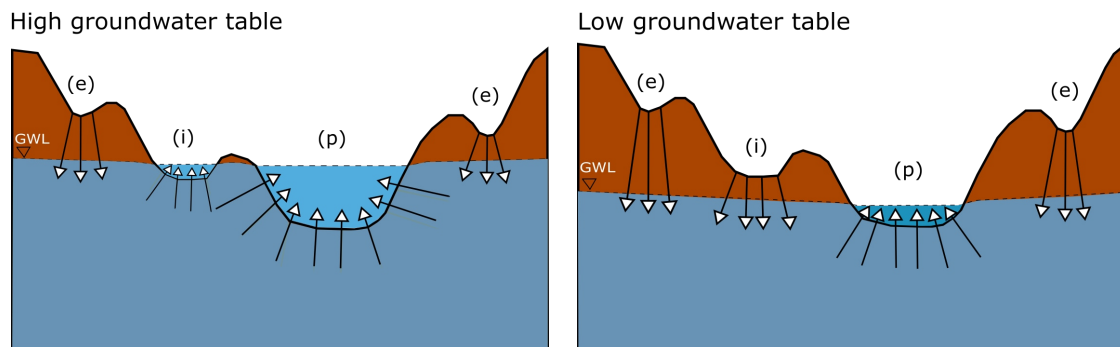


Figure 2.1.: Definitions of perennial (p), intermittent (i) and ephemeral (e) rivers and streams in terms of surface water groundwater interactions

In this dissertation, the term intermittent rivers and streams (IRS) is adapted to define rivers and streams with flow seasonality, because regardless of their sizes (i.e. width, depth) and locations, both rivers and streams may experience long or short dry periods or flow intermittency.

2.1.2. Definitions in terms of occurrence of zero flows (flow intermittency)

Traditionally hydrographs have been extensively used to determine the flow regime of rivers and streams based on the hydrological matrices such as number of zero flow days, zero flow periods, average duration of zero flow periods, percent flow permanence in a year and percent flow permanence by season (e.g. Snelder et al. 2013; Costigan et al. 2015). Snelder et al. (2013) used the hydrological data (daily flow data) from 628 gauging stations to classify the flow regime of rivers in France. Based on the frequency of zero flow periods and total number of zero flow days, the rivers are classified as single-perennial (no zero flows), rarely intermittent (infrequent brief zero flow periods), intermittent (infrequent long zero flow periods) and highly ephemeral (frequent long zero flow periods). Similarly, Reynolds et al. (2015) used historic discharge data for the determination of flow regimes for rivers and streams in the upper Colorado River basin. The mean annual zero flow days and the percent of months with zero flows for the entire month are used to classify the rivers as strongly intermittent (more than 5% of months during the period of record had zero flows and more than 20 annual zero flow days), weakly intermittent (between 0%-5% of months during the period of record and 1-19 annual zero flow days) and perennial (0%

of months during the period of record and no annual zero flow days). The international research project “International River Biodiversity Analysis and Synthesis” classifies rivers and streams with at least five zero flow days per year as intermittent.

2.1.3. Tools other than flow records for defining IRS

The use of hydrological matrices alone for defining IRS is challenging because many of them are ungauged, unmapped and inaccurately shown on the topographical maps (e.g. Hansen 2001). The challenge is even larger for the intermittent headwater streams, which are often ungauged and underrepresented by traditional mapping techniques (Meyer and Wallace 2001). Therefore, several techniques such as wet/dry mapping, use of imagery, field loggers and flow surrogates and modelling are additionally used to classify the flow regimes of headwater rivers and streams. Temporal changes in the distribution of surface flow in IRS can be tracked by on-ground mapping (e.g. Stanley et al. 1997). The on-ground mapping demands considerable time in the field, in particular when large areas are to be frequently visited. Therefore, the citizen science initiatives (e.g. Crowdwater) may help collect hydrological information of rivers and streams in areas where no other mapping tools are available.

Remote sensing techniques is another tool used to determine the status of the rivers (wet, dry, or isolated pool) and proxies for surface flow from river dimensions (e.g. river height or width) to estimate the flow regimes (e.g. Mett 2016). The limitation in using remote sensing techniques is the presence of vegetation and lack of fine resolution imagery, in particular for headwater streams. However, for large rivers, the data acquired by remote sensing can be effective for detecting flow proxies (Benstead and Leigh 2012).

Data loggers and flow surrogates can be deployed to the stations where gauges are absent. They can measure flow surrogates such as electrical conductivity (e.g. Gungle 2007; Chapin et al. 2014), water temperature (e.g. Constantz et al. 2001) and water level (e.g. Costelloe et al. 2005; Vorste et al. 2016).

Modelling has also been used as a tool for completing the information gap in understanding the flow regimes for IRS. The hydrologic matrices such as zero flow days can be calculated for flow gauges with limited data. The traditional rainfall-runoff models need to be modified to simulate the zero flows by incorporating the effects of surface and groundwater interactions or special geological formations, such as karstic zones, into the model. Ivkovic et al. (2014) developed a modified version of the IHACRES (Identification of Hydrographs And Components from Rainfall, Evaporation, and Streamflow) and successfully applied it for modelling the flow regime in an ephemeral system in New South Wales, Australia. The Soil Water Assessment Tool (SWAT) accounts for hydrological components such as precipitation, evapotranspiration, surface runoff, infiltration, lateral flow, and percolation (Gassman et al. 2007). The SWAT model is successfully used to simulate the flow regimes in IRS under existing natural conditions (e.g. Chahinian et al. 2011) as well as by implementing future scenarios (e.g. Jaeger et al. 2014). Sando and Blasch (2015) used a statistical model considering snowpack persistence coupled with climatic, geological and environmental data to predict alpine headwater streams flow in-

termittency. Flow regime assessment using models is restricted by the amount and quality of input data and the adequate understanding of the processes. Thus, a combination of the approaches and methods should be employed for understanding the flow regime of IRS. Gallart et al. (2017) have developed a software tool (TREHS) accepting inputs from any rainfall-runoff model and is compared with data from gauging records, information by citizen scientists, and remote sensing to determine the regime classifications of IRS.

2.2. Worldwide distribution and contribution of IRS

IRS are most abundant in arid and semi-arid regions. They are also found throughout the globe between 84 degrees north and 84 degrees south latitude (Tooth and Nanson 2000; Larned et al. 2010). The presence of IRS is not limited to arid and semi-arid regions rather they are also found in temperate and humid areas, where they are particularly draining headwater streams (Datry et al. 2014). IRS, in particular, drain the dryland regions of the world. According to the Millennium Ecosystem Assessment (2005) (figure 2.2), drylands contribute approximately 41.3% to the global terrestrial area, which inhibits about 35.5% of the total global population.

Based on a statistical analysis considering temperature and precipitation by Raymond et al. (2013), intermittent and ephemeral rivers roughly contribute to more than 30% of total length of the global river network of streams of order 5. In Australia, roughly over 70% of the 3.5 million kilometres of river channels are considered intermittent (Sheldon et al. 2010), and more than half of the total length of rivers in the United States, Greece, and South Africa are intermittent (Larned et al. 2010). In France, 25% to 40% of the total rivers segments are found to be intermittent (Snelder et al. 2013). The estimates of the intermittent river network often do not include low-order streams (i.e. headwater streams) because they are difficult to detect by traditional mapping techniques, including airborne photography and satellite imagery (Benstead and Leigh 2012). Low-order streams may contribute to more than 70% of river networks and are especially prone to flow intermittency (Lowe et al. 2005; Fritz et al. 2013; Robinson et al. 2016). Therefore, the proportion of IRS in the global river network is likely greater than 50% (Datry et al. 2014).

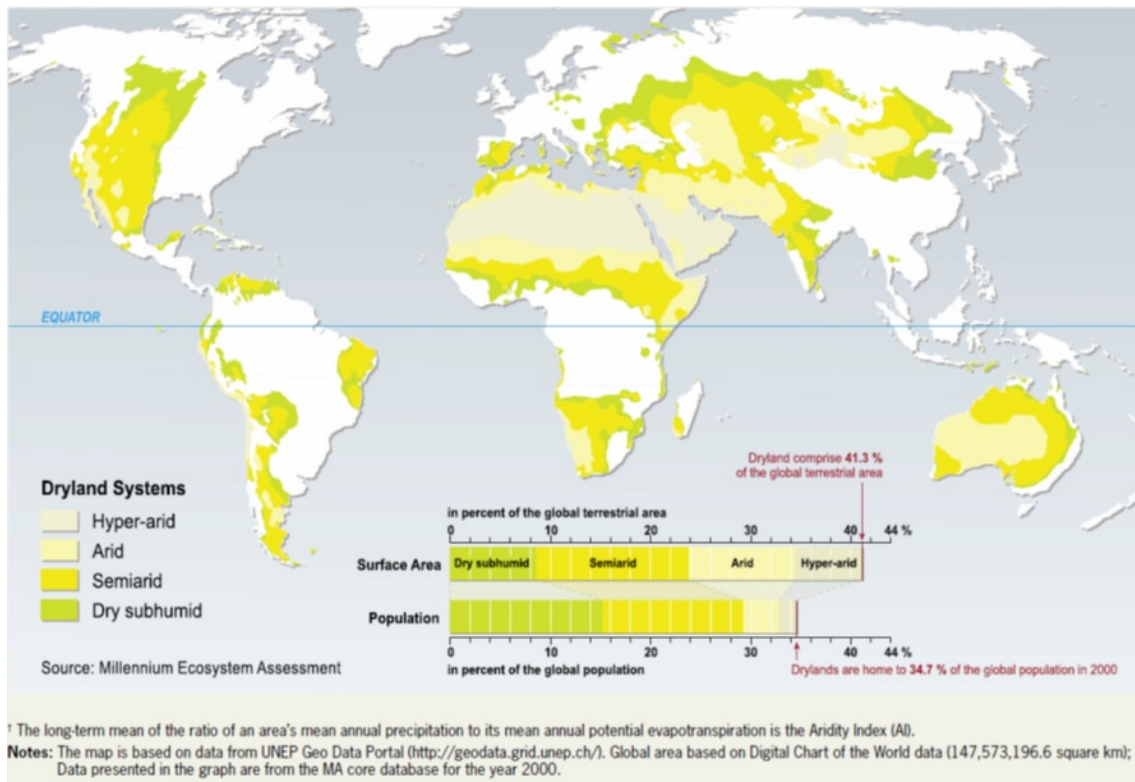


Figure 2.2.: Locations of world's dryland regions and their categories
Source: Millennium Ecosystem Assessment (2005)

2.3. Drying and rewetting patterns in IRS

Flow in IRS either ceases (stops) to flow or dries up in parts or completely. The flow cessation occurs when the surface flow along the channel stops flowing and forms isolated pools while the riffle parts of the river dry up (e.g. Datry et al. 2017). A longer dry period may lead to complete loss of surface water even from patches of isolated pools to either groundwater or evapotranspiration. The isolated pools may be internally connected through subsurface (hyporheic) flow, depending on the permeability of the riverbed and gradient between the isolated pools. Two examples of riffle drying from Dori and Harirud rivers in Afghanistan are shown in figure 2.3 a and b respectively. The riverbed drying is used to refer the disappearance of surface water due to the infiltration (e.g. infiltration into a karstic formation), evapotranspiration, water abstraction (e.g. dams, weirs) and, or due to the combined effect of all mentioned factors. Drying and rewetting often occur consecutively in some IRS, however, there may be temporary intermediate stages, where water is present in pools and then dry for some time (i.e. weeks to months) before a continued streamflow season begins (e.g. Boulton and Lake 1990; Bhamjee et al. 2016). According to Boulton et al. (2017), most common sequences of drying and rewetting are identified as (i) surface water ceases to flow without channel drying (ii) channel drying

followed by rewetting and immediate flow resumption (e.g. Farahrud River in figure 2.3 d, e) and (iii) channel drying and rewetting with several intermediate temporary false starts before a continuous surface flow resumption. Most IRS undergo a prolonged and gradual drying (Lake 2003), in contrast, rewetting is usually faster, in particular when flow resumption is due to the surface flow (Boulton et al. 2017). Drying typically occurs in both upstream and downstream directions depending on the regional geomorphology (Larned et al. 2011) and the gradient between groundwater and surface water in the channel (Shaw 2016). An example of the upstream drying extending to downstream is given in figure 2.3 c, which shows dry upstream (right side) and wet downstream (left side) of a braided river reach in Afghanistan. Downstream drying pattern that extends to upstream occur as a result of water abstraction upstream or seepage loss. IRS are generally subject to a flow volume decrease further downstream due to seepage loss or groundwater recharge (Tooth 2000; Shanafield and Cook 2014). In comparison, rewetting extends often from upstream to downstream direction either as a result of surface runoff (e.g. Fisher et al. 1982; Jacobson et al. 2000) or inputs from a surplus of springs and seeps (e.g. Shaw 2016) out of unconfined aquifers into the channel. The spatial extent of drying and rewetting varies from a basin-scale down to the reach-scale (Stanley et al. 1997; Costigan et al. 2016). At the channel reach-scale, drying and rewetting of runs, riffles, and pools are recognisable (Stanley et al. 1997) and are largely governed by channel topography, because of depressions (e.g. pools in a riffle-pool channel fill earlier and sustain water longer than surrounding areas) (Woodward et al. 2015). At the river section-scale, the drying pattern depends on how the section is constrained, namely the flow persists longer in constrained sections (i.e. narrow canyons) compared to unconstrained channel sections with a lower gradient (Stanley et al. 1997). At the tributary and river section-scale, local precipitation causes flow resumption in a channel while the neighbouring channels may still stay dry (Datry et al. 2014). At the basin-scale, water loss from tributaries is largely causing overall size changes, which may lead to fragmentation and isolation of sub-basins from the mainstem (Stanley et al. 1997).

In general, drying and rewetting of IRS occur as a result of changes in spatial and temporal water budget. Surface water flow is largely a function of water inputs (i.e. precipitation, groundwater) and outputs (e.g. seepage loss, evapotranspiration) at various scales (Gordon 2004; Godsey and Kirchner 2014). At all spatial extents, channel drying is caused when the surface water loss exceeds the gains whereas the flow is resumed when the water gains exceeds the water losses.

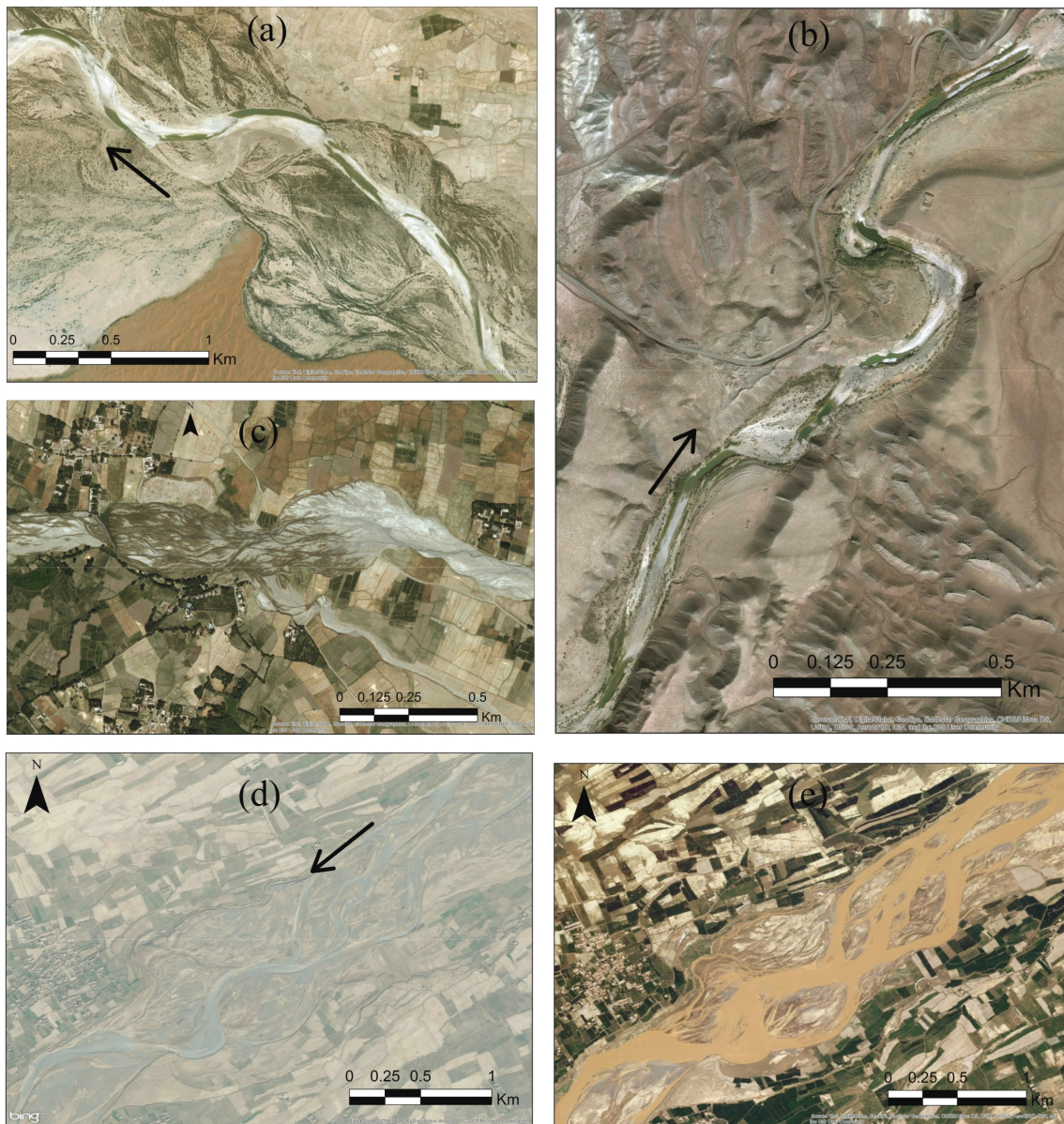


Figure 2.3.: Drying pattern of isolated pools at (a) Dori (b) Harirud rivers (c) upstream drying extending downstream in Nahreen River and Farahrud River during (d) dry period and (e) resumption of flow

source: Esri, DigitalGlobe, GeoEye, Earthstar Geographics, CNES/Airbus DS, USDA, USGS, AeroGRID,IGN, and the GIS User Community 2017 DigitalGlobe, CNES 2017 Distribution Airbus DS, 2017 Microsoft Corporation

2.4. Causes of flow intermittency

In general, the main drivers of the flow intermittency can be natural and non-natural. Under natural conditions, some causes of flow intermittency are mainly related to climate, source of water, and the water body characteristics (e.g. river width, bed material permeability). The climatic drivers are precipitation, temperature, evaporation, and evapotranspiration. For example, in arid and semi-arid regions, flow intermittency is mainly caused by low precipitation rates and high rates of evaporation and evapotranspiration through plants. In contrast, in alpine and arctic regions, freezing at the surface and shallow subsurface due to low temperature causes flow intermittency (Robinson et al. 2016). Water sources can also cause flow intermittency in rivers and streams. For example, in perched and semi-perched alluvial rivers, transmission losses, depletion of bank storage and floodplain aquifer leads to drying of rivers (e.g. Shanafield and Cook 2014).

In addition to climatic and water source drivers, physical characteristics of channels, shallow alluvium, and catchment area control the flow intermittency in many intermittent water bodies (Jaeger et al. 2017). Channel characteristics such as riverbed permeability due to the presence of coarse riverbed sediments (e.g. in gravel-bed rivers) and water table well below the main river channel facilitates the infiltration of surface water into the streambed and hence leads to higher transmission losses and finally to flow intermittency in the river (Sophocleous 2002).

In addition to naturally occurring IRS, human activities such as alteration of land use, flow regulation, surface and groundwater extraction, reduced precipitation, and increased evaporation due to climate change may cause a flow cessation (Gleick 2003; Palmer et al. 2008; Steward et al. 2012). Water abstraction and impoundment have caused many formerly perennial rivers to become intermittent in the last 50 years, including large rivers, such as the Nile, Indus, Yellow, Amu and Syr Darya, Rio Grande, and Colorado (Gleick 2003). Most of the once-perennial rivers of arid and semiarid regions are now intermittent (Gleick 2003). In the near future, the number of IRS will increase in regions where severe climatic drying or water evapotranspiration occurs (Larned et al. 2010; Döll and Schmied 2012).

2.5. Importance and challenges of IRS management

2.5.1. Increasing demand and decreasing water availability

The rapid increase in human demands for freshwater and the changing climate are altering the flow regimes of rivers and streams worldwide (Jaeger et al. 2017). IRS are the main water source for drinking water, irrigation and groundwater recharge in arid and semi-arid regions. They are closely coupled with aquatic-terrestrial systems that are spatio-temporally highly variable due to flow intermittency (Datry et al. 2014). As the population grows, the demand for drinking water and water for food production increases, which in turn imposes an additional stress on IRS. Döll and Schmied (2012) concluded that an ongoing global increase in the occurrence and spatial and temporal

extent of IRS is likely to continue to shift flow regimes from perennial to intermittent by 2050. This trend demands a research focus to fill the knowledge gap traditionally caused by unidirectional research focus on perennial rivers.

Furthermore, with the increase in population, stress on water resources will also increase, especially in areas where water availability has a high seasonality. According to FAO-Aquastat (2016), the data from 1988 to 2011 show a decrease in the available water resources per capita, in particular, for the inhabitants of arid and semi-arid regions. Population growth and climate change are considered the main causes for the increasing stress on freshwater resources. Population growth essentially contributes to a constant decrease of the available water in terms of the increased domestic and irrigation water demand for food production (Vörösmarty et al. 2000). The annual global population growth rate between 2010-2015, for instance, was estimated to be around 1.18% (UNDESA Population Division 2015). Agriculture is by far the largest consumer of freshwater worldwide, making around 70% of total annual freshwater withdrawal (FAO-Aquastat 2016).

2.5.2. Challenges in water storage and sediment management

Sediment transport in IRS is not yet well studied mainly due to the presumed higher socio-economic importance of perennial rivers. Recent investigations reveal much higher sediment transport capacities in IRS under the same flow condition (Almedeij and Diplas 2005). Very high sediment transport rates are recorded in IRS as a result of high-intensity flash floods and unarmoured riverbeds (e.g. Laronne and Reid 1993; Su et al. 2013). Unlike perennial rivers, the riverbeds of IRS are commonly unarmoured, because of the absence of varying flow discharge throughout the year or short period of flow discharges (Laronne and Shlomi 2007). Armouring is the coarsening of the surface layer as a result of the selective transport of finer grain sediments fraction during longer low or medium flow conditions (e.g. Little and Mayer 1972). Armoured riverbeds can better resist against erosion during the rising limb of the flood as the coarse sediments layer protects the finer material underneath and therefore reduces the overall sediment transport. In contrast, in an unarmoured riverbed, all grain sizes of the sediment are exposed to erosion and therefore, the sediment entrainments and transport rate is considerable even at low flows. Flash flood events of short periods transport a wide range of grain sizes and then deposit without a pronounced armouring layer (Laronne et al. 2002).

An abundant sediment supply from the catchment area due to the lack of vegetation cover especially in the arid and semi-arid regions leads to high suspended sediment transport (e.g. Verstraeten et al. 2006; Schumm 1968). This abundance of sediment supply in dry regions affects the flow characteristics, morphology and bedforms (e.g. Storz-Peretz and Laronne 2018) evolution, which behaves differently than in humid regions.

One main negative impact of the high sediment transport rates is the premature sedimentation of reservoirs and irrigation canals in arid and semi-arid regions, which reduces the storage capacity of the reservoirs and may hinder saving sufficient water for high demand summer seasons. One example of such extreme sedimentation is a 10 m high Hesarak

dam built on an intermittent river draining a catchment area of 120 km² in Nangarhar, Afghanistan, which is filled by sediments within one and a half year (Hazelton et al. 2009; Oosterkamp 2009).

This entire knowledge gap in sediment transport in IRS is requiring more researchers' focus to find solutions and engineering practices for water and sediment management. There exists some new research works on intermittent water bodies, e.g. Science and Management of Intermittent Rivers and Ephemeral Streams (SMIRES), Intermittent River biodiversity Analysis and Synthesis (IRBAS) in Europe with focus mainly on ecology and hydrology, in American south west (e.g. Reid and Frostick 2011; Graf 1988) and in central Australia (e.g. Tooth and Nanson 1999; Tooth and Nanson 1999) focused on large scale geomorphology. However, only few studies have a focus on sediment transport regime characteristics (e.g. Hassan 2005; Laronne and Reid 1993). Therefore, up to date, our knowledge of sediment transport mechanism, processes and governing parameters in IRS are far from complete and requires more research.

2.5.3. Water right issues and water conflicts

Transboundary waters are making up 60% of the global freshwater resources and inhibit 40% of the world population (Wolf 1998). The variability of river flow in arid and semi-arid areas are, in particular, causes of competitions and conflicts for the constantly decreasing water resources. As a consequence, the downstream riparian states may receive poor quality and a limited quantity of water that can lead to conflict among riparian states (Klaphake and Scheumann 2001). There have been seldom cases where international laws could have regulated a fair share of transboundary waters, in order to avoid conflicts (Wolf 1999).

Climate change, in particular global warming, may cause large-scale changes in precipitation patterns, evapotranspiration, and reduction of glaciers and snow cover (IPCC 2013 a), which in turn can cause flow intermittency in rivers and streams. This will cause conflicts among countries sharing transboundary waters, because the river water may disappear before reaching downstream regions (e.g. Milly et al. 2008; Dinar et al. 2015).

Another challenge for intermittent rivers and streams' management is the lack of data required for planning, designing, and implementing management strategies. Most of the IRS are ungauged and the information about flow discharge is hardly available. While flow data is crucial for any negotiations on transboundary waters, and their management, lack of data may also hinder a fruitful dialogue on sharing the water (e.g. King and Sturtewagen 2010; Thomas and Warner 2015). To overcome these challenges, adaptive strategies should be developed and implemented to address the growing demand, the spatial and temporal variability of flow in rivers and streams, and high sediment transport rates.

2.5.4. Climate change and increase in flow variability

Climate change is considered an important factor causing flow variability in rivers and streams. The global averaged combined land and ocean surface temperature data from 1880 to 2012 show an increase of 0.85 °C (IPCC 2013 a). The observed surface temperature changes in some regions reach up to 2.5 °C (IPCC 2013 a). Precipitation data from 1951-2010 show large-scale pattern changes in precipitations caused by climate change, in particular, a decrease in accumulated precipitations in the largest areas of the world and the occurrence of droughts (IPCC 2013 b). Combined changes in temperature, precipitation and soil moisture known as Palmer Drought Severity Index (PDSI) shows that the dry areas are becoming drier (Dai et al. 2004). According to Dai et al. (2009), changes in continental freshwater discharges of world's largest ocean-reaching rivers between 1948-2004 show a downward trend outnumbering upward trends.

Long-time observations show that both glacier and snow cover extent have shrunk as a result of global warming (IPCC 2013), for instance, satellite records over a period from 1967-2012 indicate an annual mean snow cover extent decrease of 53% for months of June.

2.6. Hydro-morphological characteristics of IRS

2.6.1. Geomorphological characteristics and sediment transport regimes

Some fundamental geomorphological characteristics of intermittent river systems can be well described with respect to their locations in the catchment area and elevation (Schumm 1977). Schumm (1977) divided the river network into three main sediment regime zones namely upland (production), piedmont (transfer) and the floodout (deposition) zones as shown in figure 2.4 a. In the production zone, sediment is eroded from hillslopes (in form of sheet, rill, and inter-rill erosions) and is transported to the channel. The transfer zone is considered to be in a morphological equilibrium condition (supply equals output) and transports the received sediments from the production zone to the deposition zone. The deposition zone is the sink area for most of the sediments from the production zone. This concept originally developed for perennial river systems is extended by Tooth and Nanson (2011) to rivers in dryland regions. Their conceptual model consists of four zones namely upland, piedmont, lowland, and floodout. This generalisation of the river system aims at facilitating the description of intermittent river systems. However, the characteristics (climatic, tectonic, and physiographic) of the four zones, as well as their spatial extent, may vary widely from one region to another (Jaeger et al. 2017). In nature, the geomorphology of IRS is diverse and may not be captured with the four zone generalisation, but it can provide a logical and physically meaningful framework for understanding the geomorphology and sediment regimes within each zone with respect to the valley characteristics and ecological conditions.

2.6.2. Upland zone

Upland zone is characterised by steep slopes, exposed bedrock in the bed and banks, and a rather small thickness of alluvium as shown in figure 2.4 c (Sutfin et al. 2014). The sediment is supplied from the hillslopes and lateral inputs are a result of delivery by overland flow as well as mass failures (landslide, debris flow)(Wohl and Pearthree 1991; van Steijn 1996). Riverbed is composed of poorly sorted coarse sediments containing large gravel and boulders. The sediments in the upland zone may have edgy shapes (low roundness)(Demir 2003). Single thread channels with low width to depth ratios are directly coupled with hillslope. Restricted or no floodplains are characteristics of upland channels. The upland zone experiences flash-floods as a result of high-intensity convective rainfall and short overland flow distances, which can transport a large amount of sediment (Métivier et al. 2004; Su et al. 2013). At steep slopes of the upland zone, selective transport processes and the availability of large immobile boulders may lead to step-pool or cascade morphologies (Powell 1988; Grant et al. 1990; Wohl and Pearthree 1991; Powell et al. 2012). At gentler slopes and high sediment supply (e.g. from landslides) channels may develop a planer bedform with low relief channel bars (Powell et al. 2012).

The upland zone may contain the majority of IRS, because it is the home for headwater streams, where most of IRS worldwide can be found (e.g. Naiman et al. 2005).

2.6.3. Piedmont zone

In this zone, the floodplains are wider, channel beds are running in thicker alluvium layers compared to the upland zone, as shown in figure 2.4 d. Sediment supply from hillslopes remains closely coupled with the channel of moderate to steep slopes by episodic lateral movements of sediments as a result of diffusive processes and mass failures (Jaeger et al. 2017). The second source for sediment is the supply of flash floods from the tributaries. In piedmont zone, sediment supply from hillslopes and tributaries are reworked and then distributed further downstream to the lowland zone, leading to smoothed river topography (Michaelides and Martin 2012; Singer and Michaelides 2014). This zone acts as an intermediate section between the upland zone (net erosion) and lowland zone (transfer), where sediment erosion, deposition, and transport occurs at various spatial and temporal scales (Jaeger et al. 2017). The sediments are composed of a wide range of sizes up to large boulders. The channels in this zone have a variety of forms ranging from a single thread, braided to narrow and anabranching shapes (Graf 1981; Tooth and Nanson 1999; Tooth 2000; Singer and Michaelides 2014).

2.6.4. Lowland zone

The rivers in this zone flow in wider fluvial valleys, thus hillslope and channel are less closely coupled by larger floodplains compared to piedmont and upland zones as shown in figure 2.4 e (Jaeger et al. 2017). In the lowland zone, an approximately balanced condition between the sediment input and output rates may exist. Unlike

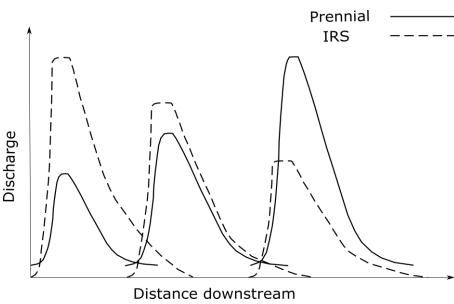
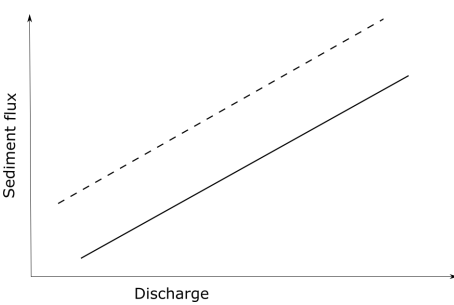
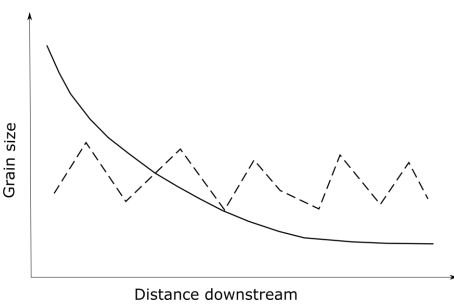
upland and piedmont zones, in lowland zone, the transmission losses into the much larger unconsolidated alluvium is causing a downstream decrease in flow volume (Lange 2005; Tooth 2013; Shanafield and Cook 2014). In addition, overbank flow to floodplains as well as evapotranspiration adds to the downstream flow volume decrease during flooding (Tooth 2013; Jaeger et al. 2017). The channel bed in the lowland zone is consisting of a variable composition of alluvium from gravel, sand to silt, and clay (Knight and Nanson 1997; Reid and Frostick 2011; Sadid et al. 2017). There is a wide variety of river morphologies found in this zone from, low sinuosity, wide and shallow channels to braiding, anabranching and anastomosing forms (Leopold et al. 1966; Tooth and Nanson 1999; Tooth 2000; Eaton et al. 2010). The riverbed and bars in this zone tend to be not well developed and may hardly maintain their form over a longer period (decades to centuries) (Hassan 2005).

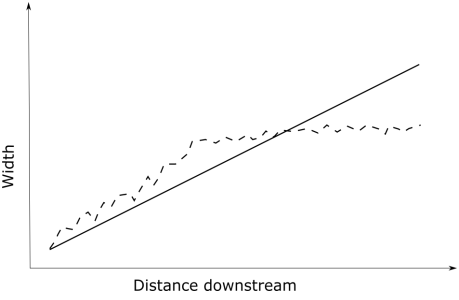
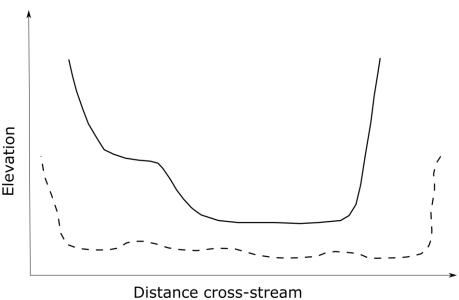
2.6.5. Floodout zone

The IRS often do not reach a coastline, rather ending in inland topographic basins or alluvial plains (Mabbutt 1977; Gore et al. 2000; Billi 2007) or they may form pans and playas (e.g. Shaw and Bryant 2011). The floodout zone is characterised by a net sediment deposition regime leading to a wide variety of geomorphological features (Jaeger et al. 2017). The sediment composition and flow in the floodout zone are largely dependent on the distance to the flow and the sediment production zones (upland and piedmont) (Jaeger et al. 2017) and on the flow and sediment characteristics in the production zone. The floodout zone can be located few kilometres downstream of IRS and the riverbed may contain coarse sediments like cobbles and even boulders (e.g. Billi 2007). It can also be further many tens or even hundreds of kilometres downstream of the upland zones, where the flow events may be very infrequent due to infiltration loss and bed sediments are typically fine (Mabbutt 1977; Tooth 2000; Jaeger et al. 2017). In floodout zones, a downstream decrease in flow magnitude and frequency can occur in association with a downstream decrease in gradient caused by an alteration in the lateral confinement as well as riverbed sedimentation (Tooth 1999 a). The decrease in flow discharge, and or gradient leads to a reduction in unit stream power and sediment transport capacity, which in turn leads to a downstream reduction in channel size, increasing floodwater overflow onto the floodplains and sediment deposition (Jaeger et al. 2017). The morphology of floodout zone can vary widely with respect to the riverbed substrate. The cross-section morphology can be wide and shallow when the riverbed substrate is gravel and sand and can be narrow and deep in muddy channel substrate (Mabbutt 1977; Tooth 1999 a). Compared to the lowland zone, the floodwater infiltration in floodout zone contributes to the groundwater recharge (Morin et al. 2009).

The main longitudinal trend characteristics of IRS compared to perennial rivers in all four geomorphologic zones are summarised in table 2.1.

Table 2.1.: Main distinctions in IRS longitudinal trends. Modified after Jaeger et al. (2017)

<p>Discharge: IRS undergo a flow decrease downstream as a result of seepage loss due to the strong gradient between surface water level and the groundwater table. In perennial rivers, discharge peak downstream increases because more downstream locations receive flow from the larger catchment. The transmission loss depends on the permeability of bed and bank materials. The flow volume decrease also reduces the forces for sediment transport (e.g. Reid and Frostick 2011).</p>	 <p>The graph shows discharge on the y-axis and distance downstream on the x-axis. Two lines represent Perennial (solid) and IRS (dashed) rivers. The Perennial line shows a single peak that increases in magnitude and shifts downstream as distance increases. The IRS line shows multiple peaks that decrease in magnitude and shift downstream as distance increases, indicating flow loss over time.</p>
<p>Sediment flux: Observations show high rates of bedload and suspended load transport in IRS. Abundant sediment availability, the absence of vegetation and armouring facilitates high sediment transport compared to perennial rivers. Field measurements tend to confirm high rates of bedload and suspended load transport in IRS (e.g. Su et al. 2013; Gellis et al. 2004; Laronne and Reid 1993).</p>	 <p>The graph shows sediment flux on the y-axis and discharge on the x-axis. Two lines represent Perennial (solid) and IRS (dashed) rivers. Both lines show a positive linear relationship between discharge and sediment flux. The IRS line is consistently higher than the Perennial line, indicating higher sediment transport rates for the same discharge.</p>
<p>Grain size: IRS are characterised by fluctuating reaches of coarse and fine sediments and no clear tendency of downstream decrease in grain sizes as in perennial rivers. Sediment supply from hillslopes and absence of base flows during infrequent flash floods for riverbed processing affects longitudinal patterns of the sediment grain size to downstream (e.g. Michaelides and Singer 2014; Frostick and Reid 1980; Thornes 1977).</p>	 <p>The graph shows grain size on the y-axis and distance downstream on the x-axis. Two lines represent Perennial (solid) and IRS (dashed) rivers. The Perennial line shows a smooth, continuous decrease in grain size as distance downstream increases. The IRS line shows a fluctuating pattern of grain size that does not show a clear overall decrease, indicating more variable sediment transport.</p>

<p>Channel width: In perennial rivers, channels often widen downstream while it is shown to be asymptotic to a value of 100 m- 200 m for drainage areas from 100 to 1000 km² in IRS (e.g. Wolman and Gerson 1978). This is partly due to the geomorphological effectiveness of rare extreme events. Secondly, effective sizes of storms are not larger than 10 to 100 km² and simultaneous runoffs from larger drainage areas are rarely achieved. Thus, the channel size is attributed to changes to accommodate the largest occurring discharges. Transmission losses may also constrain the channel widening further downstream. This trend is however not universal.</p>	
<p>Cross-section width: IRS may have an initially wide cross-section in upland and piedmont zones for a given catchment area compared to perennial rivers. This is partly due to the geomorphological effectiveness of rare extreme events and no recovery after a flash flood due to the absence of vegetation (e.g. Wolman and Gerson 1978).</p>	

2.7. Hydrological characteristics of IRS

2.7.1. Hydrological connectivity

Hydrological characteristics of IRS can be explained in terms of the hydrological connectivity in longitudinal, lateral, and vertical dimensions. Hydrologic connectivity is defined as the transfer of matter, energy, or organisms within and, or between elements of the hydrologic cycle mediated by water (Pringle 2003). The surface flow cessation in IRS disrupts the hydrological connectivity in one or more spatial dimensions, which in turn disrupts the transport of sediment and biota (Hooke 2003; Rolls et al. 2012). The hydrologic connectivity is largely governed by flow regime (magnitude, frequency, duration, timing, and rate of change of flow) as well as by fluvial geomorphology (i.e. channel and floodplain form, size, gradient, sediment composition and location) (figure 2.4 b, c, d and e) (Boulton et al. 2017). At a larger scale, the hydrologic connectivity depends on the climatic conditions (i.e. precipitation, evaporation rates), hydrogeological features (i.e.

riverbed permeability), tectonic activity (i.e. fault, volcanism) and the underlying geology and lithology (Boulton et al. 2017; Tooth and Nanson 2011; Graf 1988). However, at a smaller-scale, local processes such as microbial activity and benthic algae may change the substrate permeability (Mendoza-Lera and Mutz 2013; Hartwig and Borchardt 2015) or the vegetation may modify the surface flows, sediment and bed topography in the channel (Sandercock and Hooke 2011; Sandercock et al. 2007). The shallow channel areas such as the riffle region in a riffle-pool river geometry are often prone to drying, which may halt the longitudinal hydrological connectivity, however, the isolated pools may be interconnected through subsurface (hyporheic) flow (Boulton et al. 2017). Lake (2003) identified three common patterns of longitudinal drying, which occur in perennial rivers due to droughts that can also be applied to IRS. The first pattern of longitudinal drying occurs in streams originating from a permanent source (e.g. springs, headwater lakes), where the upper reaches retain permanent flows while the middle and lower parts dry fully or partially (isolated pools). This is a common pattern of longitudinal drying in IRS originating from mountain ranges and extending out into the more arid and permeable areas in lowland regions (Boulton and Williams 1996; Jaeger and Olden 2012). Specific hydrological conditions (e.g. high transmission losses exceeding inflows) (Datry 2012) and many karstic formations may also cause flow cessation in lowland areas (Meyer and Meyer 2000). The second longitudinal drying pattern is opposite to the first pattern, namely flow persists in lower reaches and headwater reaches dry out. The flow is sustained in most of the reaches in the piedmont and lowland zones by groundwater inputs through larger and deeper rivers downstream whereas, in the upland zone, the input from groundwater is restricted (Lake 2003; Datry et al. 2016). In the third common pattern, the mid-reaches dry while the upper and lower reaches sustain perennial flow. One example of this pattern is Selwyn River, in New Zealand's Southern Alps, where different aquifer structures and depths are causing mid-reach drying. The Selwyn River flows perennially for 3 km, is then slowly losing the surface flow in the flowing 45 km long section and emerges back (gaining-section) at the last 8 km (Arscott et al. 2010).

Lateral hydrologic connectivity of IRS depends mainly on the location (upland, piedmont, lowland, floodout) with respect to the channel topography and morphology and composition of the substrate in the geomorphological zones (figure 2.4 b, c, d and e) (Boulton et al. 2017). The channels in the upland zone are often overlaying bedrock, narrow in shape with low width to depth ratio and limited or no floodplains as schematically shown in figure 2.4 c (Sutfin et al. 2014). The surface flows down the hillslopes usually toward the channel are rapid, due to the shorter travel distances and steep slopes. The flow from the hillslope occurs as a response to precipitation, overland flow and subsurface flow (e.g. gradual snowmelt)(Lake et al. 2006).

In the piedmont zone, the river has a more rectangular cross-section, with a larger width to depth ratio and wider floodplains compared to the upland zone (Singer and Michaelides 2014). Lateral hydrologic connectivity is frequently maintained by a subsurface flow and larger transmission rates through a coarse alluvial substrate of the riverbed and the floodplains (Boulton et al. 2017). Lowland and floodout zones are characterised by a low

gradient with a large width to depth ratio, wide floodplains and fine riverbed sediments (i.e. sand, and clay), which restrict the lateral and vertical hydrologic connectivity (Boulton et al. 2017; Tooth and Nanson 2000).

The vertical hydrologic connectivity is ensured through water exchange between the surface (riverbed and floodplains) and the subsurface as well as between surface and atmosphere by precipitation and evapotranspiration. Vertical hydrologic connectivity is the main cause for surface flow intermittency in most of the rivers in piedmont, lowland and floodout zones, because in these zones the groundwater gains and losses dominate the water balance (Boulton et al. 2017). The vertical hydrologic connectivity is predominately the exchange between surface flow and the groundwater. A gaining or effluent channel is fed by groundwater whereas a losing channel or influent recharges the groundwater (Winter et al. 1998; Sophocleous 2002). The gaining and losing of surface flow can change along the river network in response to temporal groundwater table fluctuations, geology, topography, riverbed material composition and other local factors (Buss et al. 2009; Cardenas 2009). Precipitation and evapotranspiration are the main natural driving factors for reversing the vertical flow direction in response to groundwater level change.

In upland zone, the vertical hydrologic connectivity is ensured through gaining and losing water into the fractures and hyporheic corridors in the bedrock and limited alluvial deposits (Stanford and Ward 1993). However, at a reach-scale, channel geomorphological features such as cascade or step-pool forms may establish the vertical hydrologic connectivity (Buffington and Tonina 2009; Buss et al. 2009). An example is a hyporheic flow through pool-step-pool caused by a higher hydrostatic head difference between upstream pool and downstream pool separated by a step in headwater streams.

The surface-groundwater exchange in the piedmont zone is larger due to the larger permeable alluvial channel substrate compared to the upland zone. In the lowland and floodout zones, the channel cross-section and floodplains are much wider and therefore a larger area is exposed to vertical exchange between surface and groundwater. The limiting factor, however, is the lower permeability of alluvial substrate, because of fine sediments compositions, usually sand and clay. Some geomorphological forms like riffle-pool sequences may facilitate the vertical and longitudinal subsurface flow in lowland zone (Stanford and Ward 1993; Buss et al. 2009).

To sum up, flow cessation can disrupt the hydrologic connectivity in one or more dimensions. In the upland zone, the channels are often overlying bedrock which restrict the lateral and vertical hydrologic connectivity. However, longitudinal connectivity is maintained mainly by surface flow in response to precipitation or overland flow in the downstream direction. The contribution of lateral and vertical hydrologic connectivity is larger in the piedmont zone compared to upland zone, mainly due to the presence of the alluvial channel and floodplain's very permeable substrate. In the lowland and floodout zones, the channels and their floodplains are much larger in dimensions but the alluvial substrate is less permeable, hence this limits the lateral and vertical hydrologic connectivity. During the channel dry period, the subsurface (hyporheic) flow may sustain the hydrologic connectivity in all dimensions. At the reach-scale, geomorphologic features

2. *Introduction*

of the channels such as step-pool or riffle-pool and other forms may also cause hyporheic flow by providing a pressure head difference.

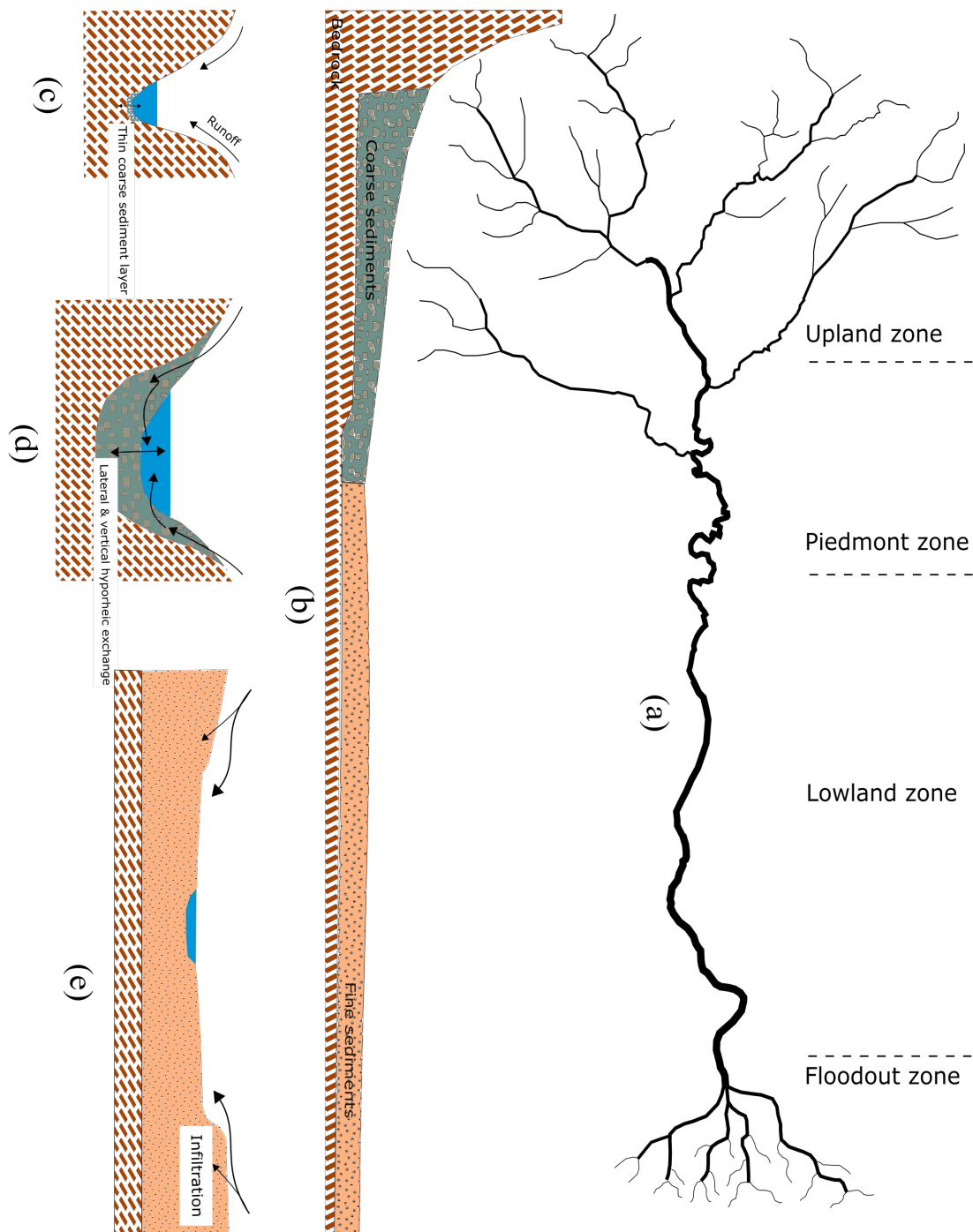


Figure 2.4.: Conceptual model showing hydro-geomorphological zones after Schumm (1977) and (b) their longitudinal material distribution. (c) Cross-sectional view of upland zone, (d) piedmont, and (e) lowland and floodout zones. The arrows indicate the lateral and vertical exchange of surface water and groundwater showing the hydrologic connectivity in different zones

2.8. Summary

The IRS are considered as important water conveyors predominantly in arid and semi-arid regions of the world. The hydro-geomorphology of the IRS maybe well described by their location and elevation in the catchment area, namely upland, piedmont, lowland, and floodout zones. The zones from upland to floodout are characterised by the cross-section shapes (e.g. narrow in upland to wide in floodout), bed substrate (bedrock in upland to fine sediments in floodout), and the associated transmission loss (low in upland, high in piedmont, and moderate in lowland and floodout zones), which are controlling parameters for the hydrologic connectivity and sediment transport. The hydrologic connectivity is ensured by the exchange of water between surface and subsurface in longitudinal, lateral and vertical directions. Hydrologic connectivity is disrupted by flow cessation and/or drying in IRS, which occurs as a result of climatic parameters (temperature, precipitation, and evapotranspiration), geologic formation (e.g. karstic formation), channel characteristics (bed permeability) and depletion of water sources (e.g. spring or lake depletion). The high variability of flow, lack of flow data, high rates of sediment transport, and lack of hydro-sedimentological knowledge and experience in IRS are the main challenges for a sustainable management of these water systems. Climate change and population increase, in particular, in arid and semi-arid regions imposes further stress on this highly variable water resource.

Semi-arid to arid mountainous regions of the world are drained by IRS. The majority of flow intermittency is occurring in headwater streams. However, even some large rivers in lowland regions (e.g. Helmand River in south-west Afghanistan) show intermittent flow behaviour. The rivers and streams dry out soon after the snowpack is melted in the summer months. The IRS in semi-arid to arid mountainous regions are characterised by mountainous flow and sediment transport regimes with steep slopes, low flow submergence, and coarse bed sediment compositions. The majority of the IRS in Afghanistan for instance are located in upland or piedmont zones, where the channel and floodplains substrate are composed of coarse sediments up to large boulders. However, the numbers of IRS in lowland and floodout zones are also increasing, mainly due to the climate change, water abstraction for agriculture. Therefore, flow and sediment transport characteristics of mountainous IRS are further studied in detail in chapter 3 in terms of shallow water depth (low flow submergence), rough surface, and steep channel slope. Additionally, methods and approaches for calculation of flow hydraulics (i.e. water depth, mean velocity, flow resistance, shear stress) and sediment transport in channels of low relative submergence, steep slope and coarse riverbed sediments are discussed in detail. Further, the effect of dry period and absence of base flows on sorting of riverbed sediments, and its implication on sediment transport is also studied.

3. Hydrodynamic and sediment transport in steep IRS

3.1. Sediment transport in rivers

Sediment particles of the riverbed are transported in one or a combination of movements such as rolling, sliding, and/ or saltating modes when the critical forces on the particles exceed the resisting forces (grain's submerged weight and friction). When the critical forces further exceed the resisting forces, the sediment particles can be lifted to a level, where the upward turbulent forces will be comparable or higher than the particle's submerged weight and as a result, the particle may go in suspension. The sliding, rolling, and saltating particles are usually referred to as bedload, which occurs by successive contacts of the particles with the riverbed restricted by the gravity forces (Bagnold 1956). Einstein (1950) defined the bedload as transport of particles within a thin layer having a thickness of two particle diameters by sliding, rolling, or moving in a succession of jumps with a streamwise distance of a few particle diameters. According to Einstein (1950), saltating particles having a jump length larger than two particle diameters are transported in suspension mode. The bedload mode of transport is shown to be a function of bed shear stress, namely at smaller bed shear stress particles move in sliding and/ or rolling mode also termed as contact load. At higher bed shear stress, the bed particles are largely transported in streamwise direction in short succession of jumping or bouncing mode also known as saltation.

As the bed shear stress further increases, finer sediment particles from the riverbed are driven up by diffusion as a result of near-bed turbulence and are transported within the water column in suspension. The particles remain in suspension as long as the upward diffusion of turbulence resists the tendency of particles to fall under gravity (Bagnold 1966). The particles transported in suspension are referred to as suspended load.

Another portion of very fine sediment particles such as silt and clay are transported by the flow such that they are nearly permanent in suspension and always remain close to the free surface without deposition. This mode of sediment transport is termed as wash-load.

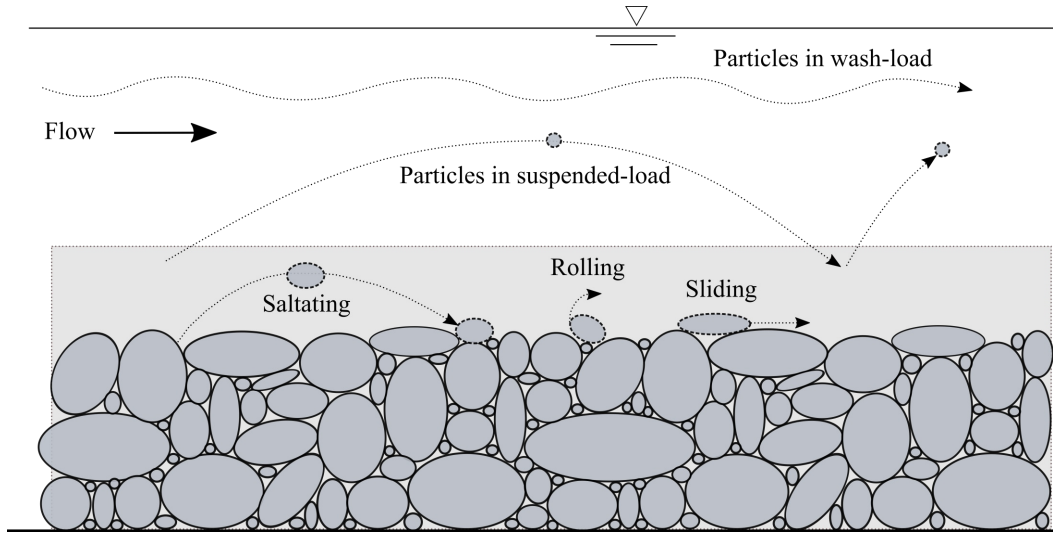


Figure 3.1.: Schematic of different modes of sediment transport

3.1.1. Bedload transport

Most of the bedload transport equations are developed based on the boundary shear stress that overcomes a critical shear stress required for the initiation of motion or grain mobility. A general form of this approach is expressed by:

$$Q_b \propto (\tau - \tau_c)^\beta \quad (3.1)$$

τ is the effective boundary shear stress applied to the bed sediments, τ_c is the critical shear stress required for the initiation of grain motion and β is an empirical exponent, typically larger than 1. The boundary shear stress is calculated as the downslope component of water weight divided by the wetted area A_w . The total volume of water is calculated by multiplying the wetted area with a unit stream length $A_w L$. The weight of the volume of water is given by $\rho g A_w L$ and the downslope component of the weight is calculated as:

$$\rho g A_w L \sin(S) \approx \rho g A_w L S \quad (3.2)$$

In the equation (3.2), it is assumed that $\sin(S) \approx S$. The boundary shear stress τ or the downslope component of flow force over the wetted area is calculated by:

$$\tau = \frac{\rho g A_w L S}{PL} \quad (3.3)$$

For wide channels, the wetted perimeter is assumed as A/h ; hence the boundary shear stress reduces to:

$$\tau = \frac{\rho g A_w L S}{(A_w/h) L} \approx \rho g h S \quad (3.4)$$

The resisting stress is basically the submerged weight of water per contact area $W = (s - 1)\rho g \pi \frac{D^3}{6}$, which is calculated by the grain's submerged weight W divided by the

Table 3.1.: Main bedload transport approaches

Approaches	Bedload equation	Incipient motion	Flow parameter dependency
Stochastic (Probablistic)	$Q_b = \frac{\alpha_1 D^3}{T_p} \sum_{n=1}^{\infty} p_n \frac{L_p}{\alpha_2 D^2}$	Probability of lift forces to the weight of sediments $p_n = \frac{W}{F_c} < 1$	Lift forces. e.g. Einstein 1950
Energy balance or stream power	$Q_b = (\omega - \omega_c)^3 / 2 D^{-2/3} h^{-1/2}$	Critical stream power $\omega_c > \omega$ $\omega_c = \tau_c \bar{u}_c$	Section average critical velocity and critical shear stress. e.g. Bagnold 1980
Excess shear stress	$q_b = \alpha (\tau - \tau_c)^\beta$	Critical shear stress $\tau_c^* > \tau^*$ $\tau_c^* = \frac{\tau_c}{(s-1)\rho g D}$	Critical shear stress based on the grain Re number from Shields diagram, which is dependent on shear velocity, and grain size. e.g. Meyer-Peter and Müller 1948
Excess discharge	$q_b = Y S^\gamma (q - q_c)$	Critical discharge $q_c > q$ $q_c = 0.065(s-1)^{1.67} g^{0.5} D_{50}^{1.5} S^{-1.12}$	Critical discharge per unit width is empirically derived based on the gravity, grain size and energy gradient. e.g. Bathurst et al. 1987

grain area $Area = \frac{2}{3} \times \pi \frac{D^2}{4} = \pi \frac{D^2}{6}$ as:

$$\frac{W}{Area} = \frac{(s-1)\rho g \pi \frac{D^3}{6}}{\pi \frac{D^2}{6}} = (s-1)\rho g D$$

The ratio of bed shear stress and grain resisting stress is termed as dimensionless shear stress:

$$\tau^* = \frac{\tau}{(s-1)\rho g D} \quad (3.5)$$

This is one of the most important variable in the sediment transport. Shields (1936) did extensive flume experiments and showed that the value of dimensionless shear stress or simply Shields parameter τ^* varies with grain Reynolds number $\frac{u_* D}{\nu}$, which is discussed in section 3.1.2. Over a century of bedload transport studies resulted in the evolution of large number of approaches and equations for bedload transport calculation. Some of the most commonly used approaches are listed in table 3.1. Channel hydraulics such as flow depth, velocity and shear stress are fundamental parameters for bedload transport calculations. In the stochastic approach of Einstein, lift forces are considered as a measure of flow hydraulics for bedload transport, which in turn is a function of flow velocity. Similarly, the stream power or energy approach uses the critical flow velocity or water depth as a measure for bedload transport. Excess discharge approach, on the other hand, assumes unit discharge as a decisive measure of flow hydraulics for bedload transport, because for coarse channel beds, water depth and velocity measurement are not straightforward. The widely used excess shear stress-based approach considers shear stress and its critical value as a significant parameter for bedload transport estimation, which is in turn linked to flow depth, velocity and shear velocity. The critical shear stress for incipient motion is a crucial parameter for bedload transport calculation using excess discharge method.

The bedload transport equations can be modified and adjusted for steep IRS by modifying the hydraulics of the channel, regardless of the background of the bedload transport equations. The adjusting parameters can be linked to the hydraulic and sedimentological characteristics of the steep channel in order to achieve a realistic estimation of bedload transport. Despite the recent efforts to adjust the bedload transport methods initially developed for low slope rivers and streams to the steep slope channels, there is still no universal approach existing. The main reason is the lack of observed data for steep channels due to the difficulty associated with acquiring extensive field data in the past. However recently indirect bedload measurement are also deployed to the fields to collect data, but they are still limited to few sites. The data is even scarcer for IRS mainly due to the remoteness of the sites and cost-intensive observation. Before discussing the approaches on how to adjust the bedload transport equations to steep IRS channels, it is logical to outline the major hydro-sedimentological parameters for bedload transport and their behaviour in steep, low flow submergence and high flow resistance conditions.

3.1.2. Sediment incipient motion

Sediment grains in alluvial streams have a finite weight and result in certain friction, which together act as resistance forces against bed shear stress. They can only be brought into motion when the acting shear stress of the fluid is exceeding the grains' resistance stress.

$$\tau > \tau_c$$

This threshold in shear stress is termed as critical stress τ_c .

Shields (1936) performed flume experiments and derived a curve showing the relationship between a dimensionless critical Shields number versus grains' Reynolds number defined as:

$$\tau_c^* = \frac{\tau_c}{(s-1)\rho g D} \quad (3.6)$$

$$Re_* = \frac{u_* D}{\nu} \quad (3.7)$$

τ_c^* denotes the critical Shields' value, Re_* is the grains Reynolds' number, u_* is shear velocity, and ν is the kinematic viscosity of water. Shear velocity $u_* = \sqrt{\frac{\tau}{\rho}}$ is a measure of the bed shear stress linked to the turbulent flow structures close to bed and can be estimated from the velocity measurement or shear stress fields (Bayazit 1976; Dittrich and Koll 1997; Katul et al. 2002). Shields (1936) suggested that the wall shear stress has a value, where the extrapolated sediment flux approaches a zero value.

Yalin and Karahan (1979) compiled a large volume of data from literature with their own results of flume experiments on sand particle sizes ranging from 0.10 to 2.86 mm under laminar and turbulent flow conditions as shown in figure 3.2. It is important to mention that the data in the Shields' diagram is considerably scattered. For small grain Reynolds' numbers $Re_* < 10$, the τ_c^* relationship with Re_* depending on the flow regime (i.e. laminar or turbulent) and can have a power law relationship. Despite the small grain

sizes of silt and clay particles, their τ_c^* increases as grain size decreases. This is mainly due to the cohesive forces that increase the critical shear stress for initiation of motion for silt and clay particles. In contrast, sand and gravel particles are lacking cohesive forces and are entrained at lower τ_c^* values. For $Re_* > 70$ or hydraulic rough conditions, the τ_c^* takes an average value of 0.045. A minimum of 0.032 for τ_c^* can be recognised for a $Re_* = 10$. Cao et al. (2006) derived explicit equations for three distinct regions of incipient motion curve by Yalin and Karahan (1979) as follows:

$$\tau_c^* = \frac{0.1414}{Re_*^{0.23}} \quad Re_* \leq 6.61 \quad (3.8)$$

$$\tau_c^* = \frac{[1 + (0.0223Re_*)^{2.84}]^{0.35}}{3.09Re_*^{0.68}} \quad 6.61 \leq Re_* \leq 282.84 \quad (3.9)$$

$$\tau_c^* = 0.045 \quad Re_* \geq 282.84 \quad (3.10)$$

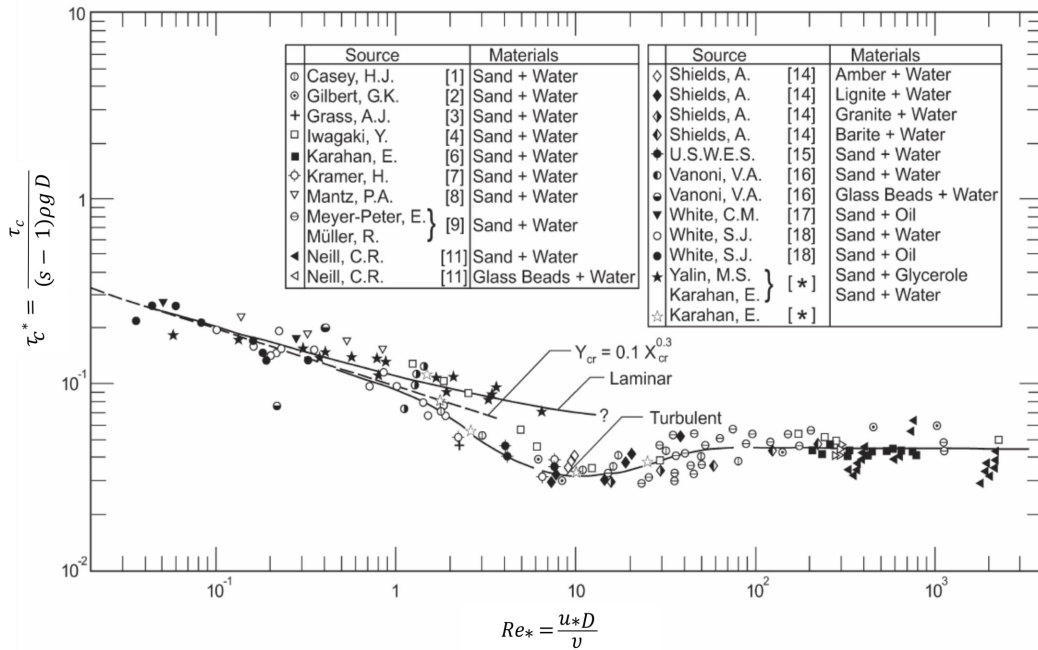


Figure 3.2.: Critical shear stress for incipient motion of sediment grains by (Yalin and Karahan 1979)

Most of the studies for determination of initiation of motion are conducted using uniform size sediments, while in natural conditions the riverbed is composed of sediment mixtures with a wide range of grain sizes. Wiberg and Smith (1987 b) used a balance of forces on individual particles of sediment mixtures considering the near-bed drag forces, lift to drag force ratio, and the particle angle of repose for deriving an expression for critical shear stress for particle movement as on the particle angle of repose. They suggested the following equation for predicting incipient motion for mixed size sediments. They

found that the incipient motion for mixed grain sizes additionally depends on the relative protrusion of the particles into the flow as well as on the particle's angle of repose as:

$$\tau_c^* = \frac{4 (\tan \phi \cos \Theta - \sin \Theta)}{3 (C_D + \tan \phi C_L)} \frac{1}{\left(u_z/u_*\right)^2} \quad (3.11)$$

u_z is the effective fluid velocity acting on the particle assuming logarithmic velocity distribution, u_* is shear-velocity, ϕ is sediment mixture angle of repose, Θ is bed slope angle, C_D is drag coefficient and C_L is lift coefficient. The angle of repose ϕ of natural particles in mixed-size sediments is calculated by the equations proposed by Miller and Byrne (1966) from observations of naturally sorted sediments.

$$\phi = \cos^{-1} \left[\frac{D_b/k_s + z_*}{D_b/k_s + 1} \right] \quad (3.12)$$

D_b is the diameter of moving particle, k_s is the equivalent Nikuradse roughness length, $z_* = -0.02$ is the average level of the bottom of moving grain from zero bed level and depends on grain sphericity and roundness. Chiew and Parker (1994) suggested a similar equation for adjusting τ_c^* based on the bed slope and mixture of sediment angle of repose as:

$$\frac{\tau_c^*}{\tau_{c0}^*} = \frac{\sin(\phi - \Theta)}{\sin \phi} \quad (3.13)$$

τ_{c0}^* denotes the critical dimensionless shear stress for a flatbed condition that can be read from Shields diagram based on Re_* .

The equations developed for accounting the channel slope effect and sediment mixture angle of repose show that higher angle of repose leads to higher τ_c^* while the channel slope has an inverse proportion with τ_c^* . This means that the downslope component of the particle weight contributes to the sediment movement.

As shown in figure 3.2, the critical Shields' value at incipient motion is varying with Re_* but at higher $Re_* > 100$, a constant average threshold of 0.045 is assumed (Yalin and Karahan 1979; Miller et al. 1977 and others).

3.1.3. Slope dependency of critical shear stress

In contrary to the usual consideration of a decreased critical Shields' value on steep slopes because of increased gravitational forces, slope dependency of critical shear stress for the incipient motion was even recognised by Shields himself (Shields 1936). Flume and field studies show that critical Shields stress for incipient motion increases with channel slope (e.g. Neill 1967; Ashida and Bayazit 1973; Aguirre-Pe 1975; Bathurst et al. 1984; Shvidchenko and Pender 2000). The same trend is found from field studies (Bartnik 1991; Mueller et al. 2005; Lenzi et al. 2006; Mao et al. 2008; Ashida and Bayazit 1973. Lamb et al. (2008) suggested the following empirical relation to account for the increasing critical Shields values with increasing stream slope (figure 3.3 a).

$$\tau_c^* = 0.15 S^{0.25} \quad (3.14)$$

Similar power relation between the critical Shields parameter and the slope is derived from investigation of 133 field and flume datasets by Parker et al. (2011) as follows:

$$\tau_c^* = 0.19 S^{0.28} \quad (3.15)$$

The increase in frictional resistance at steep and low flow submergence channel is due to the increased effect of the wake eddies from bed particles on the overall flow resistance (Shvidchenko and Pender 2000). They further showed that critical Shields stress for the incipient motion not only depends on sediment size but also on the relative submergence of the grains (figure 3.3 b).

Mueller et al. (2005) investigated the Shields stress variation with stream gradient for 45 gravel-bed streams in western North America. The reference critical shear stresses τ_r^* are calculated from the measured bedload transport rates in terms of dimensionless transport parameter proposed by Parker et al. (1982). A dimensionless transport rate is assumed to be equal to $W^* = 0.002$.

$$W^* = \frac{(s - 1) g q_b}{\rho_s (\tau / \rho)^{1.5}} \quad (3.16)$$

Where s denotes the specific gravity of sediments, ρ_s is the density of sediments. τ_r^* is estimated from the dimensionless shear stress for median grain size values τ_{50}^* . The variation of the reference critical Shields stress with the channel bed slope and relative submergence is shown in figure 3.3 c.

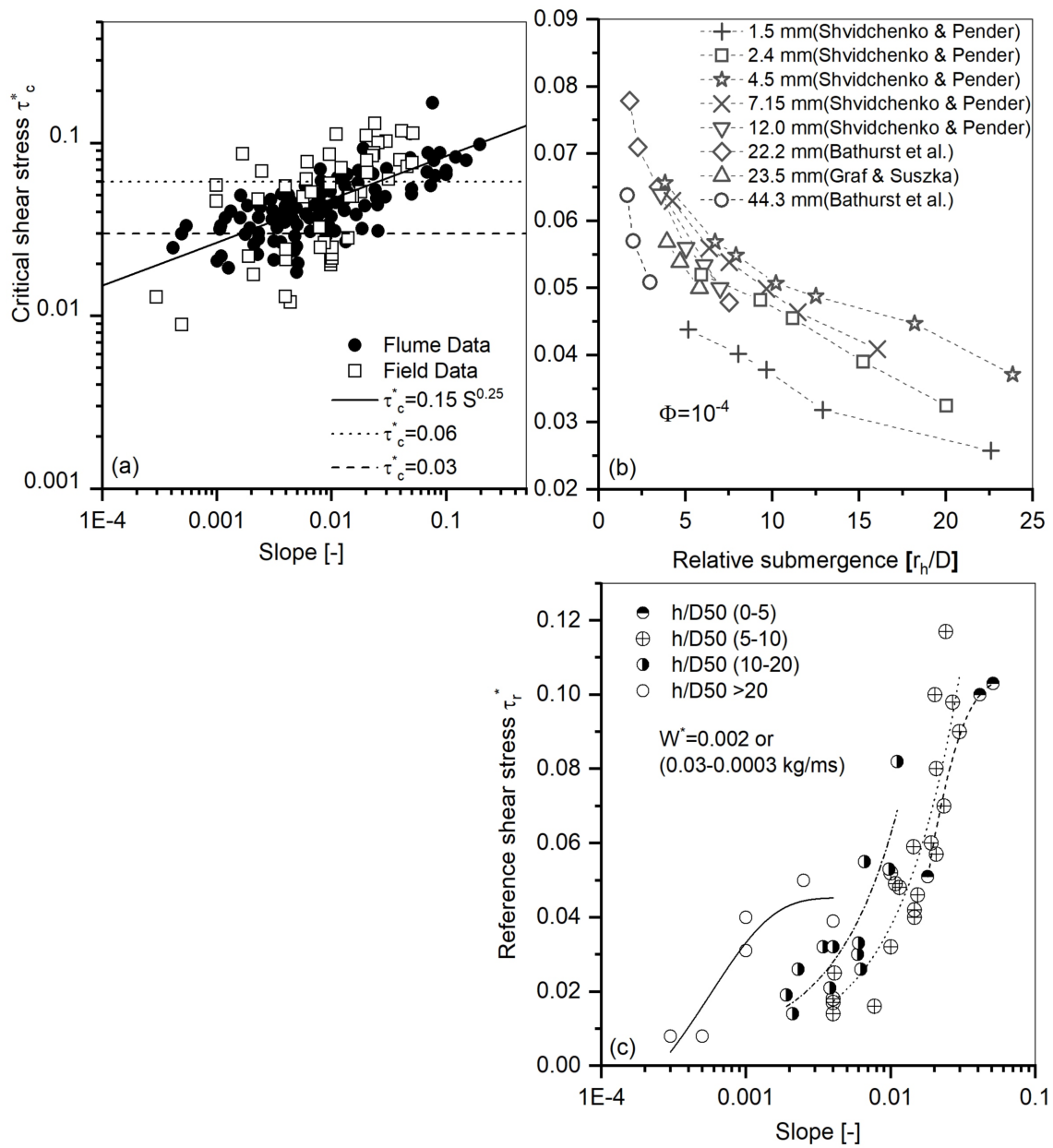


Figure 3.3.: Field and flume data showing the slope dependency of critical Shields stress (a), (b) The critical shear stress variation with grain sizes and relative submergence and (c) reference shear stress τ_r^* for different slope with data stratified by bank-full flow h/D_{50} derived from measurements of 159 gravel-bed streams in North America and the United Kingdom.

Potential slope dependent effects mentioned in literature are listed below:

- Wall drag

- Form drag from bed morphology
- Variable friction angles
- Grain emergence
- Air entrainment
- Variable drag and lift coefficients
- Local vertical velocity profile
- Structure of turbulent velocity fluctuations

Among the mentioned parameters, Lamb et al. (2008) suggested that slope's influence on the relative roughness and flow resistance is responsible for the correlation between slope and critical shear stress. Flow resistance is shown to increase with slope increase and consequently relative roughness increases (Bathurst 2002). (Ashida and Bayazit 1973; Bathurst 2002; Graf 1991; Shvidchenko and Pender 2000) suggested that this trend in increasing critical Shields' stress at higher slopes, is causing an increase in relative roughness and a decrease in local flow velocity around bed particles. If the relative roughness is held constant, the critical shear stress actually decreases with increasing channel slope as shown by Chiew and Parker (1994) after conducting an experiment in a closed conduit of constant relative roughness by changing the slope. Therefore, the flow resistance for mountainous rivers as a main factor for reduced effective shear stress on steep slopes is studied in detail in section 3.3.

3.2. Sedimentological characteristics of IRS

3.2.1. Riverbed sediment characteristics in IRS

Gravel-bed rivers and streams in humid and snowmelt areas have typically a coarse surface layer with a thickness of 1 to 2 times of the very coarse grains (i.e. D_{90} , D_{84}) known as an armoured layer (e.g. Powell 1988; Gessler 1990; Parker 2008). Field observations in dryland regions show that the surface and subsurface layer sediments are not significantly different in IRS, namely, riverbeds lacking armouring (Schick et al. 1987; Laronne et al. 1994; Hassan et al. 2006; Laronne and Shlomi 2007). The absence of an armouring layer and, or presence of riverbed clogging (colmation) (i.e. finer surface layer than subsurface layer) is observed in IRS (Almedej 2002). The weakly or unarmoured gravel-bed rivers in dryland environment occur mainly due to abundant supply of sediments, short period flash floods, which transport large amount of sediments and absence of base flows (lower discharges) necessary for segregation and vertical sorting of the riverbed sediments and formation of armouring layer (e.g. Hassan et al. 2006; Powell 2009). Flume experiments by Hassan et al. (2006) showed that sediment supply is the first order controlling parameter of the armouring process of riverbeds and hydrograph shape is termed as secondary controlling parameter. They further reported that hydrographs resembling a snowmelt case (flat hydrographs) produced a vertical sorting or armouring whereas the sharply

peaked hydrograph did not result in an armouring.

The degree of riverbed armouring can be characterised by an armouring ratio (surface median size to subsurface median size or D_{50sur} / D_{50sub}) and is found to vary between 0.5 to 2.4 for 22 desert ephemeral gravel-bed streams while the armouring ratio for snowmelt-fed gravel-bed streams ranges between 2 to 7 (Hassan et al. 2006). The armouring ratio lower than unity is indicative of an inverse layering, while a value of unity and larger than unity shows unarmoured and armoured beds, respectively. Almedeij and Diplas (2005) suggested an explanation for inverse layering based on the shear stress that exceed the bedload entrainment threshold but simultaneously remain below the particle suspension threshold condition. This leads to segregated sediment deposition in such a way that finer particles settle on the top of coarse particles. This process resembles fluidised bed that during the peak conditions, nearly all sediment sizes are suspended and subsequently when the flow energy decreases, larger particles deposit earlier than finer particles and causes an inverse layering of bed sediments (Di Felice 1988).

Hassan et al. (2006) observed a vertical sorting effect in their gravel-bed flume experiments at flat hydrographs. However, IRS are lacking the base flows in their hydrographs and often the hydrographs resemble a seasonal flash flood (Costigan et al. 2017), hence the absence of base flows may lead to an unarmoured riverbed. It can be inferred that the longer the dry period and absence of base flow persist; the more interrupted the vertical sorting process may develop. The shape of hydrograph may also affect the sediment supply, namely flash floods of short periods as common in arid regions are causing more sediment supply from traces and river banks than flatter hydrographs (Higson and Singer 2015).

In dryland environments, sediment supply from poorly vegetated hillslopes to valley floors and rivers are due to the availability of sediments and infrequent flows that often occur during the periods with abundant of sediments (Cooke et al. 1993). In mountainous dryland regions, the sediment supply from hillslopes is further intensified due to the effect of steep slopes (Michaelides and Singer 2014).

The degree of armouring as a function of sediment supply and flash floods is graphically shown in figure 3.4.

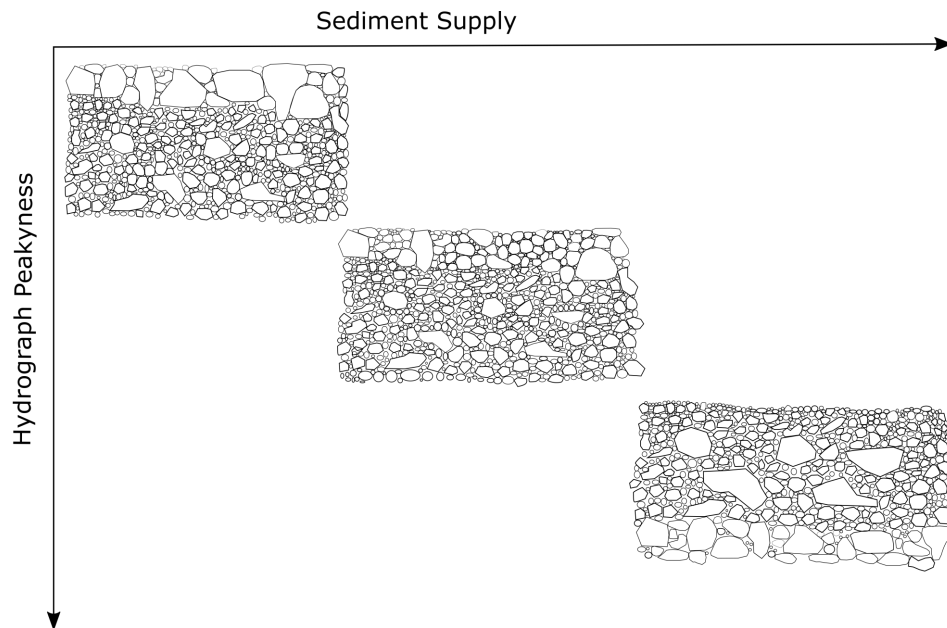


Figure 3.4.: Graphical representation of bed building in IRS with respect to the sediment supply and hydrograph shape Modified after Cooke et al. (1993)

Weakly armoured, unarmoured or even inversely layered gravel-bed rivers are main characteristics of IRS, which are mainly formed as a result of abundant sediment supply and infrequent flash floods.

High rates of sediment transport observed in dryland regions are mainly attributed to the absence of an armoured layer in IRS. The shape of the hydrograph is found to play an important role in the vertical sorting. Most of the IRS in Afghanistan for instance are originating from mountainous regions, where snowmelt controls the flow regime consisting of one peak with relatively long low flow periods. This may lead to a wide variety of armouring degrees from strongly armoured to weakly armoured but also unarmoured and inversely layered gravel-bed rivers and streams may also develop depending on the sediment supply rates. Therefore, the application of an armouring effect in predicting sediment transport should be associated with the field observation of the study area to determine the type and degree riverbed armouring.

3.2.2. Bedload transport in IRS

Few bedload transport measurements for IRS are available, which show very high bedload transport compared to rivers and streams in temperate regions (Reid and Laronne 1995). Bedload transport measurements at two ephemeral desert streams, Nahal Yatir and Nahal Eshtemoa, are providing valuable information about bedload transport in IRS. They are fourth and fifth order gravel-bed neighbouring ephemeral streams with draining basins of 19 km^2 and 119 km^2 in the northern Negev desert, respectively (Powell et al. 1996; Laronne et al. 1992). Bedload transports are recorded at both sites during flash floods

using Birkbeck-type bedload samplers (Reid et al. 1980). The bedload transport as a function of the average channel shear stress is compared with some bedload data for Goodwin creek (seasonal) (Kuhnle 1992), and perennial rivers Oak-creek (Milhous 1973), Jacoby (Lisle 1989) and East-Fork (Leopold and Emmett 1976). The comparison is plotted in figure 3.5 with respect to the mean grain size of the bed surface and the subsurface material. It is observed that despite of the insignificant difference in bed material mean grain sizes, much larger bedload transports are measured for Nahal-Yatir and Nahal Eshtemoa rivers at similar shear stress compared to others. The result is indicative of high bedload transport efficiency of flow in ephemeral IRS compared to perennial rivers (Diplas et al. 2006). The high rates of sediment transport observed in dryland regions are mainly attributed to the absence of armouring layers and the abundance of sediment of all sizes available to be transported in IRS as discussed earlier in section 3.2.1.

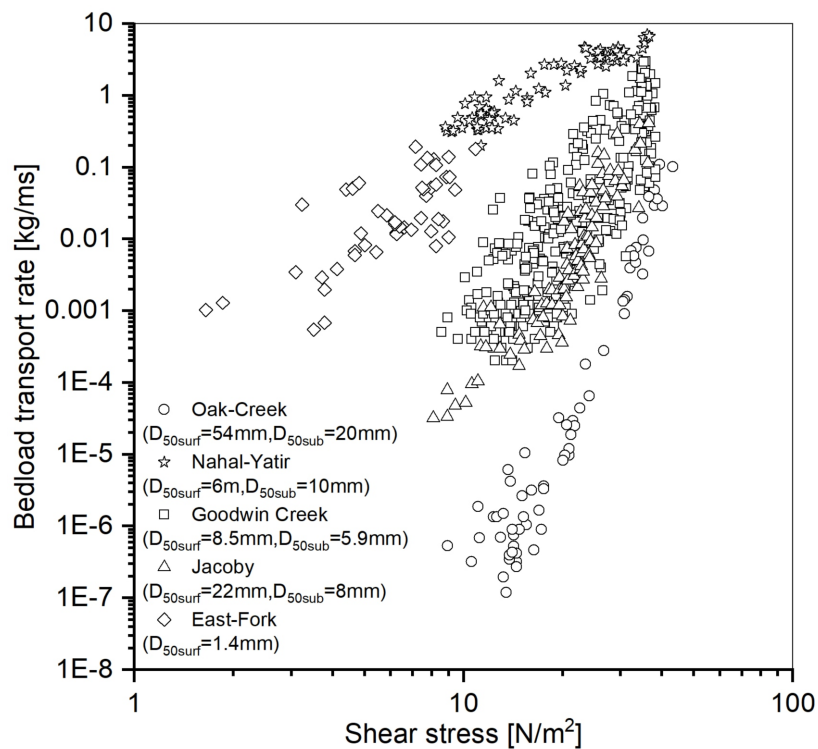


Figure 3.5.: Comparison of unit bedload transport as a function of bed shear stress in the ephemeral Nahal Yatir and Nahal Eshtemoa, seasonal Goodwin Creek, perennial rivers Oak Creek, Jacoby and East-fork rivers

3.2.3. Riverbed clogging and its implication on bedload transport in IRS

A. Riverbed clogging

The reduction in riverbed hydraulic conductivity and porosity as a result of physical,

chemical and biological processes are referred to as riverbed clogging or colmation. The physical process is mainly the deposition of fine sediments (i.e. sand, silt and clay) into pores or on top of a coarser riverbed, which may lead to a reduction in the riverbed hydraulic conductivity.

In natural rivers, two types of riverbed clogging are common. The first type occurs when the fine sediment particles deposit in the gravel matrix and intrude into the gravel-bed due to their large pores, and cause an internal clogging or colmation. The second type of riverbed clogging is termed as external clogging or colmation, which refers to the deposition of fine sediments on a coarse riverbed. Blaschke et al. (2003) observed additionally, an intermediate type clogging in Danube River called armouring layer clogging, where the fine sediments fill the existing voids in the armouring layer. All clogging types result in a decrease in hydraulic conductivity of the near-surface layer. External and intermediate clogging is visible from the surface while internal clogging can be observed after removing the surface layer. The riverbed clogging is governed mainly by the critical shear stress, the concentration of suspended sediment load, the hydraulic gradient between surface and groundwater, GSD of the riverbed (Schälchli 1992; Schubert 2002), and the water quality (Griseck and Bartak 2016). The slug test and grain-size analysis on a riverbed point bar by Nowinski et al. (2011) observed 10% of increase in fine sediments, which led to a decrease of factor 4 in hydraulic conductivity. Schälchli (1992) performed flume experiments using riverbed sediments and observed a reduction approximately of a factor 9 in hydraulic conductivity as a result of finer suspended sediment intrusion and deposition on the flume-bed. Beschta and Jackson (1979) conducted a flume experiment of gravel-bed and found that fine sediment intrusion into the voids of gravel-bed may be more influenced by suspended sediment size than by flow hydraulic variables.

In IRS, flash floods transport relatively large amount of fine sediments from the catchment area, due to the lack of vegetation in dryland regions that can otherwise act as a buffer for sediments. The suspended sediments deposit downstream as a result of the surface flow reduction due to the seepage loss, which reduces the transport capacity. The fine sediment deposition on coarse riverbed may cause clogging in IRS. Sadid et al. (2016) observed external riverbed clogging in some IRS in Kabul River basin, as a result of excessive depositions of fine sediments on the coarse riverbed as shown in figure 3.6. The external clogging of the riverbed is not universal for all IRS; but it depends, in particular on the characteristics of the catchment area (i.e. fine sediment supply and vegetation cover) and the occurrence of flash floods.

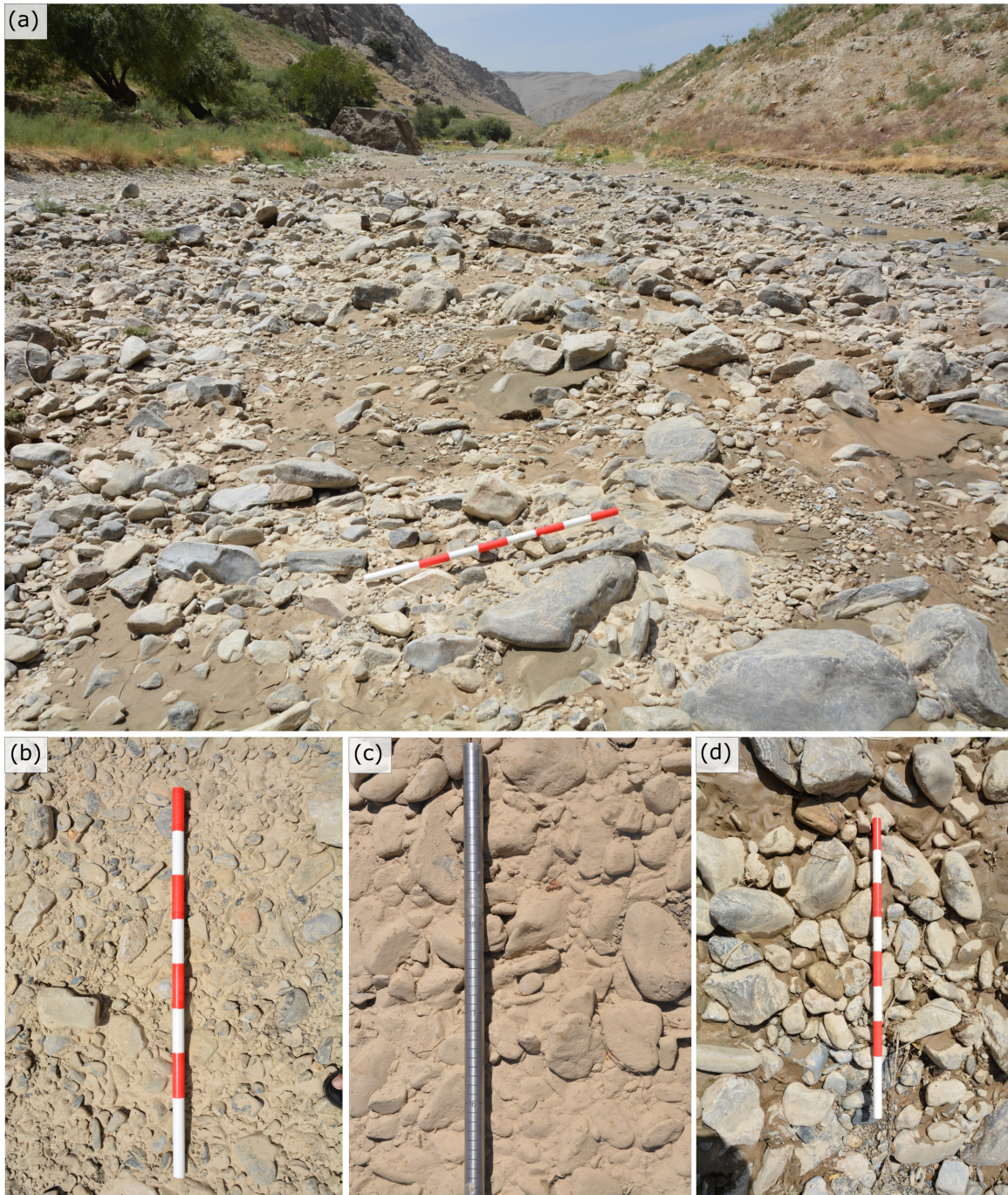


Figure 3.6.: Clogging of the riverbed by fine sediments deposition soon after flash flood recession at (a) upstream reach of Maidan River in Kabul River basin (b) closer view of the freshly clogged riverbed (c) and (d) clogged riverbed after it is dried. Note: The equal-distance markings (red and white strips) on the staff are 10 cm each.

In IRS, biological and chemical clogging of riverbed may be restricted due to the seasonality of flow that is required for microbial and chemical activities and nutrients transport. However, physical clogging of riverbed may be present mainly due to the short period flash floods, which transport a large amount of fine sediments that may deposit on the riverbed after quick flash flood recession. The deposition may also be a result of the downstream reduction in surface flow (due to the seepage loss) that can lead to external clogging.

B. The implication of riverbed clogging on bedload transport

The main impact of a clogged riverbed on the bedload transport is an increase in resistance against flow shear stress regardless of the type of clogging processes behind a clogged riverbed. Schmidt (2017) observed an increase in critical shear stress for particle entrainment due to biofilm stabilisation of flume bed sediments. Similar flume experiments confirm that biofilm slightly modifies the bed roughness and flow hydraulics and highly influences the bed sediments erosion such that bedload rates were five times lower than a bed without biofilm (Piqué et al. 2016). Both biotic and abiotic mechanisms may lead to riverbed clogging; however, their contribution may vary widely. Ulrich et al. (2015) observed larger biotic role in riverbed clogging than abiotic processes after studying time-laps grain size and biomass datasets for a river section in California.

The clogging is associated with an increase in fine sediment contents, which in turn may increase the critical shear stress for particle entrainment. Panagiotopoulos et al. (1997) observed that for increasing mud content in the sand, the critical mean shear stress also increased. Flume experiments by Kothyari and Jain (2008) showed that critical shear stress increases with clay content and unconfined compressive strength while it is inversely proportional to the void ratio of clay-gravel and clay-sand-gravel mixtures. Singh et al. (2016) varied clay content from 10% to 50% in clay-silt-gravel mixture and observed an increasing trend in critical shear stress for incipient motion of gravel particles with clay content increase. The contribution of cohesive forces due to mud content is observed to be the key parameter because some experiments show that with an addition of other fine particles such as sand into the coarse gravel-bed actually resulted in an increase in overall sediment mobility. This increase in mobility is linked to an increase in the near-bed flow velocities as a result smoothing effect of sand particles, filling of voids, which increase the bed surface and larger particles protrude that increases the likelihood of particle entrainment (Hill and Tan 2017).

The riverbed clogging is affecting the structure, roughness, critical shear stress and hydraulic conductivity of the riverbed sediments regardless of processes caused the clogging. In IRS, the biological processes of riverbed clogging is shown to have less contribution compared to the perennial rivers, due to the harsh biotic conditions (i.e. humidity, and nutrients condition). The abundance of fine sediments supply, low flow and dry periods may lead to stronger physical clogging of riverbeds in IRS.

On the other hand, in IRS, the clogging of riverbed may restrict the seepage losses of surface flow as a result of lower hydraulic conductivity in the near-bed region. This may cause the IRS to have the full surface water capacity for sediment transport with a limited

decrease in the downstream direction. This effect may counteract the effects of riverbed clogging.

3.3. Hydraulics of mountainous IRS

3.3.1. Flow regions and their characteristics

A large number of IRS in arid and semi-arid regions of the world are located in the upland regions and valleys, therefore, the hydraulics and flow regime of IRS in these regions are mountainous and are strongly controlled by steep slopes. Flow in mountainous rivers can be unsteady, non-uniform and with variable flow submergence ratios, as a result of steep hydrographs, non-uniform geometry, lateral inflow and strong bed gradient. In mountain regions, with the presence of large-scale roughness, the free surface of the flow is controlled by roughness elements. The structure of the flow in the mountain regions can, in general, be described as turbulent flow over rough-boundary. Coleman and Alonso (1983); Graf (1991) distinguished different regions of flow over depth in mountainous rivers as shown in figure 3.7 a. Each zone is characterised by different flow properties and are briefly outlined here.

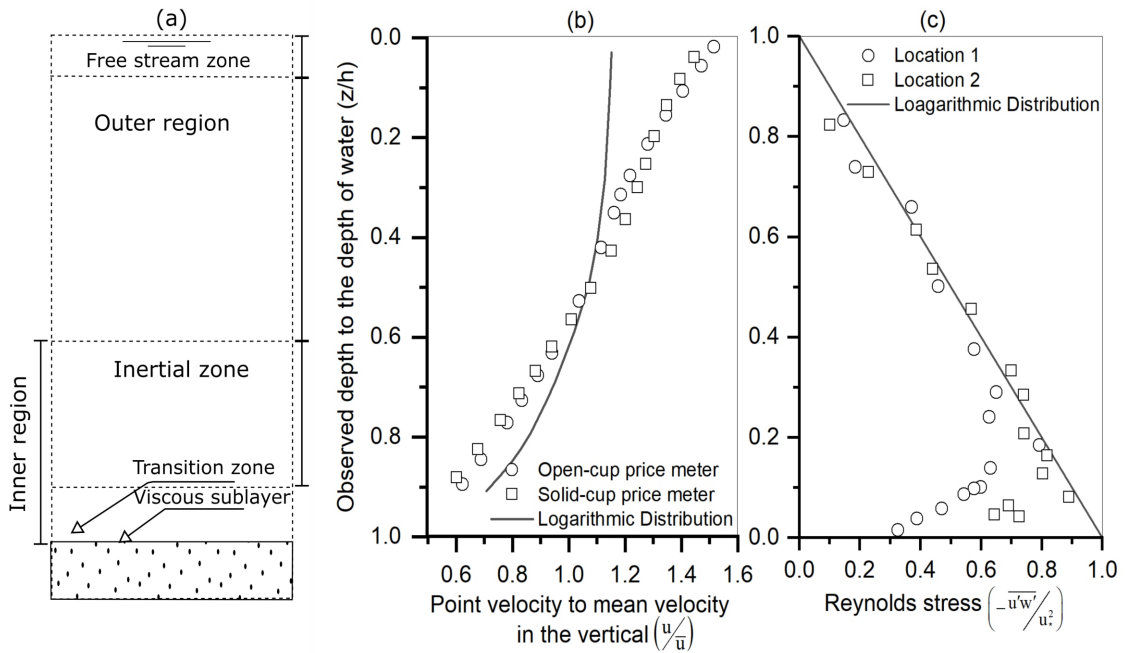


Figure 3.7.: (a) Regions in boundary layer flow (Coleman and Alonso 1983; Graf 1991), (b) measured mean flow velocity distribution normalised by mean flow velocity for mountain rivers in Colorado (Jarret 1990) and (c) measured Reynolds stress normalised by shear velocity for flow with small submergence over a flume bed composed of glass beads using Laser Doppler Anemometer (LDA) (Nakagawa et al. 1991)

In the outer or wake region, the direct effects of local roughness parameters are less significant and free-stream zone is theoretically free of shear and turbulence. In this region, viscous effects and form-induced fluxes are also negligible (Coleman and Alonso 1983; Graf 1991). The characteristic scales for outer region are shear velocity u_* , maximum flow velocity u_{max} , the distance from the bed and the flow depth h . The near surface and intermediate regions are part of this outer layer where the velocity distribution may be described by defect law (Nezu and Nakagawa 1993).

The region close to the bed is known as inner or wall region, where the actions of shear stress and roughness are dominant. This region is assumed to be part of boundary layer, where the shear stress is constant. Since the effective thickness of the inner region is small, it is convenient to assume the stress distribution for this region as constant. This assumption makes it possible to adopt the boundary layer theory results to the channel flow. The thickness of this region is related to flow submergence ratio and is often given as $z_0/h < 0.15$ (Hinze 1975; Graf 1991), where h is water depth measured from top of roughness element and z_0 is height (taken from $0.3D_s$ to $0.4D_s$), where D_s is a representative grain diameter (Graf 1991). The inner region is further divided into an inertial zone, where the logarithmic law of velocity distribution exists (logarithmic zone),

a transition or buffer zone, where a change from laminar to turbulent flow occurs and an extremely thin viscous sublayer, where the velocity linearly varies with distance from the wall surface.

The logarithmic zone ranges between $(2 - 5)k_s$ to $< 0.2h$ (Nezu and Nakagawa 1993). The roughness element height k_s is equal to surface particle size D_s in a granular bed of large particles. However, in case of small grain diameters and bedforms such as sand wave (dunes and ripples), the value of k_s is taken much larger than grain diameter. The viscous effects and form-induced fluxes are negligible as is the cases for the outer layer but the characteristic scales are differing from those for the outer layer (e.g. Nikora et al. 2001). The characteristic scales for the logarithmic layer are shear velocity u_* , the distance from the bed and the characteristic scales of the bed topography such as standard deviation of bed elevation and longitudinal and transverse correlation lengths (Nikora et al. 1998). The existence of this layer is only guaranteed when the water depth is much larger than roughness height $h \gg k_s$ (Nezu and Nakagawa 1993; Raupach et al. 1991; Raupach et al. 1980).

The transition zone is largely affected by relative roughness. In presence of large relative roughness, the transition zone is extended up in the inertial zone (e.g. Kirkgöz 1989). The viscous sublayer is present in turbulent flow with smooth and transition regimes, while it is absent in rough regime flows (Coleman and Alonso 1983; Graf 1991). The flow layers described above are depending on the relative submergence h/k_s . In case of high flow submergence $h \gg k_s$, all layers exist. As the relative submergence decreases to small relative submergence $(2 - 5)k_s > h \geq k_s$, the form-induced sublayer represents the outer layer and in the case of partially inundating rough beds $k_s > h$, the interfacial sublayer is the upper flow region (Nikora and Mclean 2001).

3.3.2. Near-bed flow characteristics

In mountain rivers, the flow field is often turbulent over rough surfaces with $R_e > 2500$, which in addition has a so-called roughness layer, where individual roughness elements occupy a region between just above the roughness crests and roughness troughs (e.g. Koll 2002) (figure 3.8 a). In case of natural and irregular beds, the flow in roughness sublayer is highly three dimensional and spatially heterogeneous, where the shear velocity and bed topography are the main characteristic scales (Nezu and Nakagawa 1993). Tsujimoto (1991) reported a thickness of approximately 0.3 to 1.2 times the bed material diameter for the roughness layer.

The roughness layer is further divided into form-induced sublayer (a thin region of 1 to 4 times roughness height above the crest of roughness element) and interfacial sublayer (with thickness from roughness element crest to troughs) (Nikora et al. 2001; Koll 2002) as shown in figure 3.8 a. The thickness of the roughness layer is shown to be invariant of flow discharge (or relative submergence) (Koll 2002; Cooper et al. 2013).

The flow in the form-induced sublayer is predominantly characterised by individual roughness elements. Flow separation from individual roughness elements causes a new feature called form-induced stress in the form-induced sublayer (Giménez-Curto and

Lera 1996), while the main feature in interfacial sublayer is the form drag. The main characteristic scales for both form-induced and interfacial sublayers are the shear velocity u_* and characteristic length of bed topography.

The roughness layer in rough beds plays a similar role as viscous and transition layers in hydraulically smooth beds (Nikitin 1963; Raupach et al. 1991), where the interfacial sublayer resembles in a manner to the viscous sublayer and form-induced sublayer is analogous to the transition sublayer (Nikora et al. 2001). Some of the most important flow parameters relevant for sediment transport are discussed in details, in particular, with regard to their characteristics in roughness layer region and their alternation with flow submergence.

i- Velocity

Velocity as a main and important driver of sediment particles' transport is strongly altered by the flow resistance in the near-bed regions. The assumption of logarithmic velocity distribution for the near-bed region is strongly overestimating the flow velocity and may lead to an overestimation of bedload transport as well. Aberle (2006) showed that within the roughness layer, a linear flow velocity distribution is valid. Similar results of more uniformity of flow velocity in the roughness sublayer than log-law profiles are also reported by (O'Loughlin and Annambhotla 1969; Mizuyama 1977; Raupach et al. 1980; Nakagawa et al. 1991). Flume experiments by (e.g. Bayazit 1976; Tsujimoto 1991; Pu et al. 2017) show that distribution of velocity and turbulence intensity in the near-bed region is no longer consistent with those known for flow with sufficient submergence. The velocity profile becomes rather uniform and turbulent intensity is suppressed in this region. Observations in mountain streams have also shown that the velocity profile can deviate strongly from the often used logarithmic (e.g. Jarret 1990; Wohl and Thompson 2000; Byrd et al. 2000). An example of velocity profiles averaged from several measurements for Colorado River using USGS AA current meter is shown in figure 3.7 b. The averaged velocity profile shows strong deviation from logarithmic distribution in the near-bed region as well as in the outer most and free stream zones (Jarret 1990).

Flume experiments by Koll (2006) show that an increase in flow submergence reduces the zero-plane displacement in roughness layer region as well as controls the shape of velocity profiles with an increase in Von Karman constant within the logarithmic region. Zero-plane displacement height d_p is defined as the distance from roughness crest into the roughness layer, where the flow velocity is zero (e.g. Nikora et al. 2002). Similarly, flume and field observations both show that water depth has a strong control over the size of large-scale flow structures. These flow structures have typically a length of three to five times flow depth and a width and height of approximately equal to flow depth (Roy et al. 2004; Shvidchenko and Pender 2001). Thus, roughness size and flow submergence, which are the determinant of flow resistance are the dominant factors for velocity suppression in the near-bed region.

A simplified schematic of velocity distributions normalised by shear velocity for three different flow submergences are shown in figure 3.8 b, which indicates velocity deviation from the logarithmic law with flow submergence in the near-bed region.

ii- Reynolds stress

Turbulent stress or Reynolds stress is a component of total stress tensor inserted on the bed by the fluid, which are the net rates of transfer of momentum resulting in from turbulence in the fluid. The Reynolds stress is developed due to the turbulent fluctuations and are represented by the time-average of the quadratic terms of the velocity fluctuations $\overline{\rho' u' w'}$. In turbulent flow, the Reynolds stress is by far outweighing the viscous stress, thus it is considered important to understand the Reynolds stress distribution in the near-bed region. In a logarithmic distribution of flow velocities, the Reynolds stress is shown by a straight line indicating zero values at the water surface, which linearly increases with water depth and reaches its maximum values over the top of roughness crest. However, flume experiments by (e.g. Nakagawa et al. 1991) shows that the Reynolds-stress distribution in the roughness sublayer region is degenerated and suppressed (figure 3.7 c). Recent flume studies employing PIV and UPV measuring techniques shows that Reynolds stress distribution degenerate right above the roughness crest and reduces rapidly below the crest toward the bed surface, while in the upper flow zone, the Reynolds stress distribution is reasonably consistent with linear law as shown in figure 3.8 c (e.g. Mohajeri et al. 2015; Manes et al. 2009). The flume results for mobile and immobile beds shows that Reynolds stress diminishes more in the mobile bed than in the immobile bed in particular in the near-bed regions, however, at upper zones, the difference is indistinguishable (Dey et al. 2011). The stronger damping in Reynolds stress for mobile bed is attributed to the provided momentum for the flow to maintain the bed particle in motion. Flow submergence is shown to have no consistent or appreciable influence on the spatial variance in the Reynolds stress (e.g. Cooper et al. 2013). Reynolds shear stress distribution provides a clear idea of the truly available shear stress in the flowing fluid in particular in the near-bed region, where the sediment entrainment occurs.

iii- Form-induced stress

Spatial fluctuations of time-averaged velocities known as form-induced stress is generated as a result of flow vortices separation from roughness elements give as $-\rho \langle \tilde{u} \tilde{w} \rangle$ (Giménez-Curto and Lera 1996). In other words, the form-induced stress is the streamwise averaged momentum flux caused by the spatial variance in the time-averaged flow. If the value of $-\rho \langle \tilde{u} \tilde{w} \rangle$ is positive, it extracts momentum from the flow in the streamwise direction while a negative value defines a situation in which the form-induced stress enhances the fluid momentum in the streamwise direction and therefore enhances the sediment entrainment as well. Inside interfacial sublayer, form-induced stress continues to increase often reaching a first peak and subsequently either decreasing or switching from a negative to positive contribution to the fluid stress depending on the sign of \tilde{u} and \tilde{w} and on the manner the time-averaged flow is coherently structured (e.g. Cooper et al. 2013).

At shallow flows, form-induced stress within the roughness layer is found to have greater significance, which is primarily driven by a higher spatial flow variance in time-averaged stream-wise velocity (figure 3.8 d). However, it is negligible at distances 1-2 k_s above the roughness crest (Cooper et al. 2013). The contribution of form-induced stress is found to

be up to the 20% of spatially averaged Reynolds stress at the roughness crest (Cooper et al. 2013) and between 15% to 35% of the total measured shear stress in the roughness layer (Campbell et al. 2005) depending on the flow submergence and occurrence of bedload transport.

Flume experiments show that form-induced stress is decreased when the sediment feeding rate is increased because the roughness geometry is changed due the sediment deposition in spaces between roughness crests (troughs) leading to a smoothed bed (Campbell et al. 2005). Bed geometry control is also shown by Cooper et al. (2013) in flume experiments for different flow conditions and a single bed surface that all produced similar profile shape for spatial flow variance and form-induced stress. These results are suggesting that bed geometry has a strong control on the vertical distribution of flow variance and on the vertical organisation of time-averaged flow within the roughness layer.

To sum up, form-induced stress is contributing significantly to total stress in the roughness layer region in particular its contribution is increasing with decreasing flow submergence. A negative contribution of form-induced stress counteracts the total shear stress and reduces the overall shear stress acting on the sediment particles on the bed, while a positive contribution increases the total shear stress.

iv- Turbulence intensity:

The degree of flow velocity fluctuations is considered as an important characteristic of turbulent flow expressed by root mean square (RMS) known as turbulence intensity. The turbulence intensity in streamwise and vertical directions are given by $\sqrt{\langle u'u' \rangle}$ and $\sqrt{\langle w'w' \rangle}$ respectively, which are often scaled by either shear velocity u_* or depth-averaged flow velocity \bar{u} .

Turbulence intensity induces an additional instantaneous shear stress to time-averaged shear stress that is termed as effective shear stress for initiation of sediment motion. On the other hand, the induced pressure fluctuations by turbulence give rise to the lift forces acting on a sediment particle, which makes it easier to dislodge (e.g. Zanke 2003).

Turbulence intensity is zero at the boundary, increases to its maximum value at the roughness crest and achieves a constant value away from the boundary in the main flow region (e.g. Lamb et al. 2017; Grass 1971). While the vertical turbulence intensity component approaches the shear velocity $\sqrt{\langle w'w' \rangle} / u_* = 1$ at the main flow region, the streamwise component is slightly larger than shear velocity $\sqrt{\langle u'u' \rangle} / u_* > 1$.

The boundary roughness has a strong control on the near-bed turbulence intensity distribution, namely as the roughness increases, the streamwise turbulence intensity decreases, whereas the vertical component increases (e.g. Grass 1971). Flume experiments with a sediment feeding show that streamwise turbulence intensity is enhanced throughout much of the flow depth in the presence of bedload compared to clear water case. This finding supports the idea that bedload extracts momentum from the mean flow (Campbell et al. 2005). The influence of flow submergence on the near-bed turbulence intensity in a permeable bed flume shows that turbulence intensity is damped at low flow submergence

above the roughness crest. It decreases linearly inside interfacial sublayer with no appreciable difference due to the flow submergence and it decays exponentially within the permeable bed as shown in figure 3.8 e (Manes et al. 2009). Similarly, Carollo et al. (2005) showed that a decrease in flow submergence also causes a decrease in the peak value of turbulence intensity at the top of roughness crest. This is confirming that more penetrating roughness elements into the flow field lead to more effective turbulence damping.

Flume experiments at shallow flows reveal that the vertical distribution of turbulence intensity and Reynolds stress are largest close to the roughness crest and reduce below the roughness crests (Aberle and Koll 2004; Cooper et al. 2013), as shown in figure 3.8 e and c respectively.

Turbulent intensity both within and above roughness layer is decreasing with increasing flow submergence in the streamwise direction, however, in the vertical direction, the spatial variance with flow submergence is considerably low (Cooper et al. 2013).

Turbulence intensity and turbulent kinetic energy are influenced by roughness and flow submergence, namely an increase in roughness or a decrease in flow submergence leads to a reduction in turbulence intensity. This indicates that at steep slope IRS, the turbulence intensity is strongly damped due to the presence of roughness elements and low water depths and hence reduces the sediment entrainment capacity of the flow discharge.

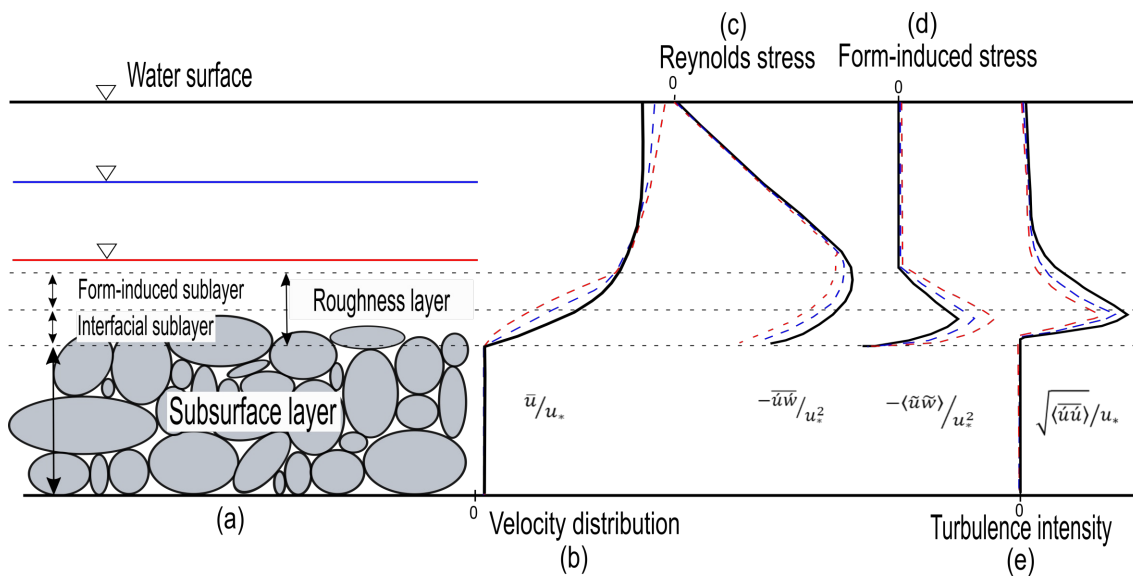


Figure 3.8.: Schematic view of permeable bed (a) average flow characteristics in the roughness layer normalised by shear velocity (b) velocity distribution (c) Reynolds stress (d) form induced stress and (e) turbulence intensity for three different flow submergences

The turbulence properties of open channel flows with hydraulically rough beds for high flow submergence reveals similar behavior to those flows over smooth beds, at least at

distances sufficiently larger than the roughness height. The logarithmic distribution of flow velocity is shown to be valid for the regions above roughness layer (inner region to water surface), however, it deviates strongly from logarithmic law in the near-bed region (i.e. within roughness layer). Similarly, Reynolds stress is strongly degenerated in the near-bed region and reduces rapidly below the roughness crest toward the bed surface. At shallow flows, form-induced stress within the roughness layer is found to have greater significance, which is primarily driven by a higher spatial flow variance in time-averaged stream-wise velocity. Turbulence intensities induce an additional instantaneous shear stress to time-averaged shear stress that is termed as an effective shear stress for initiation of sediment motion.

The near-bed flow characteristics for steep IRS indicate that the sediment entraining parameters are reduced as a result of increased flow resistance, due to the presence of coarse channel bed and low flow submergence.

3.3.3. Role of macro-roughness elements in changing the hydrodynamic forces on sediment particles

3.3.3.1. Effects on the hydraulic of the near bed regions

In mountainous IRS, MRE are composed of large rocks and boulders protruding from the channel bed (figure 3.9 a). The presence of macro-roughness alters the local flow velocity, flow resistance, as well as the near-bed turbulence and shear stress. The macro-roughness influence on the flow resistance not only depends on macro-roughness size but also on spatial density and pattern (e.g. Canovaro et al. 2004). According to a rational definition by Morris (1955), the formation of wakes behind the MRE is resulting in turbulence and energy dissipation. He further classifies the roughness flow into three basic types based on longitudinal spacing L_D , namely isolated roughness flow $L_D/D_B = 10$, wake interference flow (transitional) $L_D/D_B = 7$ and quasi-smooth flow $L_D/D_B = 3$. Large eddy simulations over the mentioned three roughness configurations show an increased turbulent and Reynolds stress fluctuations above isolated roughness compared to smooth roughness (Stoesser et al. 2004). Extensive investigation on the influence of single isolated boulder on hydrodynamic and sediment transport processes around the boulder is examined by Papanicolaou and Tsakiris (2017). Their key findings can be summarised as:

- i- Under high relative submergence (HFS) $h/D_B > 1$, a mean flow recirculation region in the near wake occurs and extends $1.0 D_B$ downstream of the boulder with decelerated and even reversal flow (figure 3.9 b). Due to the additional form-drag as a result of interaction between boulder and flow, the bed shear stress and or sediment transport capacity are reduced within the boulder wake region. As a result of the reduced bed shear stress, a depositional area downstream of the boulder forms.
- ii- Under low relative submergence (LFS) $h/D_B < 1$, velocity profile has an S-shape

profile in the proximity of, and linear shape further downstream of the partially submerged boulder. Unlike high HFS, the flow accelerates downstream of the boulder, due to the standing wave constricting the mean flow and in upstream a deceleration flow with low shear is observed. Therefore, the depositional area occurred in the stoss side of a boulder (figure 3.9 b).

Flume experiments on the regular pattern of the macro-roughness element by Canovaro et al. (2004) indicate that the maximum resistance was achieved at strip wavelength $L_D/D_B = 10$ at which the drag induced shear stress is as high as 80% of the total bed shear stress. This optimal spacing of transverse strips produced in flume is close to the geometrical spacing between step-pool frequently encountered in natural streams (Canovaro and Solari 2007). This indicates that streams step-pool form evolves to maximise the resistance to flow and therefore achieves an optimum stability (Abrahams et al. 1995). The effect of slope on flow resistance and velocity distribution in presence of MRE is found to achieve a maximum velocity gradient at steep slopes and relatively low MRE concentrations $L_D/D_B = 9 - 18$. At low slopes, however, the higher macro-roughness concentrations results in more effective flow resistance (Wohl and Ikeda 1998).

An increase in pebble concentration is found to first increase the flow resistance and achieves an asymptotic behaviour and then decreases (Hassan and Reid 1990; Canovaro et al. 2004). The spatial density between 0.2 to 0.4 and transversal strip pattern planimetric arrangement of MRE causes the highest resistance to flow and highest energy dissipation. At this setting, the maximum values for ratios of drag shear stress τ_d due to MRE to total shear stress $\tau_d/\tau_g = 90\%$ (Canovaro and Solari 2007).

Additionally, a distinctive pressure field is produced by the particle projecting from an alluvial bed by distorting the flow field around it. This distortion has a significant effect on the entrapment and entrainment of neighbouring particles and is considered as a primary cause of pebble clusters and boulder shadows. Brayshaw et al. (1983) observed a linear relationship between the lift and drag forces with the separation between obstructing particles on the wake (lee side). However, drag does not vary with separation on the stoss side, but the lift is increasing with decreasing separation.

3.3.3.2. Hiding effect of MRE

MRE on the riverbed protect the finer size sediments beneath them from erosion. Experiments reveal that MRE may also reduce the shear stress in their neighbourhoods by altering the flow velocity and turbulence. Papanicolaou et al. (2012) showed that the shear stress around a fully submerged boulder roughly reduced to 50%. The influence of the macro-roughness size is reflected in the sediment transport capacity such that at a given L_D/D_B and channel slope, the transport capacity decreases with increasing macro-roughness diameter (Ghilardi et al. 2014).

On the other hand, large MRE are immobile at most of the occurring flows and hide the finer grains beneath them, thus preventing finer grains from being transported, which also means that the exposed area to erosion is reduced.

3.3.3.3. MRE effects on the bed roughness and flow resistance

Laboratory experiments with tilting flume indicate that at higher stream power (i.e. higher discharge and bed slope), the fluctuation of bedload pulses in duration and amplitude decreased. This implies that a higher concentration of MRE increased the critical stream power for bedload transport (Ghilardi et al. 2014). Another flume experiments showed that bedload transport can be reduced by as much as 60% when 15% of the flume area is covered by boulders, compared to flume without boulder coverage (Ghilardi and Schleiss 2012). Their study included randomly placed and half buried MRE into poorly sorted flume bed sediments with $L_D/D_B = 2, 3, 5, inf$ and diameter $D_B = 0.1 m$. Their findings are outlined as (i) slope has the strongest impact on sediment critical discharge, namely at higher slope, higher sediment transport rates were observed (ii) sediment transport rates decreases with increasing distance between MRE and (iii) The sediment transport rate decreases with increasing MRE diameter at a given L_D/D_B and bed slope.

In summary, the presence of MRE such as boulders, cobbles and pebbles, may strongly control the sediment transport in rivers and streams. They may strongly reduce the total exposed riverbed area to erosion depending on their spatial density as hiding elements leading to stability of the riverbed. Secondly, isolated MRE on the riverbed alter the flow characteristics and reduce the shear stress around them otherwise available for sediment transport. Finally, their spatial arrangement is providing the rivers and streams with the highest resistance to flow to maximise the flow energy dissipation, in order to ensure optimum stability for the riverbed.

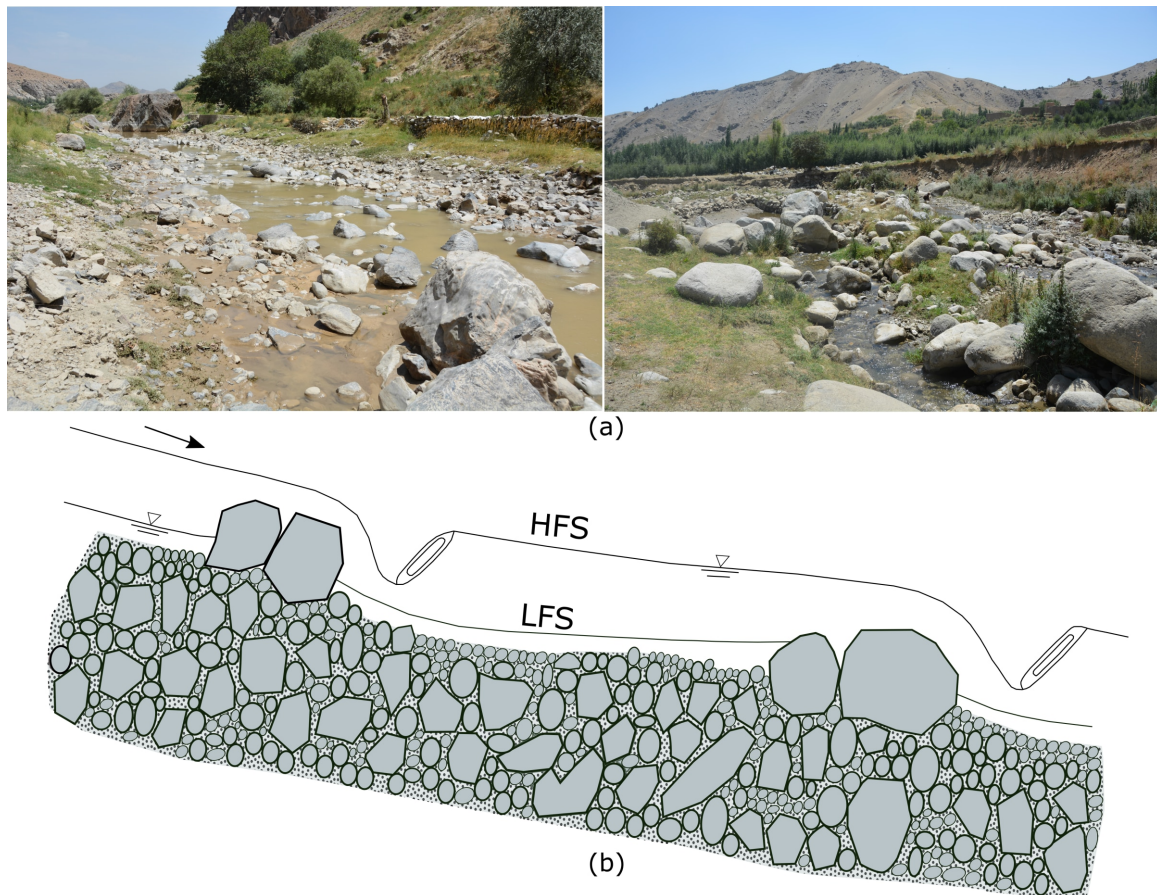


Figure 3.9.: MRE on a natural IRS riverbed (a) and (b) their impact on the flow conditions under high (HFS) and low flow submergence (LFS)

3.3.4. Methods for adjusting near-bed flow hydraulics for steep slopes

Rough-turbulent flow in steep IRS with low flow submergence shows distinct characteristics. Certain bedload transport related flow parameters such as shear stress, flow velocity, Reynolds stress, turbulence intensity, and form-induced stress strongly deviate from the flow with sufficient flow submergence.

A number of approaches have been developed for estimating the average flow characteristics for the near-bed region to account for the increased flow resistance in mountainous IRS (refer to table 3.2). Double-averaging of Navier-Stokes equations (DANS) are generated by averaging the Navier-Stokes equations twice (in time and spatial domain). As a result of DANS, additional terms such as form-induced stress, drags and viscous-induced stress due to the protruding bedforms is taken into account. Therefore, DANS are shown to perform better than Reynolds average Navier-Stokes equations (RANS) for approximating flow variables in the near-bed region with small relative submergence, three-dimensional and spatially heterogeneous flow in gravel-bed rivers (Giménez-Curto and Lera 1996;

Nikora et al. 2001). The double averaging results in two terms namely the force due to mean momentum flux for boundary disturbances (form-induced stress $(-\rho \langle \tilde{u}\tilde{w} \rangle)$) due to vorticity of disturbed motion by flow separation from roughness and force exerted by the roughness elements on the fluid while the earlier is shown to dominate the bulk resistance in low relative submergence condition (Giménez-Curto and Lera 1996; Nikora et al. 2001). The DANS equations are generated by averaging the Navier-Stokes equations twice (in time and spatial domains). The DANS apply to any instantaneous variable (θ) (i.e. velocity), a decomposition in which the spatial variability is taken into account. The decomposition is similar to Reynolds decomposition for time-averaging (Nikora et al. 2001).

The flow resistance approaches, modify the flow resistance equations like Chezy, Manning, and the Darcy Weisbach to approximate mean flow velocity for the near-bed region of mountainous IRS. The flow resistance equations are relating the average flow velocity \bar{u} to the relative flow submergence h/D_{84} assuming either a logarithmic or power-law velocity distributions.

The first approach modifies the logarithmic laws suitable for high submergence predominantly in terms of roughness height k_s , Von Karman value k and B_r value in the (Keulegan 1938) flow resistance equations as listed in table 3.2. The roughness height in the flow resistance equation is expressed as some multiple of D_{84} ranging $2.2 D_{84}$ - $3.5 D_{84}$ to include a small-scale form-drag on protruding clasts. With this modification, a better fit of field measurements are achieved (Bathurst 1985; Bray 1979; Hey 1979; Thompson and Campbell 1979). The Von Karman value is observed to have a value of 0.4 for high relative submergence flow, however, Dittrich and Koll (1997) found that with $k = 0.18$, log-profile better fitted with measured velocity in low relative submergence condition. The B_r value generally depends on the cross-sectional shape (Keulegan 1938) or relative submergence Kironoto and Graf (1994) and its variation has limited influence on the near-bed velocity estimation.

A second approach is focused on modifying the exponent $1/6$ in Strickler equation based on the flow submergence level h/k_s . A generalised power-law flow resistance equation is expressed by Strickler equation in table 3.2. The values for constants a_1 and b_1 are derived based on the best fit with the measured data. The value of b_1 is found to vary with relative submergence h/k_s . The value of exponent b_1 is reported to be $1/6$ for $10 < h/k_s < 100$, $1/2$ for $1 < h/k_s < 10$ and 1 for $1 < h/k_s < 2$ (Carson and Kirkby 1972). Bathurst (2002) analysed 27 field data from gravel-bed rivers and found that for shallow streams of gradient $S < 0.8\%$, a value of 3.84 and 0.55 and for $S > 0.8\%$ a value of 3.10 and 0.93 for the exponent a_1 and b_1 respectively, results best fits with his measurements. Similarly, for step-pool streams with emergent clasts, the best fit is achieved with $b_1 = 1$ (Comiti et al. 2007; Lee and Ferguson 2002). Smart et al. (2002) showed a good fit for rough-flume data with a value of 0.5 for b_1 .

The wide-variety of values for a_1 and b_1 indicates that these parameters are very site-specific and are chosen based on fitting with measured data. The pre-factor a_1 values have a strong influence on the velocity distribution, namely, velocity decreases with decreasing

a_1 however, at low flow submergence, the difference is decreasing. The near-bed velocity decreases with increasing values of b_1 values, however at flow submergence larger than 1, the influence of b_1 is reversed.

In the third approach, near-bed flow velocity is estimated from flow discharge using empirical relations, because in small and rough mountainous streams, the measurement of flow depth is erroneous due to the fact that a zero depth level is difficult to be defined because of irregular bed topography (Zimmermann et al. 2010; Comiti et al. 2007; Ferguson 2007; Aberle and Smart 2003; Rickenmann 1994). A general form of average flow velocity as a function of discharge is given in table 3.2. The constants C and m_1 are determined empirically. The equation $\bar{u} = CQ^{m_1}$ is similar to equations derived using the regime concept (Lacey 1930) and hydraulic geometry concept (Leopold and Maddock 1953) by employing mean water depth and mean channel width as a function of flow discharge. The exponent m_1 is found to indicate the rate of change in velocity as a result of a change in flow resistance. Bathurst (1993) concluded that at high flow submergence, bed material roughness is the dominant cause of flow resistance. He found the m_1 value to vary from $m_1 < 0.4$ for sand-bed, from 0.45 to 0.55 for gravel-bed, cobble-bed and boulder-bed streams and $m_1 > 0.55$ for step-pool and riffle-pool streams.

The fourth approach is focused on the dividing of total flow resistance in streams and channels into components related to the channel features also termed as flow resistance partitioning. The flow resistance in streams and channels are often divided into two main components namely grain and form resistance. The grain resistance also known as base level resistance f_0 is generated by grains composing the bed surface without the bedforms such as sediment grains on a plane bed, which causes energy losses as a result of skin friction on the individual particles. The form resistance is an additional resistance due to bedforms or other sources of form drag (e.g. isolated boulders, cobbles) or large woody debris, therefore the term additional resistance f_{Add} is preferably used here. The total flow resistance f_{tot} is the sum of grain resistance and additional resistance as usually shown in form of Darcy-Weisbach friction factor as $f_{tot} = f_0 + f_{Add}$. The partitioning has a wide-range of implications for hydraulic, sediment transport and channel morphology investigations. The additional resistance reduces the flow energy otherwise available for sediment transport. Thus the aim of flow resistance partitioning is to estimate the net flow energy available for sediment transport, which is often less than total flow energy. While the calculation and measurement of f_0 are straightforward, the f_{Add} is difficult to measure directly using existing approaches and methods. In natural streams and rivers, the f_{Add} is composed of several other resistance sources such as form resistance due to bars and riffle-pool in lower reaches, spill resistance and resistance due to large woody debris in step-pool streams at steep slopes. These all add to the complexity of measuring or calculating the f_{Add} , therefore, it is often estimated by measuring the total resistance and subtracting the measurable component (i.e. grain resistance) from total resistance. The flow resistance partitioning has an important implication for sediment transport in rivers and streams characterized by additional roughness elements. The variables related to flow resistance such as bed shear stress, energy slope, Darcy-Weisbach friction factor,

shear velocity and flow depth can be partitioned into distinct components. The flow resistance partitioning approach is applied for steep streams by modifying the energy slope (Chiari and Rickenmann 2011). The energy loss due to the additional roughness can be taken into consideration by multiplying the energy slope with the ratio of grain resistance to total resistance f_0/f_{tot} , which results in a reduced energy slope. The total energy slope can be calculated using Manning-Strickler or Darcy-Weisbach equations as shown in table 3.2. The reduced energy slope is associated with base level roughness or grain roughness only and is used for estimating bedload transport. The value of e is theoretically determined to vary from $4/3$ to 2 based on the best fit achieved for the flume experiments of bedload transport with $e = 1.5$ (Meyer-Peter and Müller 1948). The exponent e is used as calibration parameter and is accounting for energy loss due to macro-roughness in rough flumes and channels (Chiari and Rickenmann 2011).

The flow resistance partitioning approach modifies the energy gradient, which in turn reduces the bed shear stress to account for the increased flow resistance in steep channels. It basically determines the share of shear stress acting on sediment grains, which is a fraction of the total flow shear stress. The flow resistance partitioning approach can function independent of the type of bedload equation used for estimation of bedload. Thus, bedload transport in steep IRS can be predicted using the flow resistance partitioning approach, and to avoid the overestimation of bedload transport as a result of overestimating the actual energy gradient acting on the mobile sediments.

A fifth approach focuses only on the boundary layer (roughness layer) in shallow flows in which the velocity profile deviates from a logarithmic velocity distribution. The near-bed profile deviates from logarithmic in roughness layer and below a relative submergence $h/D_{84} < 4$, there is no boundary layer in the conventional sense. Roughness layer approaches for shallow flows are basically utilizing mixing layer analogy of turbulent flow within and above rigid vegetation canopies, where the structure of the turbulent airflow near porous roughness elements resemble the mixing layer with an inflection just over the roughness crest (Katul et al. 2002). The inflection point is connecting high-velocity region above the roughness crest to the low-velocity region below and within the porous bed. The inflection in velocity profile is mainly due to the turbulent eddies generated in and below the shear layer at the top of the canopy or roughness elements crest. Katul et al. (2002) suggested a hyperbolic tangent function for the mean velocity, assuming the thickness of mixing layer as roughness element size $L_s = k_s$, the flow resistance equation is derived as shown in table 3.2. Where L_s is a characteristic energetic eddy size (i.e. mixing length) typically generated at $z = k_s$, by a Kelvin-Helmholtz type instability and the mean reference velocity at $L_s = k_s$, is denoted by u_0 . In case of low relative submergence in which roughness element protruding the water surface $h/D_{84} < 1$, the resistance is mainly due to form-drag $f \propto h/D_{84}$ (Lawrence 1997; Nikora et al. 2001).

A brief summary of the existing approaches and their limitations for application in estimating near-bed flow characteristics for mountainous IRS are given in table 3.2. The reviewed methods and approaches to account for the increased flow resistance in steep IRS have their own application range and limitations. The double averaging of Navier-Stokes

Table 3.2.: Approaches for adjusting the near-bed flow hydraulics for steep IRS

Approaches	Principle	Governing equation	Application limitation
Double-averaging of Navier-Stokes equation	Improved flow variables estimation in the near-bed region	$\theta = \langle \bar{\theta} \rangle + \tilde{\theta} + \langle \theta' \rangle + \tilde{\theta}'$	Requires high computational capacity and high resolution riverbed geometry data
Modified logarithmic law	Reduces near-bed flow velocities by reducing k , h/D_{84} and increasing B_r values	$\sqrt{\frac{8}{f}} = \frac{1}{k} \ln\left(\frac{h}{k_s}\right) + B_r$	Requires measured velocities for validation and detailed information of flow submergence h/D_{84}
Generalised power-law or non-dimensional hydraulic geometry	Reduces near-bed flow velocities by decreasing pre-factor and increasing exponent in the Strickler equation	$\sqrt{\frac{8}{f}} = a_1 \left(\frac{h}{k_s}\right)^{b_1}$	Requires a number of parameters such as water depth, channel slope, and D_{84}
Estimating velocity from unit discharge	May lead to realistic velocity estimation in rough steep channels	$\bar{u} = CQ^{m_1}$	Requires a number of parameters such as water depth, channel slope, and D_{84}
Flow resistance partitioning	Reduces the bed shear stress by taking into account only a fraction of total shear stress for bedload transport	$S_{red} = \left(\frac{n_{tot}}{n_0}\right)^e = S\left(\sqrt{\frac{f_0}{f_{tot}}}\right)^e$	Requires additional information for the total flow resistance estimation
Roughness layer models based on mixing layer analogy or concept of form-induced stress	Reduces flow velocity over the roughness layer	$\frac{\bar{u}}{u_0} = 1 + \tanh\left(\frac{z-k_s}{L_s}\right)$	Requires the relative flow submergence data h/D_{84}

equation (DANS) is shown to well reproduce the flow characteristics in particular in roughness layer region. However, the DANS increase the computation time, because of additional terms (i.e. form-induced stress and drags, viscous-induced drags), which limit its application for larger computation domains.

The modification based on the flow resistance approaches (logarithmic and power-law) depends strongly on the relative flow submergence h/D_{84} . While the determination of h/D_{84} for flume condition is straightforward, it has very diverse spatial distribution in natural rivers and streams due to the existence of MRE and small water depths. Nevertheless, the modified logarithmic and power-law methods with average flow submergence may help improving the prediction of near-bed flow velocity.

3.4. Summary

Chapter 3 presents key controls on the bedload transport in mountaineous IRS. Regardless of types of bedload transport equations and their derivative background, the hydraulics and sedimentological characteristics of bedload equations can be modified to predict realistic rate of bedload for steep IRS. The need for such a modification is revealed from the slope dependency of bedload incipient motion from various flume and field investigations that shows increasing critical shear stress with steeper channel slopes. On the other hand, bedload transport is strongly controlled by the availability of mobile sediment particles in the IRS. Sediment supply and hydrograph peakyness is shown to strongly control the layering of sediments with larger sediment supply and high

hydrograph peakyness leads to abundance of fine sediment on the bed surface. As a result, bedload measurement in some IRS reveals much larger rates compared to their preennial counterparts in which the existing of base flows causes generation of armouring layer that protects finer subsurface sediments from erosion. A secondary control on the riverbed sediment is the phenomon of clogging, which is caused by settling of fine particles on the coarse gravel-bed and cements the riverbed as flush floods on IRS receds very quickly. The clogging increases the riverbed resistance against erosion at early stages of flow resumption in the following season.

In the second part of chapter 3, the hydraulics of steep IRS is studied in detail. Bedload transport relevant near-bed parameters such as flow velocity, Reynolds stress, form-induced stress and turbulence intensity are reviewed for rough steep IRS. The mostly used logarithmic distribution of flow velocity as major bedload transport parameter is shown to be no longer valid for steep IRS with low relative flow submergence. With exception of the form-induced stress that increases with an increase in channel roughness, the rest of the bedload moving parameters reduces in near-bed region (roughness layer). In steep IRS, channel roughness including the MRE, their arrangements (i.e. cascade or step-pool forms) and their relative submergence have significant control on the channel resistance to flow and bedload transport. The MRE not only alter the flow velocity and resistance in their locality but also reduce channel-bed area exposed to erosion.

Subsequently, some common approaches for modifyiny and adjusting the flow parameters developed for high flow submergence rivers in lowland regions to steep IRS are discussed. Double -averaging of Navier-Stokes equations (DANS) and flow resistance approaches (i.e. modified logarithmic law, generalized power-law and others) can be applied to steep IRS for a realistic estimation of flow resistance and bedload transport estimation. However, their application is limited to small computation domains and well controlled flume experients. DANS for instance requires high resolution geometry information and computation capacity, while modified flow resistance approaches require at least flow submergence h/D_{84} information. These make their application on steep IRS with variable flow submergences and scarce channel information impossible. Therefore, it is required to think of a different approach that overcomes the lack of detailed channel data but at the same time accurate enough for estimating bedload transport in IRS. Thus, in this study, a regime channel approach is used to estimate the channel flow resistance and bedload transport while assuming an IRS reach in morphodynamically equilibrium condition as disscused in detail in chapter 4.

4. Methods

4.1. Channel regime concept

The literature review in chapters 2 and 3 revealed that near-bed flow characteristics in steep IRS deviate strongly from high flow submergence rivers in lowland regions. If the flow parameters are not adjusted to steep IRS, the resultant bedload transport is overestimated. Further, the approaches on how the flow parameters (i.e. velocity, shear stress) can be modified to represent the hydraulics of steep IRS have their own limitations in particular in terms of flow submergence data and its diverse variations in nature. These all make a small spatial scale analysis of flow resistance very difficult, therefore a reach-scale study of flow resistance by a extremal hypotheses (regime channel approaches) are one viable options to test.

In mountaineous environment, most of IRS experiences regular flow as a result of snowmelt and precipitation. Sediment is delivered to the channel from upstream catchment, and hillslopes by the action of gravity, avalanches, wind or all combined. Some typical IRS reaches in north-east Afghanistan are shown in terms of flow resistance variations (recognised visually by flow areation) and channel regime slopes (derived from 5 m resolution digital surface model) in figures 4.1 (a to e) and 4.2 respectively. The relationship reveals a systematic correlation between channel slope and flow resistance. This relationship supports using a channel stability theory or regime channel approach for quantifying the relationship between relative flow resistance and channel regime slope. This approach determines the contribution of flow energy actually contributing to bedload transport in steep IRS.

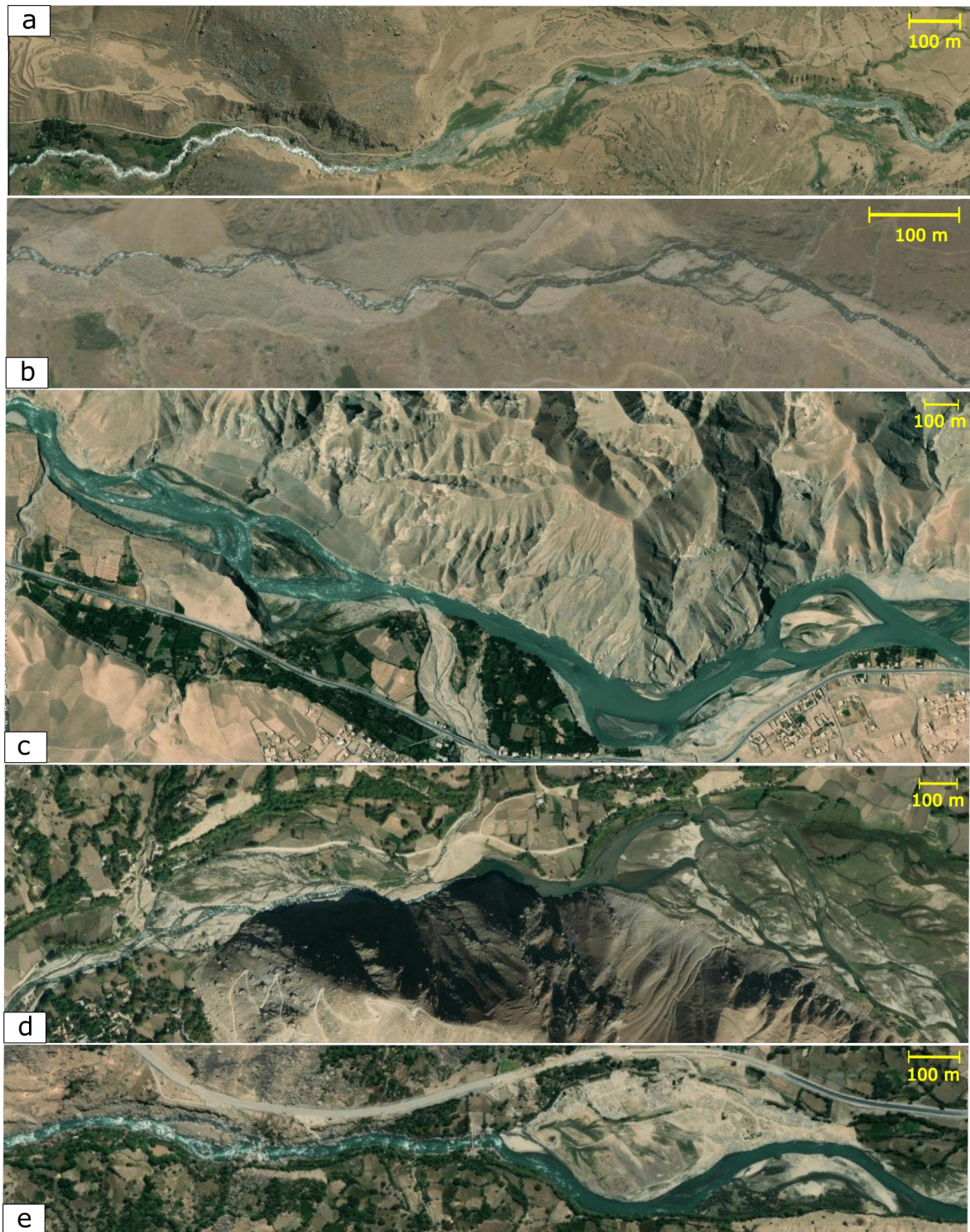


Figure 4.1.: Five river reaches in north-east Afghanistan showing variable flow resistance in (a to e)

Imageries: Esri, DigitalGlobe, GeoEye, Earthstar Geographics, CNES/Airbus DS, USDA, USGS, AeroGRID, IGN, and the GIS User Community

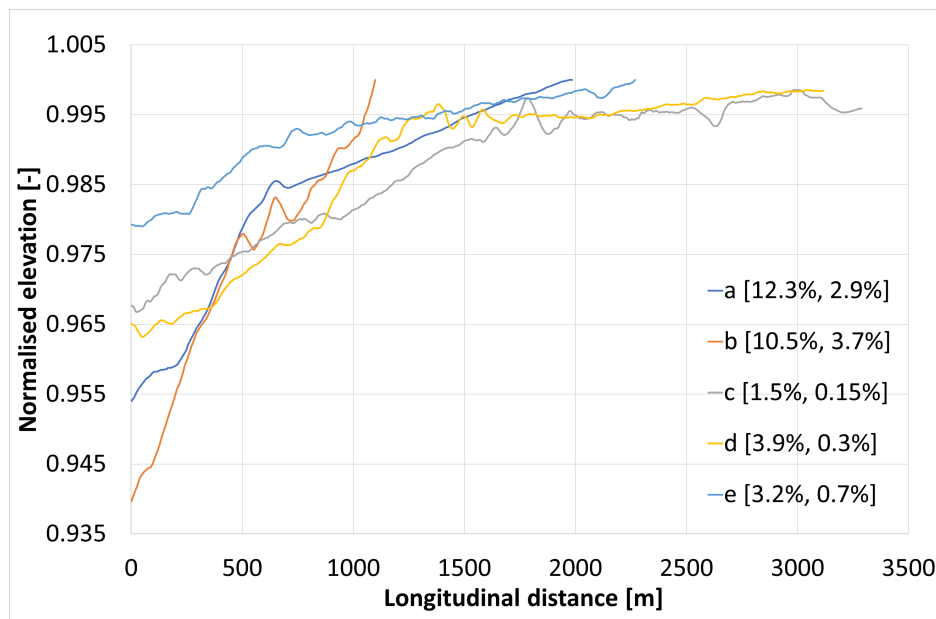


Figure 4.2.: Longitudinal profiles for river reaches in figure 4.1. For each reach two distinct slope can be recognised as listed in the legend

There are mainly three groups of alluvial channel regime methods (i) empirical (regime theory and power-law) (ii) rational or mechanistic and (iii) extremal hypothesis. Despite critiques, regime methods based on extremal hypothesis is reported to predict equilibrium geometry of rivers better than empirical and rational methods (Farias et al. 1998; Huang et al. 2014). However, there are large number of extremal hypothesis methods to use such as minimum Froude number (MFN), minimum stream power, minimum unit stream power, maximum transport rate, maximum friction factor, minimum energy dissipation rates and many more. Despite their development by different researchers, some of these approaches tend to be equivalent and give identical results (e.g. Joshi et al. 2018). In this study, the relationship between regime channel dimensions and flow resistance in steep IRS are discussed in light of MFN as it has produced good agreement with field data (Yalin and da Silva 2001; Joshi et al. 2018). Therefore, MFN is discussed as representative of extremal hypothesis for describing the steep IRS development.

4.1.1. Description of gravel-bed rivers regime theory

An alluvium stream does not accept any channel given by nature or men but modifies the provided channel to create a certain channel of its own, which is referred to as regime (equilibrium) channel (Yalin and da Silva 2001). Channel regime state represents a long term average characteristics of a river rather than an instantaneously variable state; hence under ideal condition, regime channels do not vary over time. An alluvium channel adjusts its slope and geometry (width and depth) to develop a dynamically stable state that can convey a certain discharge and sediment (Yalin and da Silva 2001).

The regime theory is as a result of pioneering works of (e.g. Lacey 1930; Inglis 1949; Leopold and Maddock 1953; Blench 1957; Wolman and Miller 1960; Yang 1976; Yang and Song 1979; Andrews 1980) based on the conviction that a stream tends to achieve regime state because one of its energy-related characteristics A_* tends to acquire a minimum value. The three unknowns namely stream regime width w_R , depth h_R and slope S_R are determined by solving simultaneously the following three equations:

$$Q = F_Q(w_R, h_R, S_R, c_R) \quad \text{Resistance} \quad (4.1)$$

$$Q_b = F_{Q_b}(w_R, h_R, S_R, c_R) \quad \text{Transport} \quad (4.2)$$

$$dA_* = 0 \quad \text{Minimum energy – related} \quad (4.3)$$

The equations 4.1 and 4.2 are flow resistance and sediment transport equations respectively. While equation 4.1 can be easily solved, equations 4.2 and 4.3 are not very straightforward, because the determination of h_R , w_R and S_R is only possible when the value of Q_b is known beforehand, and yet it is hardly available except for controlled laboratory experiments (Yalin and da Silva 2001). Further, the equation 4.3 is difficult to be solved, due to the uncertainty associated with the physical nature of A_* . Therefore, the value of Q_b in equation 4.2 is substituted by a w_R -relation, which does not involve Q_b . Similarly, to solve equation 4.3, the physical nature of A_* must be identified (Yalin and da Silva 2001).

There is yet no universal agreement for definition of energy-related characteristic A_* of the regime channel. Yalin and da Silva (2001) employed the principles of thermodynamics to reveal the energy-related characteristic A_* by a minimum stream velocity u_{min} . The rivers and streams tend to alter its slope, geometry and effective roughness to minimise its velocity, therefore:

$$A_* = u_{min} \quad (4.4)$$

The final thermodynamic equilibrium is reached when the channel mean velocity achieves zero value $\bar{u} = 0$ when no constraints are present (Yalin and da Silva 2001). In reality; however, the effect of constraints such as sediment transport rate and or bedforms impose a condition such that the channel formation is stopped before the final equilibrium is reached. At this state, the channel formation is factually terminated, which is commonly referred to as regime state (Yalin and da Silva 2001). Channel width and slope are the main adjusting parameters in a wide alluvial channel, while the flow depth is a characteristic of flow and not of the channel, however, depth establishes itself depending on an existing w and S by the fulfillment of the resistance equation. Hence, eliminating depth from the continuity $Q = wh\bar{u} = whc\sqrt{ghS}$ and resistance $F_r^2 = \frac{\bar{u}^2}{gh} = \frac{Q^2}{gw^2h^3} = c^2S$ equations results in the following equation:

$$\frac{\bar{u}^3}{F_r} = \frac{gQ}{w} \quad (4.5)$$

The adjustment of w is happening at early stages of the channel regime development, therefore, at the later stages of regime development, w can be assumed as constant. This gives the possibility to express the time derivative of the equation 4.5 as:

$$3\frac{1}{\bar{u}}\frac{d\bar{u}}{dt} = \frac{1}{F_r}\frac{dF_r}{dt} \quad (4.6)$$

The relation 4.6 is showing that at later stages of channel regime development, the relative time-decrement of \bar{u} can be considered to be related to that of F_r by a constant of proportion. The \bar{u} and F_r achieves their minimum values together; thus the F_r can be adopted as a dimensionless measure of A_* .

$$dA_* = F_r \quad (4.7)$$

4.1.2. Computation of regime channel R

Regime channel R is designated to a channel with no sediment feeding at the entrance and the sediment transport at outflow is merely due to the erosion of material forming the channel (Yalin and da Silva 2001). The sediment transport rate $(Q_b)_R$ conveyed by the regime flow along the channel length is therefore solely due to the flow itself. In this case, the $(Q_b)_R$ is a certain function of S_R , h_R , and w_R (Yalin and da Silva 2001). The following six parameters characterize this regime channel:

$$Q, \rho, \nu, \rho_s \text{ or } u_{*c}, D, g \quad (4.8)$$

From the equation 4.8, any quantity related to channel regime R is expressed by:

$$A_R = f_{A_R}(Q, \rho, \nu, \rho_s, u_{*c}, D, g) \quad (4.9)$$

All regime channels (sand and gravel) have a regime width w_R proportional to \sqrt{Q} , this proportionality is ensured if ∂_w is evaluated. It is found from various field and laboratory experiments (Yalin and Da Silva 1997a; Yalin and Da Silva 1997b) that ∂_w can be expressed as:

$$\partial_w = \phi_1(\Xi) \cdot \phi_2((c_f)_R) \cdot c_R = w_R \sqrt{\frac{u_{*c}}{Q}} \quad (4.10)$$

For rough gravel-bed rivers with $(c_f)_R < 21$, the $\phi_2((c_f)_R)$ is assumed to be inversely proportional to the grain roughness namely $\phi_2((c_f)_R) = 1/(c_f)_R$ (Yalin and Da Silva 1999). The material number Ξ reflects the influence of solid $D; \rho_s g$ and fluid $\rho; \nu$ phases and remains unchanged with flow stage because it does not include the shear velocity u_* or water depth h .

$$\Xi = \frac{D(\rho_s g)^{1/3}}{\rho^{1/3} \nu^{2/3}} = \left(\frac{R_e^{*2}}{\tau_{dms}^*} \right)^{1/3} \quad (4.11)$$

Where:

$$\phi_1(\Xi) = 0.639\Xi^{0.3}, \text{ if } \Xi \leq 15; \phi_1(\Xi) = 1.42, \text{ if } \Xi > 15 \quad (4.12)$$

Adopting $A_* = \bar{u}$ and thus $dA_* = F_r$, and replacing the Q_b -equation 4.2 by the w_R -equation 4.10, the following three regime equations are resulted than can be used for determination of w_R , h_R , and S_R :

$$(F_r)_R = Q^2 / (g w_R^2 h_R^3) \quad \text{Resistance equation} \quad (4.13)$$

$$w_R = \partial_w \sqrt{Q / u_{*c}} \quad w_R - \text{equation} \quad (4.14)$$

$$(F_r)_R = c_R^2 S_R \rightarrow \text{min} \quad \text{Minimum } F_r \quad (4.15)$$

A regime channel development can be represented on a so called $F_r; \eta_*$ -plane and is derived from large number of flume and field investigations, which sets the relationship between F_r , relative flow intensity η_* , material number Ξ and dimensionless specific flow rate N as shown in figure 4.3 (Yalin and da Silva 2001).

The relative flow intensity is also known as relative tractive force is referred to as the ratio of acting shear stress to critical shear stress for grain incipient motion:

$$\eta_* = \frac{\tau}{\tau_c} = \frac{gSh}{u_{*c}^2} \quad (4.16)$$

The dimensionless specific flow rate refers to unit flow discharge over channel width for a given grain size and critical shear velocity expressed by:

$$N = \frac{Q}{wDu_{*c}} \quad (4.17)$$

Each value of N refers to a single curve in the $F_r; \eta_*$ - plane, namely, N values are increasing from the gravel-like curves down to the sand-like curves.

The F_r for specified granular material and fluid reduces into the curve-family $F_r = F_r(\eta_*; N)$ as shown in figure 4.3, where the η_* is the abscissa and each F_r curve corresponds to a constant N (Yalin and da Silva 2001). The F_r -curves shown are computed for a single material number Ξ , which is representing a single mean particle size D .

Figure 4.3 also shows the geometric nature of F_r -curve family and the regime points for two different channel characteristics namely sand-like (with a dip point) and gravel-like. If the regime channel formation is sand-like, the regime point $P_R = P_s$, and the dip point $dF_r/d\eta_* = 0$ is located at $(\eta_*)_R \gg 1$ (Yalin and da Silva 2001). The gravel-like regime channel formation is shown by regime point $P_R = P_g$, this is exactly at $(\eta_*)_R = 1$. At $\eta_* < 1$, sediment transport does not occur and therefore no channel formation can take place, thus the F_r curves are only valid in the region $1 \leq \eta_* < \infty$ (Yalin and da Silva 2001). Yalin and da Silva (2001) described the sand-like and gravel-like channel regime formation in $F_r; \eta_*$ plane by the so called rolling ball analogy as follows:

1. The ball rolls on a rough horizontal plane initially at $\eta_* = (\eta_*)_0$ having an initial velocity $u = u_0$. The ball's kinetic energy becomes completely converted by friction into internal energy and the ball stops $u = 0$ at $\eta_* = 0$, which is termed as final equilibrium.
2. The ball cannot reach the final equilibrium $\eta_* = 0$, because it falls into a pit at $(\eta_*)_R \gg 1$, which is termed as total roughness constraint in sand-like development.
3. The ball cannot reach the final equilibrium $\eta_* = 0$, because it is stopped by a barrier at $\eta_* = 1$, also termed as Q_b constraint in gravel-like development.

The sand-like regime channel development occurs in natural sand-bed rivers and streams. The regime state is achieved when the roughness height k_s achieves its maximum value by maximizing the bedforms height (i.e. dunes). The acting shear stress is always larger than the grains' resistance forces $(\eta_*)_R \gg 1$; therefore the bedload transport occurs also in the regime state. The gravel-like regime development achieves its regime state by transporting

all mobile sediment grains until no more mobile grains are available on the gravel-bed. At this point, the acting forces on the remaining sediment grains equal the resisting forces $\eta_* = 1$. The development of a regime channel is shown by the movement of a point m on the $F_r; \eta_*$ -plane (figure 4.3). Initially, at $t = 0$ and $t = T_0^\wedge$, the point m is at P_0 and P_0^\wedge ; at $t = T_R$, it is at $P_R = P_g$ or P_s depending on either it is a gravel-like or sand-like formation (Yalin and da Silva 2001). The point m will follow a path ι within $0 < t < T_R$ to first rapidly approach its related $(F_r)_R$ -curve and subsequently follow this curve closely until it merges into it at its lowest point P_R . At the initial stage $0 < t < T_0^\wedge$, the movement of m is nearly horizontally to the left, because at this stage the channel width w is rapidly developing (increasing) to achieve its regime state, thus causing substantial reduction in η_* than at $T_0^\wedge < t < T_R$ (Yalin and da Silva 2001).

The theoretical final thermodynamic equilibrium state $\eta_* = 0; F_r = \bar{u} = 0$ can be extended for both gravel-like and sand-like $(F_r)_R$ -curves as shown by extended dashed lines in figure 4.3 for $\eta_* < 1$, which cannot be achieved in natural rivers and simply because the flow velocity cannot become zero, due to the restrictions discussed in sand-like and gravel-like regime behaviours (Yalin and da Silva 2001).

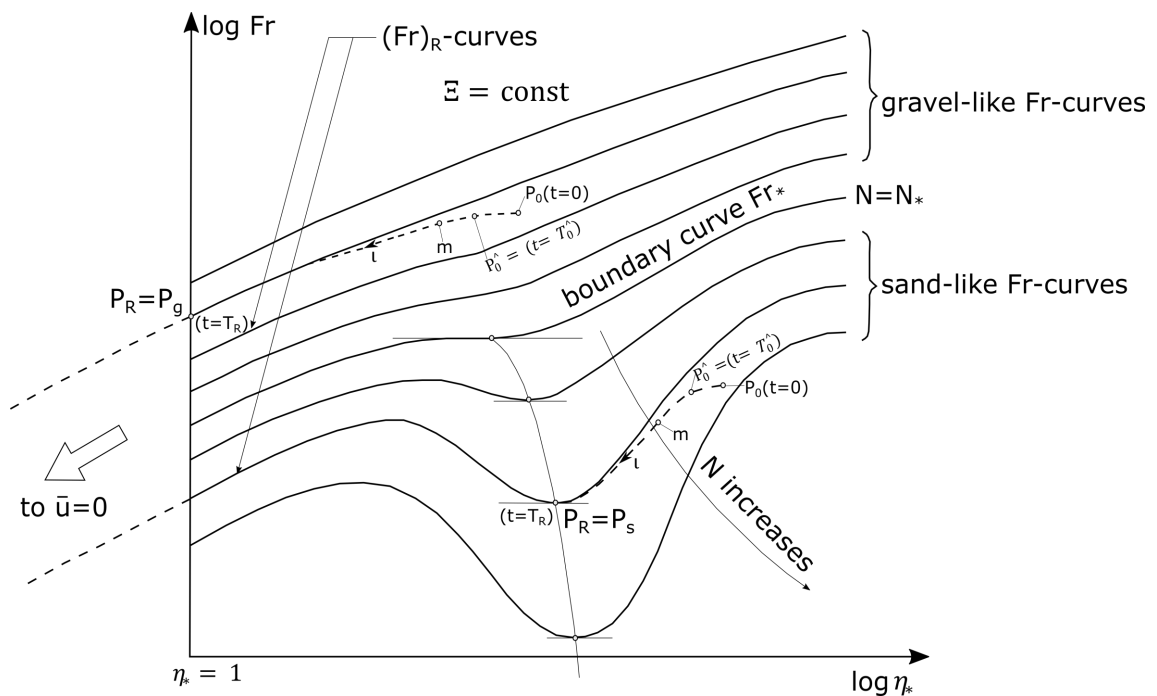


Figure 4.3.: Schematic view of geometric nature of $F_r; \eta_*$ -curve family for regime channel R

Modified after: Yalin and da Silva (2001)

The main assumption in the $F_r; \eta_*$ -plane for gravel-like regime channels is that channels are lacking additional resistance sources (i.e. MRE, bedforms). However, in nature, steep IRS develop strong additional resistance, which causes the regime development to cease

far before reaching the optimum point at $\eta_* = 1$. The tractive force exceeds the loose sediment particles weight, namely the regime development may stop at any point $\eta_* > 1$.

4.1.3. Gravel-like regime channel formation

The dimensionless flow width ∂_w for gravel-bed rivers and streams are approximated to take a value of 1.42 for all $(F_r)_R$; hence the regime width equation 4.14 is reduced to:

$$w_R = 1.42\sqrt{Q/u_{*c}} \quad (4.18)$$

The dimensionless flow width ∂_w is also calculated by the following equation:

$$\partial_w = \phi_1(\Xi) \cdot \phi_2((\mu_c)_R) = 1.42c_R/(c_f)_R \quad (4.19)$$

The $(\mu_c)_R = c_R/(c_f)_R$ is the ratio between total resistance (total dimensionless Chezy resistance factor) to grain resistance (pure grain friction component $(c_f)_R$ at regime state. In case of sand-bed rivers, the bedforms such as ripples, dunes, anti-dunes exert an additional resistance on the flow, while for gravel-bed rivers, large immobile boulders and bedforms such as step-pool, cascade are the main responsible for additional resistance.

The factor $\phi_1(\Xi)$ takes a value of 1.42 for $\Xi > 15$ and $\phi_2(c_R/(c_f)_R) = (\mu_c)_R$ for gravel-bed rivers and streams.

If the additional roughness due to the MRE and bedforms is neglected, the $(\mu_c)_R = 1$ means the total resistance is equal to grain resistance, while in the presence of additional resistance $(\mu_c)_R < 1$.

i- In case of no bedforms

If gravel-bed rivers have no bedforms, the regime parameters calculation is reduced to the following equations:

1. The flow resistance can be predicted using a power law equation as:

$$c_R = 7.66\left(\frac{h_R}{k_s}\right)^{1/6} = 6.82\left(\frac{h_R}{D}\right)^{1/6} \quad (4.20)$$

2. In the flow resistance equation $Q = w_R h_R c_R \sqrt{g h_R S_R}$, the value of c_R is replaced from 4.20:

For gravel-bed rivers, the value of $(\eta_*)_R = 1$ and therefore from the relative flow intensity equation η_* , the critical shear velocity is determined as:

$$(\eta_*)_R = 1 = \frac{g S_R h_R}{u_{*c}^2} \quad (4.21)$$

Hence the regime width and slope is obtained by:

$$h_R = 0.143 D^{1/7} \left(\frac{Q}{u_{*c}}\right)^{3/7} \quad (4.22)$$

$$S_R = \left(6.993 \frac{u_{*c}^2}{g D^{1/7}}\right) \left(\frac{Q}{u_{*c}}\right)^{-3/7} \quad (4.23)$$

If a value of 0.05 is adopted as critical Shields value for initiation of motion and $g = 9.81 \text{ m/s}^2$, the critical shear velocity can be expressed in terms of grain size as:

$$\tau_c^* = 0.05 = \frac{\rho u_{*c}^2}{g\rho_s D}, \text{ thus } u_{*c} = 0.9D^{1/2} \quad (4.24)$$

Replacing the u_{*c} in terms of grain size $0.9D^{1/2}$ in equation 4.18, 4.22 and 4.23, the regime equations for w_R , h_R and S_R can be expressed as a function of flow discharge and grain size respectively as:

$$w_R = 1.5D^{-0.25}Q^{0.50} \quad (4.25)$$

$$h_R = 0.15D^{-0.07}Q^{0.43} \quad (4.26)$$

$$S_R = 0.55D^{1.07}Q^{-0.43} \quad (4.27)$$

ii- If MRE or bedforms are available

The additional roughness due to the MRE and bedforms in gravel-bed rivers can be included in regime development equations 4.25, 4.26 and 4.27 using equation 4.19 for dimensionless flow width ∂_w in which the ratio of total roughness to grain roughness is not unity $\mu_c = c_R / (c_f)_R < 1$ leading to:

$$\partial_w = 1.42 \cdot \phi_2 \left(c_R; (c_f)_R \right) = 1.42c_R / (c_f)_R = 1.42\mu_c \quad (4.28)$$

Replacing the ∂_w in 4.28 gives 4.29 and subsequently using 4.29 in flow resistance equation, one obtains:

$$w_R = 1.5 \cdot \mu_c D^{-0.25} Q^{0.50} \quad (4.29)$$

$$h_R = 0.15(1/\mu_c)^{0.86} D^{-0.07} Q^{0.43} \quad (4.30)$$

$$S_R = 0.55(1/\mu_c)^{0.86} D^{1.07} Q^{-0.43} \quad (4.31)$$

The value of μ_c is depending on the additional roughness and is always taking a less than unity value. It can be concluded from the above equations (4.29-4.31) that additional roughness reduces the regime width, while the regime height increases as the total roughness increases. The regime channel slope increases as well with an increase in total roughness; this indicates that in the presence of additional roughness, the reduction in channel slope is compensated by larger flow resistance to achieve the minimum $(F_r)_R \rightarrow \min$.

4.1.4. Regime channel R1 (with a constant bedload transport)

The regime channel R1 is designated to a regime channel that has a constant bedload transport; therefore, it has a transport equation in addition to the resistance and minimum energy equations (see equations 4.1 to 4.3) (Yalin and da Silva 2001). The resistance equation of R1 is the same as that of R, namely, $\bar{u} = c\sqrt{gSh}$, i.e. $F_r^2 = \bar{u}^2/gh = c^2S$. Thus the graph of the resistance equation of R1 is also a F_r -curve corresponding to a certain $N = Q/wDu_{*c}$. The second equation of R1 is the transport equation, which is obtained

using Bagnold (1980) bedload transport equation as (Yalin and da Silva 2001):

$$\begin{aligned} Q_b &= \beta' w \bar{u} (\mu_c^2 \tau - \tau_c) / g \rho_s = \beta' h w \bar{u} \frac{\tau_c}{g \rho_s h} (\mu_c^2 \eta_* - 1) = \beta' Q \frac{\tau_c}{g \rho_s h} (\mu_c^2 \eta_* - 1) \\ &= \beta' Q \frac{\Psi(\Xi)}{Z} (\mu_c^2 \eta_* - 1) \\ K_* &= \left[\frac{Q_b}{Q} \frac{1}{\beta' \Psi(\Xi)} \right] = \frac{\mu_c^2 \eta_* - 1}{Z} \end{aligned} \quad (4.32)$$

Where β' is a dimensionless coefficient, $Z = h/D$, $Q = wh\bar{u}$ and $(\tau_c = g\rho_s D\Psi(\Xi))$. Further, using $F_r = Q^2/(gw^2h^3)$ gives:

$$K_{**} = \left[\frac{Q^2}{gw^2D^3} \right] = F_r Z^3 \quad (4.33)$$

Removing Z between equation 4.32 and 4.33 results in:

$$F_r = \frac{K}{(\mu_c^2 \eta_* - 1)^3} \text{ with } (K = K_*^3 K_{**}) \quad (4.34)$$

With a given w , the value for K can be calculated and equation 4.34 implies a curve Σ in the $F_r; \eta_*$ -plane for the value of $\mu_c^2 = (c/c_f)^2$, which becomes similar to 3/1-declining straight line for $\eta_* \gg 1$ as shown in figure 4.4. The curve Σ approaches a vertical asymptote when $\eta_* \rightarrow 1$. If channel width is constant (i.e. in case of flume experiment), the regime point P_{R1} is the intersection point of Σ with the F_r -curve corresponding to that particular N of given width and no minimization of any A_* is involved (Yalin and da Silva 2001). In the case of unknown channel width w_{R1} , multitude of F_r -curves for each $N_i = 1/w_i$ and multitude of Σ -curves for each $K_j \sim 1/w_j^2$ exist that results in multitude of points P , where F_r and Σ -curves corresponding to the same w .

The regime point P_{R1} must be identified with that of P , where the adopted minimum condition $A_* = u_{min}$ acquires its lowest value. If $A_* = \bar{u}$ and thus $dA_* = F_r$ as in R regime approach, then the R_1 can only coincide with R if the point P_{R1} coincides with the lowest point $P_s = P_R$; $P_g = P_R$ of the F_r -curve (Yalin and da Silva 2001). In other words, the bedload transport rate Q_b is selected to be equal to $(Q_b)_R$ of R regime.

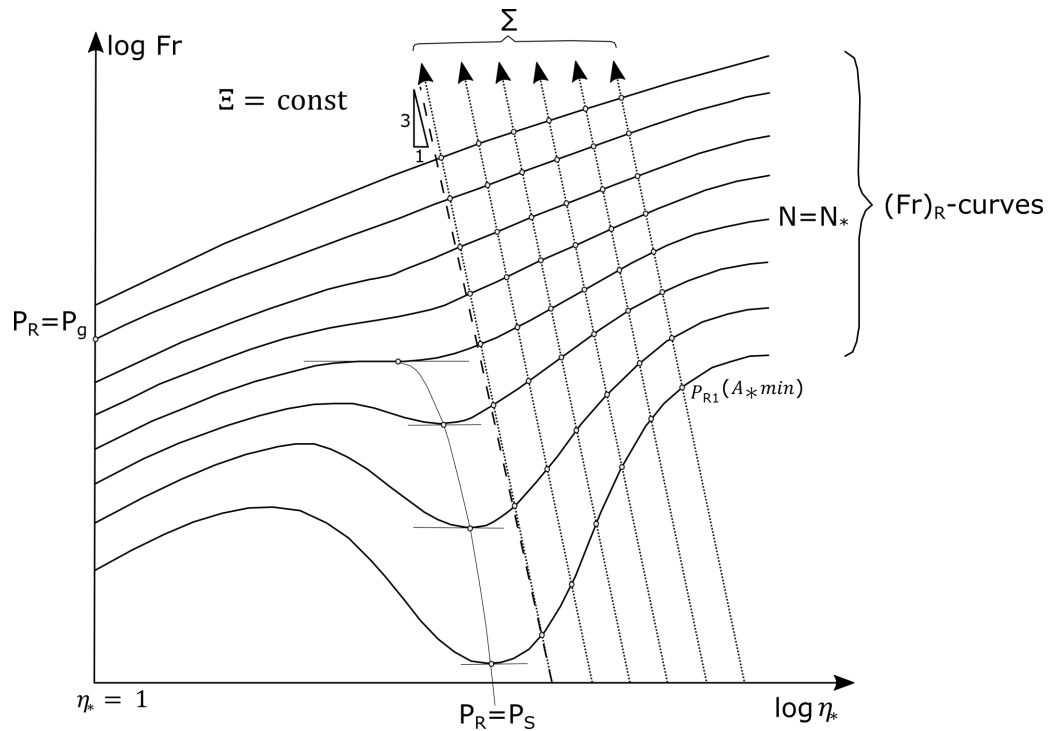


Figure 4.4.: Schematic view of geometric nature of $F_r; \eta_*$ -curve family for R1- channel regime

Modified after Yalin and da Silva (2001)

4.1.5. Channel slope and roughness development at regime conditions

The regime development of width w and slope S are leading to the formation of a wide alluvial channel (Yalin and da Silva 2001). The alteration of w and S by the sediment transporting flow is aimed to achieve the minimum value of $F_r = c^2 S$, while the channel depth h and total bed roughness c adjust themselves by satisfying the resistance formula $Q = whc\sqrt{ghS}$ and the friction factor expression $c_f = 7.66\left(\frac{h}{k_s}\right)^{1/6}$ (Yalin and da Silva 2001). As shown in figure 4.3, for a given initial condition, $N = 1/w$ and F_r continually decrease in the process of achieving the regime state $P_R = P_s$ or $P_R = P_g$. The only condition in which the w experiences an increment is when the given bedload rate at inflow is exceeding the bedload rate naturally transported by the flow (e.g. Ackers 1964; Leopold and Wolman 1957).

A large number of data (6982 points) for grain sizes $0.01 \text{ mm} < D < 52 \text{ mm}$ are compiled by Hayashi (1989) and used by Yalin (1992) to show the relationship between resistance c , η_* and N . The results indicate that with the increase of D and decrease in N , the computed c – curves tend to become monotonous as in c_g , while with a decrease of D and increase of N , they usually exhibit dips $\frac{\partial c}{\partial \eta_*} = 0$ as in c_s as shown in figure 4.5 a. The monotonous trend is associated with gravel-like behavior for $\Xi > 15$, which shows the flow resistance c_g is increasing toward its regime point.

The channel-width w and slope S are altered by the sediment transporting flow in order to achieve the minimum value for $(F_r)_R = c_R^2 S_R \rightarrow \min$. In this process, the water depth h and roughness height k_s adjust themselves by satisfying the resistance formula $Q = whc\sqrt{ghS}$ and friction factor relation $c = 7.66\left(\frac{h_R}{k_s}\right)^{1/6}$. The relationship between S and η_* for different constant values of Ξ and N as shown in figure 4.5 b on an example computed by Yalin (1992). This example shows that a decrease in η_* is always corresponding to a decrease in S for all practically possible values of Ξ and N . The development of characteristics c and h directly follows the development of w and S by satisfying the resistance equations mentioned above. Since the channel width development is occurring at the beginning of regime development, thus, the values of c and h can solely be based on the development of S , which takes place for nearly constant width $w = w_R$.

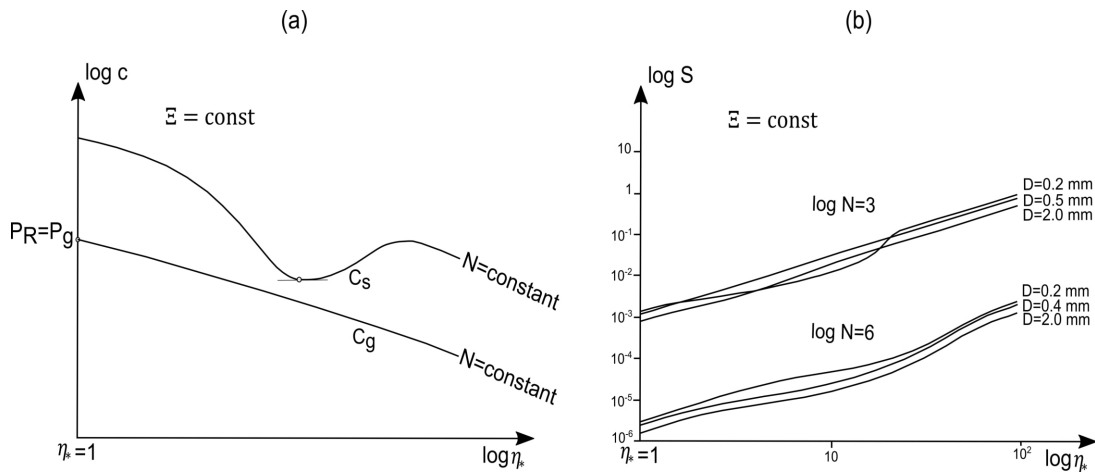


Figure 4.5.: (a) Relationship between Chezy resistance factor c with tractive force η_* and (b) relationship between S and η_* for different grain size D and N values

4.2. Determination of flow resistance using gravel-like regime approach

Most of mountainous IRS have gravel-beds and are assumed to behave as gravel-like regime development. Recalling equation (4.15):

$$(F_r)_R = c_R^2 S_R \rightarrow \min$$

Now, if it is assumed that most of natural rivers and streams with a certain bankfull discharge Q and grain size distribution (GSD) D are in regime state, then the bed slope S should also have its regime value S_R . In the regime state, the bed slope is not changing anymore as it has already reached its lowest value $S_R \rightarrow \min$. Thus, the regime channel slope S_R can be easily measured with sufficient accuracy both for laboratory and natural rivers and streams. The bed slope, however, may change as a result of extreme events such as extreme flood events and landslides that may temporarily change the bed slope

and disrupt the regime state.

Unlike regime channel bed slope S_R , the determination of regime resistance factor c_R is not straightforward. The presence of MRE (i.e. immobile boulders, cobbles) and their arrangement in step-pool or cascade bedforms in steep IRS adds to the complexity in determining the total resistance factor c_R .

Usually, the resistance is subdivided into two main parts, namely resistance due to sediment grains also known as skin resistance c_f and an additional resistance due to bedforms and MRE c_{Add} . The total resistance c is merely the sum of the skin and additional resistance as:

$$\frac{1}{c^2} = \frac{1}{c_f^2} + \frac{1}{c_{Add}^2} \quad (4.35)$$

The grain or skin resistance c_f is well approximated using a logarithmic law $c_f = \frac{1}{k} \ln \left(0.368 \frac{h}{k_s} \right) + 8.5$, power law $c_f = 6.86 \left(\frac{h}{k_s} \right)^{1/6}$ with known $h/k_s = h/2D$ or in Manning-Strickler form from GSD (e.g. $n_0 = 21(3D_{50})^{-1/6}$; $23.5(2D_{90})^{-1/6}$; $26(D_{90})^{-1/6}$) (Nujić et al. 2015b; Schöberl 1979; Müller 1943). Unlike c_f , total resistance c cannot be determined easily and is often indirectly approximated from flow velocity or bedload transport measurements, that are hardly available for mountainous IRS.

One strategy to approximate the total resistance c for steep gravel-bed IRS is to use the regime-channel concept in numerical modelling. Numerical modelling allows long-time simulation of the hydro-morphological behavior of channels aiming to achieve regime status. Two dimensional (2D) models can be employed to simulate the regime development of steep IRS. With known flow discharge Q , sediment feeding rate Q_b , GSD D , critical dimensionless shear stress τ_c^* , grain friction c_f , initial channel dimensions (width w , length L and channel initial slope S), a total flow resistance c can be determined when the following regime conditions are fulfilled.

1. The flow discharge Q and bedload transport Q_b at model's inflow are equal to those of model's outflow.

$$\begin{array}{lll} Q_{in} = Q_{out}; & Q_{b_{in}} = Q_{b_{out}} = 0 & R - \text{regime channels} \\ Q_{in} = Q_{out}; & Q_{b_{in}} = Q_{b_{out}} \neq 0 & R_1 - \text{regime channels} \end{array}$$

2. The channel slope has reached its regime state which means it does not change anymore.

$$S = S_R; \frac{\partial S}{\partial t} = 0 \quad R - \text{regime channels}$$

$$S = S_{R_1}; \frac{\partial S}{\partial t} = 0 \quad R_1 - \text{regime channels}$$

The simulation is terminated when the above two regime conditions are met. The channel regime slope S_R for a given total resistance c is read from the simulation result and are analysed to understand the relationship between them.

Similarly, for a regime channel R ($Q_{b_{in}} = Q_{b_{out}} = 0$) and $\tau_c^* = 0.05$, the theoretical equations

(see equations 4.29 -4.31) for determination of regime channel dimensions as a function of $\mu_c = c_R / (c_f)_R$, D and Q are reanalysed based on the simulation results.

4.2.1. Determination of regime relative resistance μ_c using simulations

The Hydro_FT-2D model is an extension of the Hydro_AS-2D which solves the 2D depth-averaged flow equations also known as shallow water equations (Nujić et al. 2015a) (more details about Hydro_FT-2D in section 4.4.4). The model provides depth-averaged velocity \bar{u} and water depth h , which subsequently are used for the estimation of bed shear stress. The model uses Manning-Strickler approach for estimation of energy gradient S from \bar{u} and h , which in turn is used for the estimation of bed shear stress as:

$$S = \frac{\bar{u}^2}{n_{tot}^2 h^{4/3}} \quad (4.36)$$

As it is further discussed in section 3.2.3, MRE and bedforms reduce the energy available for the transport of sediment. A correction for additional resistance due to MRE and bedforms is suggested by Nitsche et al. (2011) by introducing a reduced energy slope. The reduced energy slope represents a fraction of the calculated gradient, which is based on the flow resistance partitioning approach of Nitsche et al. (2011) and Rickenmann and Recking (2011) as:

$$S_{red} = S \left(\sqrt{\frac{f_0}{f_{tot}}} \right)^e = S \left(\frac{n_{tot}}{n_0} \right)^e = S\mu \quad (4.37)$$

Here, S_{red} is the reduced slope to account for additional roughness effects, S is the channel or hydraulic energy slope, $f_0; n_0$ are base-level flow resistance, $f_{tot}; n_{tot}$ are representing total flow resistance using Darcy-Weisbach and Manning-Strickler approaches respectively. The exponent e is ranging from 1 to 2, with a typical value of $e = 1.5$. The flow resistance ratio μ is calculated for a given grain resistance n_0 and total resistance n_{tot} as:

$$\mu = \left(\frac{n_{tot}}{n_0} \right)^{1.5} = \left(\frac{k_{st}}{k'_{st}} \right)^{1.5} \quad (4.38)$$

Hydro_FT-2D uses symbols k'_{st} and k_{st} respectively for grain and total resistance. Based on the relative resistance factor μ , the reduced energy gradient and bed shear stress are calculated. Subsequently, bedload transport equations are solved based on the reduced dimensionless shear stress.

$$\tau_{red}^* = \frac{\tau_{red}}{(s-1)\rho g D} = \frac{h S_{red}}{(s-1)D} \quad (4.39)$$

Usually, the total resistance k_{st} is determined from the hydraulic calibration of the model by fixing the measured and simulated water levels. However, data for water level and discharge are rarely available for steep IRS. While the total resistance k_{st} is used in the model for influencing the value of S , the grain resistance k'_{st} is usually used as a calibration parameter, because by varying k'_{st} , the value of μ also varies, which in turn alters the S . Therefore, the k'_{st} is used as a coefficient in the model for adjusting the S and or bed shear stress τ , which is used for bedload transport calculation. Hydro_FT-2D limits the

maximum allowable values for both k_{st} and k'_{st} to 100.

Based on the above definitions of k_{st} and k'_{st} , two scenarios of their combination is examined in this study.

i- Scenario A

In scenario A, it is assumed that original energy gradient is only affected by the grain resistance k'_{st} ; thus total resistance in the model is set equal to calculated grain resistance using the equation 4.40 for each set of GSD D . An initial value for k'_{st} can be calculated by the following empirical relation:

$$k'_{st} = 17 D_{50}^{-1/6} \quad (4.40)$$

The effect of additional resistance or the resistance ratio μ is then applied by varying the value of k'_{st} in the denominator in the range of $k'_{st} < k_{st} < 100$ because the value of μ should always be lower than 1.

This scenario resembles a condition in which based on the grain resistance, the hydraulic energy gradient S is calculated. It is then modified by the μ and the reduced energy gradient S_{red} , reduced bed shear stress τ_{red}^* and subsequently the bedload transport Q_b are calculated by the model.

$$\mu = \left(\frac{k_{st} = k'_{st}}{k'_{st}} \right)^{1.5} \frac{(constant)}{(variable)}$$

The value of nominator in the above equation remains constant for all tested channel slopes and GSD D , which means the hydraulics of the system varies due to different channel slopes only.

This scenario avoids the counterproductive effect of decreasing the value of k_{st} to achieve a $\mu \leq 1$, which increases the energy gradient (see equation 4.39) because in equation 4.39, a smaller value of k_{st} leads to a larger energy gradient and vice versa. Therefore, by keeping the k_{st} constant for given GSD D , the initial energy gradient is not exaggerated.

ii- Scenario B

The scenario B is the opposite of the scenario A, namely the initial energy gradient is calculated using total resistance. The grain resistance is constant for all slopes and a given D_{50} , and only total resistance is varied for different initial channel slopes.

$$\mu = \left(\frac{k_{st}}{k'_{st}} \right)^{1.5} \frac{(variable)}{(constant)}$$

The main problem in using this scenario is to guarantee a $\mu \leq 1$, because, for any k'_{st} , the value of $k_{st} \leq k'_{st} \leq 100$ is limited by the model, and only for certain channel regime slopes, the value of $\mu \leq 1$ is fulfilled. The problem, in particular, arises for low channel slopes and fine grain GSD, where for $\mu \leq 1$ bedload transport and channel regime development are hardly initiated. Therefore, scenario A is comprehensively experimented and compared with the results of scenario B.

4.2.2. Channel slope combinations

Scenario A and B are applied on the number of initial channel slopes, and the relative resistance values are observed at channel regime states. Wide ranges of channel slopes from a low slope 0.5% up to steep slope 10% are investigated because these ranges of channel slopes are often present in mountainous IRS. In general, two cases of channel slopes are studied, namely constant slope channels and combined slope channels. Constant slope channels represent a single stretch of a river or stream having a constant slope. Combined slope channels resemble a whole river network, which is composed of several constant slope stretches.

Furthermore, the initial channel width can be fixed (i.e. in laboratory flume or rigid boundary channels) or can have extensive floodplains. Both of these two conditions termed in this study as fixed-width and extended-width channels are investigated with respect to their regime dimension w, h, S development with the relative resistance μ .

I- Constant slope channels

Constant slope channels are making the bulk of the investigations, which consists of both fixed-width and extended-width channels. The fixed-width channels represent a controlled laboratory flume condition or a channalised river stretch with rigid banks, while the extended-width channels represent natural river stretches with broad and erodible floodplains.

The fixed-width constant slope channels are consisting of ten sets of constant slope channels with lengths of 200 m, widths of 5.5 m and slopes of 0.5 %, 1.5 %, 2.5 %, 3.5 %, 4.5 %, 5.5 %, 6.5 %, 7.5 %, 8.5 % and 10 %. The meshes are kept identical in terms of their resolution namely the number of nodes and elements are the same for all channel slopes. The initial channel width is calculated using the equations of the regime channel for gravel-like channels proposed by Yalin and da Silva (2001) as discussed earlier in section 4.1.3 for $\tau_{cm}^* = 0.05$. The initial channel width is selected such that it just exceeds the regime width for the finest set of GSD, which according to equation 4.29 ought to develop the largest regime width. The aim of limiting the initial channel width near to regime width for the finest GSD is to avoid long computing time due to additional large mesh domain.

The equation 4.29 is considered for the case of maximum channel regime width for the relative resistance value $\mu_c = 0.9$, which assumes a minimal additional roughness due to MRE or bedforms. When additional roughness is present $\mu_c \ll 1$, smaller regime width for the same flow discharge Q and GSD D is developed, compared to a condition with no additional resistance.

The flow discharge Q is considered to be the bedload transport relevant discharge or bankfull discharge, which is initially derived from continues discharge measurement and field investigation of a natural river Shakar-Dara (see details in chapter 6). Based on the natural hydrograph of the investigated river with $Q_{min} = 0.04 \text{ m}^3/\text{s}$ and $Q_{max} = 7.0 \text{ m}^3/\text{s}$, the bankfull discharge is determined to be around $Q = 2 \text{ m}^3/\text{s}$.

The representative grain size D often taken as D_{50} is determined from field measurements

(details in 4.4.3). As it is observed from the equation 4.29, the finer the D_{50} , the larger the channel width is required for regime development. Thus, the finest set of GSD for subsurface layer $D_{50} = 19.0 \text{ mm}$ is selected for the calculation of initial channel regime width. Therefore, by inserting the values of $\mu_c = 0.9$, $Q = 2 \text{ m}^3/\text{s}$ and $D_{50} = 19.0 \text{ mm}$ into the equation 4.29, the initial channel width w is estimated as:

$$w_R = 1.5 (0.9) (0.019)^{-0.25} (2.0)^{0.50} = 5.14 \text{ m}$$

The channel width is selected to have a size of 5.5 m slightly larger than the calculated regime width of 5.14 m for the finest GSD set which sets the upper threshold for regime channel width because for coarser grain sizes, the regime width significantly decreases. The extended-width constant slope channels are merely assumed to have three-times larger width compared to fixed-width channels, in order to allow bank erosion as a result of secondary currents and to represent a natural condition with erodible banks. Therefore, the channel width is chosen as $3 \times 5.5 \text{ m} = 16.5 \text{ m}$, while the channel length is kept identical to fixed-width channels (200 m). The extended-width channel is constructed by combining three fixed-width channels such that the middle part is the same as the fixed-width channel and the left and right parts are added as floodplains as shown in figure 4.6. The left and right parts $+0.7 \text{ m}$, in order to avoid overflow of the water on the floodplains right at the beginning of the simulation, because based on the hydraulic simulations results, the maximum water depth for lower slope channels 0.5% reaches about 0.7 m . If the overflow occurs, the transport capacity reduces strongly, and this will lead to zero bedload transport and no regime development is initiated.

The length of the channels is selected based on the findings of Schmutz (2003) that proposes a regime length to be around 35-times regime of the width. Therefore, for a regime width of 5.5 m , a regime length of $35 \times 5.5 \text{ m} = 192.5 \text{ m}$, thus a length of 200 m is considered to be sufficient for regime and planform developments as well as to account for boundary effects at the inflow and outflow of the model.

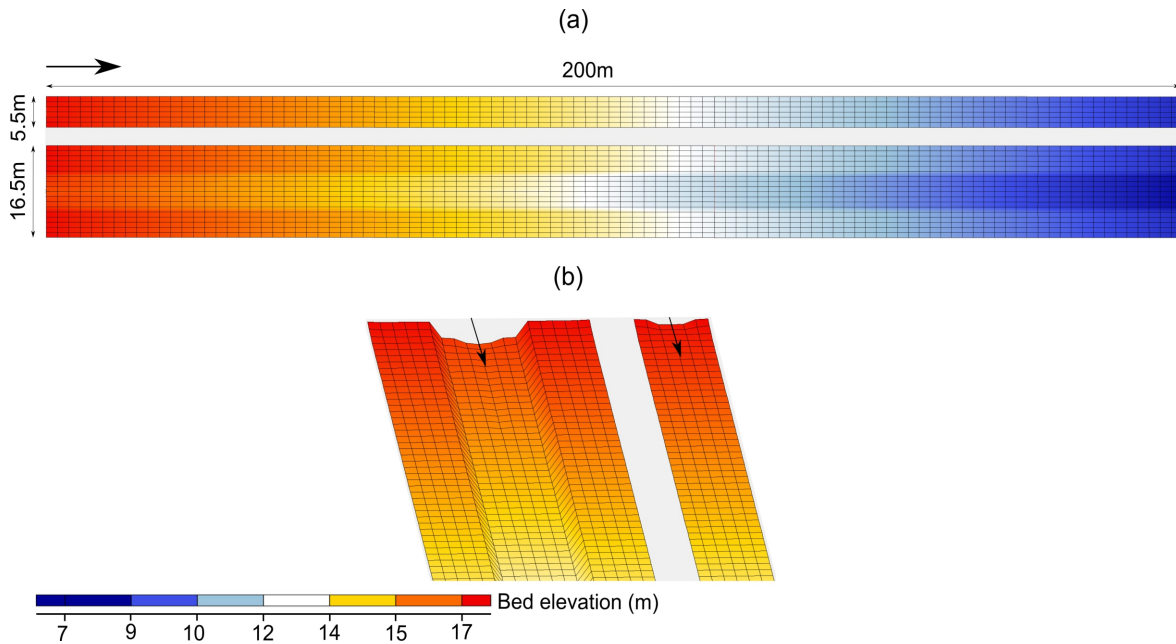


Figure 4.6.: Fixed and extended-width meshes for a 4.5% slope channel (a) 2D view and (b) 3D view of the inflow region

II- Combined slopes cases

While a constant slope channel can represent a controlled laboratory flume or a single stretch of a river or a stream, a natural river may consist several stretches of different slopes along its course. Thus, different patterns of channel slope combinations are studied using the regime channel concept for gravel-bed channels, in order to understand their regime behavior (i.e. regime slope relationship with relative flow resistance).

The combined slope case 1 is designed to represent a condition in which two steep slope $S \geq 7.5\%$ stretches are connected by a gentler slope $S \leq 2.5\%$ stretch. The combined slope case 2 is the opposite of the case 1 and is designed to represent a condition in which two gentler slope $S \leq 2.5\%$ stretches are connected by a steep slope $S \geq 7.5\%$ stretch. Finally, the combined slope case 3 is a combination of the case 1 and 2 and represents an alternate series of steep slope $S \geq 7.5\%$ and low slope $S \leq 2.5\%$ stretches. This combination of slopes includes gradual and abrupt slope changes as also occurs in natural IRS as shown in figure 4.7. The channel width is kept the same as constant slope case for all combined slope cases, and the channel length is the sum of all constant slope channels' lengths. Therefore, the channel slope combination case 1 and 2 are composed of three single constant slope channels, thus have a total length of $3 \times 200 \text{ m} = 600 \text{ m}$, while the slope combination case 3 is built from six single constant slope channels, hence has a total length of $6 \times 200 \text{ m} = 1,200 \text{ m}$.

The slope combinations aims to show the regime development of a channel system of different slopes and their interaction in the long term. Besides, it is to test the development of channels regime geometries $w_R; S_R; c_R$ in combined slope system cases and single

channel cases under the same hydro-sedimentological conditions $Q; Q_{br}$. In nature, a single slope channel rarely exists, often the channel slopes decrease from upstream to downstream directions. Additionally, the channel slope combination study is aimed to reveal the slope-driven plan-form development.

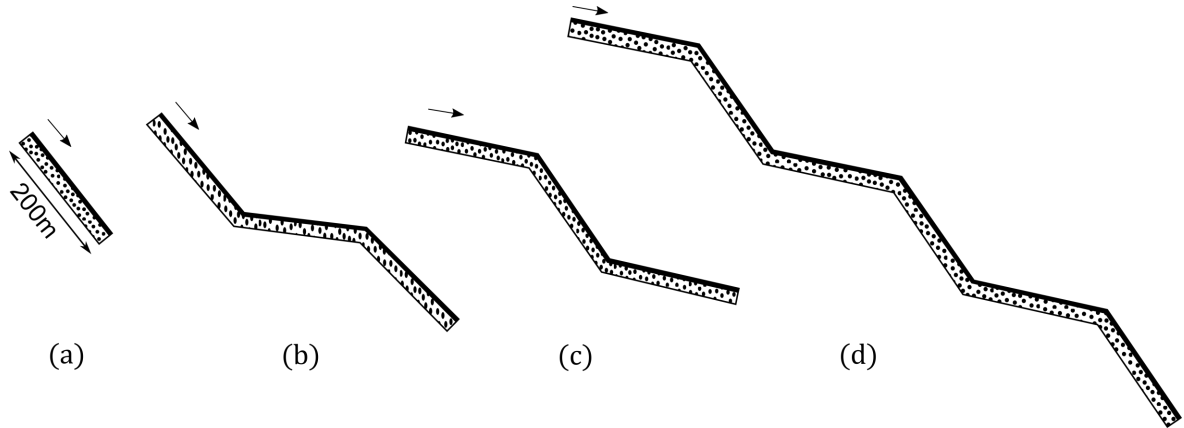


Figure 4.7.: Channel slopes and slope combination cases used in the simulations (a) constant slopes from 0.5% to 10% (b) slope combination case 1 (c) slope combination case 2 and (d) slope combination case 3

4.3. MRE as geometry (immobile boulders and step-pool bedforms)

4.3.1. MRE as geometry

While the first method under the framework of regime channel approach focuses on the relationship between relative resistance μ and channel slope S at regime state, in the second method, the MRE are built as non-erodible geometrical shapes, which induces an additional resistance. In the first method, the relative resistance μ is numerically varied to achieve regime condition for different regime channel slopes, but in this method, the MRE concentrations on the channel-bed are varied to obtain a regime condition for a particular channel slope. In this case, the value of μ in the model is equal to 1, since the additional resistance is only imposed by MRE rather than by numerical values as in the first method. The MRE changes the velocity magnitude and direction and therefore reduce the shear stress for sediment transport. As discussed in detail in section 3.2.3 of chapter 3, MRE changes the flow regime in their vicinity depending on the flow submergence condition. If MRE is submerged, a flow recirculation in the near wake region occurs. The recirculation extends about one diameter size of MRE downstream with a decelerated and even reversal flow, which leads to a reduced shear stress. In case of protruding MRE, a standing wave condition occurs in the upstream of MRE with a deceleration of flow and reduced shear stress, while at the downstream side, the flow is accelerating.

The hydraulic simulation results for a 4.5% channel slope of a flatbed 0.0% MRE and beds with different MRE concentrations show that velocity for the flatbed is uniformly distributed, while in the presence of MRE as geometry, velocity distribution varies widely (see figure 4.8 a). Velocity decreases significantly in all regions, but the more significant reduction in velocity is consistently observed in the leeward side of a MRE (shown by red rectangles in figure 4.8 a and b). The velocity increase is observed in rare cases and in particular in micro channel regions formed among MRE and between wall regions and MRE. The velocity vectors change from unidirectional (in longitudinal) for the flatbed to multi-directional (longitudinal and transverse directions) around MRE in the presence of MRE.

More importantly, the presence of MRE causes a substantial reduction in shear stress compared to flatbed as shown in figure 4.8 b. The longitudinal profile of shear stress for flatbed (shown by solid red line) and MRE (shown by dashed color lines) shows that on average, around 27 to 35% decrease in bed shear stress compared to the flatbed case as shown in figure 4.8 c.

As the concentration of MRE increases, the bed shear stress decreases accordingly, except for some regions around some MRE, which experience spots of increase in shear stress. These spots of high shear stress may have larger magnitudes than the flatbed case in some regions and their occurrence increases with an increase in MRE concentrations. Since the MRE areas are set as rigid or non-erodible bodies in the model. Therefore an increase in shear stress in some spots should not increase the total bed erosion. However, they may lead to local scour around the MRE. The reduced shear stress in the presence of MRE on the channel bed lead to a reduced bed erosion and bedload transport, thus leading to channel slope stability. On the other hand, the MRE on channel bed protects the area underneath them from erosion and reduces the total exposed channel bed area to erosion. Often mountainous IRS have a large number of MRE of different sizes, which are immobile at most of the occurring flow discharges. This information is almost always not collected during the river geometry measurements, because usually the river cross-section measurements conducted from a zero-bed level and exclude MRE. Secondly, the information about the distribution of MRE is lost in the process of interpolation for generating meshes for the simulations. Even if very detailed river topography data is available, the computing mesh cannot be generated with fine resolution as this requires high computation capacity, else this will lead to very long computing time. As a result, computation meshes often does not include individual MRE due to their coarse resolution. However, with the advancement in computing technology, it is becoming more plausible to perform long time simulations of fine resolution meshes in a relatively acceptable time.

To understand the collective effect of MRE on the steep channel stability and bedload transport, MRE are built as rigid trapezoidal bodies into fine resolution meshes for long-time simulations. The simulations results are analysed concerning MRE concentrations, for which a particular channel slope is achieving its regime state. For a particular channel slope S , GSD D , flow discharge Q and sediment feeding rate Q_b , the MRE total areas are set to achieve an equilibrium condition. The MRE are distributed randomly over the

entire channel with an initial trapezoidal shape of one mesh element size. The trapezoidal shapes are built by increasing elevations of four nodes by 0.5 m as shown in figure 4.9 d. The MRE concentration on a channel bed is expressed as the percentage of the total channel area.

The channel dimension is kept identical as used in the first method of regime channel approach namely having a width of 5.5 m and length of 200 m but the mesh resolution is made finer (i.e. element size is $0.5 \times 0.23\text{ m}$). The fine resolution mesh makes it possible to distribute the MRE well throughout the channel. Distances 5 to 10 m from inflow and outflow boundaries are set free of MRE to allow stable flow development at model's boundaries.

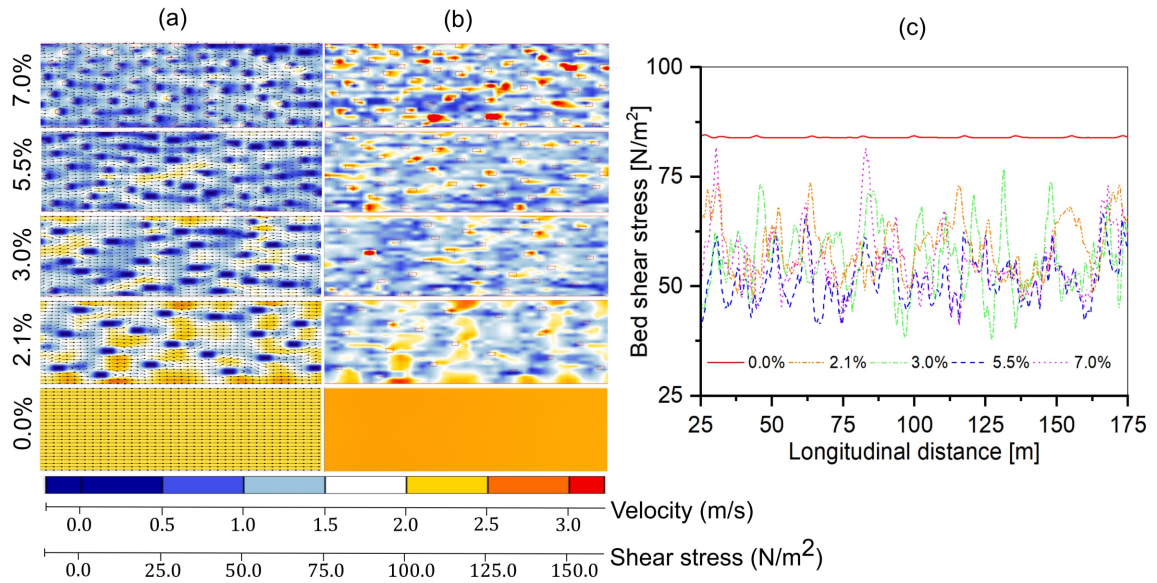


Figure 4.8.: MRE as geometry and their influence on (a) velocity field (b) bed shear stress and (c) longitudinal profile of bed shear stress as a function of MRE concentrations for an example of 4.5% constant channel slope

The initial trapezoidal shape of MRE may deform into various geometrical shapes depending on the erosion depths around the MRE. These deformed trapezoidal shapes are either submerged or protruding or mixture of both at a specific time during simulation and may change from one phase to another depending on their relative submergence h/D_B . This condition also exists in natural channels in which parts of the MRE may be submerged while the rest may protrude from the water surface during the same flow event Q . The second parameter which has a firm control on the water depth is the channel slope S . At gentler slopes, larger MRE may become submerged, while at steep channel slopes water depth reduces significantly. The hydraulic simulation shows that elements heights lower than 0.2 m is often submerged, while those taller than 0.5 m are often protruding from the water surface.

The simulation results with rigid initial trapezoidal shapes as MRE show that the erosion

occurs around the MRE and after the passage of time, the MRE shapes deform significantly. The deformation causes trapezoidal MRE to become thin (enlarge in height), while the base dimensions remain constant as the channel bed is eroded. These very tall MRE (height > 2m) may impose an adverse effect on the bedload transport and erosion because thin MRE provide micro-channels of large shear stress that may lead to unrealistic bed erosion. More importantly, since these types of tall MRE are seldom found in nature, therefore, it is essential to keep the MRE height comparable to water depth. In order to overcome this issue, the MRE height is reduced with time. This reduction is made by extracting a volume of sediments from the surface of the MRE such that the heights of MRE remain comparable with water depth at all stages of simulation. Sediment extraction is performed by simply cutting from top of the MRE to keep their height comparable to water depth. The channel bed experiences different erosion depths (decreasing from upstream to downstream) and at different rates at different simulation time. Therefore, the rate of sediment extraction from MRE are also set to decrease with time for all extraction zones as shown in figure 4.9 b and c for an example of 8.5% channel slope having a 4.6% MRE concentration.

The sediment extractions zones near the inflow boundary (1, 2, 3, 4 and 5) undergo large volume of sediment withdrawal, in particular at the beginning of the simulations, because the inflow regions experience considerable erosion depths. Similarly, with the passage of time, the sediment extraction volume is also decreased, because the erosion rates decrease with time. At the final stage of the simulation, the sediment extraction from MRE is set to zero, because the erosion depth tends to zero as well. The diagram of sediment extraction rates at different simulation time and different extraction zones are shown in figure 4.9 b. By applying the sediment extraction strategy, the MRE original trapezoidal shape deforms into various geometrical shapes due to differential erosion rates at neighboring nodes. The total given volume of sediment extraction in the model is divided over the total surface area of the MRE within each zone, and if any neighboring node is undergoing larger erosion than others, the initial trapezoidal shape is deformed as shown in figure 4.9 d. The sediment extraction is conducted at each time step by dividing the total sediment extraction volume by the duration for instance for zone 1, at early simulation stage $350 \pm 50 \text{ m}^3$ sediment is extracted during 83 hours of simulation.

The simulations with MRE concentrations from 1.7% to 7.0% for channel slopes from 2.5% to 10% are conducted using three GSD sets with $D_{m0} = 19 \text{ mm}$, 38 mm , and 57 mm . The simulations are performed with constant flow discharge $Q = 2 \text{ m}^3/\text{s}$ and bedload transport rate $Q_b = 0 \text{ to } 5 \frac{\text{kg}}{\text{s}}$. The outflow boundary condition is assumed as channel slope.

The regime state is achieved when at the specific MRE concentration, the channel slope $S = S_R$ does not change anymore with time and the bedload transport rate at the model inflow is equal to model outflow $Q_{b_{in}} = Q_{b_{out}}$. As a result, at the regime state, the relationship between channel regime slope S_R and MRE concentrations are analysed.

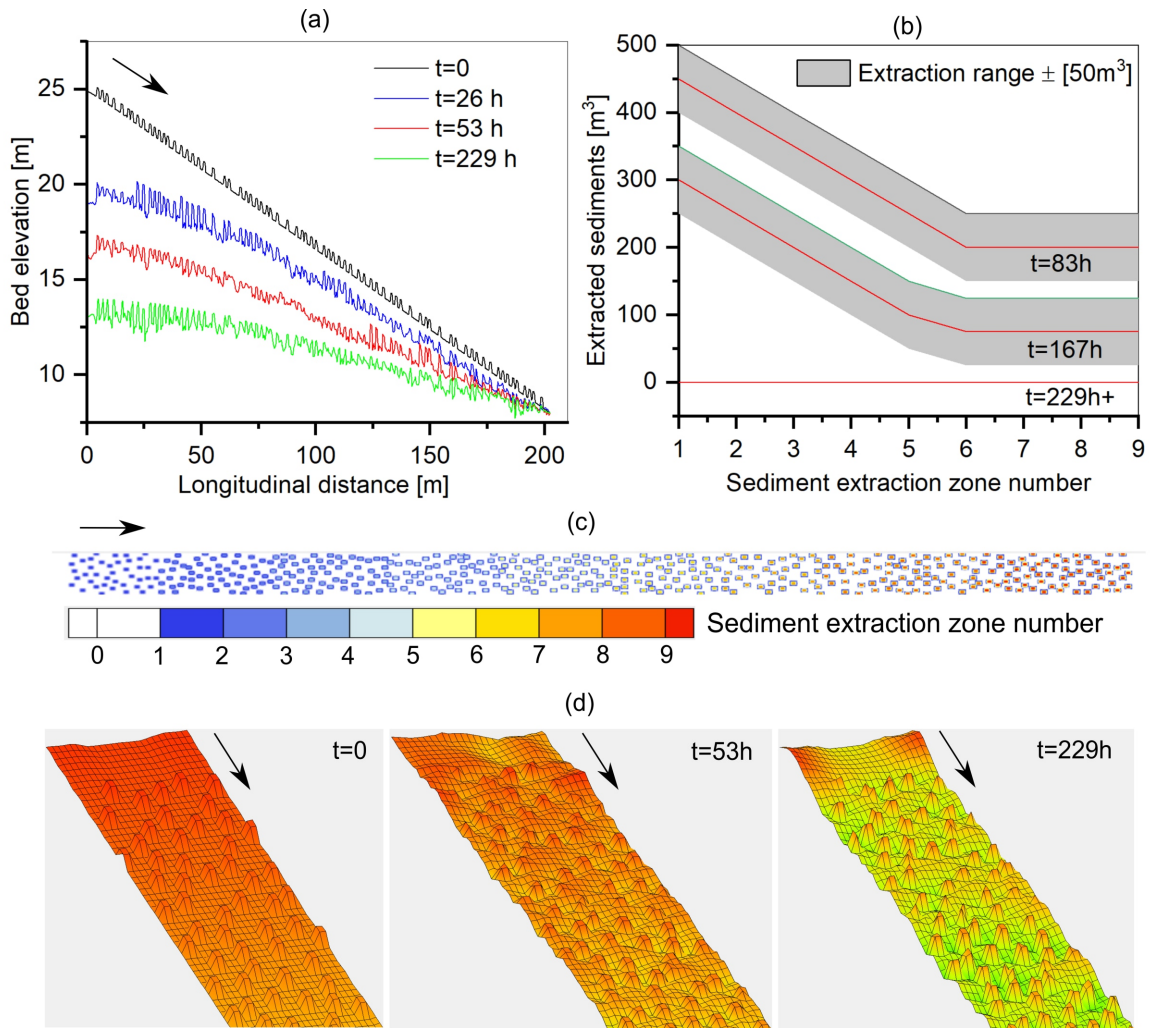


Figure 4.9.: Example of channel-bed evolution development for initial channel slope of 8.5% with MRE concentration of 4.6% (a) initial and time-development of channel bed longitudinal profile (b) sediment extraction volume from MRE for different extraction zones and at different simulation time (c) sediment extraction zones and (d) initial and time-development of MRE trapezoidal shapes deformation

4.3.2. MRE as step-pool or cascade bedforms

In step channels, MRE are water worked and arranged in the form of cascades or step-pool sequences, which are dissipating energy in the form of fill and spill in the pool and step regions respectively. The self-organisation process of MRE in step-pool sequences increases flow resistance, while it decreases the local slope and as a result the stream power is minimised (Chin and Phillips 2007). Since the step-pool bedform is the main morphological characteristics of step rivers and streams, therefore they are

thoroughly investigated concerning their role in increasing the flow resistance under the regime-channel approach using long-term morphological simulations.

As discussed in detail in section 3.2.3 of chapter 3, the distance between cascades or steps of step-pool bedform to produce maximum resistance depends on the MRE sizes, GSD of bed sediments D , channel slope S , flow discharge Q and bedload transport rate Q_b . In this study, the step-pool channel bed of a specific slope S is simulated to understand the relationship between step-pool dimension L_D/D_B and the channel regime slope S_R .

The steps are built in the mesh by increasing the elevation of elements covering the whole cross-section. The original mesh elements in the step area are further refined to keep the size of steps' width nearly equal to steps' height as shown in figure 4.10 c because it is assumed that MRE building the steps dimensions are of trapezoidal shapes. The cross-section of a step has a shape of an isosceles trapezoid with an extended base width 1.0 m, small base width 0.5 m and variable initial heights from 0.1 m to 0.3 m for different initial channel slopes.

The steps are built over the entire channel width as non-erodible elements. In nature, however, extreme flow events may destroy the steps, but under normal flow condition, the steps can be assumed as stable bedforms. The initially built steps in the model are adjusting their dimensions often demonstrated by step-length wave (clear distance between two adjacent steps) to step-depth D_B (distance between step-crown to step toe). The L_D/D_B value varies based on the channel slope S at a particular flow discharge Q , bed sediment GSD D and sediment feeding rate Q_b .

The simulation results for a step-pool channel of 4.5% slope shows sediment deposition in the upstream of steps and erosion right at the downstream of the steps as shown in figure 4.10 c. This type of bed evolution results in an increase in step-depth from the initial condition at $t = 0$ to final step-pool bed at $t = 80 h$ leading to a regime status. In this state no further bed evolution takes place and therefore the channel slope is reaching its regime value $S = S_R$.

The flow velocity and bed shear stress distribution for a section of the step-pool channel and flatbed channel shows a sharp reduction in velocity and bed shear stress at the upstream of the steps and an increase at the top and right at the downstream of the steps as shown in figure 4.10 a. Similarly, the longitudinal profile of bed shear stress shows around 45% to 50% reduction in bed shear stress in most of the pool regions of the channel, but it nearly doubles at step's top and at the downstream of the steps as shown in figure 4.10 b. Since steps are set as rigid bodies in the simulations, therefore, the increase in shear stress in steps' tops are not imposing any change in steps geometry during the bed evolution development.

The outcome of this study should reveal the relationship among parameter L_D/D_B , channel slope S , flow discharge Q and sediment feeding rate Q_b , GSD D by fulfilling the regime channel status.

The simulations for step-pool bed channels are performed for slopes ranging from 2.5% to 10% using GSD sets with $D_{mo} = 19 \text{ mm}$, 38 mm , and 57 mm . The simulations are run with constant flow discharge of $Q = 2 \text{ m}^3/\text{s}$, and bedload transport rate of $Q_b = 0 \text{ to } 5 \frac{\text{kg}}{\text{s}}$

and the outflow boundary condition is assumed as the initial channel slope. The relative resistance factor is given a value of $\mu = 1$ because the aim in this investigation is to determine the total resistance (in the form of step-pool dimensions L_D/D_B) imposed by MRE arrangements in step-pool bedforms only for achieving regime status. Therefore, the result of this study will reveal the relationship between channel regime slope $S_R; S_{R1}$ and regime step-pool dimensions L_D/D_B .

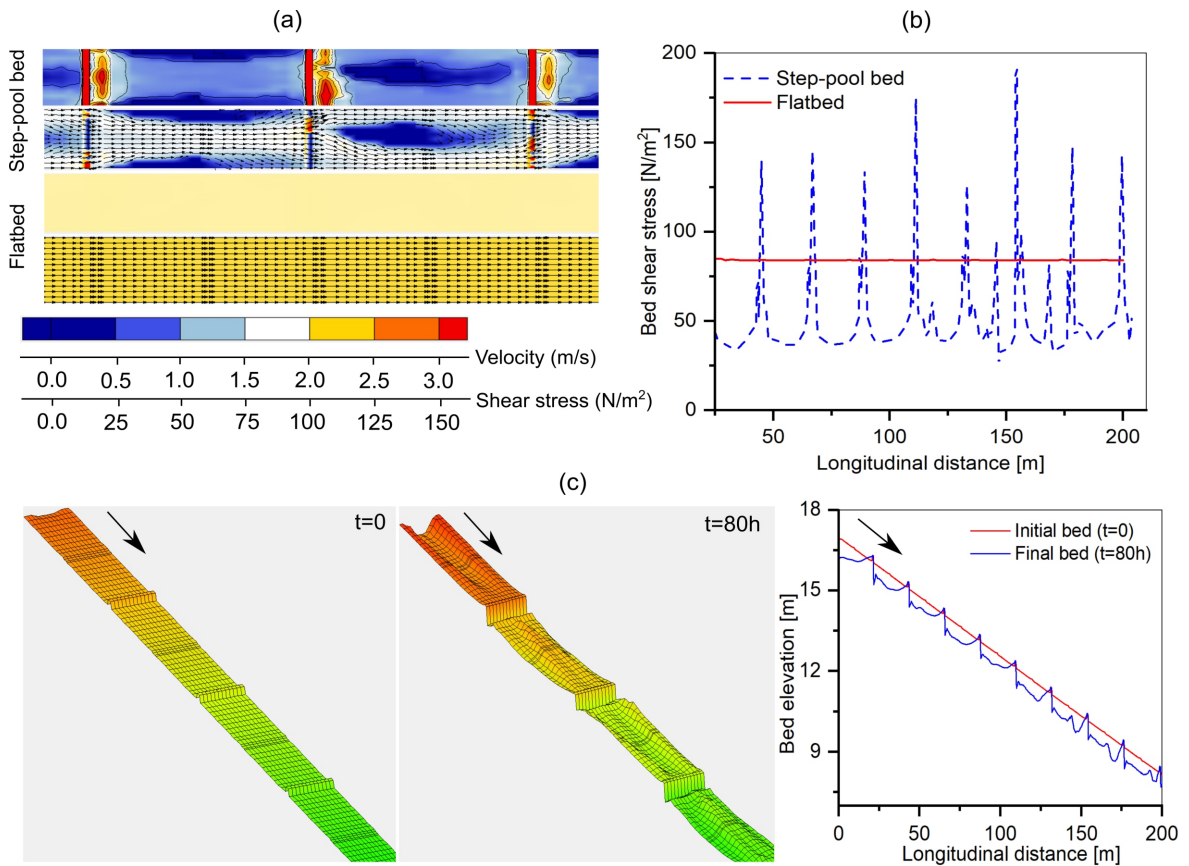


Figure 4.10.: Step-pool channel regime development and their effects on the flow characteristics for an example of 4.5% initial channel slope (a) 2D bed shear stress and velocity distribution and (b) longitudinal profile of shear stress for flatbed and step-pool bed channel and (c) channel bed evolution with time for step-pool bed channel

4.4. Hydro-morphological simulations

4.4.1. Mesh conditioning

Mesh conditioning is aimed to modify the inflow regions to ensure stable simulation runs. The inflow region with a dimension of $1.85\text{ m} \times 10\text{ m}$ is modified such that the main flow is concentrated over two central elements rather than six elements. This modification is made by reducing the elevation of nodes by 0.2 m for the two central elements at the inflow boundary. Similarly, adjacent elements nodes' elevation are also linearly reduced such that after four elements length or 10 m in the direction of flow, it follows back the average gradient of the mesh. Thus, the modified region has a lower gradient than the rest of the mesh as shown in figures 4.6 b, 4.9 d and 4.10 c.

This modification has two main objectives. First, by reducing the gradient at the inflow region, the chances of potential simulation instability reduces as well. The simulation instability more often occurs for steep gradient channel geometry than gentler slope channels. Secondly, this modification induces higher shear stress right at the inflow region in order to trigger bedload transport and bed evolution. The bed dynamic is then propagating downstream in the direction of flow. The modification is made for inflow regions of all sets of meshes including single slope, combined slope, fixed and extended-width meshes as well as for MRE and step-pool arrangements of MRE channels. Since the inflow boundary regions are set as erodible for all simulations, thus this mesh modification helps achieve a good start at the initial phase of the simulations.

4.4.2. Boundary conditions

The inflow and outflow boundary conditions can be divided into three main phases, namely initial, intermediate and final phases as shown in figure 4.11. The initial condition consists of constant flow discharge of $Q = 2\text{ m}^3/\text{s}$, zero sediment feeding rate $Q_{b_{in}} = 0$, and six sets of GSD for exchange layer (AS), subsurface layer (US) and base layer (GS) as listed in table 4.1. The extended-width channels are also simulated using a constant flow discharge of $Q = 1\text{ m}^3/\text{s}$ in order to investigate the effect of flow distribution over the relatively larger area compared to other channels, due to their larger available widths. The channel bed slope is assigned at the outflow boundary as energy gradient E because, at uniform flow condition, the channel bed slope can be assumed as energy gradient. The initial phase also consists an initial condition in which an initial water depth h and flow velocity components are assigned to the long-term morphological simulation model Hydro_FT-2D. The initial condition variables are exported from the result of a pure hydraulic simulation with a flow discharge of $Q = 1\text{ m}^3/\text{s}$ using Hydro_AS-2D model. The initial condition helps improve the stability of the simulation for long-term morphological simulations.

The initial grain roughness k'_{st} in Manning-Strickler values are estimated using equation 4.40 for each set of GSD as listed in table 4.1. As discussed in section 4.2.1, in scenario A, for both fixed and extended-width channels, the value of total roughness k_{st} is assumed

as grain roughness k'_{st} and the value of relative resistance $\mu = k_{st}/k'_{st}$ is varied by varying the value of grain roughness k'_{st} for different channel initial slopes. In scenario B, the μ is varied by the variation of total roughness k_{st} , while the grain roughness k'_{st} is kept constant. The values of both k_{st} and k'_{st} are kept constant for simulations of MRE and step-pool, namely the value of $\mu = k_{st}/k'_{st} = 1$ because the additional roughness is induced to the flow by MRE and step-pool bedforms themselves.

The initial phase for the simulation of MRE as geometry also consists of sediment extraction volumes from the MRE in order to keep their size comparable to water depth $D_B \approx h$. The sediment extraction volumes are given in m^3 for the given initial time spans, which are withdrawn from the MRE areas within the given time duration.

The intermediate phase of simulations is a stage at which the channel width w is already fully developed and almost achieved its regime dimension. The channel plan-form development is visualized to identify this phase of the simulations, which strongly depends on the boundary conditions such as flow discharge Q , GSD D and channel initial slope S . While the channel width w does not change significantly with time after this stage, the channel slope S continues to decrease until it reaches its regime condition. At this stage, bedload transport rates at outflow of the model can be recirculated to inflow of the model for R1 regime channel simulations. The recirculated bedload (bedload feeding rate) is given to the model for the third stage of regime channel simulation. The magnitude of the bedload feeding rate is selected to be smaller or equal to bedload transport rates at model' outflow $Q_{b_{in}} \leq Q_{b_{out}}$, because the bedload transport capacity is reducing with time and larger feeding rates $Q_{b_{in}} > Q_{b_{out}}$ may not be entirely transported. The GSD of the recirculating bedload is assumed as that of subsurface (US) because the transported sediments grain sizes do not differ significantly from subsurface (US) GSD.

The bedload feeding at model's inflow will stop the further reduction in channel slope S , because now the erosion of the channel bed that is causing the slope reduction is compensated by the feeding sediment. In other words, once the sediment is fed at the inflow of the model, the transport capacity of the flow is saturated, and hence the erosion from the channel bed, as well as the reduction of channel slope, is stopped. At early stages, after the sediment feeding is introduced, there may be slight changes in channel slope depending on the transport capacity of the flow at this stage. If the transport capacity $Q_b^* > Q_b$, there would be a further reduction in slope as a result of bed erosion, while for $Q_b^* < Q_b$, the slope may slightly increase due to the sediment deposition right at the inflow boundary. This non-equilibrium condition right at the beginning of sediment feeding introduction is overcome after the passage of time. If the feeding rate is considerably larger than the transport capacity $Q_b^* \ll Q_b$, the sediment deposition right at the inflow boundary will lead to unstable simulation, and thus no regime state can be achieved. After the introduction of sediment feeding at model's inflow, the simulation is restarted and let run until the regime state is achieved. However, for the simulations with zero feeding rate (R regime channels) throughout the simulation; no intermediate boundary condition is required.

Based on the description of the intermediate phase, several intermediate boundary

conditions with different bedload feeding rates can be introduced depending on the time when the initial phase is stopped. Since the bedload transport rate at model's outflow is decreasing with time due to the channel slope decrease, therefore after the development of channel width w , several bedload feeding rates can be recirculated at several simulation time instants. At early stages, larger bedload feeding can be defined based on the bedload transport rates at model's outflow and with the passage of time, it decreases. Thus, depending on the time instant when the recirculation is made, its rate can differ strongly. Additionally, for the simulation of MRE as geometry, the intermediate phase may also contain modification of the sediment extraction volumes, because the initially given extraction volumes are often leading to either over-withdrawal or under-withdrawal that can respectively lead to very small MRE or very tall MRE. Thus, a modification is made based on the observation of initial phase results, and new sediment extraction volumes are provided.

The final phase of the simulation is recognised based on the criteria set for regime status, namely $S = S_R$ and $Q_{b_{in}} = Q_{b_{out}}$ or in the case of zero feeding rate $Q_{b_{in}} = Q_{b_{out}} = 0$. The values of $Q_{b_{out}}$ can be read from the output file of the Hydro_FT-2D. The channel slope can be visualized by plotting the simulated channel bed or water surface elevation (WSE) along the thalweg of the channel in post-processing tool Surface-water Modelling System (SMS). If the WSE does not change between two time-steps, it can be concluded that the channel slope has reached its regime value S_R .

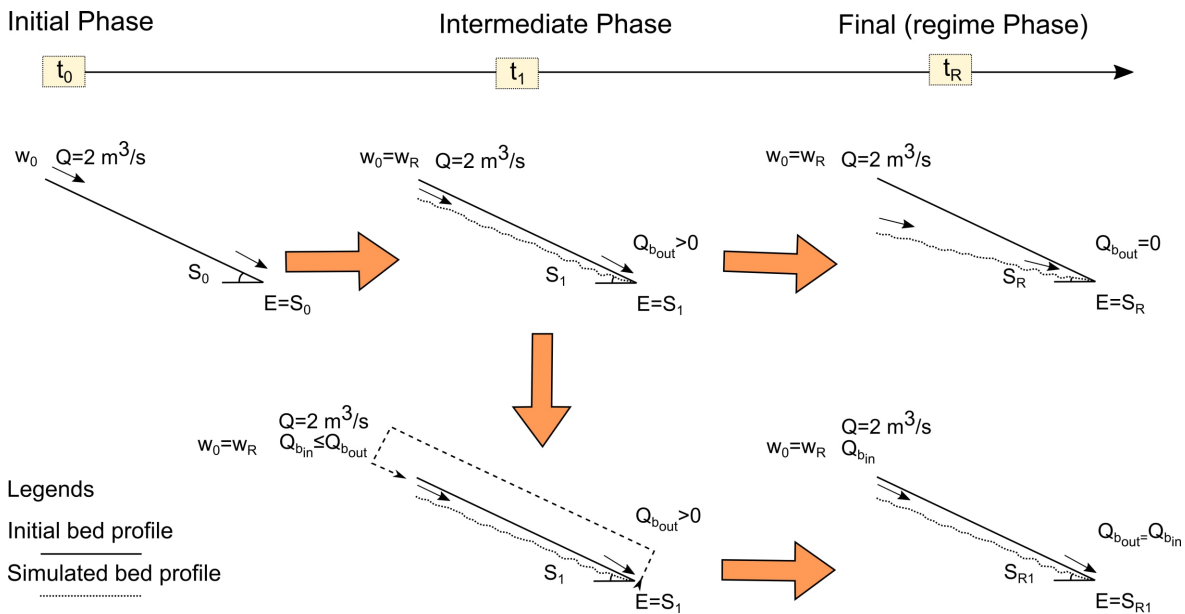


Figure 4.11.: Schematic diagram of boundary conditions for initial, intermediate and regime phase of simulations

4.4.3. Riverbed sediment grain size distribution (GSD)

Riverbed sediment characteristics are adopted from Shakar-Dara River, a natural mountainous intermittent river in the Kabul region of Kabul River basin in Afghanistan. Detailed information about Shakar-Dara River and its hydro-sedimentological characteristics are discussed in the chapter 6.

Five riverbed sediment samples, one surface, three subsurface and one mixed layer samples from different locations of about 2.0 km reach of Shakar-Dara River are used for this study. The surface layer sample is taken from a depth of about one-grain size to approximately a depth of 0.25 m, mixed layer sample is taken from a depth of about 0.25 m to 0.35 m, and the subsurface layer samples are taken from a depth of about 0.35 m or more. Additionally, as many as nine photographs from different locations of the riverbed surface are taken and analysed granulometrically to achieve a spectrum of GSD for the surface layer. Some photographs were manually improved by drawing boundaries around individual grains for a better detection by Basegrain photogranulometric analysis tool (Detert and Weitbrecht 2013) (details in appendix E).

The average GSD for the surface layer (AS) is derived from the average of the riverbed sediment sample from the first layer and the granulometric analysis results. The mixed and second layer samples are averaged to represent the GSD for the subsurface (US) layer. The GSD is discretized into 12 classes and used in the model.

Due to the diverse nature of sediment GSD for mountain rivers, the average measured GSD is made manually coarser and finer, in order to cover a wide range of sediment GSD that may occur in natural rivers and streams. The coarsening is made by multiplying each grain size class by the factors of 1.25, 1.50, and 1.75 respectively, while the percentages of grain sizes are kept constant. The same distributions are also made finer by multiplying the grain sizes by factors less than unity namely 0.75, and 0.50 as shown in figure 4.12. The main characteristics of the measured average GSD together with sets of coarsened and refined GSD for surface layer (AS) and subsurface (US) are listed in table 4.1.

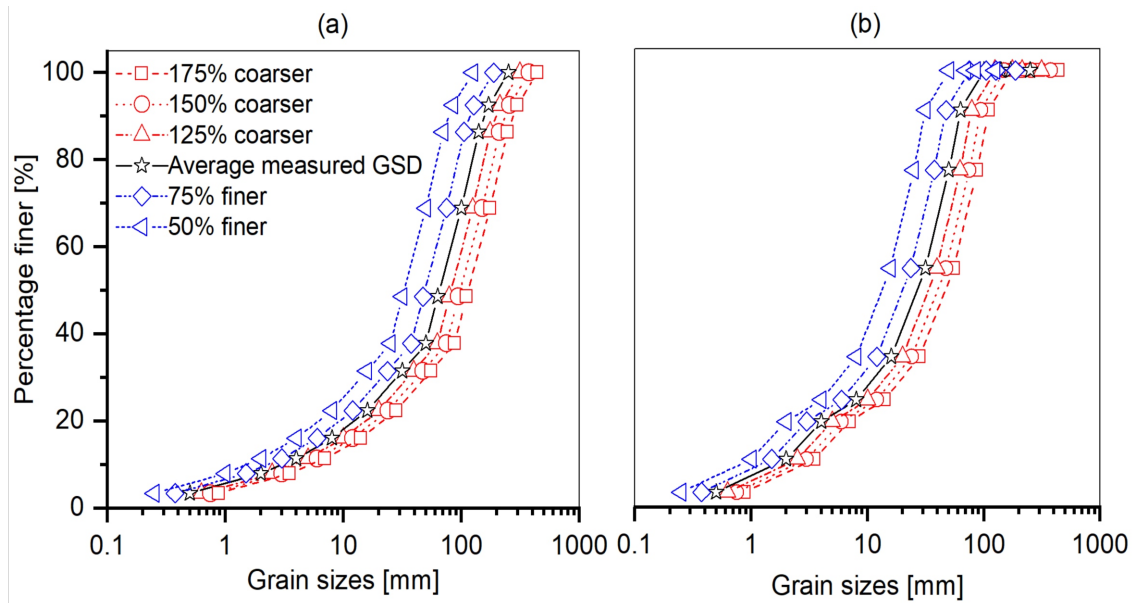


Figure 4.12.: Measured (shown by stars) and generated GSD curves for (a) surface layer (AS) and (b) subsurface (US), base layer (GS) and sediment feeding.

Table 4.1.: Main sediment GSD characteristics and calculated grain roughness for measured and generated sets of GSD used for surface (AS), subsurface (US) and base layer (GS)

Finning/Coarsening [%]	D_{50} (AS) [mm]	D_m (AS) [mm]	D_m (US) [mm]	D_m Sediment feeding [mm]	Grain roughness k'_{st} [$m^{1/3}/s$]
50	32.0	44.3	19.0	19.0	29.52
75	48.0	66.5	28.4	28.4	28.25
Measured data	64.0	88.5	38.0	38.0	26.93
125	79.0	110.6	47.3	47.3	25.87
150	95.0	132.7	57.0	57.0	25.11
175	111.0	155.0	66.3	66.3	24.53

In summary, simulations for fixed and extended-width channels concerning GSD sets, constant and combined slopes channels, as well as simulations of MRE as geometry and their step-pool arrangement, are listed in table 4.2.

Table 4.2.: List of simulations performed for various sets of GSD

Simulations	Grain sizes sets [%]	Constant slopes	Combined slopes	MRE as geometry	MRE as step-pool	Variable flow Q=1.0[m ³ /s]
Fixed-width ✓ Extended-width ✓	50	✓ ✓		✓	✓	✓
	75	✓				
	Measured data	✓ ✓	✓	✓	✓	✓
	125	✓				
	150	✓				
	175	✓ ✓			✓	✓

Further input parameters for hydraulic and morphologic simulations with Hydro_FT-2D are given in appendix A.

4.4.4. Model Hydro_FT-2D description

Hydro_FT-2D is an extension of the 2D numerical flow simulation program Hydro_AS-2D developed by Nujić et al. (2015). The abstraction “FT” is for the German word “Feststofftransport”, which means solid transport including both bedload and suspended load transport, but the program provides the option to simulate only bedload transport as well. It is assumed that the suspended sediment does not significantly contribute to the regime development of channels; thus only bedload transport simulations are performed. Hydro_FT-2D solves the two dimensional free surface flow or shallow water equations (also known as Saint-Venant equation), sediment transport equations (bedload and suspended load) and Exner equation for bed evolution. The equations originate from the integration of the three-dimensional continuity equation and the Reynolds-averaged-Navier-Stokes equations for incompressible fluids over the water depth, assuming hydrostatic pressure distribution (Pironneau 1989; Yörük 2008; Nujić et al. 2015a). Finite volume method (FVM) is used for the spatial discretization of the linearly unstructured mesh of triangular or rectangular forms. As a temporal discretization procedure, Hydro_FT-2D uses an explicit second-order Runge-Kutta method for free surface flow equations system. The time step duration in an explicit procedure is limited due to the stability issues and is controlled by the so-called CFL or Courant number as:

$$\Delta t \leq \min \frac{\Delta L}{|\vec{u}| + \sqrt{gh}} \quad (4.41)$$

Δt is the simulation time-step, ΔL is the characteristic length between the connected pair of nodes and \vec{u} represents the depth-averaged velocity in the direction of the connected pair of nodes in the simulation mesh. Thus the given time-step is adjusted such that CFL-number is less than unity.

Hydro_FT-2D employs a combination of an algebraic eddy viscosity approach and a constant eddy viscosity. This enables the model to simulate domains with intense flow mixing or

significant shear flow and thus, strong turbulence can be modelled by the additional constant viscosity term (Nujić et al. 2015a).

Bedload transport can be simulated using one of the three bedload equations namely Mayer-Peter –Müller (MPM), Acker –White (AW) and Engelund- Hansen (EH). The critical Shield parameter can either be given as a constant value or calculated by the Hydro_FT-2D using the equation of Yalin and da Silva (2001) as a function of grain Reynolds number. The original MPM bedload transport equation in Hydro_FT-2D is modified by Hunziker (1995) for mixed grain sizes based on the equal-mobility concept. The MPM bedload transport was developed based on the laboratory models of single grain sediment transport. In natural conditions, however, due to the presence of a large number of grain sizes, mixing and sorting processes of sediments can influence the bedload transport. Thus, the ideal single grain bedload transport equation is modified to account for mixing and sorting processes to allow fractional bedload transport estimation. Sorting process plays a significant role in particular for mountainous rivers and streams, where various grain sizes are present, and the critical shear stress or mobility parameter value $\tau_c^* < 0.11$ is essential for a realistic simulation of morphological processes (Hunziker 1995). The laws of sorting processes are rather complex to include them simply in a model, but Hunziker (1995) showed that by employing the concept of equal-mobility, the basic mechanic of sorting process could be built in rather simple models. He, therefore, developed the fractional transport of multi-grain sediments based on the Meyer-Peter and Müller (1948) equation in the Hydro_FT-2D model as follows:

$$\Phi_{dms,i} = F_i \cdot k_f \cdot 8 (\varphi_i (\tau_{dms}^* - \tau_{cm}^*))^{3/2} = F_i \cdot \varphi_i^{3/2} \cdot k_f \cdot 8 (\tau_{dms}^* - \tau_{cm}^*)^{3/2} \quad (4.42)$$

$$\Phi_{dms,i} = \frac{q_{b,i}}{\sqrt{(\rho_s/\rho - 1)} \cdot g \cdot d_{ms}^3} = \frac{q_{b,i}}{\sqrt{(s - 1)} \cdot g \cdot d_{ms}^{3/2}} \quad (4.43)$$

$$q_b = \sum_{i=1}^n q_{b,i} \quad (4.44)$$

The sum of dimensionless transport parameters for each fraction can be written as:

$$\sum_{i=1}^n \Phi_{dms,i} = k_f \cdot 8 (\tau_{dms}^* - \tau_{cm}^*)^{3/2} \cdot \sum_{i=1}^n (F_i \cdot \varphi_i^{3/2}) \quad (4.45)$$

$$\sum_{i=1}^n \Phi_{dms,i} = \frac{1}{\sqrt{(s - 1)} \cdot g \cdot d_{ms}^{3/2}} \sum_{i=1}^n q_{b,i} = \frac{q_b}{\sqrt{(s - 1)} \cdot g \cdot d_{ms}^{3/2}} \quad (4.46)$$

The total bedload transport can be obtained as:

$$q_b = \sqrt{(s - 1)} \cdot g \cdot d_{ms}^{3/2} \cdot k_f \cdot 8 (\tau_{dms}^* - \tau_{cm}^*)^{3/2} \cdot \sum_{i=1}^n (F_i \cdot \varphi_i^{3/2}) \quad (4.47)$$

The F_i is the percentage of grain class F_i , and k_f is a pre-factor modifier that provides the option to adjust the bedload transport rate to achieve a target calibration and its value varies between 0.25 and 0.625. These values for k_f is resulting in pre-factor values between 2 and 8 for MPM bedload transport equations.

The hiding/exposure parameter φ_i for grain size class i is defined as the ratio of mean grain diameter of grain class d_{mi} to the mean grain size diameter of the surface layer or exchange layer sediment d_{ms} as:

$$\varphi_i = \left(\frac{d_{mi}}{d_{ms}} \right)^{-\alpha_A} \text{ for } \frac{d_{mi}}{d_{ms}} \geq 0.3 \quad (4.48)$$

The hiding function exponent α_A can be determined using a regression analysis of a series of flume studies by Günter (1971) and Suzuki and Hano 1992. The equation (4.49) considers the sorting process by effective shear stress τ_{dms}^* and calculated as:

$$\alpha_A = 0.011 \cdot \tau_{dms}^{*-1.5} - 0.3 \text{ for } \alpha_A \leq 2.3 \quad (4.49)$$

The equation 4.49 is a result of regression of rather complex original function and is tested to be valid for the mobility parameters ranging between $0.035 < \tau_{dms}^* < 12$. It will lose some accuracy outside this range, in particular at small effective shear stress, (Hunziker 1995).

Although the regression equation 4.49 is based on a single grain size composition used in the study of Suzuki and Hano (1992), Hunziker (1995) showed that it could be used for other grain size distributions as well. Nujić et al. (2015) explain the limitation of hiding function exponent $\alpha_A \leq 2.3$ as a controlling parameter to avoid an unrealistic increase of fine grains transports. The exponent α_A may also take a negative value at very large shear stress, which inversely affects the mobility parameter, namely increasing the mobility of larger grains $d_{mi} \geq d_{ms}$, while decreasing mobility parameter of fine grains $d_{mi} < d_{ms}$. The hiding function φ_i may also take a unity value and thus does not change the relative mobility parameter when:

$$\varphi_i = 1 \rightarrow \alpha_A = 0 \rightarrow \tau_{dms}^* = \left(\frac{0.011}{0.3} \right)^{2/3} = 0.11$$

I- Incipient motion in Hydro_FT-2D

The transport-begin for the single size grains are thoroughly investigated by Shields (1936). He presented his flume results that show dimensionless critical shear stress as a function of grain Reynolds number known as Shields diagram. In Hydro_FT-2D, the user can set the critical shear stress as a constant, or it can be calculated by the equation proposed by Yalin and da Silva (2001) as a function of grain Reynolds number as:

$$\tau_{ce}^* = 0.13\Xi^{-0.392}e^{-0.015\Xi^2} + 0.045 \left[1 - e^{-0.068\Xi} \right] \quad (4.50)$$

The material number Ξ includes the influence of solid $D; \rho_s g$ and water $\rho; \nu$ phases and its value is independent of flow stage as it does not include the shear velocity u_* or water depth h .

$$\Xi = \frac{D(\rho_s g)^{1/3}}{\rho^{1/3} \nu^{2/3}} = \left(\frac{R_e^{*2}}{\tau_{dms}^*} \right)^{1/3} \quad (4.51)$$

The critical shear stress for incipient motion in Hydro_FT-2D is treated as transport-begin of uniform grain size τ_{ce}^* . Thus, the program modifies it based on the approach of Günter

(1971) for mixed size sediments as:

$$\tau_{cm}^* = \tau_{ce}^* \left(\frac{D_{mo}}{D_{ms}} \right)^{0.33} \quad (4.52)$$

τ_{cm}^* is the critical shear stress for the incipient motion of mixed size sediments, D_{ms} and D_{mo} is the mean grain diameters for surface and subsurface layers sediments respectively. In the case of an armoring layer generation, the ratio of D_{mo} and D_{ms} is smaller than unity, which indicates that the critical dimensionless shear stress for incipient motion related to D_{ms} for the sediment mixture is smaller than that for the uniform size sediments. The reason is a differential sediment depositions of different grain sizes that causes riverbed armoring. The equation (4.52) also resembles a condition at which the finer particles under a very coarse surface layer are easily brought in motion than a condition in which the mean grain diameters of surface and subsurface layers sediments are not much different. The critical dimensionless shear stress τ_{cm}^* in Hydro_FT-2D is further modified to account for bed longitudinal Θ and transverse slope ψ effect using the equation proposed by Van Rijn (1993) as:

$$\tau_{cm,\Theta,\psi}^* = k_{\Theta} k_{\psi} \tau_{cm}^* \quad (4.53)$$

The factors k_{Θ} and k_{ψ} considers the influence of longitudinal and transverse to flow slopes on the critical dimensionless shear stress for flatbed τ_{cm}^* , mainly as a result of the downslope component of gravity forces.

The longitudinal slope effect is defined concerning bed longitudinal slope Θ and internal friction angle also known as the sediment angle of repose ϕ as:

$$k_{\Theta} = \frac{\sin(\phi - \Theta)}{\sin \phi}; k_{\Theta} < 1 \quad (4.54)$$

$$k_{\Theta} = \frac{\sin(\phi + \Theta)}{\sin \phi}; k_{\Theta} > 1 \quad (4.55)$$

In case of a downward slope in the direction of flow, the factor k_{Θ} takes a value less than unity, and in upward slope case, the factor k_{Θ} is larger than unity; thus the τ_{cm}^* is reduced in the case of the downward slope while it is increased during upward slope.

The transverse slope factor k_{ψ} is determined from the forces balance on a grain resting on a transverse slope ψ as:

$$k_{\psi} = \cos \psi \left(1 - \frac{\tan^2 \psi}{\tan^2 \phi} \right)^{1/2} \quad (4.56)$$

II- Impact of the secondary current on the bed shear stress and its direction

In a depth-averaged model, a number of simplification is undertaken, which can significantly impact the bed shear stress and its direction. In a 2D model, among others, it is assumed that the bed shear stress has the same direction as the depth-averaged flow velocity. However, in nature, the effect of secondary current and downslope component of gravity changes the bed shear stress direction from the direction of depth-averaged flow velocity as shown in figure 4.13. A 3D numerical model, in comparison can simulate

explicitly the near-bed flow and shear stress directions. However, 3D models application is limited to small domains due to the required high computing capacity and longer computing time. Therefore, a number of factors are applied in 2D Hydro_FT-2D model to account for the effect of flow and shear stress direction on the bedload transport.

Natural rivers have often meanders and curvatures, where the occurrence of secondary currents initiates a bedload transport in the inward direction of a bend. Due to the secondary currents form a helical motion, the water in the upper part of the river is driven outward, whereas the water near the bottom is driven inward in a bend. As a result the riverbank is eroded in the transverse direction and deposits in the outward curve, which gradually builds river bars. The deposition on the outward curve pushes the streamlines further toward the inward bend and as a result of this process rivers begin to meander. This complex three dimensional process in river bends is approximated and corrected in 2D- depth averaged models with the help of a approaches that use local geometrical curvature radius R_{Sec} from streamlines as a main input. Hydro_FT-2D estimates a dynamic curvature radius from the changes in velocity component vectors for every mesh node and time step. The value of R_{Sec} is used to estimate the shear stress in transverse and main flow directions as well as to determine the deviation angle δ_{Sec} , where the bed shear stress direction differs from flow direction (Rozovskiĭ 1957; Bridge 1992) as follows:

$$\tan \delta_{Sec} = \frac{\tau_{Sec}}{\tau_{\Gamma}} \cong \frac{\tau_{Sec}}{\tau_{\alpha}} = -A_{Sec} \frac{h}{R_{Sec}} \quad (4.57)$$

The dimensionless coefficient A_{Sec} is used as calibration parameter und is found to vary between 7 and 12 (e.g. Engelund 1974; Olesen 1987; Zimmermann and Naudascher 1979). The larger the A_{Sec} value is selected, the higher would be the bedload transport in transverse direction. In this study, a moderate value of $A_{Sec} = 10$ is used for all regime channel simulations.

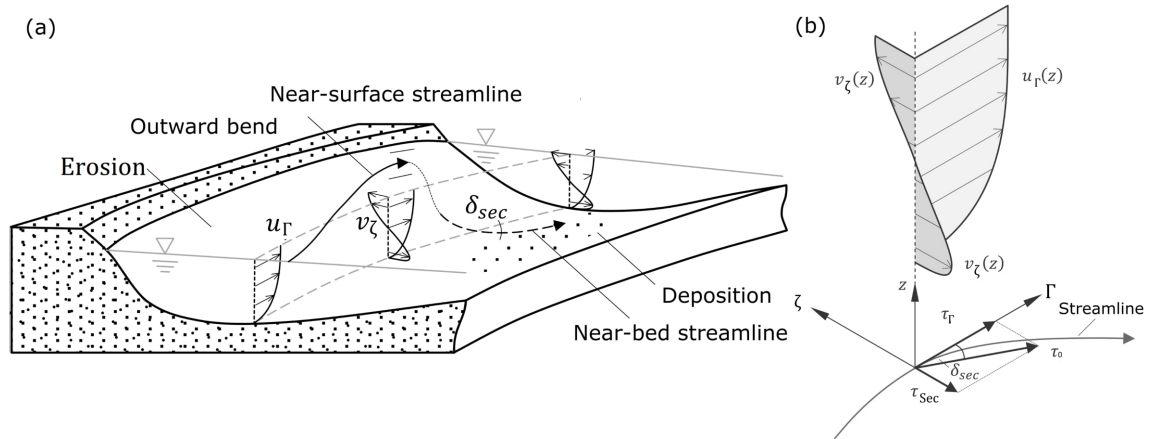


Figure 4.13.: Schematic illustration of flow in a river bend (a) Flow and bedload transport in river bend (b) profiles of main flow and secondary currents and the resultant near-bed shear stress components and their direction modified after Hafner (2008)

III- Bedload transport direction on inclined surfaces

Hydro_FT-2D model considers the effect of channel slope or gravity on the direction of bedload transport by introducing a global parameter $c_{f\Theta}$, which is used to calculate the direction angle α_b of bedload transport as shown in figure 4.14 (Nujić et al. 2015b). The tangent of bedload transport direction angle α_b is determined using a specific function $f(\tau_{dms}^*)$ and geometry term describing respectively the mode of transport and bed changes in x and y directions (Schmautz 2003) as follows:

$$\tan\alpha_b = \frac{q_{b,y}}{q_{b,x}} \approx \frac{\sin\delta - f(\tau_{dms}^*) \cos^2\epsilon \frac{\partial Z_b}{\partial y}}{\cos\delta - f(\tau_{dms}^*) \cos^2\epsilon \frac{\partial Z_b}{\partial x}} \quad (4.58)$$

$q_{b,y}$ and $q_{b,x}$ are respectively bedload transport in x and y directions, ϵ represents the angle between inclined plane and horizontal plane, τ_{dms}^* is effective dimensionless shear stress, $\frac{\partial Z_b}{\partial x}$, and $\frac{\partial Z_b}{\partial y}$ are bed change in x and y directions. The coefficient $c_{f\Theta} > 0$ is found from flume experiments to vary between 0.85 and 1.7, while the lower values are valid for natural channels (e.g. Talmon et al. 1995). Therefore, in this study, $c_{f\Theta} = 0.85$ is assumed for determination of $f(\tau_{dms}^*)$ and bedload transport angle α_b . For $c_{f\Theta} > 0$, the equation 4.58 is simplified by assuming $\cos^2\epsilon \approx 1$, the function $f(\tau_{dms}^*)$ is calculated by the following equation:

$$f(\tau_{dms}^*) = \frac{1}{c_{f\Theta} \cdot (\tau_{dms}^*)^{\frac{1}{2}}} \quad (4.59)$$

The flow direction or shear stress direction angle δ in Hydro_FT-2D is calculated from the tangent of depth-averaged flow velocity components in x and y directions $\tan\delta = \frac{u_y}{u_x}$ without taking into account the effect of secondary currents.

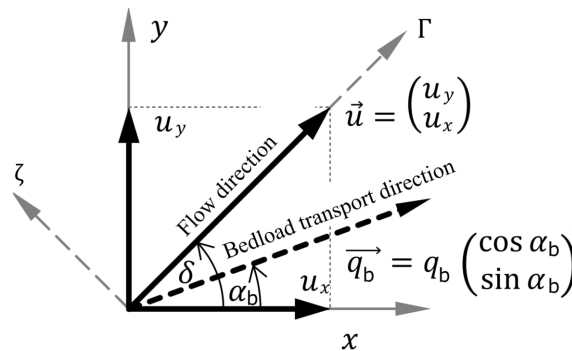


Figure 4.14.: Flow and bedload transport directions in a Cartesian coordinate system. Modified after Klar (2016)

IV- Gravity induced mass movement and river bank-failure

The bank-collapse in natural channels often occurs when the gravitational forces (primarily weight of the bank sediments) exceeds the frictional forces (due to inner grains' friction angle). The river bank-failure is accelerated by the fluvial erosion of river banks in

particular, in outward bends. Hydro_FT-2D simulates the bank-collapse when the channel bank angle exceeds the sediment frictional angle. As a result the material is extracted from higher-positioned elements and is piled to lower-positioned elements in a tilt-shaped movement until an equilibrium state is reached (Nujić et al. 2015b). Therefore, the maximum river bank angle is defined by the sediment frictional angle (often between 32° to 40°) for granular materials. In this study, all regime channel simulations are performed with a frictional angle of 37°, which allows the channel banks to have a maximum angle of 37°. The bank-failure can have significant impact on the movement of sediment mass in transverse direction, on the erosion process of river bends and eventually on the river morphology development.

V- Shear stress fluctuations

The stochastic nature of generating and dissolving turbulence eddies in the flow leads to temporal fluctuations of shear stress. These fluctuations of shear stresses may exceed the threshold of critical shear stress and may induce a bedload transport even during low flow discharges at which the average shear stress is lower than critical shear stress for initiation of bed sediments motion.

As a result of shear stress fluctuations, the exposed sediment particles will be transported during low discharges. Despite low bedload transport rates, if the contribution of low discharges in a hydrograph is significant, this may lead to a total of a significant amount of bedload transport, in particular for long-time simulations.

Günter (1971) differentiated three cases of shear stress fluctuations with time, all of them are relevant to a so-called weak sediment transport cases. Case 1 represents a condition in which the shear stress τ_m^* fluctuation peaks (maximum values) reach the bed critical shear stress τ_{cm}^* of a sediment mixture with the mean grain diameter of the surface layer D_{ms} . In this case, the mean bed shear stress $\overline{\tau_m^*}$ is equal to critical mean dimensionless shear stress $\overline{\tau_{cm}^*}$.

Case 2 occurs when the mean dimensionless shear stress $\overline{\tau_m^*}$ is equal to critical shear stress τ_{cm}^* . In this case, the dimensionless shear stress τ_m^* exceeds the critical condition during 50% of the time, which means 50% of the exposed particles are already in motion.

Case 3 represents a condition in which the mean bed shear stress $\overline{\tau_m^*}$ exceeds the critical dimensionless shear stress τ_{cm}^* at all the times, namely $\overline{\tau_m^*} = 2\tau_{cm}^* - \overline{\tau_{cm}^*}$ and all grains are in motion.

Günter (1971) defined the bed shear stress fluctuations ζ as the ratio of the critical shear stress for a sediment mixture τ_{cm}^* to the average critical shear stress $\overline{\tau_{cm}^*}$ and found a linear relationship between ζ and the flow Reynolds number as:

$$\zeta = \frac{\tau_{cm}^*}{\overline{\tau_{cm}^*}} \quad (4.60)$$

$$\zeta = \begin{cases} 1.03 + 3.4410^{-6} \cdot Re & \text{for } Re \leq 150000 \\ 1.03 + 3.4410^{-6} \cdot 150000 = 1.546 & \text{for } Re \geq 150000 \end{cases} \quad (4.61)$$

Thus the mean critical shear stress for the actual sediment grains incipient motion is

calculated as:

$$\overline{\tau_{cm}^*} = \frac{1}{\zeta} \tau_{ce}^* \left(\frac{D_{mo}}{D_{ms}} \right)^{0.33} = \frac{1}{\zeta} \tau_{cm}^* \quad (4.62)$$

In Hydro_FT-2D, this parameter is implemented based on the approach of Pazis and Graf (1977) For the so-called weak sediment transport for $\zeta = 1.546$ as:

$$\Phi_{dms,i,weak} = F_i \cdot \varphi_i^{3/2} \cdot k_f \cdot 8(1.764410^{-5} \tau_{cm}^*{}^{3/2}) \left[\left(\frac{\tau_{dms}^*}{\tau_{cm}^*} \right)^{8.15} - 0.0287 \right] \quad (4.63)$$

Although all simulations are performed with a constant flow discharge in this investigation, the shear stress fluctuations are considered in the model because, for long-time simulations of regime channels, the local shear stress fluctuations may influence total bedload transport and thus also the regime dimensions.

VI- The Layering concept in Hydro_FT-2D

1. Layering structure and vertical discretization

Hydro_FT-2D is a multi-layer model built upon an active layer or exchange layer (AS) followed by a subsurface layer (US), which in turn is followed by multiple base layers (GS). The exchange layer AS is the uppermost layer, where sorting process or selective transport may lead to coarsening or armoring of the surface layer in gravel-bed rivers, is in direct contact with water. The AS is implemented in the model as a storage layer to enable the exchange of sediments between the subsurface layer and bedload sediments. The thickness of the surface δ_{al} and subsurface δ_{ul} layers can be selected based on the maximum grain diameter of the surface layer sediments D_{max} as:

$$\delta_{al} = pal \cdot D_{max} \quad (\text{AS}) \text{ thickness} \quad (4.64)$$

$$\delta_{ul} = pul \cdot \delta_{al} = \delta_{ul,max} \quad (\text{US}) \text{ maximum thickness} \quad (4.65)$$

$$\delta_{ul} = pul/2 \cdot \delta_{al} = \delta_{ul,0} \quad (\text{US}) \text{ initial thickness} \quad (4.66)$$

$$\delta_{ul} = \delta_{al} = \delta_{ul,min} \quad (\text{US}) \text{ minimum thickness} \quad (4.67)$$

The parameters pal and pul serves as variables for controlling the thickness of AS and US. They can be given by the user, often a value of $pal = 1$ and $pul = 4$ are assumed. There is initially one base layer GS extending from a rigid (fixed) level up to the subsurface layer US. The program generates new base layers GS in the case of sediment deposition as soon as the set criterion is met (see details in figure 4.15).

The AS and US layers' grain size distribution (GSD) directly affects the bedload transport rate. In contrast, the GS represents the geological structure of soil far below the riverbed and is rarely activated, in particular, in the case of extreme bed changes. If the GSD of the GS is not known, the program assumes it to be the same as that for US layer. The control volume variables, as well as the vertical exchange of material between layers, are schematically shown in figure 4.15.

2. Layering management in Hydro_FT-2D

Layering management concepts set the interactions between layers, their GSD that change due to the sediment erosion and deposition in the model. The GSD of the layers are determined by volume balancing of sediment input (due to deposition) and sediment extraction (due to erosion). The model layering concept is based on the work of Hirano (1971) for calculation of changes in GSD of exchange layer AS, which is derived from a single layer model of flatbed and uniform flow condition. The first formulation of mixing layer is given by Armanini and Silvio (1988) between these three layers, accounting for the different adaptation-length of each grain size class. The thickness of mixing layer is assumed to remain constant and this simplifying hypothesis has a substantial impact on the morphological evolution times (Armanini 1995). According to Hirano (1971), temporal changes in GSD as a result of erosion and deposition is separately calculated as:

$$\frac{\partial p_{i,AS}}{\partial t} + \frac{1}{(1 - \eta_p) \delta_{al}} \left(\frac{\partial (p_{i,Tr} \cdot q_b)}{\partial \Gamma} - p_{i,ul} \frac{\partial q_b}{\partial \Gamma} \right) = 0 \quad \text{erosion} \quad (4.68)$$

$$\frac{\partial p_{i,AS}}{\partial t} + \frac{1}{(1 - \eta_p) \delta_{al}} \left(\frac{\partial (p_{i,Tr} \cdot q_b)}{\partial \Gamma} - p_{i,al} \frac{\partial q_b}{\partial \Gamma} \right) = 0 \quad \text{deposition} \quad (4.69)$$

The $\frac{\partial}{\partial \Gamma}$ is the partial derivative in the direction of flow, $p_{i,Tr}$ is the percentage of grain class i of bedload material, and η_p is the porosity of sediment.

In Hydro_FT-2D, the single-layer model of Hirano (1971) is modified for a multi-layer model by considering the rate of sediment input, output in a control volume as shown in figure 4.15. In case of erosion $q_{b_{in}} \leq q_{b_{out}}$, the material from US with GSD of subsurface layer $p_{i,ul}$ is fed via a material flow rate $M_{f,i}$ into the control volume. In the case of sediment deposition $q_{b_{in}} \geq q_{b_{out}}$, the material with the GSD of active layer $p_{i,al}$ is given to the US. The GSD of active layer AS is calculated at each time step from balancing sediment input rate b_{in} , output rate $q_{b_{out}}$ and material flow $M_{f,i}$ between active and subsurface layers as:

$$\frac{\Delta p_{i,AS}}{\Delta t} = \frac{p_{i,AS_{t1}} - p_{i,AS_{t2}}}{\Delta t} \quad (4.70)$$

$$\frac{\Delta q_b}{\Delta \Gamma} = \frac{q_{b_{in}} - q_{b_{out}}}{\Delta \Gamma} \quad (4.71)$$

$$q_{b,i} = p_{i,Tr} \cdot q_b \quad (4.72)$$

$$p_{i,AS_{t2}} = p_{i,AS_{t1}} + \frac{\Delta t}{(1 - \eta_p) \delta_{al} \Delta \Gamma} (q_{b,i,in} - q_{b,i,out} - p_{i,ul} \cdot \Delta q_b) \quad \text{erosion} \quad (4.73)$$

$$p_{i,AS_{t2}} = p_{i,AS_{t1}} + \frac{\Delta t}{(1 - \eta_p) \delta_{al} \Delta \Gamma} (q_{b,i,in} - q_{b,i,out} - p_{i,al} \cdot \Delta q_b) \quad \text{deposition} \quad (4.74)$$

The layering management for multi-layer approach in Hydro_FT-2D is schematically shown in figure 4.15 and explained for both erosion and sediment deposition cases in terms of exchange processes, layers GSD changes as a function of time (Nujić et al. 2015b).

1. Erosion case:

- When the critical shear stress is exceeded, the bed is eroded, and the material is taken from the subsurface layer US and transported downstream. In a control volume,

when the specific sediment input from the upstream is smaller than sediment output to the downstream, the erosion occurs, and the net sediment transport is calculated.

- The thickness of the active layer δ_{al} remains constant, and during an erosion, initial bed level z_b moves downward, and the thickness of the subsurface layer δ_{ul} reduces.
- The GSD of active layer alters as described by the equation 4.73 due to the vertical material flow M_f from the subsurface layer US, which imposes changes on each grain size fractions $p_{i,AS}$ as well as on the mean grain size diameter of surface layer D_{ms} .
- The GSD of the subsurface layer $p_{i,US}$ remains unchanged, but its thickness δ_{ul} reduces.
- If the erosive condition continues, the subsurface layer continues to decrease accordingly until the minimum thickness $\delta_{ul,min}$ is reached. The subsurface layer thickness remains constant afterward, and the material flow M_f is made from the base layer GS, hence GS is eroded.
- In case of erosion from GS, the GSD of US is equal to the GSD of GS.
- The GSD of the active layer $D_{ms}; p_{i,AS}$ during the vertical material flow from the base layer $M_{f,G}$ changes based on the GSD of GS.

2. Deposition case:

- Sediment deposition occurs when the specific sediment input from the upstream $q_{b,in}$ is larger than specific transport capacity $q_{b,out}$ inside a control volume.
- The initial bed level z_b moves upward while the thickness of the active layer δ_{al} remains constant.
- The GSD $D_{ms}; p_{i,AS}$ of the active layer AS changes and is calculated by balancing all sediment input and output inside a control volume using Hirano (1971) as described by equation 4.74.
- The vertical material flow downward from the active layer AS to the subsurface layer US leads to an increase in the thickness of this layer δ_{ul} as well as changes its GSD $D_{mo}; p_{i,US}$.
- When the thickness of subsurface δ_{ul} reaches its maximum value $\delta_{ul,max}$, a new base layer GS is generated with an initial thickness of half of $\delta_{ul,max}$. At this point, the thickness of the subsurface layer is reset back to its initial value, which is half of $\delta_{ul,max}$. The GSD of the new base layer GS is taken the same as the subsurface layer $D_{mGS} = D_{mo}; p_{i,GS} = p_{i,US}$.

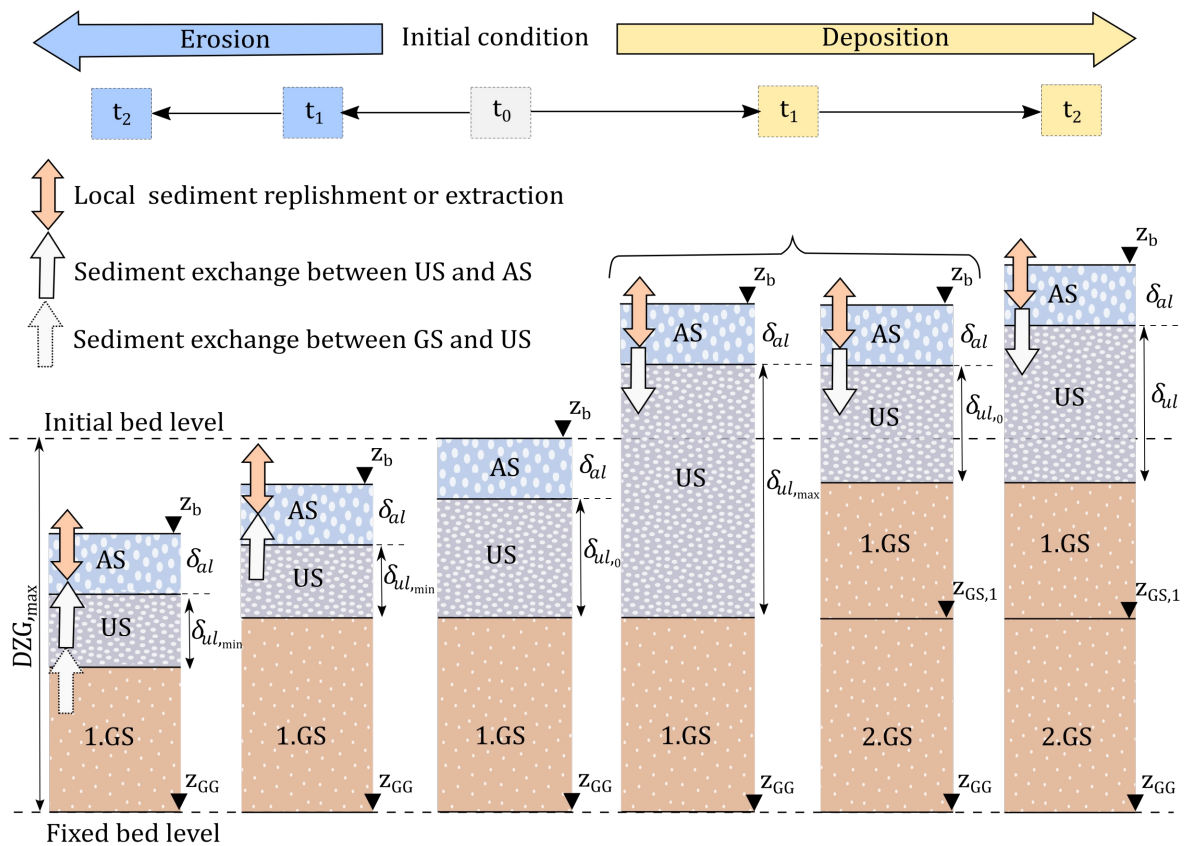


Figure 4.15.: Layering management in Hydro-FT-2D for both erosion and deposition cases
Modified after (Klar 2016; Nujić et al. 2015b)

4.5. Summary

In this chapter, four main topics are covered. First, a brief overview of channel regime approaches is provided and details are given to a central question on why an extremal approach can be useful for application to steep IRS. Further, the extremal regime theory of minimum Froude number (MFN) by Yalin and da Silva (2001) is discussed in detail. The MFN approach is further studied in terms of its application for estimating regime channel dimensions and flow resistance. In the second part, the steps are described on how the modelling tools can be employed to reproduce the channel regime development. The second part describes the steps for estimating relative flow resistance at regime state using 2D hydromorphological simulations. The methodology further shows the procedure for selecting initial channel dimensions and scenarios for setting the relative flow resistance in the Hydro_FT-2D model. Based on the initial channel dimensions, single and constant slope reaches and variable slope channel combinations are produced. Additionally, initial channel width is considered in two scenarios namely a fixed-width and extended-width resembling respectively a well controlled laboratory flume and natural channel conditions.

The third part explains the procedure for modelling MRE as geometrical shapes and their arrangement in step-pool or cascade bedforms in regime channel simulations. Further, the steps are described for preserving the MRE trapezoidal shapes throughout the channel regime development.

The last part focuses on describing the procedures for running hydro-morphological simulations including steps for mesh preparation and setting the boundary conditions including a brief description of the model Hydro_FT-2D.

5. Regime channel simulation results

5.1. Simulation results for flow resistance as numerical values

5.1.1. Channel regime dimensions development

I. Channel regime width

The channel regime width $w_R; w_{R1}$ for R and $R1$ regime channels are derived at the regime state from different cross-sections (CS) along the longitudinal distance and perpendicular to channel thalweg as shown in figure 5.1 for example of extended-width channel (a) and fixed-width (b). Regime channel R and $R1$ respectively represents a condition with zero and a constant bedload feeding at model's inflow. At least five cross-sections are defined for determination of regime width. The channel regime widths are determined based on the water depth, namely regions in a cross-section where $h > 0$ is assumed as the channel width as shown in figures 5.1 a_1 and b_1 for extended and fixed-width channels respectively. According to the above definition, two threshold regime channel widths can be estimated from the regime channel simulations. Minimum regime channel width $w_{R_{min}}; w_{R1_{min}}$ occurs at least at one of the cross-sections, while maximum regime channel width $w_{R_{max}}; w_{R1_{max}}$ occurs often near the bends. The average channel regime widths vary between $w_{R_{min}}; w_{R1_{min}}$ and $w_{R_{max}}; w_{R1_{max}}$.

The channel regime width $w_R; w_{R1}$ for R and $R1$ regime channels are plotted in x-y scatter, where the x-axis shows the channel regime slope $S_R; S_{R1}$, y-axis shows the channel regime widths $w_R; w_{R1}$. Each point in the scatter-plot displays the result of a single simulation as shown in figure 5.2 for the three out of six grain size distribution (GSD) for the subsurface layer $D_{mo} = 19 \text{ mm}$, $D_{mo} = 38 \text{ mm}$ and $D_{mo} = 57 \text{ mm}$. The regime channel width results for GSD $D_{mo} = 28.4 \text{ mm}$, $D_{mo} = 47.3 \text{ mm}$ and $D_{mo} = 66.3 \text{ mm}$ are respectively shown in figure 1 a, b and c in appendix B.

Maximum and minimum regime channel widths for both R and $R1$ regime channels are shown by red and blue colours respectively in figure 5.2 a, b and c for fixed-width, and a_1 , b_1 , and c_1 for extended-width channels. The regime widths values are shown by rectangles, circles and diamonds for GSD $D_{mo} = 19.0 \text{ mm}$, $D_{mo} = 38.0 \text{ mm}$, and $D_{mo} = 57.0 \text{ mm}$ respectively. The hollow symbol shapes represent the result for R and the filled ones show the results of $R1$ regime channels. The symbol shapes with center-bar and half-filled represent the results for extended-width of $Q = 1.0 \frac{m^3}{s}$.

As shown in figure 5.2, the channel regime widths do not vary with channel regime slope until roughly a slope of $S_R = 5.0\%$. For steeper channel slopes, a tendency toward larger channel widths with steeper slope is observed. This tendency of larger channel widths at

steeper channel slopes is more pronounced for extended-width channels.

The channel regime width for fixed-width channels in average vary between minimum of 1.8 *m* to 2.8 *m* to a maximum of 3.4 *m* to 6.0 *m*, however the latter may even take values of up to 9.0 *m*, in particular for channel regime slopes $S_R > 5.0\%$. The majority of large channel regime widths at $S_R > 5.0\%$ occurs for *R* regime channels compared to *R1* regime channels (see figure 5.2 a, b and c), because the sediment feeding in latter case saturate the transport capacity and therefore restricts the channel bank erosions.

The extended-width channels have in average about .0 *m* larger regime widths compared to fixed-width channels, namely minimum values between 2.8 *m* to 3.8 *m* and maximum values between 4.4 *m* to 6.5 *m*. However, for regime channels slopes $S_R > 5.0\%$, as large as 11.5 *m* regime widths are also observed (see figure 5.2 a₁, b₁, and c₁). Similar to fixed-width channels, extra-large regime widths for $S_R > 5.0\%$ occur in *R* regime channels only. The larger regime widths for the extended-width channels may be associated to the availability of large initial channel widths ≈ 16 *m* compared to fixed-width channels ≈ 5.5 *m*, which allows channel plan-form to develop freely in the transverse direction. The simulation results with $Q = 1.0 \frac{m^3}{s}$ for extended-width channels show lower regime widths in average by about 1.0 *m*, namely the minimum values between 1.85 *m* to 2.8 *m* and maximum values between 4.4 *m* to 5.5 *m*.

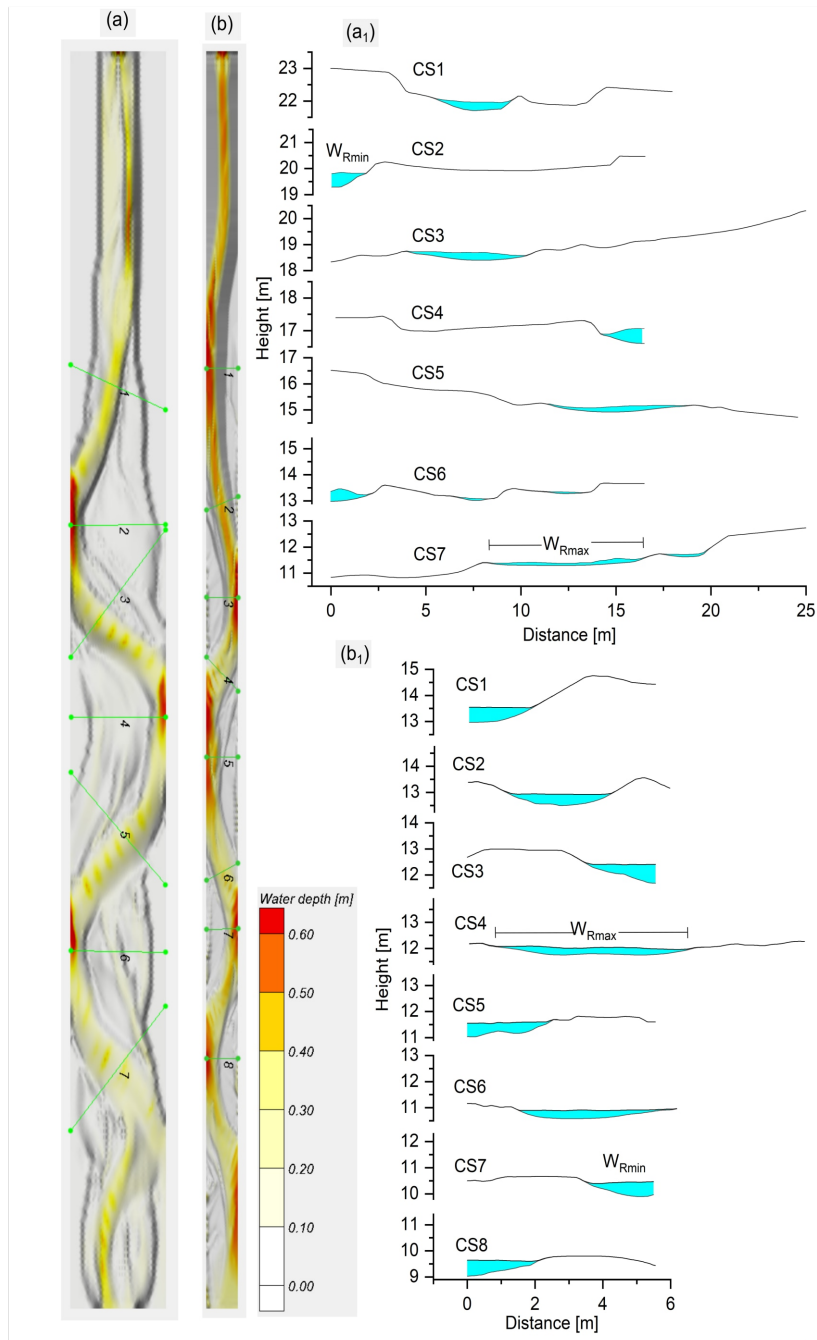


Figure 5.1.: Determination of regime channel width and depth at cross-sections shown on two examples of regime channels (a) and a₁ extended-width channel and its cross-sections and (b) and b₁ fixed-width channel and its cross-sections

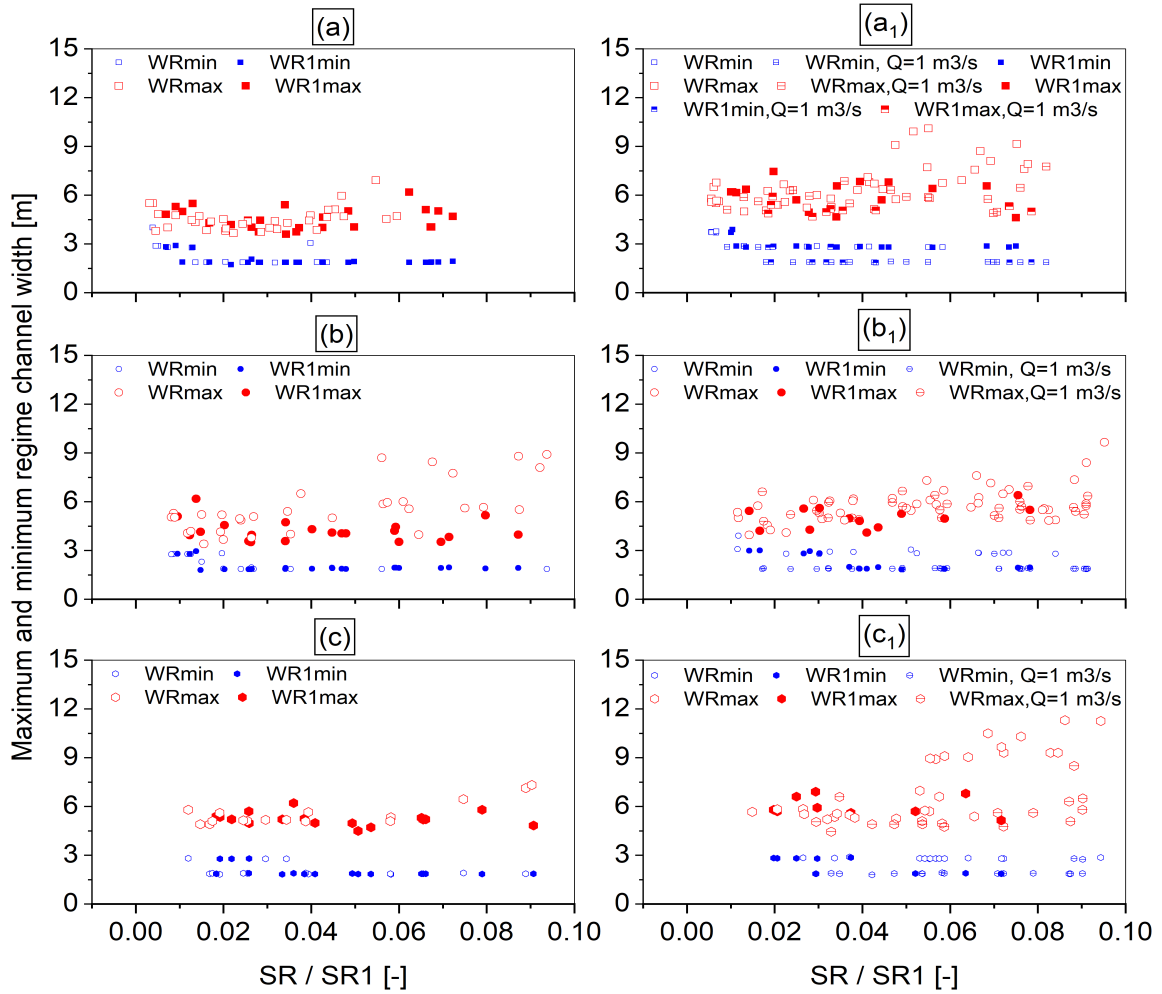


Figure 5.2.: Maximum and minimum regime channel width variations with channel regime slope (a) and (a₁) $D_{mo} = 19.0$ mm, (b) and (b₁) $D_{mo} = 38.0$ mm, (c) and (c₁) $D_{mo} = 57.0$ mm for fixed-width channels and extended-width channels respectively.

II. Channel regime depth

Channel regime depth h_R and h_{R1} is not a characteristic of a regime channel rather it adjusts itself based on the channel regime slope and width. The h_R and h_{R1} are extracted along the thalweg for the whole longitudinal profile of the regime channel. Three values for h_R and h_{R1} can be recognised in the thalweg as a result of the channel bedforms, namely a maximum value $h_{Rmax}; h_{R1max}$, a minimum value $h_{Rmin}; h_{R1min}$ and an average value $h_{Rave}; h_{R1ave}$. The maximum, minimum and average values are shown by red, blue and green colours in figure 5.3 a, b, c, and a₁, b₁, and c₁ for fixed-width and extended-width regime channels respectively. Each point in the scatter-plot displays the result of a

single simulation as shown in figure 5.3 for three out of six GSD D_{mo} values of 19.0 mm, 38.0 mm, and 57.0 mm. The regime channel depths results for GSD D_{mo} of 28.4 mm, 47.3 mm, and 66.3 mm are respectively shown in figure 1 a₁, b₁ and c₁ in appendix B.

The $h_{Rmax}; h_{R1max}$ are found in the deepest regions of the thalweg (e.g. in the pools of riffle-pool channel or pools of step-pool channel), while the $h_{Rmin}; h_{R1m}$ happens in the regions between two deep regions (e.g. in the riffle regions of a riffle-pool channel bed). Average regime channel depths $h_{Rave}; h_{R1ave}$ are derived by averaging the regime channel depths along the whole thalweg of a regime channel. The relationship between the regime channel depths $h_R; h_{R1}$ and slope $S_R; S_{R1}$ is plotted in x-y scatter as shown in figure 5.3. As expected, the regime depth decreases for steep regime channel slopes, while it increases for gentler regime channel slopes. On average, regime channel depths vary linearly with channel regime slopes.

Channel regime slope has a predominant control on the regime depth. However, the scatter in the values of regime depths may also be affected by the number of simulation results for each GSD, total roughness, bedforms, fixed or extended-width, and R or R1 regime cases. The scatter may also be as a result of different number of simulation results for each GSD, in particular for D_{mo} values of 19.0 mm, regime depth and width data up to a channel regime slope of 7.2% are achieved, which is comparatively less than those for 38.0 mm, and 57.0 mm. Total roughness values for GSD 19.0 mm, 38.0 mm, and 57.0 mm are respectively estimated to be $k_{st} = 29.52 \frac{m^{1/3}}{s}$, $k_{st} = 26.93 \frac{m^{1/3}}{s}$, and $k_{st} = 25.11 \frac{m^{1/3}}{s}$, which slightly increases the water depth as well as the regime channel depth with coarser GSD. Bedforms may also influence the average regime channel depth. An increase in riffle regions of riffle-pool channel may significantly decrease the average regime depth while for plane-bed regime channels, the bedform effect diminishes. The sharper decrease in regime channel depth with slope for fixed-width channels occurs due to the high concentration of flow in the main flow region as a result of small initial channel widths $\approx 5.5 m$. The high concentration of flow in the narrow main flow region induces large shear stress, which lead to erosion and deepening of channel bed. In case of extended-width channels, the large initial channel widths $\approx 16 m$, facilitate bank erosion and channel development in the transverse direction, which in turn allows spreading of flow over a larger area and therefore, the regime depth significantly decreases.

Regime channel depths for R1 regime channels show comparatively larger depth than R regime channels, especially for larger regime slopes roughly $S_R > 5.0\%$. The larger regime depths occur as a result of smaller regime widths for R1 regime channels, because the sediment feeding at model's inflow saturates the sediment transport capacity and therefore reduces the bank erosion. The results of regime depth for extended-width channels with both $Q = 2.0 \frac{m^3}{s}$ and $Q = 1.0 \frac{m^3}{s}$ show similar behaviour, because the difference in flow discharge is partly compensated by the larger regime width for earlier. In other words, the unit flow discharge q in $\frac{m^2}{s}$ for $Q = 2.0 \frac{m^3}{s}$ is not necessarily two times larger in magnitude than $Q = 1.0 \frac{m^3}{s}$, because larger regime width for $Q = 2.0 \frac{m^3}{s}$ results in a distribution of flow over a larger width. The larger regime width for $Q = 2.0 \frac{m^3}{s}$ reduces the bed shear stress and therefore, the erosion depth as well as the regime depth of

channel bed do not double compared to $Q = 1.0 \frac{m^3}{s}$.

Another important parameter namely the ratio of regime width to regime depth $w_{R;R1}/h_{R,R1}$, which shows the degree of channel entrenchment can be determined with known regime width and depth values. Based on the data of regime widths and depths, two threshold $w_{R;R1}/h_{R,R1}$ values are recognised. A maximum $w_{R;R1}/h_{R,R1}$ occurs at regions of maximum regime width and the smallest regime depths $w_{R;R1,max}/h_{R,R1,min}$. In contrast, a minimum $w_{R;R1}/h_{R,R1}$ occurs at regions with smallest regime width and largest regime depths $w_{R;R1,min}/h_{R,R1,max}$ as shown respectively for fixed-width and extended-width regime channels in figure 2 (a to f) and figure 3 a, b and c in appendix B. The results show that $w_{R;R1}/h_{R,R1}$ varies widely from extremely narrow channels with $w_{R;R1,min}/h_{R,R1,max}$ values of 1.5 to 7.6 to very wide channels with $w_{R;R1,max}/h_{R,R1,min}$ values of 7.0 to 60 for fixed-width regime channels. Similarly for extended-width channels, $w_{R;R1}/h_{R,R1}$ varies from extremely narrow channels with $w_{R;R1,min}/h_{R,R1,max}$ values of 2.3 to 8.5 to very wide channels with $w_{R;R1,max}/h_{R,R1,min}$ values of 9.6 to 75. The largest $w_{R;R1}/h_{R,R1}$ occurs more often for large channel regime slopes roughly $S_{R,R1} > 6.0\%$ and $S_{R,R1} > 5.0\%$ for fixed-width and extended-width channels respectively. R1 regime channels reveal lower $w_{R;R1}/h_{R,R1}$ compared to R regime channels, in particular they have lower $w_{R;R1,max}/h_{R,R1,min}$, mainly due to the smaller maximum regime widths $w_{R1,max}$ values.

A second parameter which consistently changes with channel regime slope is the width to depth ratio at the regime state $w_{R;R1}/h_{R,R1}$. Channels develop more entrenched channel widths form for low regime slopes, while for large regime slopes, the regime channel width may increase. On the other hand, the regime depth is larger for low regime slopes; in contrast it shrinks significantly for large regime slopes as can also be observed in figure 5.2. The w_R/h_R values for bulk of the simulations vary from 3 to 15 for low and large regime slopes respectively. However, w_R/h_R at regime channel slopes roughly $S_{R,R1} > 5.0\%$ may increase to 60 for fixed-width regime channels. This range of w_R/h_R occurs mostly for steep, entrenched, cascading, step-pool as well as in riffle-pool channels of moderate gradients (e.g. Rosgen 1996).

Regime channel pool regions occur often along the boundary and are comprised of narrow channel shapes, while wide channel regions happen in the riffle areas of shallow water depths and comparatively large regime widths between two successive pools (see details in section 4.1.5). It worths mentioning that the maximum and minimum $w_{R;R1}/h_{R,R1}$ shows the threshold condition for the regime channels and the average $w_{R;R1}/h_{R,R1}$ values occur for most of the regions in between the threshold values.

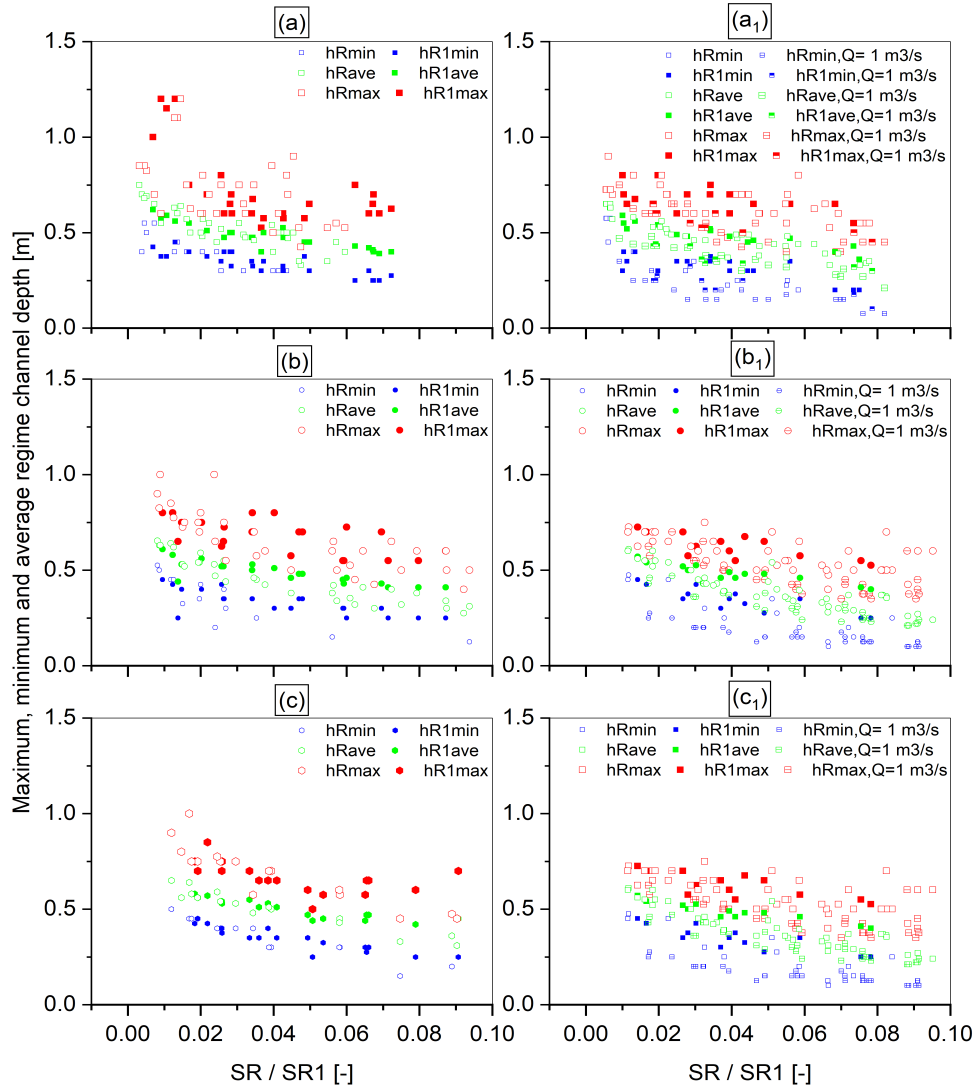


Figure 5.3.: Maximum, minimum and average regime channel depth variations with channel regime slope (a) and (a₁) for $D_{mo} = 19.0 \text{ mm}$, (b) and (b₁) for $D_{mo} = 38.0 \text{ mm}$, (c) and (c₁) for $D_{mo} = 57.0 \text{ mm}$ for fixed-width channels and extended-width channels respectively.

5.1.2. Relationship between regime slope and relative flow resistance

The relationship between relative resistance μ and channel regime slope $S_R; S_{R1}$ for R and $R1$ regime channels are plotted in x-y scatter, where the x-axis shows the channel regime slope and y-axis shows the relative flow resistance. The hollow symbols and solid symbols respectively represent the results of R and $R1$ regime channels. The symbol shapes rectangle, triangle, circle, diamond; pentagon and star in scatter graph respectively represent the results for GSD D_{mo} values of 19.0 mm , 28.4 mm , 38.0 mm , 47.3 mm , 57.0 mm ,

and 66.3 mm. Each point in the scatter-plot displays the result of a single simulation for a specific initial $S_R; S_{R1}$ and μ . As shown in figures 5.4, 5.5 and 5.6 for fixed-width scenario A, scenario B, and extended-width channels respectively, the relationship between μ and $S_R; S_{R1}$ can be well described by power-law relations as:

$$\mu = a(S_R; S_{R1})^{-b} \quad (5.1)$$

The values of a and b vary depending on the GSD D_{m0} , bedload feeding rate Q_b , flow discharge Q , and the initial channel width (fixed-or extended-width).

The μ and S_{R1} relationship in the case of bedload feeding Q_b are shown by the so-called equal-transport line (solid red line), which represents a trend line for a constant bedload feeding for different initial channel slopes S and μ . The red-dashed line represents the trend line for zero-sediment feeding case or R regime channels. The goodness of the regression fitted trend lines are shown by R-squared values. The shaded area above and below the trend lines represents the maximum and minimum range of the scatter variations shown in percentage. The light darker shaded area shows the variation range for R and $R1$ regime channels respectively. The relationship between relative resistance μ and channel regime slopes $S_R; S_{R1}$ are discussed below in details for fixed-width channels (scenario A and B), and extended-width channels.

I. Fixed-width channels

Scenario A:

The relationship between μ and $S_R; S_{R1}$ are shown for all six GSD sets in figures 5.4 (a to f). The power-law relationships factors a and b are ranging from 0.079 to 0.073 and 0.473 to 0.637 for GSD sets D_{m0} values of 19.0 mm to 66.3 mm respectively. It indicates that the value of a decreases with increasing grain sizes, while the value of b increases with larger grain sizes.

Similarly, the values of a and b for equal transport-lines for bedload feeding rates $Q_b = 5 \text{ kg/s}$ vary between 0.133 to 0.135 and 0.395 to 0.524 for GSD sets D_{m0} values of 19.0 mm to 66.3 mm respectively. The change in the values of a and b caused by the introduction of sediment feeding rate $Q_b = 5 \text{ kg/s}$ for $R1$ regime channel can be interpreted by a pure horizontal shift in regime slope ΔS_{R1} at low slopes and a pure shift in relative resistance $\Delta\mu$ at steep slopes. The shift in ΔS_{R1} means that for the same relative resistance μ , larger regime slopes $S_{R1} = S_R + \Delta S_{R1}$ are required to transport the sediment introduced as feeding at model's inflow. In other words, for the same regime slopes, flow resistance must be lower by $\Delta\mu = \mu - \Delta\mu$ in order to transport a given specific sediment feeding rate.

An increase in the value of a is interpreted as an increase in relative resistance shift $\Delta\mu$ for all channel regime slopes. A 5% increase in value of a for instance, leads to 4.76% increase in value of μ .

The value of b has a similar behaviour with μ as a , however an increase in the

value of b induces a differential increase in μ for different regime channel slopes. A 5% increase in the value of b causes about 8.7% and 4.4% increase for regime slope 1% and 10% respectively.

Similar to sediment feeding effect, GSD induces a shift in the fitted power-law trend line to differ by a ΔS and $\Delta\mu$ between finer GSD and coarser GSD. At low slopes $\Delta S_R \leq 2.5\%$, the shift is purely a ΔS -shift, while at high slopes $\Delta S_R \geq 7.5\%$, a pure $\Delta\mu$ -shift is observed. It indicates that at low slopes $\Delta S_R \leq 2.5\%$, a coarser GSD can achieve larger regime slopes for the same μ value and at high slopes, it requires larger μ value to achieve the same regime slope as for a finer GSD.

GSD has two major effects on the relationship between μ and $S_R; S_{R1}$. First, the coarser GSD has larger total roughness (see details in table 4.1, in chapter 4), which results in larger energy gradient based on the equation 4.39; thus increases the bed erosion. The different roughness values k_{st} based on the six sets of GSD show minimal effect on the bed shear stress. The bed shear stress slightly increases in an average range of 2.5% to 3.5%, 2% to 6.5%, and 5% to 9.5% for $k_{st} = 25.87 \frac{m^{1/3}}{s}$, $k_{st} = 25.11 \frac{m^{1/3}}{s}$, and $k_{st} = 24.53 \frac{m^{1/3}}{s}$, while it decreases by 3.5% to 8%, and 0.5% to 4% for $k_{st} = 29.52 \frac{m^{1/3}}{s}$, and $k_{st} = 28.25 \frac{m^{1/3}}{s}$ respectively compared to the result with roughness value of $k_{st} = 26.93 \frac{m^{1/3}}{s}$. A detailed analysis of the effect of total roughness difference on the bed shear stress for varying channel regime slopes are shown in figure 4 appendix B.

Secondly, the dimensionless shear stress or mobility parameter τ_{dms}^* is calculated based on the mean grain diameter of the surface layer D_{ms} by $\tau_{dms}^* = \frac{\mu \cdot S \cdot h}{(s-1)D_{ms}}$. The mobility parameter is significantly influenced by the value of D_{ms} , which indicates that for coarser GSD, lower mobility values are calculated compared to finer GSD for the same bed shear stress. Mobility parameter is interpreted as lower bedload transport rates for $\tau_{dms}^* - \tau_{cm}^* \geq 0$ and more importantly for $\tau_{dms}^* - \tau_{cm}^* < 0$, no bedload transport rates may occur. Therefore, lower bed erosion or channel slope reduction is observed for the same relative resistance values μ for coarser GSD compared to finer GSD of surface layer. The effect of the mobility parameter may dominate the counter effect of larger energy gradient for coarser GSD based on the equation 4.39.

The scatter in the data shows that certain channel regime slopes can be achieved at different μ values. There is no unique μ value for a single channel regime slope, rather a numbers of μ values roughly in the range of $\pm 5\%$ to $\pm 15\%$ can correspond to a single channel regime slope. The main reason for this behavior is the sorting process in the gravel-bed rivers and streams. The sorting process occur as a result of selective transport of fine sediment grains from the channel-bed leading to coarsening of the channel bed. At a certain relative resistance μ , the larger the difference between initial channel slope and regime slope is, the coarser the regime bed surface layer sediment D_{ms} is resulted. An example for $\mu = 0.492$

5. Regime channel simulation results

corresponds to two regime slopes $S_R = 2.03\%$ and $S_R = 2.16\%$ for initial channel slopes $S = 2.5\%$ and $S = 4.5\%$ respectively. The associated mean diameter of the surface or exchange layer sediments at the regime state are observed to be $D_{ms} = 30 \text{ mm}$ and $D_{ms} = 34 \text{ mm}$ respectively.

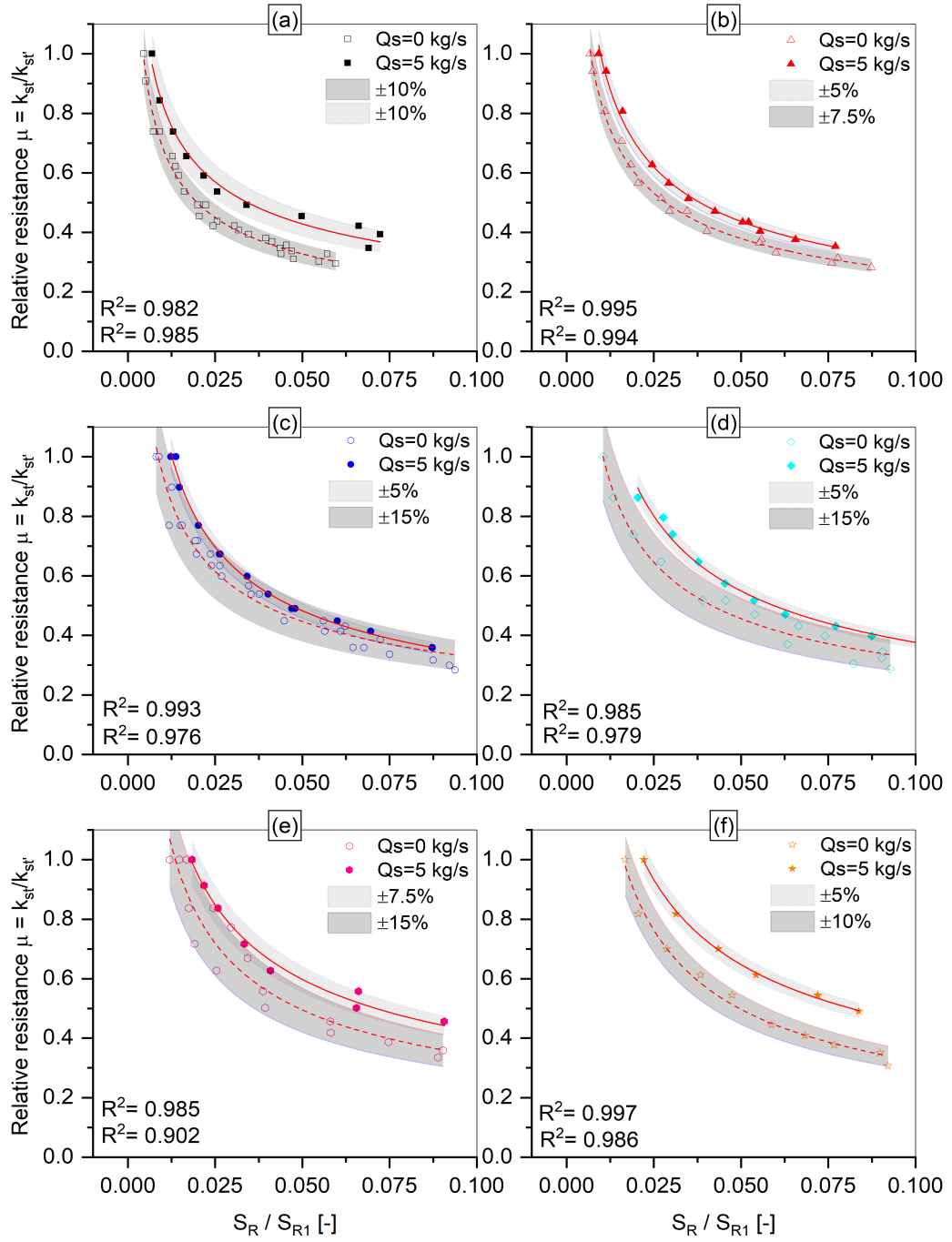


Figure 5.4.: Relationship between relative resistance μ and fixed-width channel regime slope S_R/S_{R1} for regime channels R and R1 with a feeding rate of $Q_b = 5$ kg/s for D_{mo} values of (a) 19.0 mm (b) 28.4 mm (c) 38.0 mm (d) 47.3 mm (e) 57.0 mm and (f) 66.3 mm

Scenario B:

The simulations for scenario B are performed for fixed-width channels only to find out the differences in relative resistance and channel regime slope relationships. Therefore, the relationship between μ and S_R for both scenario A and B are shown for GSD sets D_{mo} values of 19.0 mm, 38.0 mm, and 57.0 mm in figure 5.4 a, b and c respectively. The hollow and dot-center hollow symbols respectively represent the results for scenario A and B in the scatter graph. The dashed lines show the trend lines and the shaded area represents the variation range of data in figure 5.4 a, b and c.

Similar to scenario A, the relationship between μ and S_R is well expressed by a power-law $\mu = a(S_R)^{-b}$. The value of a and b vary between 0.011 to 0.021 and 0.822 to 0.935 for GSD sets D_{mo} values of 19.0 mm to 57.0 mm respectively.

The relationship between μ and S_R for both scenarios starts at $\mu = 1$, which corresponds to a condition, where the total roughness is equal to grain roughness or the form roughness or any other additional roughness is absent, namely $k_{st} = k_{st'}$. As the total roughness k_{st} value for scenario B is decreased $\mu < 1$, the difference between scenario A and B accordingly increases. In comparison to scenario A, much lower μ values are observed in order to achieve the same regime slope S_R , because as per definition of μ in scenario B $\mu = k_{st}/k_{st'}$, the value of total roughness k_{st} is decreased for varying the value of μ , which in response to the reduced value of total roughness k_{st} , the bed shear stress increases. Thus, lower μ values partly compensate the increased shear stress as a result of decrease in total roughness, while the value of grain roughness $k_{st'}$ is held constant for a GSD set. Based on the definition of $\mu = k_{st}/k_{st'}$ in scenario B, regime state in particular for larger channel slopes can only be achieved when the value of k_{st} is drastically decreased to as low as $2.5 m^{1/3}/S$. The very low total roughness values at the regime state achieved in scenario B occur to some extent also in natural rivers and streams of steep slope with presence of macro-roughness elements (MRE) and large bedforms (i.e. step-pool, cascade, and rapids) (e.g. Reid and Hickin 2008; Yochum 2010).

The effect of GSD is similar to scenario A, namely coarser GSD causes a horizontal shift to the left as well as a vertical shift upward. An early detachment of scenario B graph from scenario A for simulation results with D_{mo} values of 19.0 mm figure 5.5 a represents the effect of mobility parameter, which is much larger for finer GSD compared to coarser GSD. The decrease in total roughness k_{st} values in scenario B strongly increases the energy gradient, which in turns increases the mobility parameter. Thus, the detachment of scenario B graph from scenario A occurs later for coarser GSD (see figure 5.5 b and c).

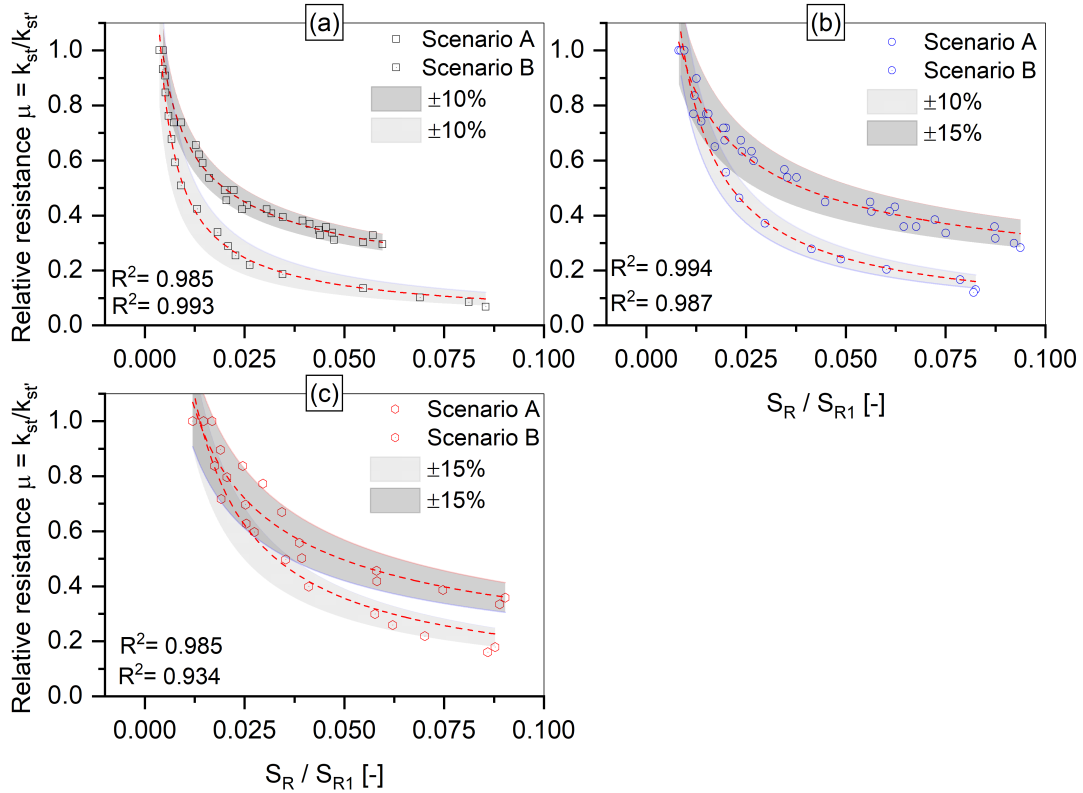


Figure 5.5.: Relationship between relative resistance μ and fixed-width channel regime slope S_R for D_{mo} values of (a) 19.0 mm (b) 38.0 mm and (c) 57.0 mm for both scenario A and B

Both scenario A and B have their limitations in terms of naturally occurring total roughness, grain roughness and addition roughness. The distribution of total roughness, grain roughness and additional roughness (form roughness plus MRE roughness) with channel regime slope is presented for GSD with D_{mo} values of 38.0 mm in figure 5.6. In scenario A, the k_{st} in Strickler values are calculated based on the GSD, $k_{st'}$ are varied such that $k_{st} < k_{st'}$ and the k_{add} is calculated by $1/k_{add} = 1/k_{st} - 1/k_{st'}$. The k_{add} follows a power-law relationship with channel regime slope, namely k_{add} values are decreasing with S_R . This behavior of increasing role of k_{add} with channel slope is also observed in nature that larger bedforms such as cascades, antidunes, chutes and dunes are developed for steep channel slopes compared to riffle-pool bedforms for gentle slopes. The bedforms developed for steep channel slopes at regime state tend to develop by the simulations results (see details in 4.1.5). The increasing contribution of k_{add} in the model is made possible by decreasing the role of $k_{st'}$, namely by increasing their Strickler values with S_R . The increasing $k_{st'}$ with S_R is not occurring in natural

channels, because the GSD does not refine as the channel slope increases. The increasing value of $k_{st'}$ with S_R is therefore treated here as an academic example to influence the model's k_{add} values with S_R . Nonetheless, it is also observed in the nature that with increasing contribution of k_{add} in k_{st} at steep channel slopes, the contribution of $k_{st'}$ becomes insignificant.

In scenario B, $k_{st'}$ value is calculated based on the GSD of surface layer sediments and held constant for all channel slopes. The k_{st} values are decreased with increasing channel slopes and the calculated k_{add} values shows a power-law relationship with S_R . Scenario B is shown to agree better with natural observation in terms of $k_{st'}$ values that does not change with channel slope unless there is significant downstream coarsening or fining of GSD. The contribution of k_{add} is similar to scenario A, namely increasing with S_R , however, the role of k_{add} is increasing much sharper compared to scenario A. Unlike scenario A, the k_{st} and k_{add} values are decreasing with S_R for scenario B and their values become as low as $2.5 \text{ m}^{1/3}/\text{s}$ to achieve regime state for $S_R > 7.5\%$. Such very low Strickler values for k_{st} and k_{add} do not occur in nature. More importantly, such low values of k_{st} in the model leads to very large water depths $h > 2.0 \text{ m}$ even for channel slopes $S_R > 7.5\%$, which is not realistic, because at steep slopes, water depth should significantly decrease. On the other hand, very low Strickler values for k_{add} is interpreted as conversion of large bed geometry elements into roughness Strickler values, which should be critically observed, because larger geometry of bed should be treated as geometry and not as roughness values. Therefore, scenario B should be dealt with caution and should be applied only in the range of k_{st} and k_{add} values, which are also observed in natural channels.

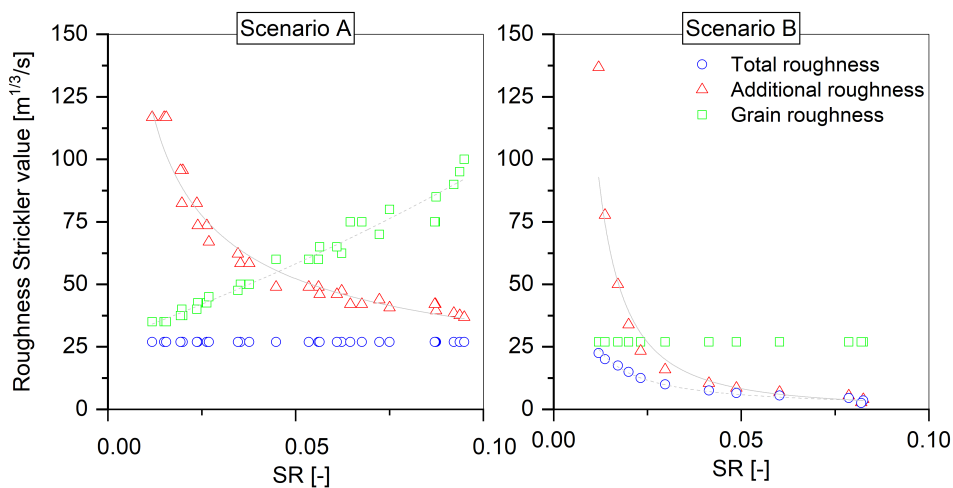


Figure 5.6.: Relationship between total roughness k_{st} , additional roughness k_{add} and grain roughness $k_{st'}$ with channel regime slopes for scenario A and B

II. Extended-width channels

The relationship between μ and $S_R; S_{R1}$ for extended-width channels are shown for GSD with D_{mo} values of 19.0 mm, 38.0 mm and 57.0 mm respectively in figure 5.7 a, b and c. Additionally, the results for $Q = 1.0 \frac{m^3}{s}$ for the extended-width channels are shown by hollow symbols with center line and half-solid symbols in the scatter graph in figure 5.7 a₁, b₁, and c₁ for GSD with D_{mo} values of 19.0 mm, 38.0 mm, and 57.0 mm respectively.

The relationship between μ and $S_R; S_{R1}$ follow similar to fixed-width channels a power-law. The power-law relationships factors a and b are ranging from 0.109 to 0.102 and 0.413 to 0.566 for GSD sets with D_{mo} values of 19.0 mm to 57.0 mm respectively. Similarly, values of a and b for equal transport-lines for bedload feeding rate $Q_b = 5 \text{ kg/s}$ for R1 regime channel vary between 0.161 to 0.100 and 0.386 to 0.616 for GSD sets with D_{mo} values of 19.0 mm to 57.0 mm respectively. The results show larger a and b values for extended-width channels compared to the fixed-width regime channel results. Larger a and b values means that for the same relative resistance values μ , larger regime slopes are achieved. In other words, same regime slopes are resulted with larger μ values. The main reason for the larger a and b values for the extended-width channels are because of the larger regime channel widths by about 1.0 m compared to fixed-width channels. This allows the flow to spread over a larger area and therefore causes a reduction in bed shear stress. The decrease in bed shear stress leads to larger regime slopes for the same μ values, GSD and flow discharge.

The μ and $S_R; S_{R1}$ relationship shows larger scatter in particular for larger regime slopes compared to fixed-width channels. The scatter in the data is in the range of roughly $\pm 5\%$ to $\pm 15\%$ from their average trend line as shown by the shaded areas in figure 5.7. The scatter in relationship of μ and $S_R; S_{R1}$ is mainly as a result of more dynamic channel plan-forms and their random changes during the regime development. The plan-form dynamic is facilitated by the larger initial widths of the extended-channels. Plan-form development is usually completed at the initial phase of regime development; however some channels showed random plan-form change even after initial phase. The random plan-form change temporarily disrupts the already stable channel plan-form and increases the erosion, which leads to lower regime channel slopes compared to no plan-form change. The random plan-form change occurs as a result of instant variation of flow discharge partially in the channel bank regions, where the D_{ms} are much finer than main channel region. The D_{ms} in the main channel region coarsens strongly as a result of selective transport, while the bank regions have much smaller D_{ms} . Thus with even a smaller overflow onto the bank region, a sediment transport and bed erosion may be initiated that can significantly change the plan-form and further reduce the channel regime slope (more details in 4.1.4 and 4.1.5).

The simulation results with $Q = 1.0 \frac{m^3}{s}$ induces a horizontal shift to the left and a vertical shift upward of the average relationship between μ and $S_R; S_{R1}$ for $Q = 2.0 \frac{m^3}{s}$. This is shown by the power-law relationship factors a and b that vary from 0.112 to 0.107 and 0.539 to 0.631 for GSD sets with D_{m0} values of 19.0 mm to 57.0 mm respectively. Larger a and b means that the simulation with $Q = 1.0 \frac{m^3}{s}$ and same relative resistance μ values leads to larger channel regime slope compared to simulations with $Q = 2.0 \frac{m^3}{s}$. Furthermore, the difference in channel regime slope ΔS_R for the same values of relative resistance μ increases with coarser GSD as shown in figure 5.7 a_1, b_1 and c_1 for D_{m0} values of 19.0 mm, 38.0 mm, and 57.0 mm respectively. The ΔS_R is caused as a result of lower bed shear stress for $Q = 1.0 \frac{m^3}{s}$, which induces lower channel bed erosion and therefore, larger regime slopes are achieved for the same μ . Further, the effect of sediment mobility parameter which decreases with coarser GSD becomes very obvious for flow discharge of $Q = 1.0 \frac{m^3}{s}$.

The investigation for varying flow discharge from $Q = 2.0 \frac{m^3}{s}$ to $Q = 1.0 \frac{m^3}{s}$ reveals that flow discharge magnitude and GSD are the primary control parameters for the regime channel slope and relative resistance relationship. The important point in the relationship between μ and $S_R; S_{R1}$ is their power-law relationship regardless of flow discharge magnitude, GSD and channel initial dimensions (e.g. fixed-or extended-width). The μ and $S_R; S_{R1}$ relationship shows that for regime channels, the role of total resistance is increasing with regime channel slope and in contrast, the role of grain resistance diminishes with increasing channel slope. The scatter in the simulation results for the μ and $S_R; S_{R1}$ relationship is caused predominantly by the magnitude of difference between initial and regime channel slopes. However, channel plan-forms dynamic in particular for extended-width channels may also play a significant role.

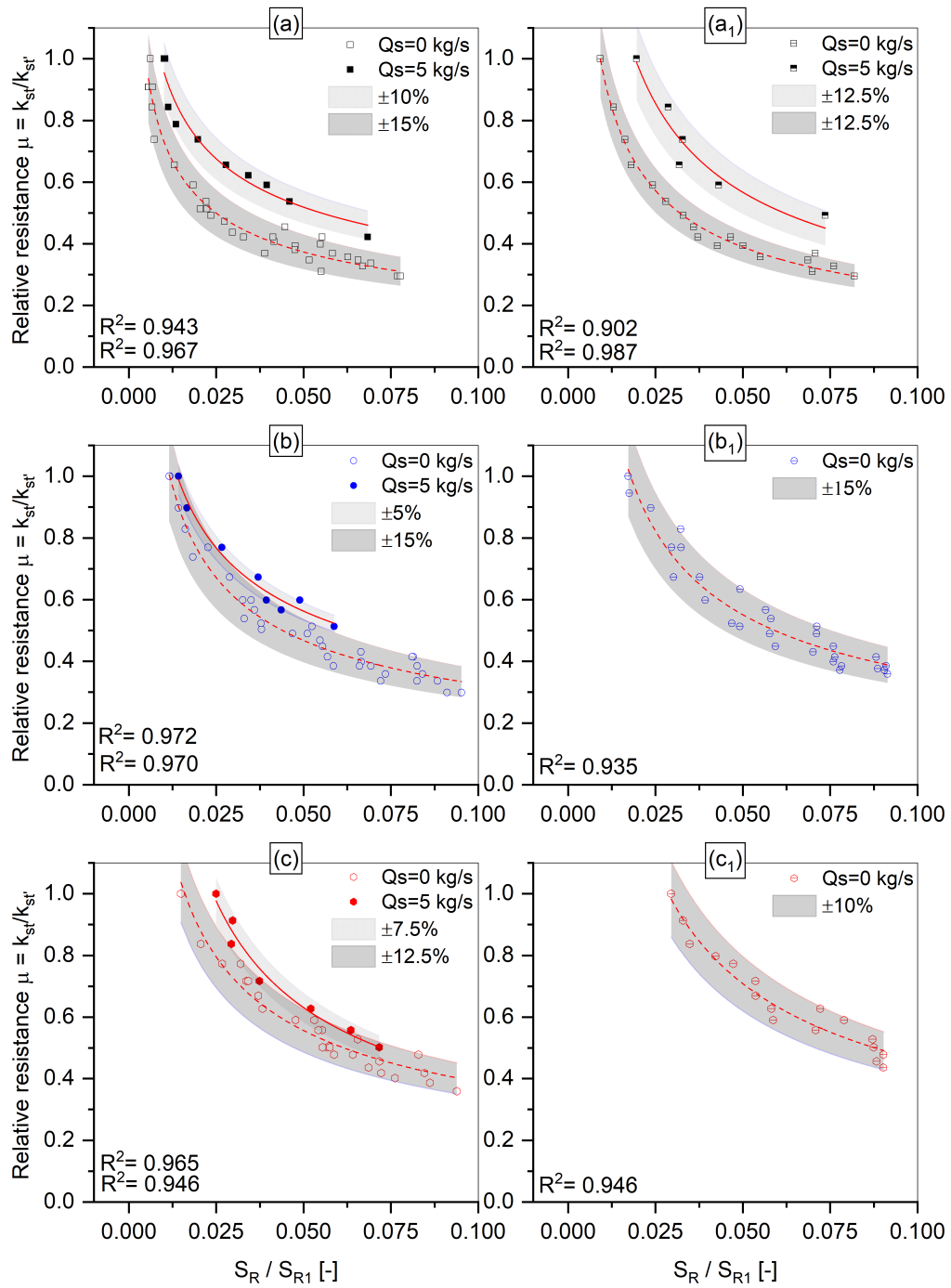


Figure 5.7.: Relationship between relative resistance μ and extended-width channel regime slope $S_R; S_{R1}$ for regime channels R and R1 with a feeding rate of $Q_b = 5$ kg/s for (a), (a₁) $D_{m0} = 19.0$ mm (b), (b₁) $D_{m0} = 38.0$ mm (c), (c₁) $D_{m0} = 57.0$ mm for flow discharge of 2.0 m³/s and 1.0 m³/s respectively

III. Channel slope combination results

In nature, the channels are composed of constant slope stretches, thus the relationship between the relative resistance μ and regime slope S_R for GSD with D_{m0} values of 38.0 mm is applied on three simple slope combination cases. The regime slope of a channel stretch in a slope combination can be smaller, larger or the same as initial channel slope depending on the given μ , location of channel stretch in a channel slope combination and its upstream and downstream stretches' initial slope and μ values. In figure 5.8 a, b, and c, one example of regime longitudinal profiles (in blue) for channel slope combination case 1, 2 and 3 are respectively shown. In general, a flattening tendency of initial channel slopes toward a single channel for the sum of all stretches can be observed from the longitudinal profiles of all three cases.

The channel regime development starts from a stretch, where for the given μ value and initial channel slope, the bed sediment starts moving. The sediment erosion therefore may start from an inflow stretch, middle stretch or outflow stretch. If the erosion starts from the inflow stretch, it propagates downstream. At the same time, the erosion from a middle stretch may propagate in both directions, while the erosion from outflow stretch may propagate in the upstream direction. The erosion propagations from different stretches meet each other at some point to form a continuous channel plan-form, which further develops to achieve a regime state.

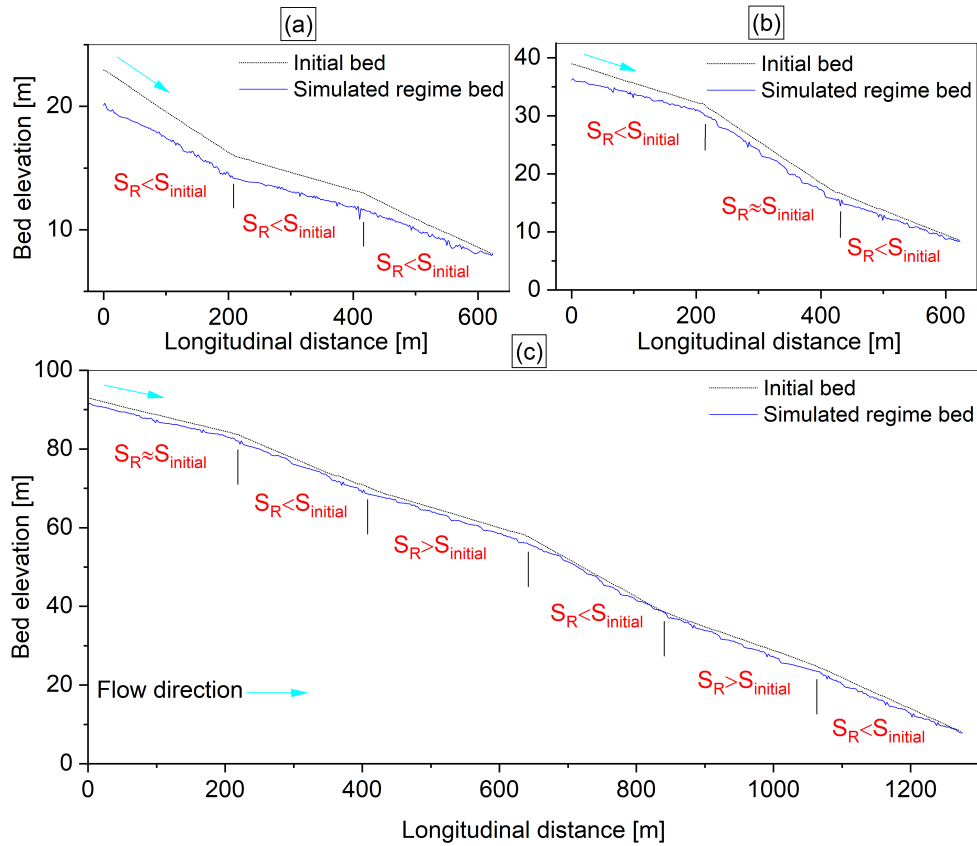


Figure 5.8.: Channel regime profiles and their initial values for examples of channel slope combinations (a) case1 (b) case 2 and (c) case 3

The relationship between relative resistance μ and channel regime slope S_R for the channel slope combination cases are plotted together with the results of single constant slope channels in figure 5.9. Despite the effect of boundary and stretch combinations, the overall trend in μ and S_R relationship agrees well with those from the single constant slope results. The μ and S_R relationship for combined slope cases show that for a single μ values, several S_R can exist depending on the location of initial channel stretch in a channel slope combinations. The inflow channel stretch in a slope combinations is found to have the lowest S_R for a single μ value, while larger S_R values are observed for the end and middle stretches respectively. The S_R values for $\mu = 0.6$ for instance results in the lowest $S_R = 0.025$ for the inflow stretch, $S_R = 0.037$ for a middle stretch and $S_R = 0.032$ for end stretch of a slope combination. The results of the inflow stretches in a slope combination agrees well with the single slope results of no sediment feeding. However, the results for middle and end stretches are comparable with a R1 regime channel with a sediment feeding rate at model's inflow. The difference

in S_R for the same μ values for middle and end stretches can be caused due two main reasons. First, the effect of boundary condition in particular for the middle stretches are less pronounced compared to inflow and outflow stretches. The boundary condition for the inflow and outflow of middle stretches in particular, are controlled by their upstream and downstream stretches and their flow and sediment transport conditions. Secondly, the middle and end stretches in a slope combination are behaving as $R1$ regime channels, because the bed erosion from the inflow stretch or upstream stretches supply sediments to downstream stretches. Therefore, several S_R values may develop for a μ value depending on the location of the channel stretch in a slope combination.

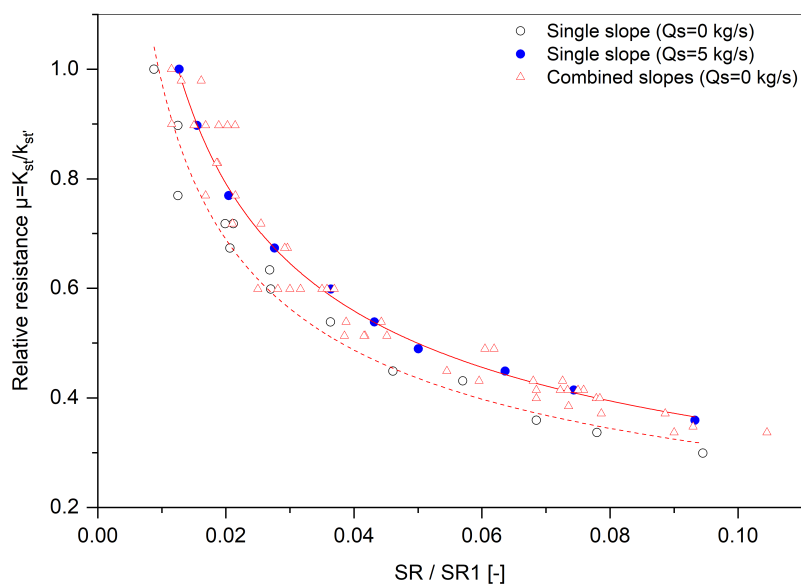


Figure 5.9.: Relationship between relative resistance and channel regime slope for single slope channels (circles), single slope with sediment feeding (filled circle) and combined slope cases (triangles)

5.1.3. Comparison of simulation results with field observations

The relationship between relative resistance μ and channel regime slope S_R acquired from simulations results by fulfillment of regime status are compared with some data from field observations. The relative resistance data are derived by comparing measured bedload transport in steep natural channels and steep flume experiments. Bedload transports in natural steep channels are either measured by a bedload sampler (e.g. B-69) during a specific flow discharge or a cumulative total bedload transport volume is measured at the end of a specific flow event (e.g. one year flood, five year flood). Steep flume experiments show higher bedload

transport compared to natural steep channels, because flume experiments do not include the effect of flow resistance due to bedforms (step-pool, cascade, and existing of MRE) and availability of mobile grains as a result of riverbed armouring. The additional resistance due to bedforms and MRE dissipate large part of flow energy at steep channel slopes otherwise available for bedload transport. On the other hand, the availability of mobile sediments may be limited in natural channels, due to selective transport process leading to riverbed surface armouring. The flume experiments often lack the effect of additional resistance, and the resistance to flow is as a result of grain resistance therefore higher bedload transport is measured in steep flume experiments. The grain resistance in the case of flume experiment can be approximated using for instance the equation developed by Meyer-Peter and Müller (1948) assuming D_{90} as a characteristic sediment grain diameter for calculation of grain roughness $k_{st'} = 26/(D_{90})^{1/6}$. The total roughness k_{st} in the case of natural steep channels are estimated from velocity measurements. The ratio of $k_{st}/k_{st'}$ represents the relative share of flow resistance based on which the bed shear stress and subsequently bedload transport are calculated. Based on the flow resistance equation of Manning-Strickler, the energy gradient is proportional to the square of Manning n value, therefore the reduced energy gradient S_{red} is expressed by $S_{red} = S(k_{st}/k_{st'})^2$. The energy gradient in bedload transport formula developed based on the steep flume experiments is replaced by the reduced energy gradient and therefore a better agreement between bedload transport data of flume experiments and natural steep channels are achieved.

The first dataset of bedload transport based on which the relative resistance is derived are from 19 gravel-bed rivers and torrents of bed slopes up to 17% (Rickenmann 1994; Rickenmann 1996) shown by dot center red circles in figure 5.10. The second bedload transport data are measured at 17 mountainous rivers and streams of average slopes raging between 2.3% and 15.3% in Himalaya-Karakorum region (Palt 2001). The total flow resistance is derived from velocity measurements and the grain resistance is calculated by $k_{st'} = 26/(D_{90})^{1/6}$ using the D_{90} of bed sediments. The relative resistance $k_{st}/k_{st'}$ is shown by green triangles as a function of channel slope in figure 5.10. The third bedload data are from six steep torrent channels of steep slopes ranging from 0.7% to 52% in Switzerland and Austria, where the cumulated sediment budgets as a result of specific flood events are available (Chiari and Rickenmann 2010). The relative resistance $k_{st}/k_{st'}$ is determined from a back-calculation of reduced energy slope $S_{red} = S(k_{st}/k_{st'})^2$ by a one dimensional SETRAC sediment transport model for reproducing the cumulative sediment budget at the end of specific flow event as shown by blue rectangles in figure 5.10.

The results of simulations using regime approach for fixed and extended-width are shown by stars and dot center stars respectively in figure 5.10. The black and

grey stars refer to the results of scenario A, and B respectively. The simulation results are comprised of results for all six used GSD with mean grain size diameters D_{m0} values of 19.0 mm, 28.4 mm, 38.0 mm, 47.3 mm, 57.0 mm, and 66.3 mm, and three GSD with D_{m0} values of 19.0 mm, 38.0 mm, and 57.0 mm for fixed and extended-width channels simulations respectively. The comparison addresses three main points regarding the variation of relative flow resistance with channel slope. The relationship between relative flow resistance and channel slope can be well expressed by power-law $\mu = a(S_R)^{-b}$ despite different a and b values for each dataset, which can be strongly influenced by the approach the μ is derived as well as by the boundary conditions. All datasets show a general trend that at high slopes, the role of grain resistance minimises, while the role of additional resistance dominates. The regime channel approach results cover a large spectrum of GSD show good agreement with field observations by following an average trend. The large scatter in the data are mainly as a result of different boundary conditions for the datasets in consideration. In this regard, the important parameters are the unit flow discharge q in m^2/s , GSD D_{m0} and relative flow submergence often represented by h/D_{90} .

The flow discharge varies widely for the datasets used in this comparison. While the flow discharge for regime approach in this study is constant $2.0 m^3/s$, it varies between $1.0 m^3/s$ to $342.0 m^3/s$, $0.0 m^3/s$ to $140.0 m^3/s$, and $0.03 m^3/s$ to $2400.0 m^3/s$ for the datasets of (Palt 2001), (Chiari and Rickenmann 2010) and (Rickenmann 1994; Rickenmann 1996) respectively. Despite large variation in flow discharges, the flow discharge per unit bed, which is considered more relevant in inducing bed shear stress remains significantly comparable. Since larger flow discharges lead to larger channel regime dimensions, as discussed in section 4.1.2 chapter 4, the channel width adjust based on the bankfull flow discharge and bed GSD $w_R = 1.5D^{-0.25}Q^{0.50}$, while water depth is as a result of adjustment by satisfying the resistance $h_R = 0.15D^{-0.07}Q^{0.43}$. On the other hand, during the flood events, water depth may also rise, which in turn increases the relative flow submergence h/D_{90} . As a result the relative flow resistance may also increase, because the effect of additional roughness decreases with increasing flow submergence. The effect flow submergence can be clearly observed in figure 5.10 that for the same channel slope, several relative resistance values are observed and each of them belongs to a single flow discharge event. Riverbed GSD affects the grain resistance, relative flow submergence h/D_{90} and finally the bedload transport.

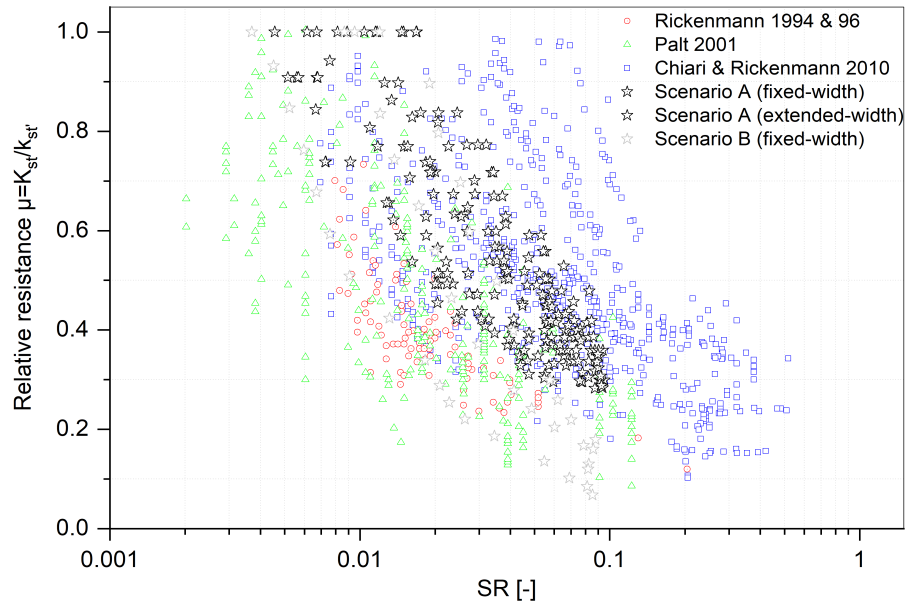


Figure 5.10.: Comparison of relative resistance relationship with channel regime slope acquired through regime channel simulations (stars) and field observations

5.1.4. Bedload transport

Bedload transport rates in kg/s and their cumulative total transport in (tons) at models' outflow are plotted as a function of regime development duration for regime channel R and $R1$ for simulations results of GSD with D_{mo} values of 38.0 mm in figure 5.11 and 5.12 respectively. The bedload transport rates and their cumulative total transport at model's outflow for R regime channels are presented in figures 5.11 a, a₁ and b and b₁ for fixed-width and extended-width regime channels respectively. The results for GSD with D_{mo} values of 19.0 mm and 57.0 mm are shown in figure 1 and 2 in Appendix C for fixed and extended-width regime channels respectively.

The bedload transport rates are selected from large number of simulations results covering a wide range of regime channel slopes. The solid black line represents the sediment feeding rates at model's inflow and the color dotted lines show bedload transport rates at model's outflow for some selected channel regime slopes S_R .

The bedload transport in general shows two stages of regime development, namely an initial and a late or final stage. In the initial stage, the bedload transport starts from zero at $t = 0$ and increase rapidly until reaching to a peak value. It recedes afterwards and decreases gradually by lower rate of change compared to rising limb (figure 5.11 a and b). The cumulative total transport at the initial stage shows a rising trend before reaching an asymptotic trend in the final stage of regime

development (figure 5.11 a₁ and b₁). The larger bedload transport rate in the initial stage is associated with large channel dimension adjustment to the flow field, in particular, as a result of channel regime width and large part of channel regime slope development.

Bedload transport rates may contain several smaller peak values between start and end of the initial stage, in particular for larger regime slopes. The intermediate peaks inside the initial regime stage occur as a result of significant plan-form changes. Random plan-form change may also occur during the final stage of regime development, because the GSD of surface layer sediment D_{ms} in the main flow region coarsens significantly, while it remains comparatively finer in the channel bank regions (see section 5.1.5). The finer GSD in the bank regions can initiate a bedload transport even for low flow discharge's deflection over the bank region from the main flow region. The instant or random plan-form change during the final stage of regime development initiates new bed sediment erosion. The intermediate peaks as a result of plan-form change occurs more often for extended-width channels compared to fixed-width channels predominantly due to the larger width offered by the earlier.

The late or final stage contains a further decrease in bedload transport approaching a zero value with low fluctuation. This is largely because major channel regime adjustments such as regime width and large part of regime slope are developed in the initial stage. The late stage does not involve any further regime width development but the channel slope further decreases at significantly lower rates toward the regime state. The cumulative total transport in this stage approaches toward a close to perfect asymptote. Since a small bedload transport rate may even be present at the final regime stage, in particular for large regime slopes, therefore a perfect asymptote is hardly achieved. The bedload transport approaches a zero value for regime slopes roughly $S_R \leq 5\%$, while for $S_R > 5\%$, a minimum bedload transport may also be present at end of final regime stage. The existence of such low bedload transport even by the end of regime development may not significantly affect the channel regime slopes. However, it definitely contributes to the cumulative total transport at model's outflow. These low bedload transport at large regime slopes may be due to the effect of weak transport as a result of shear stress fluctuations.

The initial and late stage duration depends on variables such as GSD, initial channel slope and the difference between initial and regime channel slope. In case of small difference between initial and regime channel slope ΔS , the initial stage may take longer, because the regime development is relatively slow due to the lower shear stress exceeding the critical values for sediment entrainment. The solid and grey dashed lines respectively represent the bedload transport rates at model's outflow for an initial and regime channel slopes $\Delta S = 1.5\% - 0.88\% = 0.62\%$ and $\Delta S = 2.5\% - 1.30\% = 1.20\%$ respectively see (figure 5.11 a, and a₁). The initial

stage respectively takes approximately 5 days for $\Delta S = 1.20\%$ and 10 days for $\Delta S = 0.62\%$.

The total regime development duration is observed to reduce with increasing GSD, namely the regime development duration reduces from average of 40 days for $D_{mo} = 19.0 \text{ mm}$ to 25 days for $D_{mo} = 57.0 \text{ mm}$ as shown in figure 1 and 2 (a, b, e, and f) in appendix C. The main reason for the longer regime development duration for finer GSD is due to the higher mobility parameter, which is inversely related to the GSD of the surface layer sediments D_{ms} . In case of large difference between initial and regime channel slope, the bedload rates increases rapidly to a larger peak value in relatively shorter time, largely due to the large shear stress as a result of large initial slope. The durations of late stage in this case are much longer compared to the initial stage, because of the large difference between initial and regime slopes (e.g. dotted red and solid lines in a and a₁ respectively). Additionally, large ΔS results in accordingly large cumulative total transport values compared to low ΔS simulations.

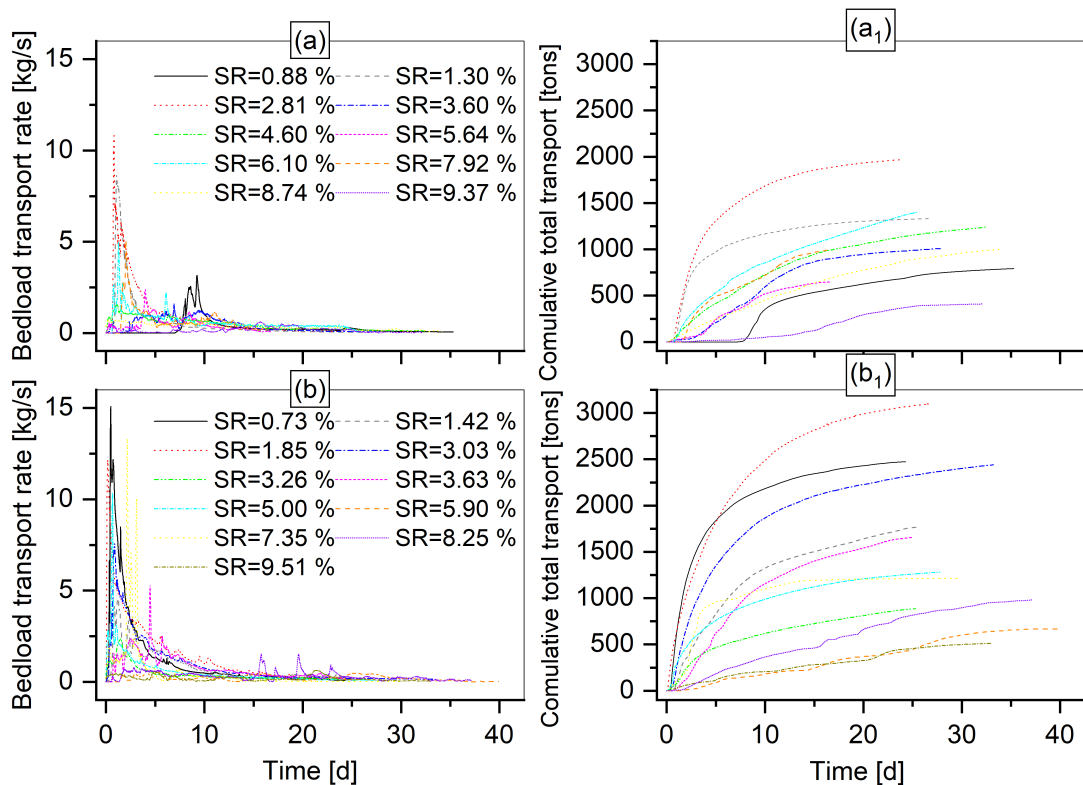


Figure 5.11.: Bedload transport rates and their cumulative total transport at model's outflow for R regime channels of GSD D_{mo} value of 38.0 mm (a) and (a₁) for fixed-width channel (b) and (b₁) extended-width channel

Bedload transport and their cumulative total transport for the *R1* regime channels with a constant feeding rates at the model's inflow is shown for constant feeding rate of $Q_b = 5.0 \text{ kg/s}$ in figure 5.12 a, a_1 and b, b_1 for GSD with D_{mo} value of 38.0 mm for fixed and extended-width channels respectively. The results of *R1* regime for GSD with D_{mo} values of 19.0 mm and 57.0 mm are shown in figure 1 and 2 (c, d, g, and h) in appendix C for fixed and extended-width regime channels respectively.

Similar to regime channel *R*, bedload transport for regime channel *R1* have initial and late or final phases with earlier having large bedload transport with fluctuations, while the latter is following the sediment feeding rate. The cumulative total transport for *R1* regime channels is represented by lines of constant slopes. At the regime state, the slope of cumulative total transport line for the sediment feeding at model's inflow and bedload transport at model's outflow should be approximately the same. Larger cumulative total sediment transport at model's outflow than input feeding sediments at model's inflow means stronger channel slope reduction. In rare case, channel regime slope may slightly increase to achieve the transport capacity required to transport the fed sediments at model's inflow (see for example dash-dotted pink line in figure 5.12 a), which has lower cumulative total transport than the fed sediments (solid line).

At first look at the figure 5.12, one can differentiate that regime channel *R1* development for fixed-width channels (figure 5.12 a) is slightly faster compared to extended-width channels (figure 5.11 b). The average total time for fixed-width channels regime development is ranging from 15 to 30 days, while it takes between 15 to 45 days for extended-width channels. The contribution of initial phase and late phase also differs for fixed-width and extended-width channels. The initial regime development phase's duration vary between 10 to 15 days and 15 to 20 days for fixed-width and extended-width channels respectively. Additionally, the fluctuations of bedload transport in the initial phase is much larger for extended-width channels compared to their fixed-width counterparts. The main reason for the longer regime development and large fluctuations in bedload in the initial phase is due to the large bank erosions the extended-width channels provide compared to fixed-width channels.

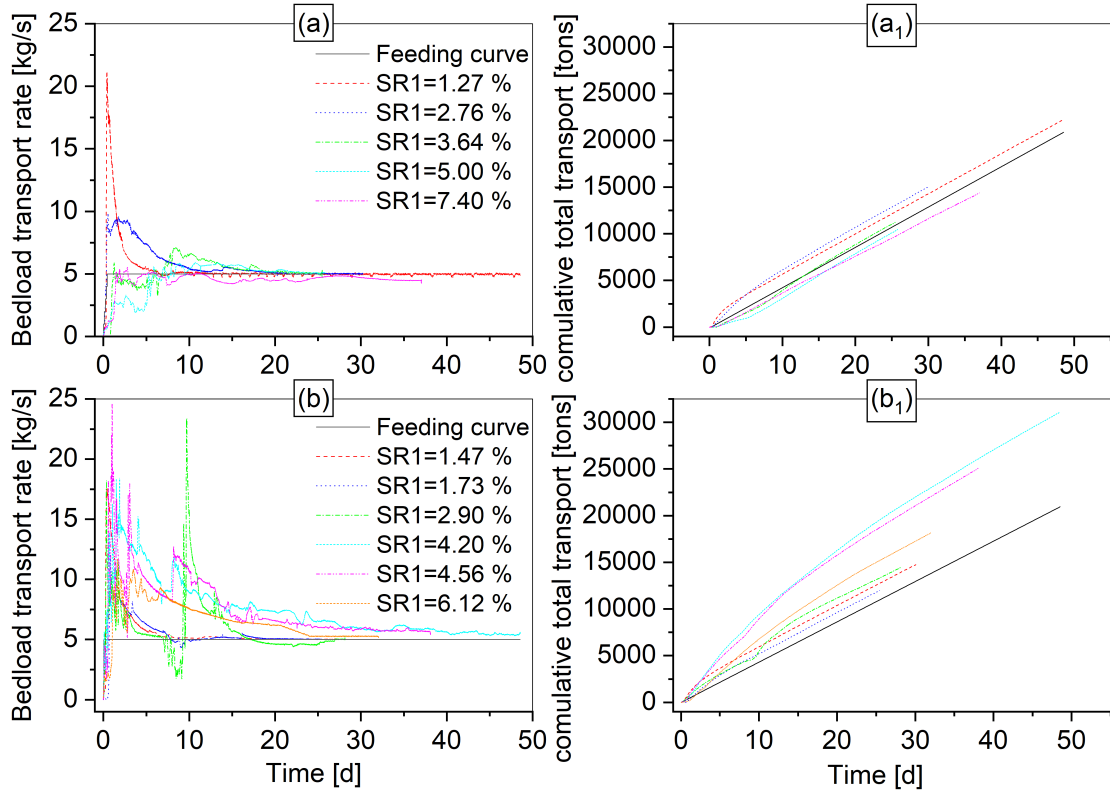


Figure 5.12.: Bedload transport rates and their cumulative total transport at model's outflow for $R1$ regime channels of constant feeding rate $Q_b = 5.0 \text{ kg/s}$ for GSD with D_{mo} value of 38.0 mm (a) and (a₁) for fixed-width channel (b) and (b₁) extended-width channel

5.1.5. Grain size distribution (GSD) at regime state

Channel bed GSD is shown for four examples of extended-width regime channels of initial GSD with D_{mo} values of 38.0 mm for both R and $R1$ regime development in figure 5.13. The GSD of the surface or exchange layer is significantly coarsened for R regime channel development. The coarsening is shown to be a function of difference between initial channel slope and regime slope, namely larger difference in slope ΔS leads to coarser channel bed sediments. The difference between mean grain diameter for the surface layer at regime state D_{msR} (dashed blue lines) and initial values D_{ms} (solid grey lines) are shown for two R regime channel cases of $\Delta S = 2.65\%$ and $\Delta S = 1.5\%$ in figure 5.13 a and b respectively. The main flow region of the channel bed surface shows significant coarsening, while the bank regions show fining compared to initially given GSD. The channel with larger ΔS shows much coarser surface GSD compared to smaller ΔS . Additionally, the

coarsening is shown to have a downstream decreasing tendency as also shown in the longitudinal profiles of D_{msR} along the channel thalweg in figure 5.13 a₁ and b₁. The simulation results show that at beginning of regime development, D_{ms} decreases strongly from the initially given values, because of the large erosion rates, which feed much finer sediments from the second layer D_{mo} (red dotted lines in figure 5.13 a₁ and b₁). As the erosion rate decreases as a result of channel slope decrease, the transport capacity decreases accordingly. Therefore only finer grains can be transported and the D_{ms} coarsens (blue dashed lines in figure 5.13 a₁ and b₁). The longitudinal profiles of D_{ms} for $\Delta S = 2.59\%$ and $\Delta S = 1.5\%$ in figure 5.13 a₁ and b₁ respectively show that at initial stage (1 Day and 2 Days), the D_{ms} decreases. It then gradually coarsens significantly at regime state D_{msR} (26 Days and 27 Days). The channel bed sediment coarsening occurs as a result of selective transport, which transports all the fine grains and coarser grains remain on the bed surface. Channel bed armoring is caused when the sediment supply in gravel-bed rivers and streams is restricted, which resembles *R* regime channels. The D_{ms} for *R1* regime channel is strongly controlled by the GSD of feeding sediments D_m , which is the same as GSD of the second layer D_{mo} . The D_{ms} decreases gradually as a result of mixing with the feeding sediments at inflow and erosion from second layer D_{mo} (figure 5.13 c and d). The decrement in D_{ms} decreases with regime development and eventually stops at the regime state. Unlike *R* regime channel, ΔS has no significant influence on the regime GSD of surface layer D_{msR1} , mainly due to the strong control of feeding sediment GSD. Since the outflow boundary nodes are set as non-erodible in Hydro_FT-2D, therefore, both D_{msR} and D_{msR1} values equal initial given D_{ms} shown by solid grey line in figure 5.13 a₁ to d₁. Unlike *R* regime channels, *R1* regime channels resemble natural gravel-bed rivers and streams with a continuous sediment supply from upstream that controls the GSD of bed sediments. Further, the GSD of bedload transport D_{mTr} (orange dash-dotted lines) is shown to follow closely the GSD of feeding sediments (in green dashed line) throughout the longitudinal profile of the channel as shown in figure 5.13 c₁ and d₁. However, some deviation is observed at inflow and outflow regions as a result of the boundary effect. The results of GSD at regime state for the fixed-width channels behave in general similar to extended-width channels as presented in figure 3 (a₁, c₁, e₁, g₁, and i₁) of appendix C. However, it is observed that the D_{ms} coarsening as a result of selective transport is not as intense as for the extended-width channels. Three-times larger initial channel width in case of extended-width channels allows free channel-width development in transverse direction. Thus, larger channel bed area are exposed to selective transport. In contrast, fixed-width channels have width of 5.5 m and the flow in transverse direction is limited. The selective transport occurs inside a 5.5 m channel, therefore the D_{ms} is largely controlled by the mixing with sediments from D_{mo} . Similarly, the channel bed sediments coarsening for *R* regime channels and strong control of

sediment feeding GSD on the bed sediments in *R1* regime channels are shown to be independent of initial GSD values. The simulation results for the rest five GSD with D_{m0} values of 19.0 mm, 28.4 mm, 47.3 mm, 57.0 mm, and 66.3 mm produce similar behaviour as for the one discussed here as shown in figure 3 (b_1 , d_1 , f_1 , h_1 , and j_1) of appendix C.

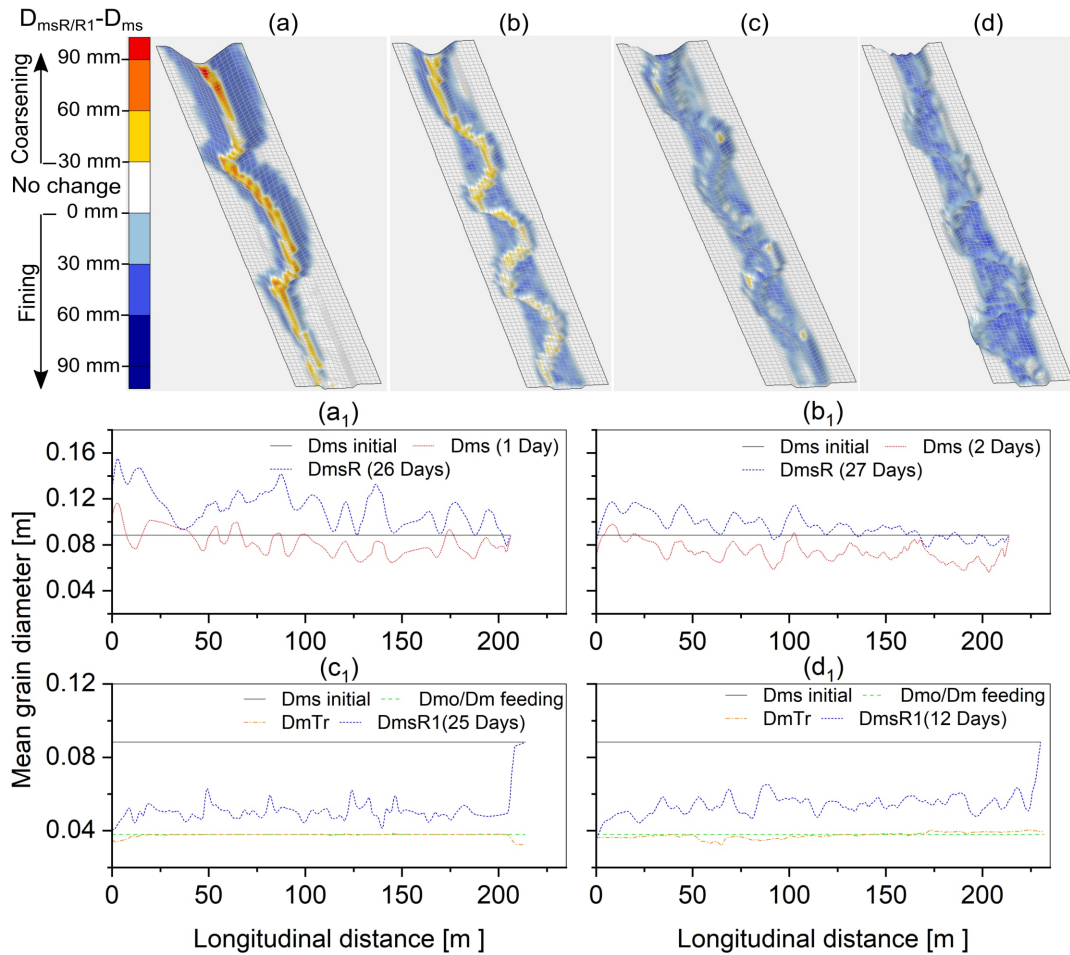


Figure 5.13.: Difference between GSD of channel bed sediments at regime state and their initial values for (a) $\Delta S = 2.65\%$ (b) $\Delta S = 1.5\%$ (c) $\Delta S = 2.59\%$ (d) $\Delta S = 1.5\%$ and their associated longitudinal distribution in (a_1) (b_1), (c_1) and (d_1) respectively

5.1.6. Channel regime morphology development

The morphology of the regime channels are analysed in terms of their plan-form development (figure 5.14) and their bedform development shown in longitudinal profiles in figures 5.15 and 5.16 for fixed and extended-width channels respectively.

The plan-forms for some selected regime channels with regime slopes from 0.89% to 9.40% are shown in figure 5.14 a, and b, for examples of fixed-width, extended-width channels respectively.

The regime plan-forms show a meandering tendency regardless of channel regime slope, GSD, and fixed or extended-width channels. The sinuosity of the regime channels varies between 1.0 and 1.1 for most of fixed-width regime channels, while it ranges between 1.0 and 1.2 for the extended-width regime channels as shown in figure 1 appendix D. The larger channel sinuosity for extended-width channels are merely due to the large initial channel widths offering sufficient space for channel plan-form development in the transverse direction.

Fixed-width and extended-width channels reveal slightly different plan-forms with channel regime slopes. The fixed-width channel produce alternate bar formation for all tested channel slopes as shown in figure 5.14 a. The wavelength of the alternate bars in average varies between 65 m to 80 m, which agrees well with the findings from flume experiments (e.g. Ikeda 1984).

The extended-width channels' plan-forms vary from single thread deep incised for channel slopes roughly $S_R < 6\%$ to multi-thread or braiding for $S_R > 6\%$. Despite existence of a single main channel, several smaller channels also develop, which conveys part of the total flow to downstream. The channel course develops extensively in transverse direction before reaching the rigid boundaries, which act as stabilising factor for plan-form development as shown in figure 5.14 b. The channel plan-forms, in particular at larger slopes $S_R > 6\%$, undergo large erosions in the downstream regions until the channel-width reaches either of the rigid or fixed boundaries. Due to the large side erosions that occurs because of the availability of large channel erodible beds, the sinuosity slightly increases compared to fixed-width channels. The channel regime slope at which the plan-form development reaches a rigid boundary is observed to vary with GSD. The plan-form development reaches fixed-boundary for D_{mo} values of 19.0 mm, 38.0 mm and 57.0 mm at regime slopes $S_R > 4\%$, $S_R > 5\%$, and $S_R > 6\%$ respectively. The side erosion causes comparatively larger channel regime widths, which in turn leads to larger w_R/h_R ranging from 3 to 80.

The plan-form development for $R1$ regime channels in general shows similar pattern as R regime channels. However, the plan-form dynamic is significantly intensified for $R1$ regime channels due to the introduction of constant sediment feeding at the model's inflow. The channel plan-form dynamic is more pronounced for extended-width channels compared to fixed-width channel for $R1$ regime channels. The channel plan-form dynamic for instance, for an initial channel slope $S = 4.5\%$ and $\mu = 0.7$ develops its plan-form inside about 10 m of total 16 m width, while it reaches the rigid boundary 16 m after introduction of sediment feeding $Q_b = 5.0 \text{ kg/s}$. The plan-form development for $R1$ channels are shown for some selected channel regime slopes in figure 2 appendix D.

The combined slope channels reveal similar plan-forms with channel regime slope as single slope channel cases. However, the plan-form is strongly influenced by the neighbouring stretches as shown in figure 3 of appendix D. Three examples of slope combination cases (1), (2) and (3) shown in figure 3 of appendix D reveal that in general alternate bars wavelength decreases with increasing regime channel slope.

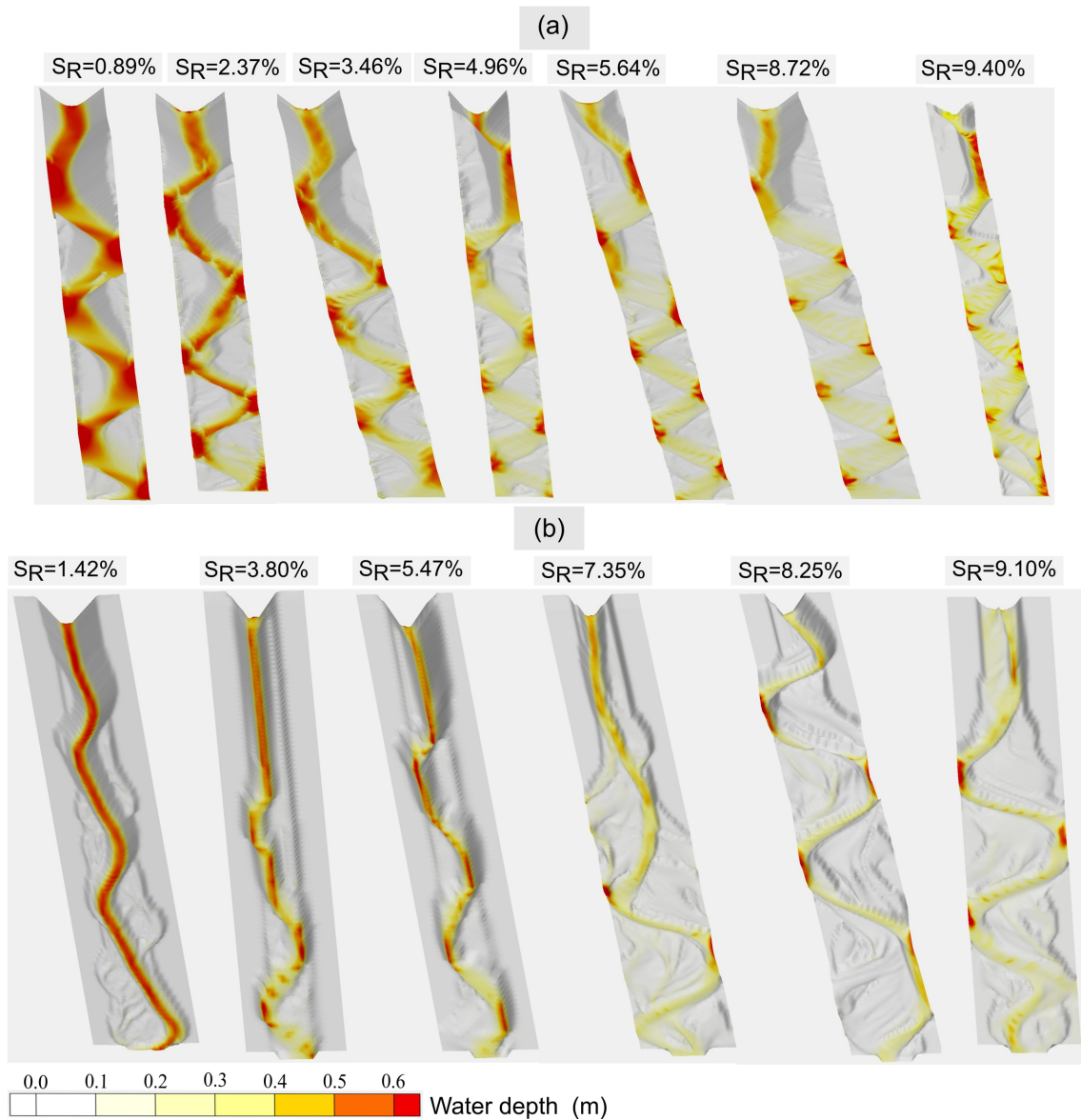


Figure 5.14.: 3D view of channel plan-forms for some selected regime slopes using $D_{mo} = 38.0 \text{ mm}$ (a) fixed-width channels (b) extended-width channels

The longitudinal profiles derived along the thalweg of the regime channels R are

shown for all six sets of GSD for regime slope ranges 0-1.5%, 1.5-3.0%, 3.0-4.5%, 4.5-6.0%, 6.0-8.0%, and 8.0-10.0% respectively in figure 5.15 a, b, c, d, e, and f. The longitudinal profiles are shown by solid black, green dashed, red short dashed, grey dash-double-dotted, blue dotted, and magenta short dash dotted lines for the mean diameter of subsurface layer sediments D_{mo} values of 19.0 mm, 28.4 mm, 38.0 mm, 47.3 mm, 57.0 mm, and 66.3 mm respectively.

The Froude number F_r has a strong control on the channel bedforms, thus for each channel slope ranges, F_r are derived for the lowest and largest channel regime slopes. The F_r is calculated using the definition adopted by Yalin and da Silva (2001) as $\frac{U^2}{gh}$. The F_r is averaged from large number of values from the thalweg region occurring throughout the channel course. The F_r values are not the largest F_r values occurring rather represent an average F_r distribution. The longitudinal profiles reveal three major bedforms. The regime channels develop riffle-pool bedforms with infrequently spaced pools roughly up to a regime slope of about $S_R \leq 6\%$ and at larger slopes $S_R > 6\%$, a step-pool, cascade or antidune bedforms can be recognised. The peaks observed in most of the riffle-pool bed profiles occur due to the scours in regions between riffles and pools. Despite the fact that simulations for all grain size sets develop similar channel regime bedforms, a tendency can be observed that fine grain size sets changes its bedform from riffle-pool to cascade at comparatively lower regime channel slopes than coarser ones. The finest grain size set with D_{mo} value of 19.0 mm for instance, develops step-pool forms for regime slope $S_R > 5\%$, while for the coarsest set with D_{mo} value of 66.3 mm, it occurs for a regime slope $S_R > 7\%$. For larger F_r values, Hydro_Ft-2D Model may run at its limit and can lose accuracy, however some studies reported reliable results by Hydro_FT-2D Model for $F_r > 1$ (e.g. Cui et al. 1996).

The results for fixed-width regime channels R1 with sediment feeding rate of $Q_b = 5.0 \text{ kg/s}$, follow in general similar trend as R regime channels as shown in figure 4 appendix D. A difference however, is observed in terms of bedforms development for steep channel slopes, namely R1 regime channels develop more cascades rather than antidunes as observed in R regimes channels.

The longitudinal regime profiles of extended-width channels for the three sets of GSD namely D_{mo} value of 19.0 mm, 38.0 mm, and 57.0 mm are shown for different regime slope ranges 0-1.5%, 1.5-3.0%, 3.0-4.5%, 4.5-6.0%, 6.0-8.0%, and 8.0-10.0% respectively in figure 5.16 a, b, c, d, e, and f. The results for $Q = 2.0 \frac{m^3}{s}$ and $Q = 1.0 \frac{m^3}{s}$ are respectively shown by solid black and grey lines for D_{mo} values 19.0 mm, the red dashed and dash dotted lines for D_{mo} value 38.0 mm, and finally, the blue dotted and dash dotted lines for D_{mo} value 57.0 mm.

A change in flow discharge does not significantly impact the channel regime bedforms, because the reduced flow discharge $Q = 1.0 \frac{m^3}{s}$ results on average a regime width of approximately 1 m smaller $w_R - 1$ compared to $Q = 2.0 \frac{m^3}{s}$. The

reduced regime width leads to a reduced wetted area and hence the flow forces per unit area (shear stress) remains in the same range as for $Q = 2.0 \frac{m^3}{s}$.

The longitudinal profiles show riffle-pool bedform for regime slopes 1.5-3.0% and step-pool or cascading bedforms for larger slopes 3.0-10%. The cascading forms become less pronounced or show a plane-bed tendency at slopes $S_R > 6\%$. The occurrence of antidunes at high regime channel gradients are as a result of supercritical flow $F_r > 1$ (figure 5.16 e and f), because at supercritical turbulent flow, antidunes bedforms are dominant bedforms (Southard and Boguchwal 1990). The supercritical turbulent flow occurring at high channel slopes of mobile bed generates breaking free-surface waves and migrating hydraulic jumps (surges) flow, which leads to breaking antidunes as well as chutes-and-pools bedforms (e.g. Cartigny et al. 2013).

Channel profiles for $F_r > 1$ reveal plane-bed bedforms than antidunes or chutes-and-pools predominantly as a result of coarse mesh resolution. Mesh resolution is shown to have a strong control on the channel bedforms for all channel regime slopes. As the channel slope increases, the bedforms such as chutes and pools and antidunes are averaged over larger distance and thus their actual form is lost. The results of bedforms for steep channel slopes using coarse mesh 2 m x 0.93 m appear rather plane-bed and their bedforms are less pronounced. Therefore, the simulations for steep slopes are repeated with a refined mesh 0.50 m x 0.23 m and the results significantly improve and bedforms are more pronounced compared to coarser mesh. The finer mesh in addition produced smoothed bedforms for riffle-pool channels and resolved the large scour depths evolved using coarse mesh resolution 2 m x 0.93 m. It can be concluded that mesh resolution has strong control on the development of bedforms for steep slopes and smoothens the bedforms for low slopes.

The results for extended-width regime channels $R1$ with a sediment feeding rate of $Q_b = 5.0 \text{ kg/s}$, follow in general a similar trend as R regime channels as shown in figure 5 appendix D. At channel slopes $S_R > 3\%$, $R1$ regime channels develop abrupt and sharp drops in their longitudinal profiles. The abrupt change in channel profile occurs when the channel plan-form is diverted to either of the rigid boundaries and develops along this rigid boundary to downstream. Except inflow region, the channel develops entirely along the rigid boundary resembling a flume condition with one side erodible and one non-erodible (rigid) boundary. The introduction of sediment feeding at model's inflow increases the plan-form dynamic. The channel plan-form changes rapidly until it reaches a rigid boundary, which acts as stabilising factor.

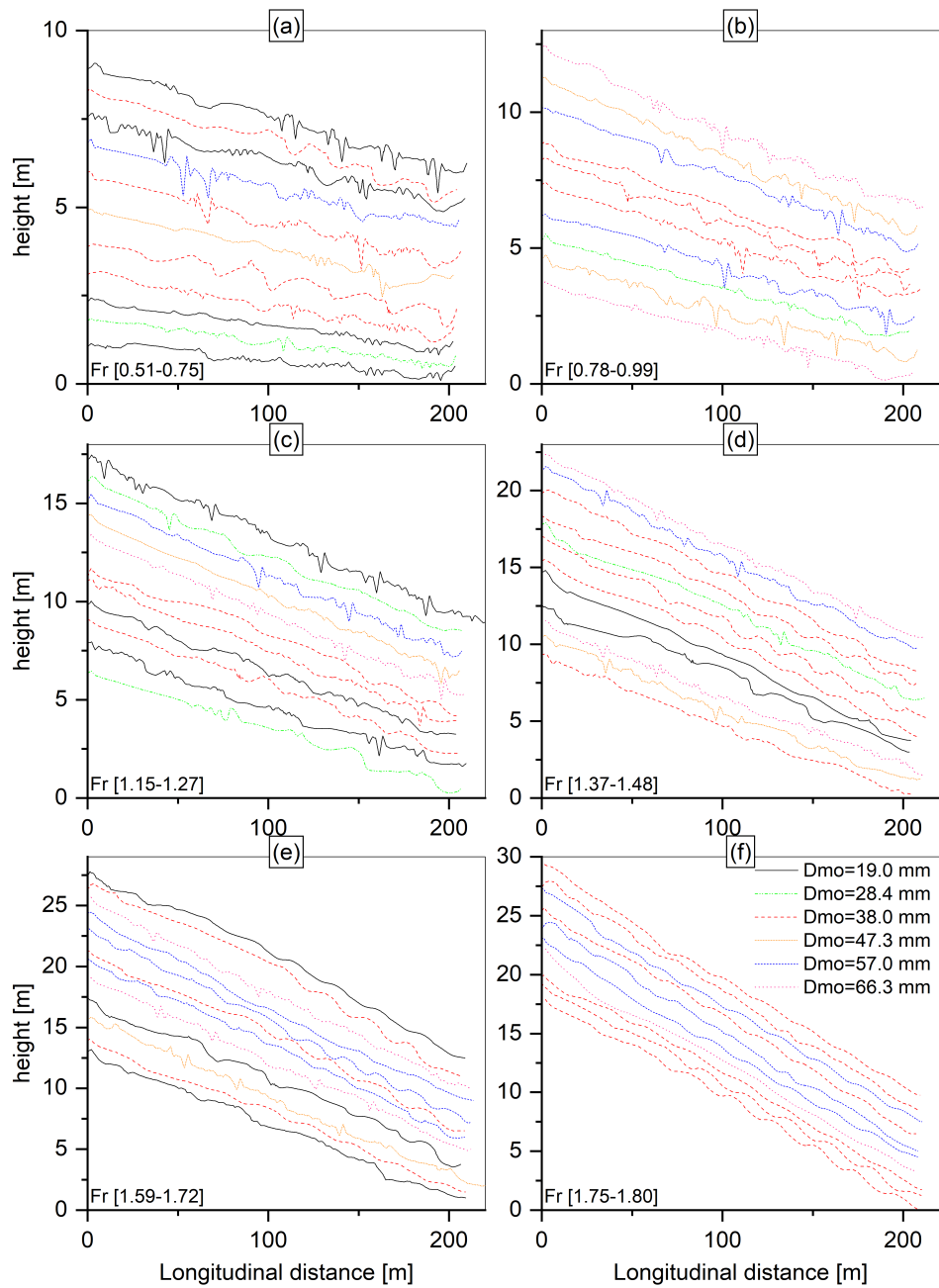


Figure 5.15.: Plan-form development for fixed-width channels for channel regime slopes (a)0.0-1.5% (b) 1.5-3.0% (c) 3.0-4.5% (d) 4.5-6.0% (e) 6.0-8.0% and (f) 8.0-10.0%

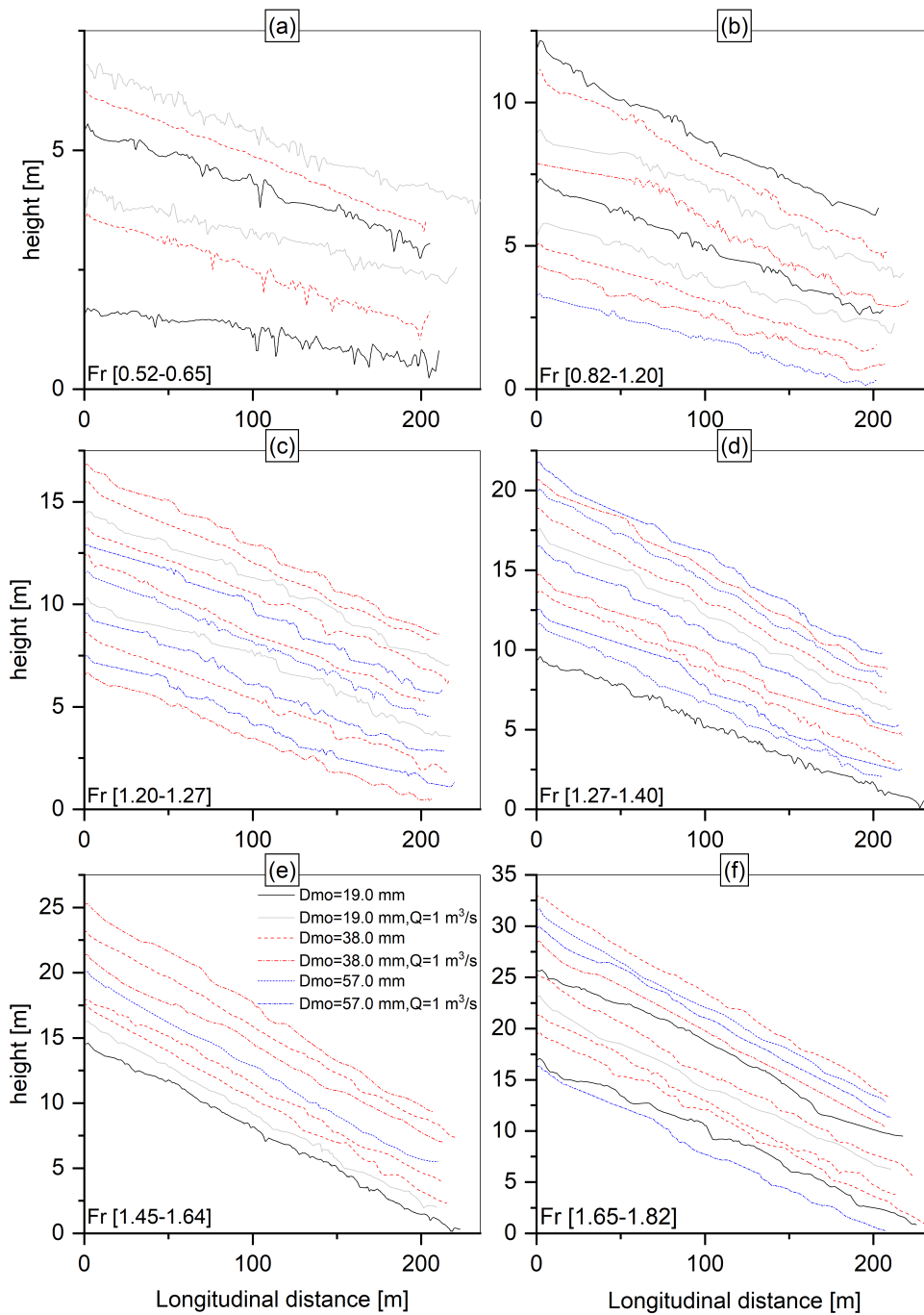


Figure 5.16.: Plan-form development for extended-width channels for channel regime slopes (a)0.0-1.5% (b) 1.5-3.0% (c) 3.0-4.5% (d) 4.5-6.0% (e) 6.0-8.0% and (f) 8.0-10.0%

5.2. Simulations results for MRE as geometry

5.2.1. Relationship between MRE concentration and channel regime slope

The results of MRE simulations are expressed in terms of MRE areal coverage concentrations and channel regime slope S_R in figure 5.17 a, b and c for GSD sets with D_{mo} values of 19.0 mm, 38.0 mm, and 57.0 mm respectively. The x-axis represents the regime channel slope and the y-axis shows the MRE concentration as percentage of total bed surface area coverage. Each point in the graphic shows the result of a single simulation and the dashed lines represents the best fit of the data.

The results indicate that initially by increasing the MRE concentration larger channel slopes can be stabilised to achieve their regime state, however after reaching a certain MRE concentration; further increases in MRE will not necessarily result in larger regime channel slopes. The relationship between MRE concentrations and channel regime slopes follow a logarithmic law with a horizontal asymptote occurring roughly at slopes between 3.0% to 4.0%, 4.2% to 6.2% and 4.5% to 7.0% for GSD with D_{mo} values of 19.0 mm, 38.0 mm, and 57.0 mm respectively.

The trend in relationship between MRE concentrations and S_R is shifted to the right as the channel bed GSD coarsens. In other words, at a certain MRE concentration, a coarser GSD for channel bed may lead to larger channel regime slopes S_R compared to a finer GSD.

The maximum MRE concentration implemented in the simulations is limited to 50%, because with resolution of the channel mesh, higher MRE concentrations were abstracting the free flow in many regions. This limitation can be lifted by increasing the channel mesh resolution to allow well distribution of MRE in smaller clusters, however finer mesh resolution leads to longer computation time. The computation time for the channel mesh resolution 23 cm x 50 cm used for the simulations are ranging between 3 to 4 days on a four node computer. However it took 12 to 14 days for a test simulation using a finer mesh resolution of 11.5 cm x 25 cm to achieve regime state. Therefore, long computation time limited the use of MRE concentration to 50%.

At low MRE concentrations, the individual elements are located at relatively longer distances from each other, thus the flow is disturbed only in the vicinity of MRE and the rest of the regions are not strongly influenced. The individual MRE generate vortices in their wake regions around them, which propagate downstream and diminish after traveling some distances (e.g. Canovaro et al. 2004). These vortices are the primary sources of energy loss in steep boulder streams (e.g. Morris 1955; Canovaro et al. 2004). With an increase in MRE concentration, the distance between individual elements decreases and the wake regions of MRE interact with each other resulting in a higher energy loss, flow resistance and drag shear stresses (e.g. Thappeta et al. 2017). With further increase in MRE, the

distance between individual elements diminishes and the MRE tend to behave as a single roughness element. Studies show that the energy loss in case of very dense MRE concentration tend to attain an asymptotic value (e.g. Thappeta et al. 2017).

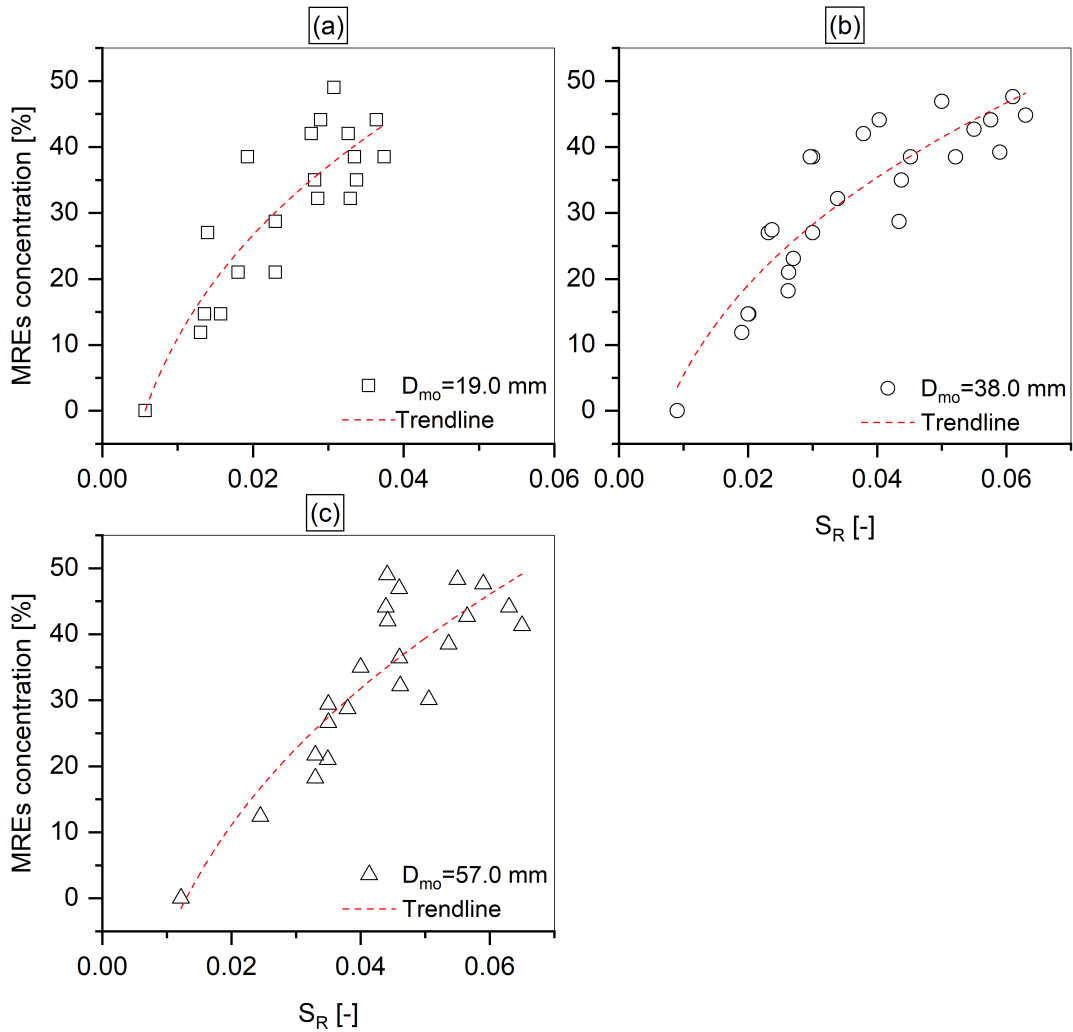


Figure 5.17.: Relationship between regime channel slope S_R and MRE concentrations in percentage of total area coverage for GSD subsurface layer sediments (a) $D_{mo} = 19.0$ mm (b) $D_{mo} = 38.0$ mm and (c) $D_{mo} = 57.0$ mm

MRE impose different effects on the channel bed shear stress under submerged and protruding conditions. In the case of submerged MRE, The effect of MRE on the channel bed shows two distinct behaviors depending on the channel slope. At channel slopes roughly $S < 4.5\%$, the effect of MRE is predominantly due to the

reduced bed surface area exposed to erosion, namely higher MRE concentrations protects more channel bed surface area from erosion. The bed shear stress is observed to increase in the micro-channel between MRE compared to plane-bed channel regardless of MRE concentrations as shown in figure 5.18 a_1 and b_1 . At channel slopes roughly $S < 4.5\%$, MRE in addition to their channel bed protection effect, significantly reduces the bed shear stress in the micro-channels between MRE compared to MRE-free channel figure 5.18 c_1 , d_1 , and e_1 . Furthermore, for $S < 4.5\%$, low MRE concentrations roughly $< 20\%$ reveals a counter effect of increasing the bed shear stress compared to higher MRE concentrations. This counter effect is observed to increase with channel slope as shown in figure 5.18 c_1 , d_1 , and e_1 . MRE concentrations roughly $> 30\%$ is observed to impose relatively similar bed shear stress in micro-channels between MRE.

Similarly in the case of protruding MRE, channel bed shear stress are increased for all MRE concentrations for channel slopes roughly $S < 2.5\%$ and the effect of MRE are merely due to the reduction of bed exposed area to erosion. For $S \geq 4.5\%$, MRE reduces the bed shear stress significantly compared to MRE-free bed as shown in figure 5.18 c, d and e. Further, it is observed that for $S \geq 4.5\%$, higher MRE concentrations $> 27\%$ causes larger reduction in bed shear stress compared to concentrations $< 27\%$. As the channel slope increases, lower MRE concentrations induces a counter effect of increasing the bed shear stress in most of channel bed regions, while higher MRE concentrations consistently reduce the bed shear stress.

Both submerged and protruding MRE cases can occur in simulations of MRE as geometry as well as in nature. In case of rich sediment supply from upstream, the spaces around the MRE may fill with deposited sediments and the size of MRE above the bed reduces accordingly and therefore MRE may be submerged under bedload transport relevant discharges. In contrast, when the sediment supply from upstream is restricted, finer sediment grains around MRE may be eroded and MRE size above the bed increases, therefore MRE may protrude from the water surface.

Mesh resolution is also observed to have an influence on the bed shear stress distribution around MRE. Hydraulic simulations for three mesh resolutions $0.5 \text{ m} \times 0.23 \text{ m}$, $0.25 \text{ m} \times 0.116 \text{ m}$, and $0.124 \text{ m} \times 0.058 \text{ m}$ show that water depth, velocity and shear stress are distributed more evenly for finer mesh resolutions compared to the coarser one. More importantly, the bed shear stress is over-estimated in the case of coarse mesh resolution $0.5 \text{ m} \times 0.23 \text{ m}$ used for regime simulations compared to finer resolution meshes. Unfortunately, due to the extra-long computation time, the use of finer mesh resolutions were limited to hydraulic simulations only to understand the effect of mesh resolution on the bed shear stress.

The second important parameter affecting the flow resistance apart from MRE

concentration is the degree of flow submergence. Field and flume investigations show that flow resistance is inversely proportional to the degree of submergence of MRE. Since the simulations in this study is performed with a constant discharge of $Q = 2.0 \text{ m}^3/\text{s}$, the relative submergence may remain constant for all simulations. However, marginal changes in relative submergence are observed as a result of the channel slopes only, because steep channel slopes have lower water depths for the same flow discharge compared to gentler slope channels. The simulations results for a constant channel slope, MRE concentration and different sizes of MRE, which induces different flow submergence. This indicates that with a decrease in flow submergence a decrease in bed shear stress is resulted. The bed shear stress in the particular, nearby the MRE regions is strongly influenced.

Majority of MRE in this study are non-submerged (protruding) due to the erosion around MRE. The erosion around MRE provides micro-channels conveying the bulk of the flow, thus the water depth lowers and MRE are protruding from water surface. The initially trapezoidal shapes of MRE change significantly into different unstructured shapes as a result of different sediment erosion and deposition rates around them as well as due to the sediment extraction from the surface of the MRE. Despite the sediment extraction from the MRE to preserve their height comparable to water depth and to avoid skinny MRE that would otherwise cause instability, majority of them remain protruding throughout the simulations. The MRE resembles natural step channels with large immobile boulders and low water depths, which are protruding during most of bankfull discharges.

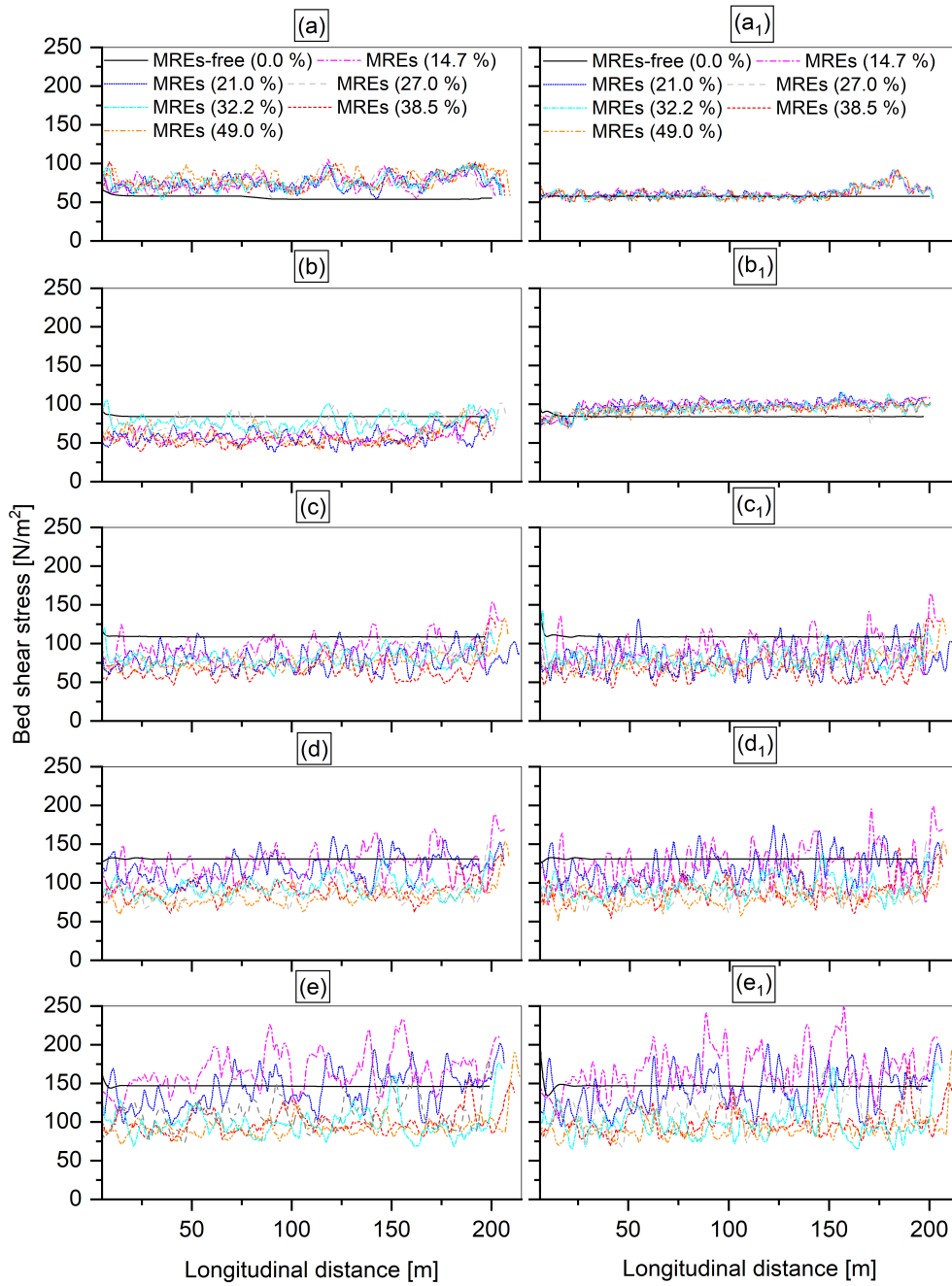


Figure 5.18.: Bed shear stress distribution along the longitudinal distance of regime channel for MRE-free bed (solid lines) and different MRE concentrations (colored lines) as a function of channel slopes (a), (a₁) 2.5% (b), (b₁) 4.5% (c), (c₁) 6.5% (d), (d₁) 8.5% and (e), (e₁) 10% for protruding and submerged MRE cases respectively

5.2.2. Comparison of MRE as geometry results with field observations

A direct comparison between the result of simulations using regime approach and field and flume experiments are not possible for two reasons. First, because a comprehensive field data that show the relationship between the MRE concentration and channel regime slope is not available to data. Secondly, the results of many flume experiments cannot be expressed in terms of MRE concentrations and channel regime slope. Therefore, the results of some studies are qualitatively compared in terms of relevant parameters affecting the channel slope stability such as energy loss, flow resistance, and contribution of drag shear stress as a function of MRE concentrations.

In general most of the flume experiments confirm that an increase in MRE concentration leads to an increase in flow resistance, provided the individual MRE are sufficiently distant (e.g. Ferro 1999; Lawrence 2000; Pagliara and Chiavaccini 2006; Canovaro and Solari 2007). The flow resistance reaches a maximum value with a MRE concentration below 50%, while it subsequently decrease when the MRE concentration is increased beyond 50% (e.g. Ferro 1999; Lawrence 2000; Pagliara and Chiavaccini 2006; Canovaro et al. 2007). Investigation of protruding MRE of spherical shapes in steep flumes show that MRE concentration increase leads to an increase in flow resistance to about a concentration of 25% and then the flow resistance does not increase anymore when the concentration of MRE are further increased. Similar results are also reported by Schlichting (1968).

Laboratory experiments by Canovaro and Solari (2007) show that MRE concentration has a non-monotonic behaviour with the ratio of drag shear stress to total shear stress. The ratio of drag shear stress to total shear stress increases rapidly with MRE concentrations and reaches asymptotically the maximum value about 40% when the MRE concentration is the range of 20% to 40%. The increase in drag shear stress as a result of MRE concentrations implies lower effective shear stress at the bed for sediment entrainment. Since the MRE are not mobile at most of occurring flow discharges, therefore drag shear stress may not contribute to the sediment transport, thus the bed erosion is limited and channel bed stabilises.

5.2.3. Bedload transport in MRE as geometry channel

Bedload transport variation at model's outflow at initial and final phase of channel regime development are shown in figure 5.19 a and b for two examples of initial channel slopes 4.5% and 6.5% and GSD set with D_{m0} values of 38.0 mm for regime channels *R* and *R1* respectively.

Temporal variations of bedload transport rates at model's outflow are plotted for MRE concentrations of 15% (blue dotted line), 28% (green dash dotted line), 39% (orange dashed line) together with results of MRE-free channel (red short dashed line) in figure 5.19 a. In general, the bedload transport curves have similar be-

haviour, namely their initial phase has peak and their final phase has a decreasing bedload transport rates for both MRE and MRE-free channels. However, two distinct behaviours outline the effect of MRE on the bedload transport during the regime development. First, the channels with presence of MRE have much shorter initial phase <2.5 days compared to > 5 days for MRE-free channel. The presence of MRE restricts the bed erosion by increasing the resistance to flow and reducing the total erodible area exposed to erosion. Therefore, for MRE channels, the total sediment volume transported to downstream as a result of erosion is strongly decreased.

Secondly, the peak bedload transport occurs slightly earlier for MRE channels compared to MRE-free channel, because the arrival of bedload transport peak to the outflow of the model is associated with the velocity of planform development. In MRE-free channels, the channel plan-form takes some time to reach the outflow boundary; while for MRE channels, no specific plan-form develops and the bedload transport peak propagation is independent of channel plan-form development. MRE channels disrupt the channel plan-form development and the higher the concentration of MRE is; the stronger is the plan-form disruption. However, for low MRE concentrations, a tendency toward developing a plan-form similar to MRE-free condition is observed. Unlike MRE-free channels, channels with MRE develop a network of micro-channels in between individual elements allowing downstream of bedload transport. The dimension of these micro-channels depends strongly on the net distance between the neighboring MRE.

The bedload transport rates at the initial phase of regime development are much larger due to the intensive erosion occurring right at the beginning of the regime development. However, the duration of initial regime development phase is much shorter for MRE channels compared to their MRE-free counterparts. The shorter the period of initial regime development (phase of large bedload transport rates) is, the lower erosion at this phase occurs, because the bulk of channel slope reduction occurs in the initial phase of regime development as a result of large erosion rates.

The sediment feeding at the model's inflow in *R1* MRE regime channels propagates downstream by filling the spaces between MRE, which reduces the exposed area of the MRE and in turn strongly reduces the bedload transport rate peaks as shown in figure 5.19 b. This effect can be well described by the standard deviation of the bed surface geometry. The regime channels *R* have larger standard deviation of bed surface geometry compared to *R1* channels with sediment feeding. The standard deviation of bed surface geometry can be interpreted as roughness height, thus *R1* channels have lower roughness values compared to *R* channels due to the effect of sediment deposition on the spaces between MRE. Similar results are also reported from flume and field observations that MRE surface exposure is a measure of bedload supply from upstream. A rich supply of sediments from

upstream leads to low exposure of MRE by filling the spaces between them, while a poor supply causes erosion of the free spaces between MRE (e.g. Ghilardi 2014).

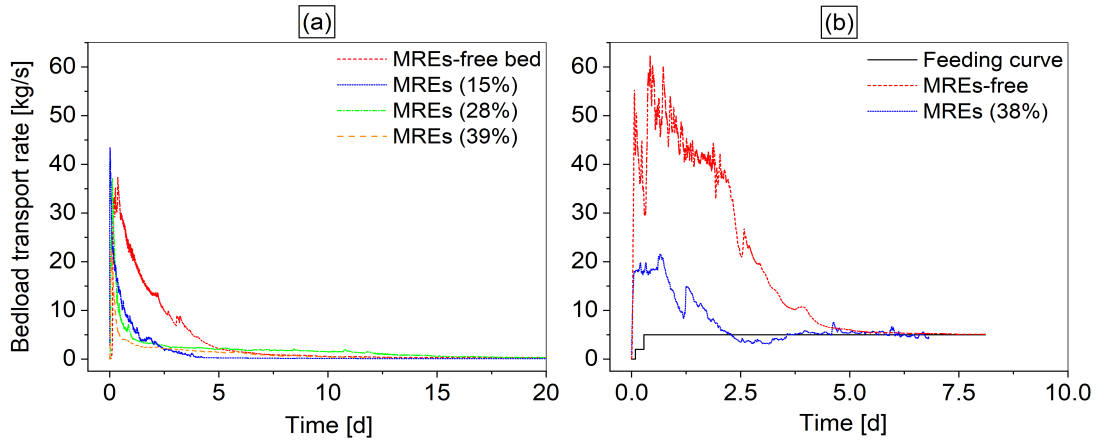


Figure 5.19.: Bedload transport rates at model's outflow with and without presence of MRE for (a) *R* regime channel and (b) *R1* regime channel with a sediment feeding rate of $Q_b = 5.0 \text{ kg/s}$

5.2.4. GSD in MRE as geometry channels at regime state

The GSD for the surface layer and transported bedload sediments are analysed for an example of regime channels with MRE concentrations of 39% and initial channel slopes of $S = 4.5\%$ and $S = 6.5\%$ for regime channels *R* and *R1* respectively.

The GSD for the surface layer at the regime is D_{msR} and D_{msR1} are analysed with respect to their difference from initial value D_{ms} for the regime channels *R* and *R1* respectively. The difference in initial GSD and regime GSD for upstream section of channels (see figure 5.20 a and b for *R* and *R1* respectively) shows a strong coarsening of channel bed GSD for both regime channels. However for *R1*, the inflow region is strongly affected by GSD of feeding sediments $D_{mo} = 38.0 \text{ mm}$ at the model's inflow (see figure 5.20 b₁). A slight fining occurs right at the inflow boundary region as a result of flow recirculation due to the MRE near the inflow boundary. The *R* regime channel bed coarsens in all flow regions except over the MRE themselves, where no sediment transport occurs (see figure 5.20 a).

Similarly, flow recirculation in the inflow region for the *R1* regime channels causes the transported bedload mean diameter D_{mTr} (in red) to be slightly lower than the feeding sediment GSD D_{mo} (green dashed line), which in turn leads to fining of D_{msR1} at the flow region (blue dashed line). The inflow boundary effect diminishes at a distance about 40 m from the inflow boundary, where the D_{mTr} becomes even larger than the feeding sediment $D_{mTr} > D_{mo}$. The intensive fluctuations in the distribution of $D_{msR/R1}$ and D_{mTr} are associated with the

variations in the bed surface geometry (black lines in a_1 and b_1) caused by MRE. The fluctuation in channel bed surface geometry strongly affects the hydraulic of the flow such as velocity, water depth, energy gradient and finally the bed shear stress. Furthermore, the bed surface geometry fluctuations can cause large number of local-scale slope changes from downslope to upslope and vice versa. The extensive slope changes induces also changes in bed critical shear stress for sediment incipient motion because Hydro_FT-2D considers a slope effect for modifying the bed critical shear stress for bedload transport initiation, which means the grains easily move on a downward slope than on upslope regions.

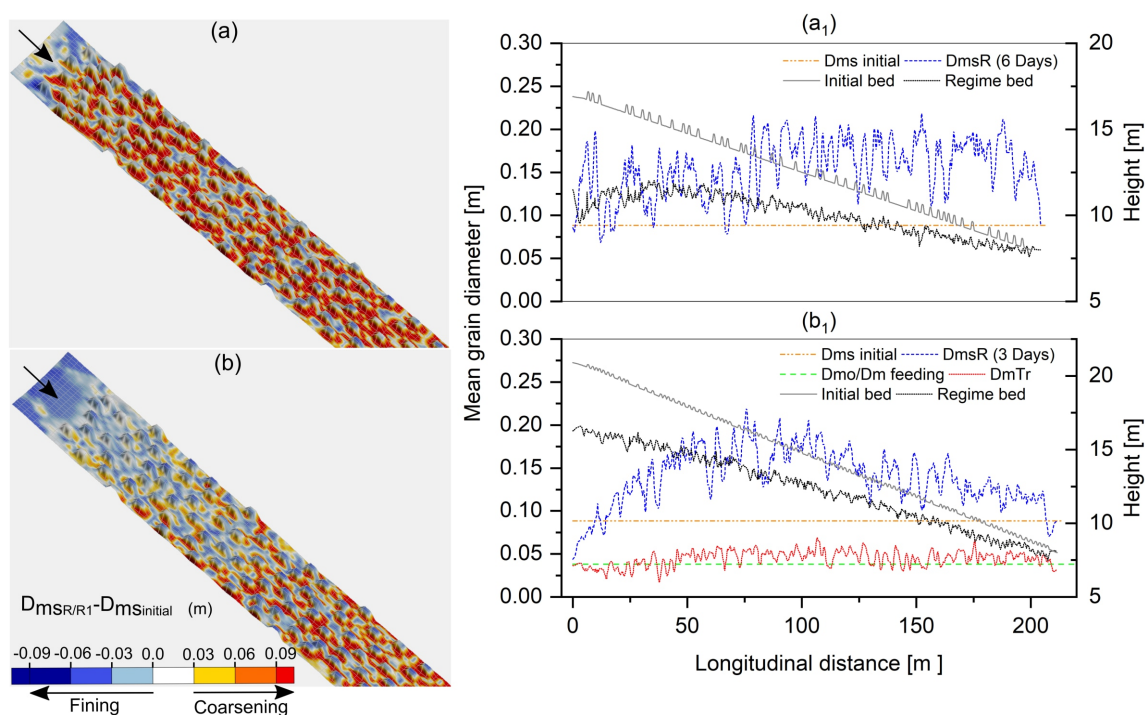


Figure 5.20.: The effect of MRE on the GSD of bed surface layer sediments in terms of difference between regime $D_{msR/R1}$ and initial D_{ms} values and their longitudinal bed profiles in (a) (a_1) and (b), (b_1) for R and R1 regime channels respectively

5.3. Simulations results for MRE as step-pool bedforms

5.3.1. Relationship between channel-regime slope and step-pool dimensions

The relationship between step-pool dimensions $\lambda = L_D/D_B$ and channel regime slopes $S_R; S_{R1}$ is shown for three GSD sets with D_{m0} values of 19.0 mm, 38.0 mm, and 57.0 mm in figure 5.21 a, b, and c respectively. The step-pool dimension is cal-

culated from the clear distance between adjacent steps also known as step-length L_D and step-height D_B . Step-height D_B is the distance between step-crown to bottom level of scour right downstream of the steps. The step-lengths are known from the distance between two adjacent non-erodible sets of MRE implemented across the whole channel width prior to the start of the simulation. The step-heights are formed as a result of regime development depending on the flow discharge, sediment GSD and sediment feeding rate. The step-heights may differ in a single simulation and also from one location to another within a cross-section due to the differences in erosion depths downstream of the steps. Thus, the step-height values are the average of several values both within a single cross-section and over the total numbers of existing steps in the channel. The step-pool dimensions are derived from the simulation results after the fulfillment of regime conditions.

The step-pool dimensions $\lambda = L_D/D_B$ and channel regime slopes $S_R; S_{R1}$ relationship can be best described by a power-law $\lambda = a(S_R; S_{R1})^{-b}$. The value of a varies from 0.56 to 0.39 and 0.41 to 0.37, while the value of b ranges between 1.0 to 1.26 and 1.2 to 1.35 for GSD with D_{m0} values of 19.0 mm to 57.0 mm for regime channels R and $R1$ respectively. The scatter in the data is roughly in the range of $\pm 10\%$ to $\pm 15\%$ from their average trend line as shown by the shaded areas in figure 5.21. The effect of GSD is observed to slightly shifting the graph of λ and $S_R; S_{R1}$ relationship to the right, which means for the same channel slope, larger λ values are achieved for coarser GSD. The simulation results for $R1$ regime channels with a constant feeding rate of $Q_b = 5.0 \text{ kg/s}$ show that at the same channel regime slopes, larger λ or smaller step-depth D_B are resulted, because part of the flow transport capacity is used to transport the sediments fed at the inflow. The effect of sediment feeding diminishes as the regime channel slope increases, namely at high slopes, the step-depths do not differ much from R regime channels.

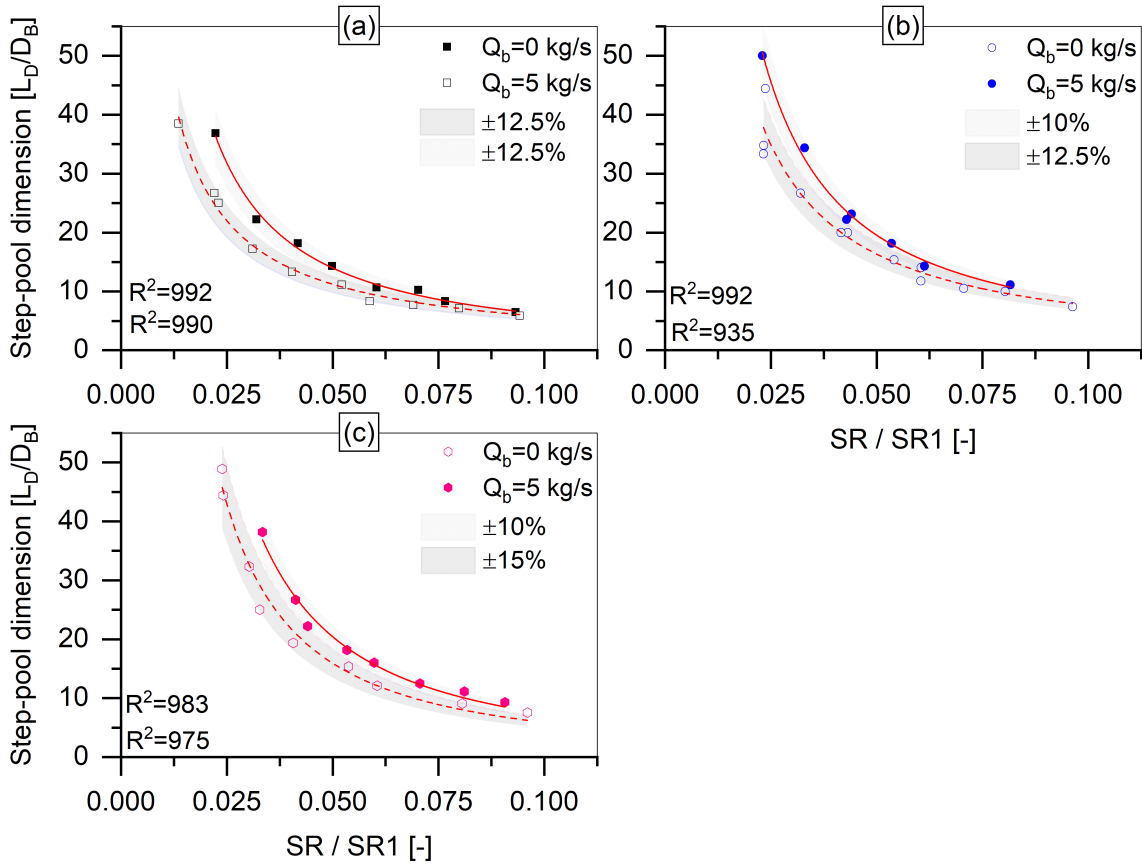


Figure 5.21.: Relationship between step-pool dimensions λ and channel regime slopes $S_R; S_{R1}$ for (a) $D_{mo} = 19.0 \text{ mm}$, (b) $D_{mo} = 38.0 \text{ mm}$, and (c) $D_{mo} = 57.0 \text{ mm}$

5.3.2. Regime channel profiles for MRE as Step-pool

Channel regime profiles are shown for some selected regime channels for three sets of GSD with D_{mo} values of 19.0 mm, 38.0 mm, and 57.0 mm respectively presented for channel slopes $S_R < 4.5\%$ and $4.5\% < S_R < 10\%$ by solid, red dashed and blue dotted lines in figure 5.22 a and b. The initially plane-bed is deformed into step-pool form by sediment deposition at the upstream of step region (set as non-erodible in the model) and erosion right in the downstream region.

The step-height D_B is clearly shown to increase with channel slope for a constant step-length L_B . Similarly, the D_B increases when the L_B is reduced and vice versa as shown in figure 5.22 b for channel regime slope $S_R = 6.15\%$, which develops a $D_B = 2.4 \text{ m}$ for a $L_B = 20 \text{ m}$, while for $S_R = 7.18\%$ and $L_B = 10 \text{ m}$, a $D_B = 1.3 \text{ m}$ is developed.

Additionally, for the same channel slopes and L_B , the D_B slightly decreases for

coarser GSD, namely the values of D_B are smaller for D_{mo} values of 57.0 mm compared to 38.0 mm and 19.0 mm. The main reason for the smaller (D_B) for coarser GSD is due to its lower mobility compared to finer GSD.

The channel regime plan-form development in presence of MRE steps follow in general a similar trend as MRE-free channel. The channel tends to a meandering plan-form between two adjacent steps at low slopes, while it straightens as the channel slope increases as shown in figure 5.23. For gentle channel slopes, the channel point bars develop on the inside turn of the bends as a result of sediment deposition, where the GSD becomes coarser compared to thalweg region over the period of channel regime development. At steeper channel slopes, the bars are formed on both channel sides and in the middle of channel and are less pronounced with increase in channel slope.

5. Regime channel simulation results

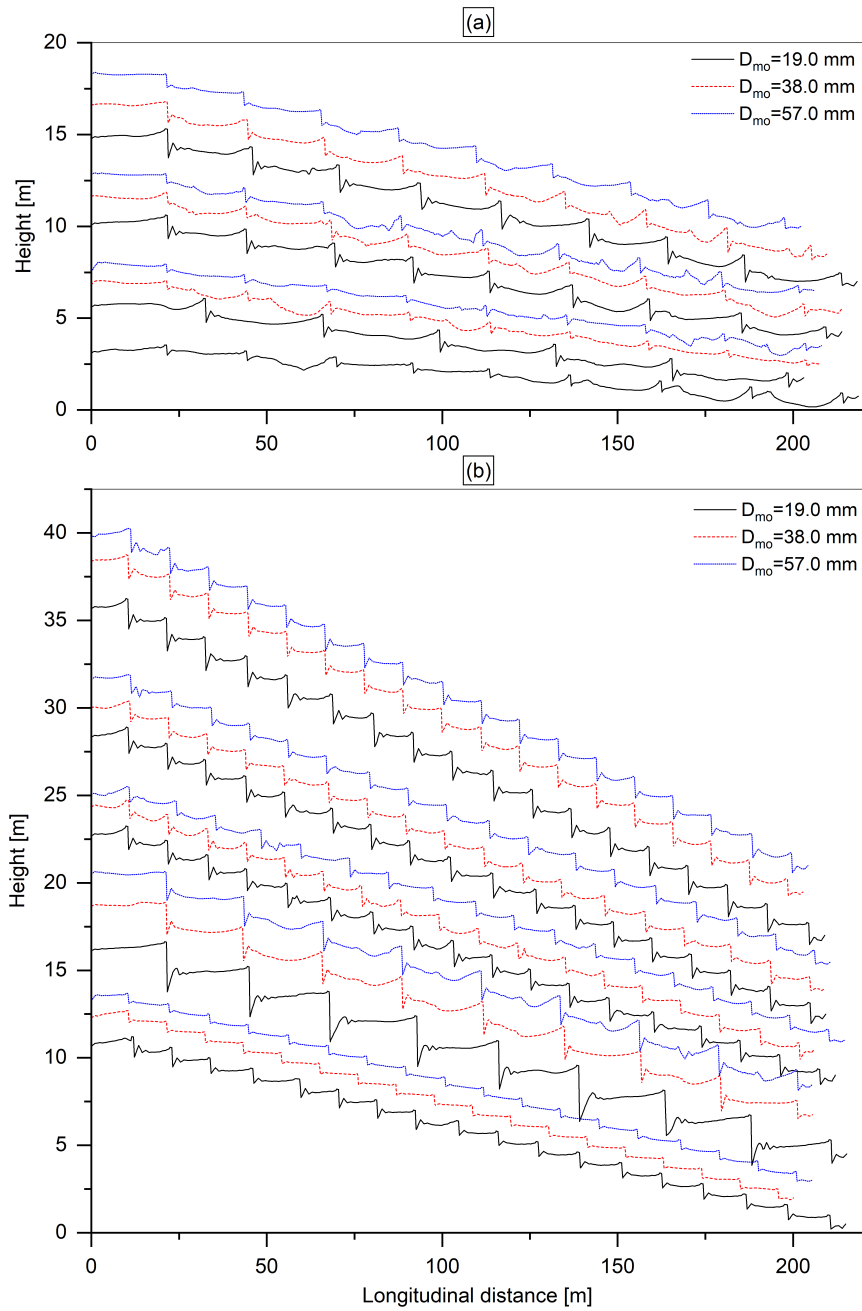


Figure 5.22.: Regime channel profiles for the MRE as step-pool for regime channel slopes
(a) $S_R < 4.5\%$ and (b) $4.5\% < S_R < 10\%$

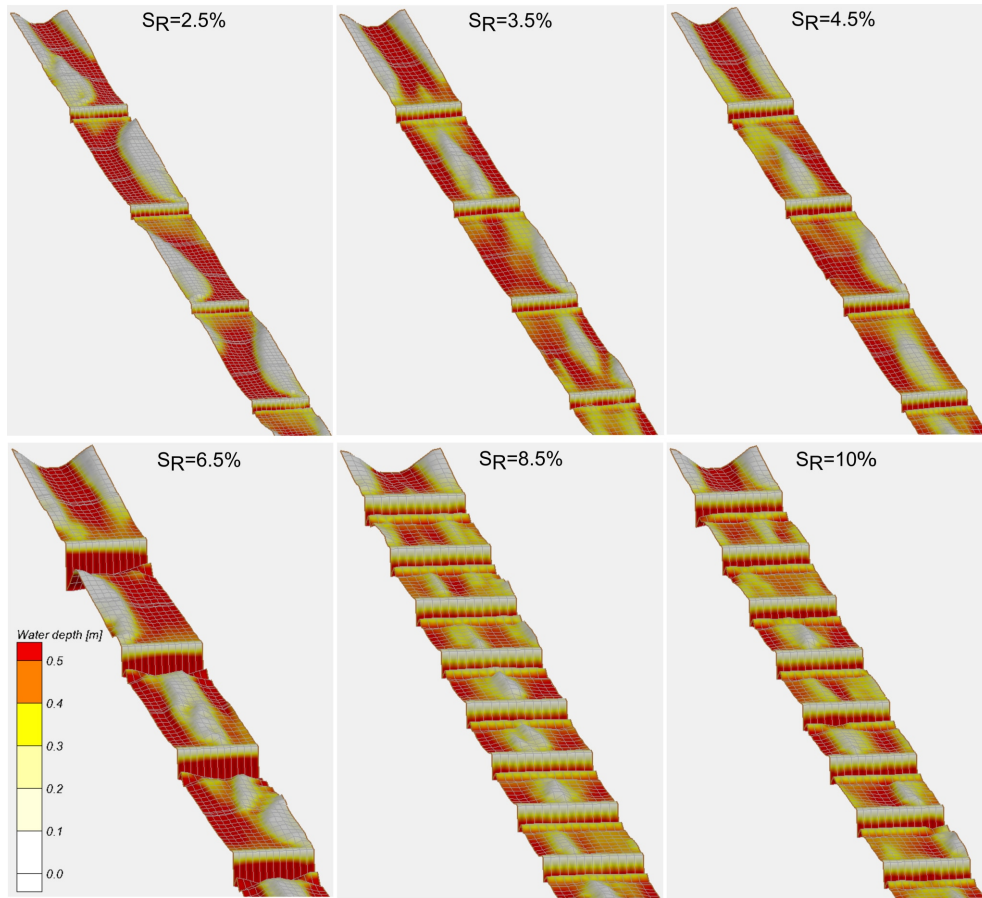


Figure 5.23.: 3D-view of MRE as step-pool channel plan-form development for different regime channel slopes from simulations results with $D_{mo} = 19.0 \text{ mm}$

5.3.3. Comparison of simulated step-pool dimension with field observations

The relationship between step-pool dimension $\lambda = L_D/D_B$ and channel regime slopes from the simulations results are compared with some field investigation data in figure 5.24. In total nine datasets from USA, Italy, Japan and Canada are compiled for comparison with the regime channel simulations results. The first data is from 52 step-pool reaches of 32 streams of catchment area 0.5 km^2 to 11.5 km^2 and reach average gradients between 0.033 and 0.16 in the north-western Montana (Wohl et al. 1997). The second data is from 13 reaches of catchment area 0.52 km^2 to 14.93 km^2 and average reach gradients 0.017 to 0.115 in Saint Monica mountains of southern California (Chin 1999). Third data is from 34 reaches of 13 rivers and streams with average reach gradient 0.015 to 0.175 in central and western-central Idaho high mountains (Chartrand et al. 2011; Chartrand and Whiting 2000). The fourth data is from 20 step-pool streams with large woody debris (LWD) and 20 streams without large woody debris respectively

with catchment areas of 0.55 km^2 to 9.6 km^2 and 0.45 km^2 to 4.2 km^2 with average gradients 0.06 to 0.18 and 0.051 to 0.14 in Washington (Curran and Wohl 2003; MacFarlane and Wohl 2003). The fifth data is from 35 reaches of 8 rivers and streams with catchment areas of 0.12 km^2 to 5.72 km^2 and reach average gradients of 0.016 to 0.317 in some mountainous basins in Japan (Okazaki et al. 2006). The sixth data is from fifteen reaches of three streams with catchment areas of 0.69 km^2 to 8.73 km^2 and average reach gradients of 0.017 to 0.195 in Colorado (David 2011). The seventh data is from eight step-pools reaches of Rio Cordon river in north-eastern Italy with a catchment area of 5 km^2 and reach average gradient 0.05 to 0.22 before and after a flood event (Lenzi 2001). The last data is from four reaches of Shatford creek in Okanagan valley of British Columbia with total catchment area of 60 km^2 and average reach gradients of 0.049 to 0.087 (Zimmermann and Church 2001).

Despite large scatter in the data, they all show an inverse relationship between step-pool dimensions λ with channel regime slopes. The scatter may be due to the different boundary conditions such as GSD, bankfull discharge and site specific characteristics such as existence of (LWD) and others. The results of the regime channel simulations are shown to agree well to an average trend of the considered field data, despite the fact that steps are artificially implemented in the model as non-erodible bodies. Simulation results produce relatively larger $\lambda = L_D/D_B$ values for channel slopes roughly $S_R < 3.5\%$ compared to field data. Comiti et al. (2005) observed that natural and artificial step-pools systems have similar behaviour of inverse relationship with step-pool dimensions and channel regime slopes. Artificial step-pools are used as grade-control structures such as check-dams and bed sills. In case of artificial step-pools, the distance between steps are prefixed and scour depth due to the falling jets forms plunge pools under each structure resembling to natural steps determining the formation of pools.

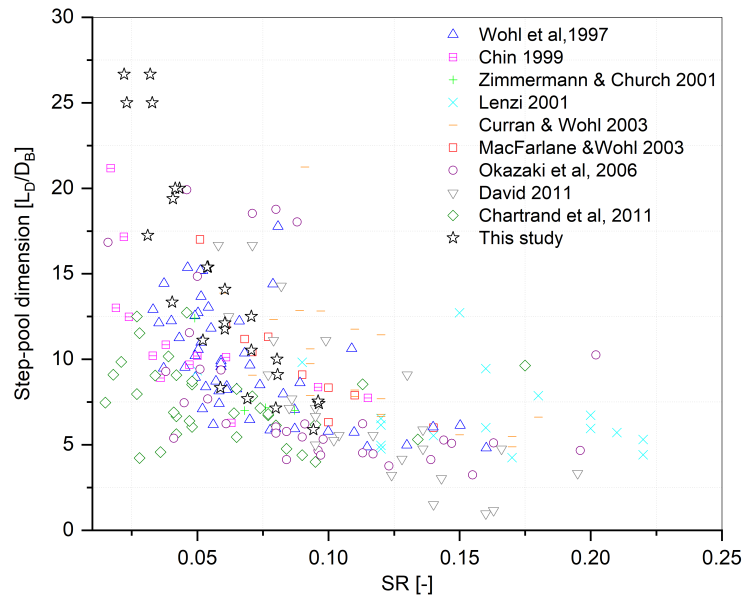


Figure 5.24.: Relationship between step-pool dimension and channel regime slopes for nine datasets from field observations and regime channel simulations using MRE as non-erodible steps (stars)

5.3.4. Bedload transport and GSD in MRE as step-pool channels

Temporal variation of bedload transport at model's outflow (red dashed line) are shown in figure 5.25 for channels with MRE arranged as step-pool or cascade forms together with those of MRE-free channels (blue line). The bedload transport rates at model's outflow are shown in figure 5.25 a, b and c respectively for three examples of MRE as step-pool channels together with their MRE-free counterparts of initial slope $S = 4.5\%$ and GSD with D_{m0} values of 19.0 mm , 38.0 mm , and 57.0 mm . Similarly, the results for R1 regime channels with MRE as step-pool and their MRE-free counterparts are shown for three examples of initial channel slopes $S = 2.5\%$, $S = 6.5\%$, $S = 3.5\%$ respectively for GSD with D_{m0} values of 19.0 mm , 38.0 mm and 57.0 mm in figure 5.25 a₁, b₁, and c₁.

The results show two major differences imposed by the MRE cascades. First, the bedload transport rates peak in the initial regime development phase is dumped significantly due to the erosion limiting analogy of MRE cascades. The bedload transport peak occurs as a result of intensive erosions in the initial phase of regime development for MRE-free channels. However for MRE cascade beds, erosion is restricted by the non-erodible steps to channel bed evolution between successive steps.

Secondly, the duration of initial and final phases of regime development for the MRE as step-pools are strongly reduced compared to MRE-free channel beds. The

regime development for MRE step-pool channels take in average 2.5 days, while it takes more than 10 days for MRE-free bed channels to achieve a regime state. The longer regime development duration is predominantly associated with larger erosions and channel slope reduction in MRE-free channels.

The peak of bedload transport rates propagation to downstream are slightly delayed as a result of slower plan-form development for MRE cascades compared to MRE-free channel beds.

The R1 regime channel development (with a constant feeding rate of 5.0 kg/s at model's inflow) with presence of MRE as step-pools show that bedload transport rates fluctuates about the feeding rate value as shown in figure 5.25 a₁, b₁, and c₁. The bedload transport rates fluctuation is shown to follow the feeding rates but did not reduce over time (see figure 5.25 a). The bedload transport rates at model's outflow approaches the feeding bedload rates very well for low channel slopes (figure 5.25 a₁). However, it fluctuates above and below the feeding bedload rates for steeper channel slopes. Therefore the channel slope is shown to have a strong control on the bedload transport rates fluctuations at model's outflow. The fluctuations in bedload transport rates are also associated with the presence of MRE step-pools, which disrupt a continuous bedload transport to downstream. A comparable field or flume experiments could help verify the bedload transport results for such a artificially implemented MRE as step-pools channels.

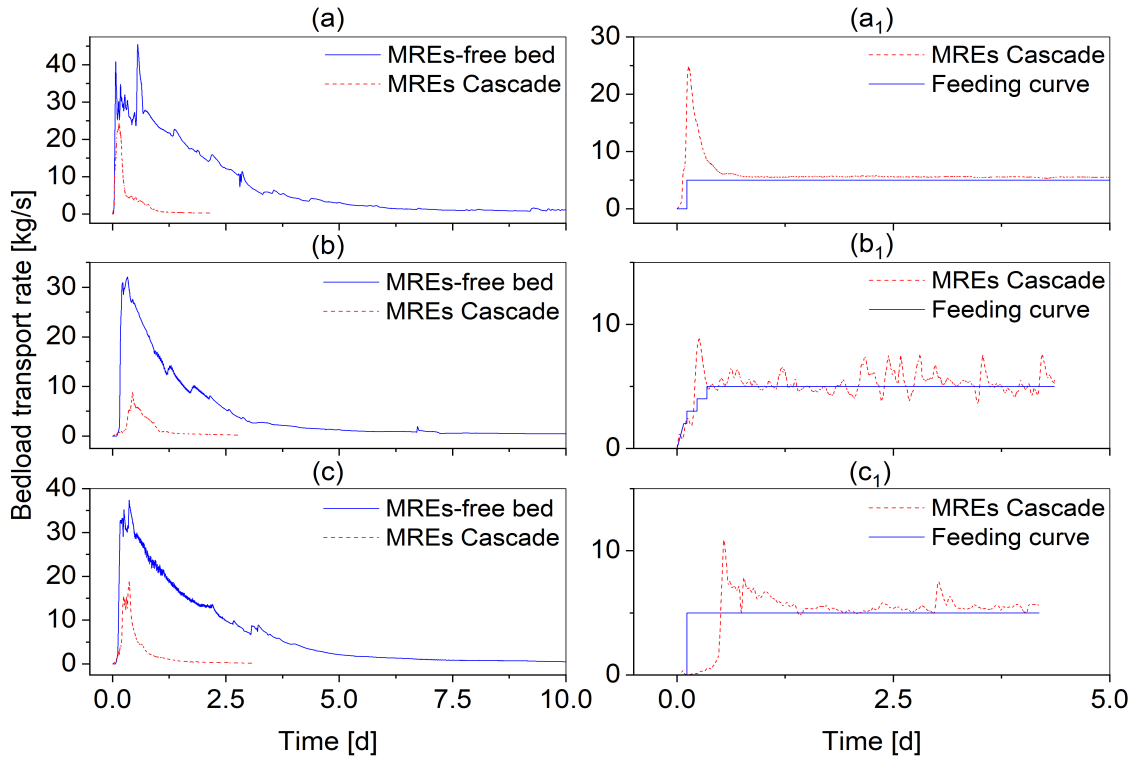


Figure 5.25.: Bedload transport rates at model's outflow for R and $R1$ regime channels with sediment feeding rate of $Q_b = 5.0 \text{ kg/s}$ for six channels of MRE as step-pools and MRE-free channels respectively for GSD (a), (a₁) $D_{mo} = 19.0 \text{ mm}$ (b), (b₁) $D_{mo} = 38.0 \text{ mm}$ and (c), (c₁) $D_{mo} = 57.0 \text{ mm}$

GSD at regime state for MRE as step-pools channels are analysed in terms of difference in surface layer sediment GSD at the regime state and its initial value for R and $R1$ regime channels to understand their coarsening and fining behaviour. The difference in GSD for surface layer at the regime state $D_{msR/R1}$ from its initial value is shown on two examples of MRE cascades of initial channel slopes 4.5% and 6.5% for regime channels R and $R1$ respectively in figure 5.26 a and b. The GSD for MRE step-pool regime channels follow closely the flow and channel geometry. Right downstream of the steps, coarse D_{msR} is observed as a result of strong energy gradient and downslope slope effect, which enables the flow to transport large number of grain sizes, thus only very coarse sediments remain immobile in this region. The upslope condition leads to sediment deposition in the upstream of steps, because on one hand the flow slows down in this region and on the other hand, the critical shear stress increases due to the upslope effect and the grains are hardly brought into motion. Therefore, the GSD gradually becomes finer from toe of one step to the crown of the next step in the direction of flow as

shown by (blue dashed line) in figure 5.26 a₁. For regime channel R1, the GSD of the feeding sediments D_{mo} strongly controls the D_{msR1} . However, similar to R regime channel, right downstream of the steps, D_{msR1} partly coarsens as a result of large energy gradient (see figure 5.26 b and b₁). In this region, the transported bedload D_{mTr} is larger than D_{mo} , thus only larger grains remain immobile leading to coarser D_{msR1} . In the scour regions, the transported bedload D_{mTr} is slightly lower than D_{mo} due to the upslope effect (see the grey line showing regime bed in b₁), which increases the critical shear stress of sediment incipient motion.

Unlike regime channel R, the channel bed between two successive steps does not develop an upslope condition but remains quasi horizontal in R1, thus the D_{msR1} does not change considerably except at short upslope area downstream of scour region. The scour region for R1 regime channels differs partially from R regime (see figure 5.26 b), namely the scour depth reduces as a result of sediment supply from upstream. However, the depth reduction is limited to a portion of total channel width, where the bulk of supplied sediments are transported to downstream.

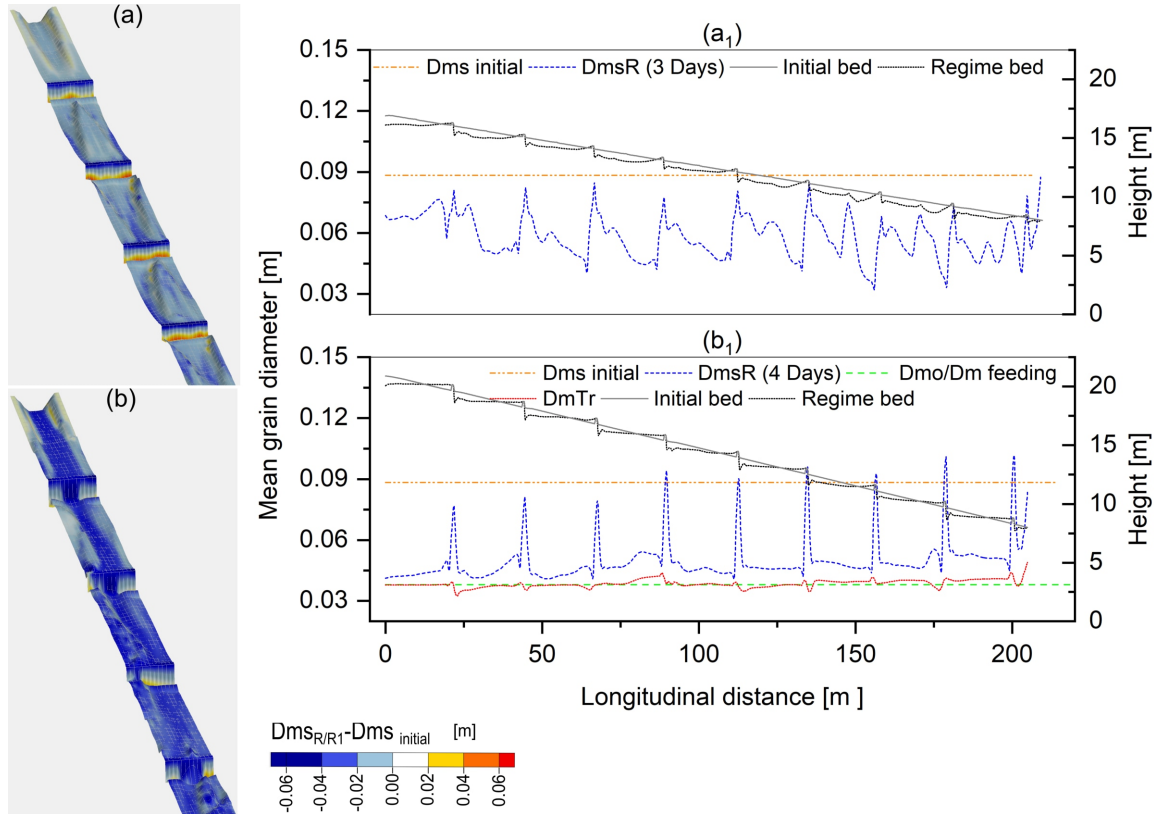


Figure 5.26.: The difference in mean grain diameter for surface layer between regime state D_{msR} and initial condition D_{ms} for inflow section of regime channels R and R1 in (a) (b) respectively. (a₁) longitudinal profiles of channel bed, D_{msR} and D_{ms} at initial and regime state for R and (b₁) longitudinal profiles of channel bed, D_{ms} , D_{msR} at initial and regime state, sediment feeding D_{mo} and transported bedload D_{mTr} for regime channel R1

5.4. Summary of the regime channel simulation results

Based on the field and flume observations, a channel with a specific regime slope develops a certain resistance to flow in order to preserve its slope and minimise its energy. The resistance to flow is observed to be proportional to the channel slope, sediment characteristics and flow magnitude. The regime channel resistance to flow may develop due to the bed sediment grains, bedforms, bed sediments interlocking and existing of large immobile macro-roughness elements MRE. Depending on the value of total resistance, only a portion of total flow energy is effectively used for bedload transport. Therefore, a reduced energy gradient, representing a fraction of the total energy gradient is estimated to be effective in bedload transport based on the flow resistance partitioning approach. The

reduced energy gradient is achieved by multiplying the relative flow resistance $\mu = k_{st}/k_{st'}$ with the original energy gradient, which in turn is used for the calculation of bed shear stress that actually used for bedload transport. The value of flow resistance is observed to decrease with increasing channel regime slope, which means for steep slopes, the contribution of total flow energy actually used for bedload transport is much lower than for gentler slopes.

While the value of grain resistance $k_{st'}$ can be relatively accurately approximated from the GSD of riverbed sediments, estimation of the total resistance k_{st} is not very straightforward. One strategy to estimate the value k_{st} for a wide range of channel slopes and GSD is to use regime channel simulation. In this chapter, the results of the regime channel simulations are presented in terms of relative resistance μ variations with channel regime slopes S_R, S_{R1} . The regime channel approach is employed in series of 2D computer simulations to determine the relative flow resistance μ relationship with channel regime slopes S_R, S_{R1} . Two regime channel approaches are applied, namely zero and a constant feeding rate at model's inflow respectively termed as *R* and *R1* regime channels. The regime state is achieved when the bedload transport at model's outflow approaches zero $Q_{bin} = Q_{bout} = 0$ for *R*, bedload transport at model's inflow equals the sediment feeding rate at model's inflow $Q_{bin} = Q_{bout}$ for regime channels *R1* and the change in channel slope with time is diminishing $\frac{\partial S_R}{\partial t} = 0, \frac{\partial S_{R1}}{\partial t} = 0$.

The simulations are performed using two types of channel domain, a fixed-width of 5.5 m and extended-width of 16.5 m and length of 200 m resembling respectively long flume and a wide natural channel. The fixed-width channels of different slopes are also combined together to study the effect of slope combination on the regime development. Simulations are performed for the channels of slopes between 0.0% and 10% and six GSD for surface and subsurface layers with mean grain diameter D_{m0} of 19.0 mm, 28.4 mm and 38.0 mm, 47.3 mm, 57.0 mm, and 66.3 mm.

The simulations are performed with a constant flow discharge of $2 \frac{m^3}{s}$. The extended-width channels are also simulated with a flow discharge of $1 \frac{m^3}{s}$ to understand the effect of flow discharge on the regime development. The 2D channel simulations are performed using Hydro_FT-2D program employing two layer sediments and critical dimensionless shear stress for transport begin as $\tau_{ce}^* = 0.05$. Two scenarios of relative resistance relationship are tested. In the scenario A, grain resistance $k_{st'}$ is varied to change the value of $\mu = k_{st}/k_{st'}$ for different channel slopes and total resistance k_{st} is held constant. In contrast, in scenario B, grain resistance $k_{st'}$ is held constant and total resistance k_{st} is varied to influence the value of μ .

The results perfectly agree a power-law relationship between relative resistance and channel regime slopes regardless of whether the channel is a fixed-width or extended-width, combined slope cases, *R* or *R1* regime channels and coarse or

fine GSD.

The effect of different GSD is predominantly due to the decreasing sediment mobility $\Phi_{dms,i} = q_{b,i} / \sqrt{(\rho_s/\rho - 1) \cdot g \cdot d_{ms}^3}$ with mean diameter of surface layer sediments D_{ms} . The program Hydro_FT-2D uses the equal-mobility concept, which assumes transport begin for all grain sizes when the critical condition for mean grain diameter D_{ms} is exceeded. Since for all GSD, a single critical dimensionless shear stress for transport begin of $\tau_{ce}^* = 0.05$ is used, therefore the effect of GSD is merely as a result of different mobility parameter $\Phi_{dms,i}$. Thus, with coarser GSD larger regime channel slopes for the same relative resistance $\mu = k_{st}/k_{st'}$ values can be achieved compared to a finer GSD.

The effect of larger channel bed area provided by the extended-width channels is observed to achieve larger regime channel slopes for the same relative resistance $\mu = k_{st}/k_{st'}$ values compared to fixed-width channels. The simulations for extended-width channels reveal larger regime channel widths, which in turn causes a distribution of flow over larger bed area compared to fixed-bed channels. Therefore, the shear stress decreases and bed erosion decreases accordingly, thus larger regime channel slopes can be achieved for the same GSD and μ values. The simulations with the reduced flow discharge by 50% ($Q = 1.0 \text{ m}^3/\text{s}$) for the extended-width channels induces a significant shift in the relationship between μ and regime channel slope. Simulations with flow discharge of $Q = 1.0 \text{ m}^3/\text{s}$ and $Q = 2.0 \text{ m}^3/\text{s}$ and same values of GSD and μ lead to larger regime channels slope S_R, S_{R1} for earlier but S_R, S_{R1} do not doubles as one may assume. Because, the simulations with $Q = 1.0 \text{ m}^3/\text{s}$ do not develop an exactly half channel regime width compared to simulations with $Q = 2.0 \text{ m}^3/\text{s}$, rather the channel regime width reduces on average by 1.0 m for $Q = 1.0 \text{ m}^3/\text{s}$.

Regime channel R1 with a constant sediment feeding rate at model's inflow has an opposite effect as GSD or flow discharge reduction. For the same regime channel slope, the relative resistance should be lowered or the μ values should be larger to transport the sediment feeding at model's inflow. In other words, for R1 regime channels, larger channel slopes may be achieved for the same μ values compared to R regime channels. The channel bed sediments is observed to develop strong coarsening from initial GSD for R channels, while it is controlled by the GSD of sediment feeding for R1 regime channels.

The increase in relative resistance with channel slope is partly reflected by the bedforms developed during the regime channel simulation similar to those observed in natural rivers and streams. The regime channel develops riffle-pool at gentle slopes and step-pool, cascade, pools and chutes and antidunes at steep slopes, which is indicative of larger relative resistance with channel slope.

In the second part of chapter 5, MRE are implemented as non-erodible geometrical bodies of trapezoidal shapes. The MRE on one hand strongly affects the flow hydraulics such as velocity, water depth and shear stress compared to the

plane-bed condition and on the other hand they reduce the total bed area exposed to erosion. The regime channel simulations reveal that initially an increase in MRE concentrations leads to an increase in regime channel slopes. However, with further increase in MRE concentration their relationship reaches an asymptote. The asymptote behaviour occurs between MRE concentrations of 30% to 40%. Similar asymptotic behaviour of ratio of drag shear stress to total shear stress with MRE concentrations are also reported in flume experiments.

In the last part, MRE are implemented as artificial non-erodible steps over the whole channels width for channel slopes ranging from 2.5% to 10%. The distance between MRE steps are therefore fixed and the only variable for regime development is the step depths. For a fixed distance between MRE steps, larger step depths are developed for steep slopes compared to gentle slope conditions. The relationship between step-pool dimension $\lambda = L_D/D_B$ and channel regime slope is shown to follow a power-law relationship. The simulations results in terms of step-pool dimension with channel regime slopes reveal good agreement with field observations of natural step-pool dimensions variations with channel regime slope.

6. Application

6.1. Case study of Shakar-Dara and Maidan rivers

6.1.1. Shakar-Dara River

Shakar-Dara is one of the fifteenth districts of Kabul province, the capital of Afghanistan, which is located in the north-west of Kabul city. The river flowing down the valley of Shakar-Dara draining a catchment area of around 93 km^2 at its hydrometeorological station in Dashtak village located at latitude $34^\circ 41' 0''\text{N}$ and longitude $68^\circ 59' 0''$. The altitude of this valley in the study area is varying from approximately 2190 down to 2090 meters above sea level (m a.s.l). Rangeland with sparse vegetation covers most of the surface area. The irrigated agricultural lands and vineyards are directly supplied by the Shakar-Dara River, as the majority of agricultural land is located right on the floodplains.

Shakar-Dara River is a steep gradient riffle-dominated type with rapids and infrequently spaced scour pools at its bends. The cross-sections are very irregular and at some sections (mostly at upstream), the river has many bars and bends. The main source of flow for Shakar-Dara River is the snowmelt in the summer and early spring rain. The so far record of the discharge shows a peak flow of $7.1 \text{ m}^3/\text{s}$ recorded on April 2012 and average daily discharge of $1.37 \text{ m}^3/\text{s}$. Shakar-Dara River also dries up or ceases to flow at some reaches during late summer months. The riverbed sediments are ranging from large boulders to fine sand and silt. The main sediment source for Shakar-Dara River is the supply from hillslope in upland zone. Moreover, the riverbanks' erosion are observed to be extensively high, since riverbanks at most of the reaches in the upstream of hydrometeorological station in particular are natural and prone to erosion. However at some locations, bank erosion is limited due to the presence of dense vegetation cover. Therefore, sediment erosion from the riverbanks has significant contribution to the total sediment budget of Shakar-Dara River.

Shakar-Dara River represents a typical mountainous IRS with varying stretch slopes and bedforms. This makes it a good study site for applying the regime channel approach examined on artificial channels in previous chapter. Further, Shakar-Dara River can be considered as natural river of almost zero anthropogenic influence, however recently a medium size Shah-wa-Arus gravity dam is under construction at the farthest downstream of the study site. The result of this study can also help Kabul water authority to better understand the bedload transport to

the dam site and to develop accordingly their reservoir sedimentation management strategies.



Figure 6.1.: Shakar-Dara River at downstream of hydrometeorological station

6.1.2. Maidan River

Maidan River is one of the tributaries of Kabul River originating from Maidan Wardak province in the south-west of Kabul province in Afghanistan. The river flows down to Kabul through a narrow valley known as Tangi-Sayedan area, where there is a hydrometeorological station at latitude $34^{\circ} 24' 0''\text{N}$ and longitude $69^{\circ} 05' 0''\text{E}$ with an average altitude of 1875 (m a.s.l). Maidan River drains a catchment area of about 1625 km^2 . The main flow source for Maidan River is mostly snow and early spring rains. The peak discharge period is from March to June, which indicates snowmelt period as the ambient temperature starts to rise. The historic data shows the highest monthly mean flow discharge of $44 \text{ m}^3/\text{s}$ in April 1980. Maidan River is an IRS with long dry period from July to October. However, during these months most of Maidan River's water is used via diversion channels for irrigation purposes. Maidan River transports large amount of suspended sediments during the flow season and due to abrupt recession of flow peak, large amount of suspended sediments deposit on the riverbed surface leading to

clogging of riverbed surface (Sadid et al. 2016).



Figure 6.2.: Maidan River section at upstream of Tangi-Sayedan hydrometeorological station

6.1.3. Field campaigns

During the two field campaigns conducted in 2013 and 2016, river geometry, riverbed sediments and flow velocity were measured for both rivers. The river geometry measurements were conducted for the first time in July 2013 and repeated after three water years in August 2016. A reach of 2057 *m* long is surveyed with total numbers of 41 cross-sections covering reach length of 783 *m* upstream and 1274 *m* downstream of the hydrometeorological station. The width of Shakar-Dara River in the study reach varies from approximately 9.0 *m* in the single thread regions to 30.0 *m* in braiding regions.

Riverbed sediments for Shakar-Dara River range from boulders and cobbles to silt. The surface layer sediment is consisting mostly of cobbles and coarse gravel covering a subsurface layer containing mostly coarse gravel to coarse sand. The grain size composition of the surface layer sediments is determined by a photogranulometric analysis tool (Basegrain)(Detert and Weitbrecht 2013) using a number of bed surface photographs taken from different locations as shown in figure 1 a of appendix E. The subsurface layer's sediments grain size distribution

is determined by sieve analysis of four sediment samples taken from mixed layer samples from four different locations along the study site.

Flow velocity measurements were conducted at a selected cross-section near the hydrometeorological station. Propeller current meter device was used to measure the flow velocity at several points of the selected cross-section. An average flow velocity for the whole cross-section is then calculated that links the average water depth and flow discharge with the flow velocity.

In total, 3720 *m* long Maidan River reach is surveyed, 380 *m* upstream and 3340 *m* downstream of the hydrometeorological station in Tangi-Sayedan area. The river cross-sections are measured in distances ranging from 20 *m* to 200 *m* depending on their locations.

Four riverbed sediment samples from different locations of the Maidan River study reach (see figure 6.3 b) are collected from mixture of surface and subsurface layers and are sieve analysed. While the mixed layer sediments are assumed to represent the GSD of subsurface layer, the GSD of surface is layer is determined using photogrammetric analysis of 20 riverbed surface photographs as shown in figure 1 b in appendix E.

Maidan River reach in the study area has plane-bed to riffle-pool morphology. In the upstream section of Tangi-Sayedan station, natural riverbanks provide part of suspended and bedload sediments while downstream of the station, mostly riverbanks are protected by stone masonry retaining walls. Therefore, the river at downstream of the station has an erosive regime with intensive erosion from the riverbed in particular in outer curved regions.

Riverbed sediment excavations from at least four locations are observed. The extracted sediments from the riverbed are mainly used for construction purposes and unfortunately no valid data about the amount and rate of sediment excavation exists.

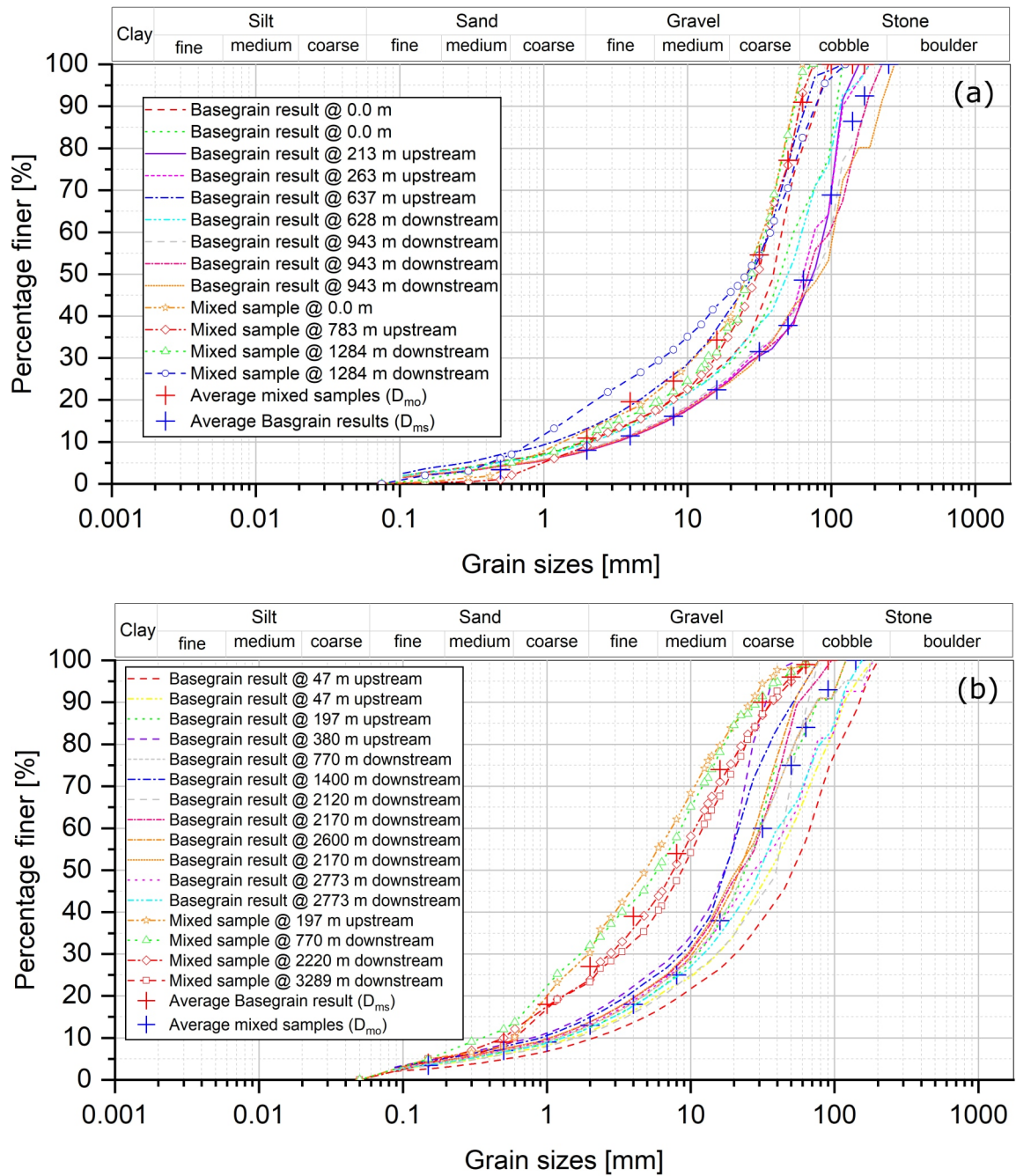


Figure 6.3.: Surface and subsurface layers' sediment GSD determined by Basegrain and sieve analysis respectively for the study reaches (a) Shakar-Dara River (b) Maidan River

The initial relative flow resistance values $\mu = k_{st}/k'_{st}$ are determined for each stretch of constant slope based on the results acquired in scenario A of extended-

width channels (see 5.1.2, chapter 5). The value of k_{st} is estimated based on the slope of each stretch using the power-law relationship between relative resistance to flow μ and stretch slope S derived from regime channel simulations. The value of total roughness k_{st} for model is assumed to be constant (as in scenario A) and is estimated from the mean diameter of the surface layer sediments D_{ms} using the equation $k_{st} = 17.5(D_{ms})^{-1/6}$. With known values of μ and k_{st} , values for grain roughness k'_{st} for each stretch are calculated. The variable k'_{st} values for each stretch is implemented by defining unique material via Surface-water Modelling System (SMS) interface for Hydro_FT-2D model as shown in figure 6.4. Similar procedure is used to assign the initial μ for Maidan River as shown in figure 2 in appendix E.

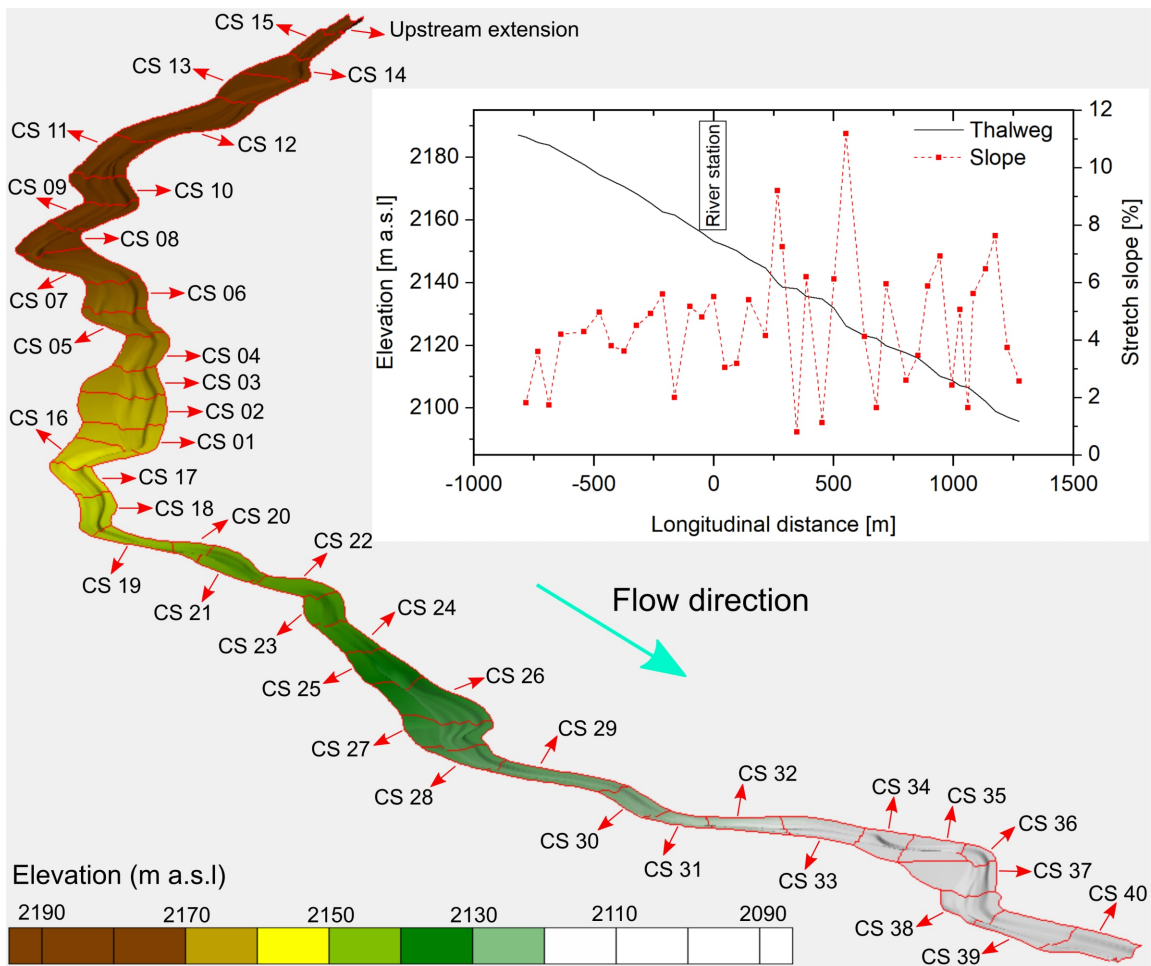


Figure 6.4.: Shakar-Dara River reaches and their associated slopes for assigning initial k'_{st} and μ values

6.1.4. Hydromorphological modelling results

i- Riverbed evolution

The result of the simulation is shown in terms of the measured and simulated riverbed evolutions. The riverbed evolution is determined from the difference in measured river cross-sections in 2013 and 2016. The simulated riverbed evolution is achieved by varying the values of μ such that a best agreement with measured riverbed evolution is resulted. The longitudinal profiles of observed and simulated riverbed evolution are also compared as shown in figure 6.5 .

The simulation result for shakar-Dara River shows that larger riverbed changes trend are well reproduced, while minor riverbed evolutions are partly reproduced (figure 6.5). Since the two dimensional visualization of riverbed geometry is produced using linear interpolation between measured cross-sections, it therefore, shows more uniform evolution distribution in longitudinal direction compared to the simulation result. Simulation result exhibits more dynamic (more diversity) in terms of erosion and deposition's magnitude and variation in longitudinal and transverse to flow directions. Riverbed change as a result of sediment in particular, is overestimated at least in two sections in the downstream reaches. As a whole, the simulated riverbed evolution is in good agreement with observed values and the deviations are also in acceptable range.

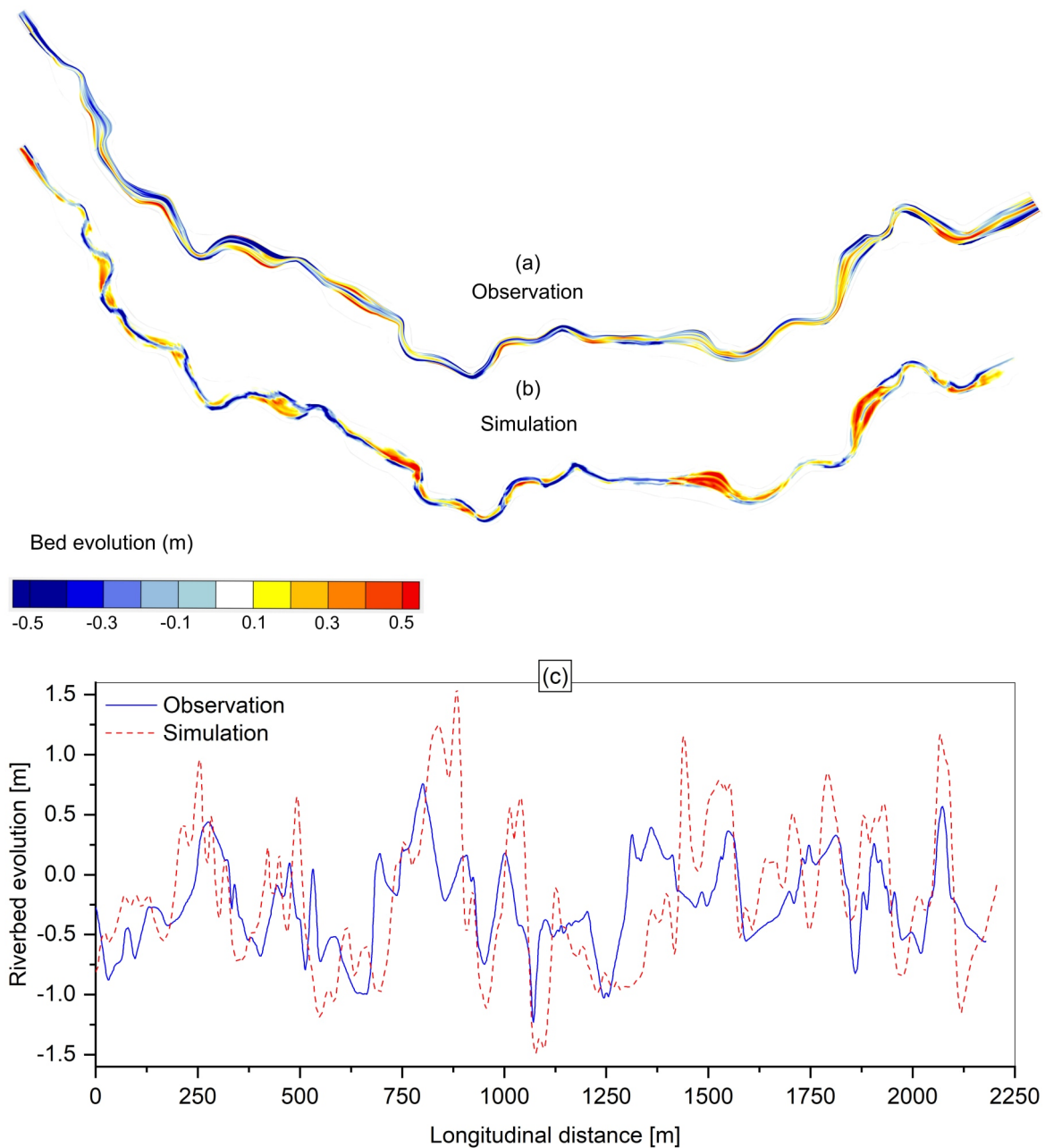


Figure 6.5.: Riverbed evolution of Shakar-Dara River occurred between 2013 to 2016 (a) observed evolution (b) simulated evolution and (c) their longitudinal profiles

Similarly, the result of the simulation for Maidan River shows as a whole good agreement between measured and simulated riverbed evolutions as shown in figure 6.6. The simulation results exhibits much better agreements for regions with larger measured riverbed evolutions, compared to regions with lower riverbed

changes during 2013 to 2016. In general, both measured and simulated riverbed evolution reveal an erosive regime in the investigated reach of Maidan River, because the inflow of sediments from upstream reaches does not satisfy the transport capacity and therefore, sediment from riverbed is mobilised. In addition, sediment supply from riverbanks is limited due to riverbank protection with stone masonry walls.

Despite general erosive regime, simulation result shows regions with large sediment deposition in particular at 200 *m* in upstream and at 400 *m*, 720 *m* and 920 *m* downstream of Tangi-Sayedan hydrometeorological station as shown in figure 6.6 c, d, e and f respectively. Field observations also confirm that from abovementioned regions in particular, sediment is extracted for construction purposes. There is no data of sediment removal available to compare with the simulated sediment deposition; nonetheless, the sediment extractions can qualitatively explain the large sediment depositions from simulation results. There are also locations where the discrepancy between simulation and observation cannot be explained. For example, at the 90 degrees meander, erosion is observed while simulation result shows a sediment deposition.

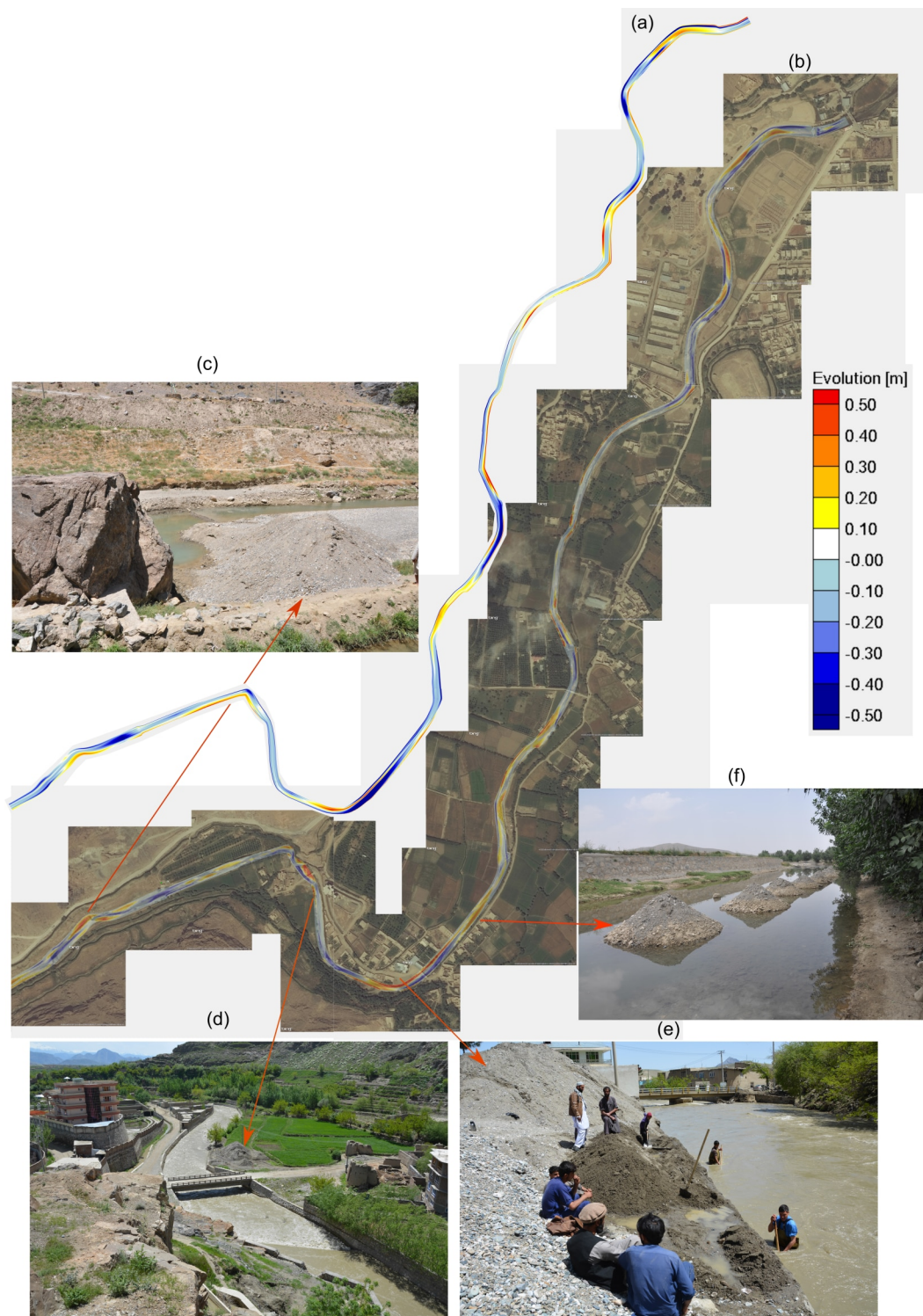


Figure 6.6.: Observation and simulation of riverbed evolution for Maidan River for 2013 to 2016 (a) observation (b) simulation (c) sediment extraction areas at 200 *m* upstream (d) 400 *m* (e) 720 *m* and (f) 920 *m* downstream of Tangi-Sayedan hydrometeorological station

Imageries: Esri, DigitalGlobe, GeoEye, Earthstar Geographics, CNES/Airbus DS, USDA, USGS, AeroGRID, IGN, and the GIS User Community

Longitudinal profiles of observed and simulated riverbed evolution for Maidan River exhibits good agreement between them as shown in figure 6.7. The major erosion and sedimentation areas are well reproduced, despite some differences in their magnitude.

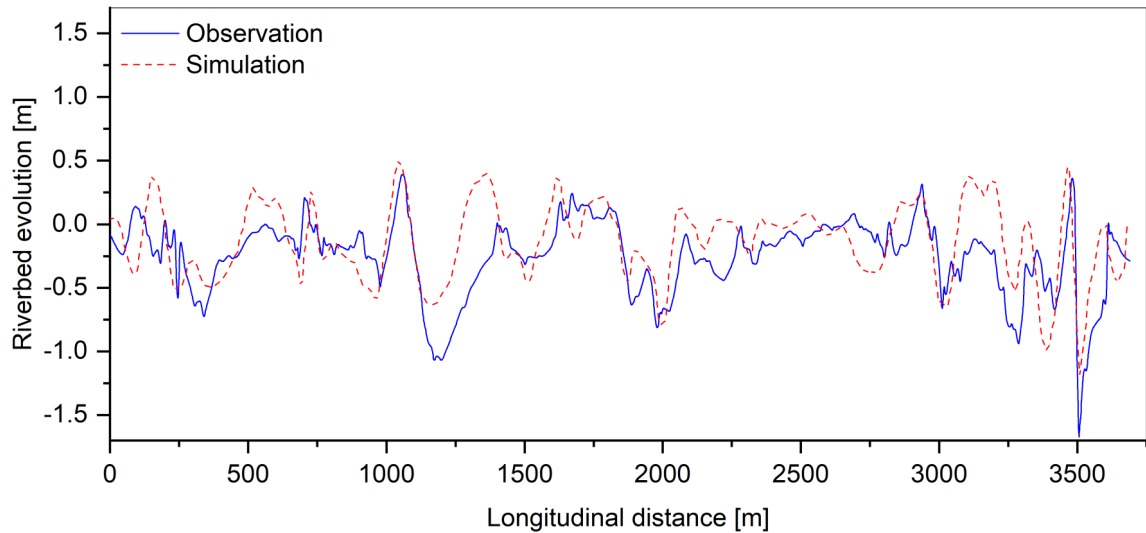


Figure 6.7.: Longitudinal profiles of observed and simulated riverbed evolution for Maidan River

ii- Bedload transport

Bedload transport as a function of flow discharge is analysed at four control sections of Shakar-Dara River as shown in figure 6.8. Bedload transport at all sections of Shakar-Dara River shows a general increase with increasing flow discharge, however in a more discontinuous form. The discontinuity is representing a natural condition where the supply of sediments from upstream and riverbank have large influence on the downstream section. The large bedload transport difference and scatter shapes are also indicative of a discontinuous transport, which also occurs in natural condition.

The initiation of bedload transport for all control sections occurs at a flow discharge of around $3 \text{ m}^3/\text{s}$ to $4 \text{ m}^3/\text{s}$. At the flow discharges larger than $3 \text{ m}^3/\text{s}$, the relationship between bedload transport and flow discharge can be expressed by a power-law. At model's outflow, $Q_b = 0.005(Q)^{4.6}$, which agrees well with bedload transport observations for steep mountainous rivers and streams.

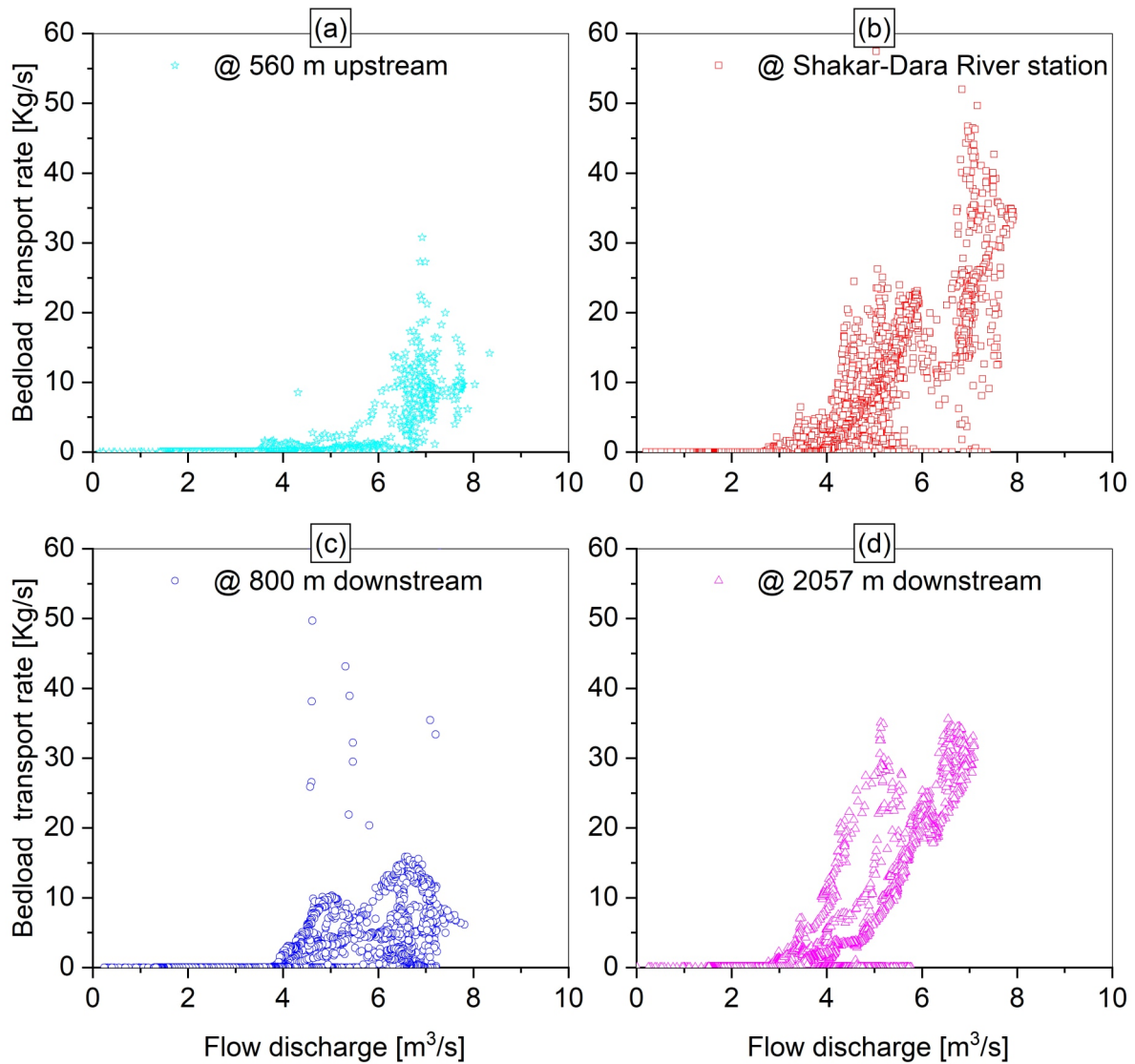


Figure 6.8.: Bedload transport from calibrated model obtained at different sections (a) 560 m upstream (b) 0 m (c) 800 m and (d) 2057 m downstream of Shakar-Dara River hydrometeorological station

Bedload transport for Maidan River is analysed at six control sections placed at specific locations of Maidan River as shown in figure 6.9. The bedload transport as a function of flow discharge for all control sections show similar polynomial trend of order two with R^2 value between 91 and 97. The relationship between flow discharge and bedload transport can be expressed by a quadratic polynomial equation with variable ranges of constants as $Q_b = [0.01 - 0.03](Q)^2 + [0.5 - 1.2](Q)^{[2-5]}$. While the pre-factors of Q^2 and Q represents the rate of change

in bedload transport with a flow discharge, the constant value between [2-5] represents the initiation of bedload transport. This indicates that for Maidan River, bedload transport starts at flow discharges larger than $2 \text{ m}^3/\text{s}$ to $5 \text{ m}^3/\text{s}$ depending on river cross-section. The results also show that up to a flow discharge of $10 \text{ m}^3/\text{s}$, weak bedload transport occurs with a minimum of rate of 0 kg/s to a maximum rate of 10 kg/s .

The bedload transport and flow discharge relationship exhibits a counter clockwise hysteresis effect, due to the armouring of riverbed sediments. Riverbed armouring leads to lower bedload transport during rising limb of a flow event and larger bedload transport during falling limb. Field investigation including riverbed sediment analysis shows riverbed armouring for Maidan River (see figure 6.2).

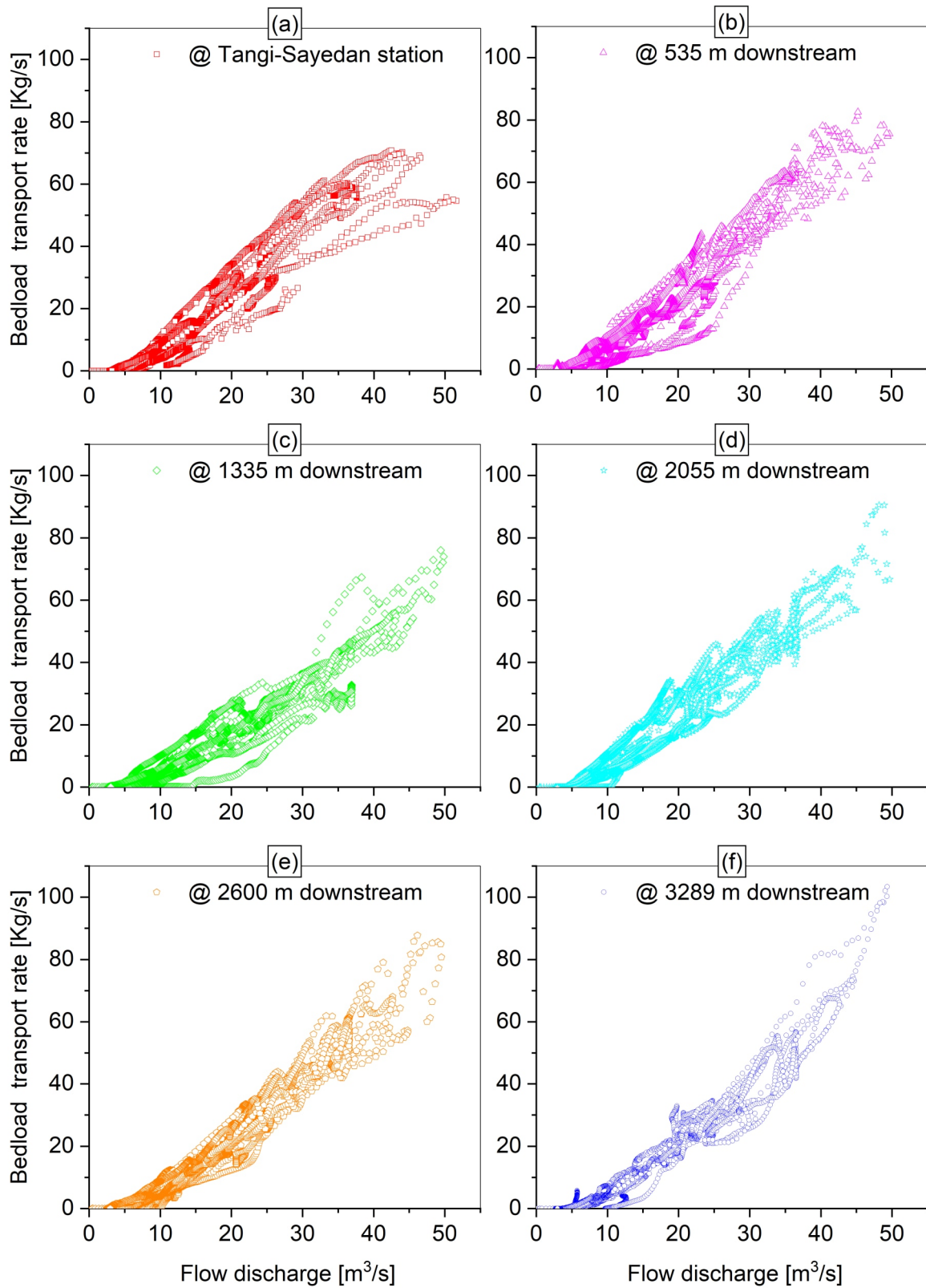


Figure 6.9.: Bedload transport from calibrated model obtained by using control sections at different locations Maidan River (a) 0 m (b) 535 m (c) 1335 m (d) 2055 m (e) 2600 m and (f) 3289 m downstream of Tangi-Sayedan hydrometeorological station

iii- Variation of relative flow resistance μ

The initially given μ values that are calculated merely based on the channel stretch slope may change for some stretches in order to achieve a best agreement between measured and simulated riverbed changes. The results indicate that despite strong variations of μ values above and below average values derived from regime channel R1 simulations, as a whole a general trend of decreasing μ value with increasing reach slope persists (figure 6.10 a). The change in μ values derived from regime channel simulations and calibration of Shakar-Dara River is not unexpected, because of the different boundary conditions (e.g. flow discharge, bedload rating curve). Similarly, for Maidan River the final or calibrated relative resistance μ values and stretch slopes follow a power-law relationship, which in general agrees with trend observed from regime channel simulations as shown in figure 6.10 b. The difference in relationship between μ and reach slope is primarily due to different boundary condition than regime channel simulations such as large flow discharges and bedload feeding from upstream of the model. The initial μ values are significant reference values for starting calibration of a bedload transport model. However, for fine calibration of the model, μ values are modified for most of river stretches, in order to achieve an optimal result.

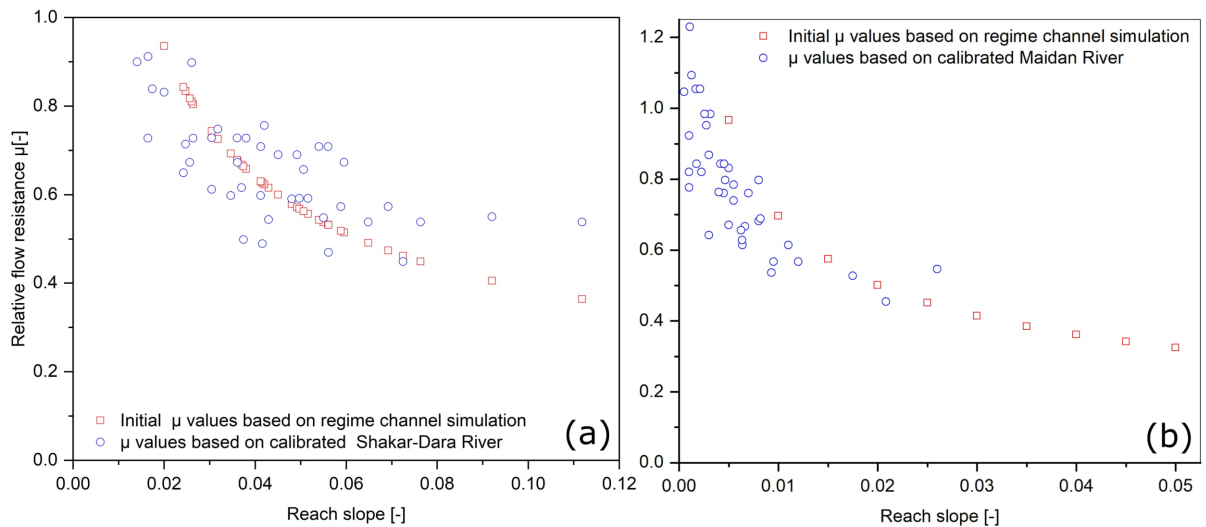


Figure 6.10.: Relative flow resistance relationship as a function of channel reach slope for an average regime channel R1 simulations and (a) Shakar-Dara River (b) Maidan River

The application of regime channel approach for determining an initial relative flow resistance μ based on an average reach slope produced acceptable results for Shakar-Dara and Maidan rivers. The relationships between μ and channel stretch slopes derived using regime channel approach set a starting point for

morphological models calibrations when the data for model calibration is available. This will help achieve calibration goals in much shorter time compared to usual case of starting the calibration with a single constant μ value for the whole model. For the IRS with no data for model calibration, assigning μ values based on channel stretch slopes and specific GSD can produce realistic results and help avoid overestimating bedload transport. IRS channel dimensions, slope, GSD and hydrograph are sufficient data to run a morphological model and estimate bedload transport. Nevertheless, the approach needed to be tested and applied on more case studies with data for calibration to improve its confidence and shortcomings. In particular, the variation of μ values with channel stretch slope should be field validated. Steep channel stretches with low μ values should also exhibit more prominent bedforms to justify higher resistance to erosion.

7. Conclusion and outlook

7.1. Conclusion

The present research covers the extensive topic of bedload transport under consideration of the complex morphological processes in mountainous Intermittent Rivers and Streams (IRS) for the prognosis of long-term bed evolution and bedload transport. Rivers and streams with flow, sediment transport and habitat seasonality are termed in this study as IRS. IRS develop unique hydrosedimentological characteristics due to the intermittency of flow (i.e. absence of base flows), which differs strongly from well researched perennial rivers and streams. The location of IRS in mountainous arid and semi-arid regions of the world adds to their complex nature of hydromorphological characteristics. Shallow water depths, diverse grain size distribution (GSD), large bedforms, existing of macro-roughness elements (MRE) (i.e. immobile boulders, large woody debris (LWD)) increase the resistance to flow, which in turn strongly affects the bedload transport. The increased flow resistance in particular for shallow and low flow submergence channels are shown to strongly influence the near-bed flow properties, namely decreases the shear stress for bedload transport. Bedload transport studies for steep channels reveal that conventional bedload transport equations typically overestimate the bedload transport up to three orders of magnitude. A realistic estimation of bedload transport can help develop sustainable sediment management strategies for reservoir, irrigation canals and other water structures.

A good estimation of flow resistance can help determining the effectiveness of the total flow transport capacity in bedload transport. Despite development of numerous methods and approaches for quantifying the flow resistance for low flow submergence in steep channels, yet their applications are limited to flume studies and require data such as relative submergence, boulder size-resolution of riverbed geometry, which are hardly available for natural river systems. Another major deficit in the existing approaches is the absence of the role of bedforms, MRE, sediment interlocking effects and other site-specific variables. Therefore, in this research work, flow resistance is estimated at river stretch scale using a regime channel approach. A natural channel of specific bankfull discharge and GSD adjusts its slope and geometry (width and depth) to develop a dynamically stable state that can convey a certain discharge and sediment. Regime channels develop a total flow resistance in order to resist the change imposed by bankfull

discharge and maintain a specific regime geometry, slope, and GSD.

The channel regime development is simulated using 2D computer models, where an initial channel geometry, slope, GSD, bedload feeding rate and bankfull discharge achieves a specific regime status for a given flow resistance. Initial channel slopes between 0.0% and 10% and six GSD covering a large spectrum of GSD occurring in natural alpine environment are examined to determine the effect of initial channel slope and GSD. In nature, a channel reach is composed of several stretches of constant slopes, thus to understand the effect of different slope combinations, regime simulations are also performed for three cases of channel slope combinations. In the regime channel approach, a relative flow resistance is numerically given to the model based on which the energy gradient of the system is modified. Based on the regime resistance partition approach, the ratio between total flow resistance k_{st} and grain resistance k'_{st} is termed as relative resistance μ also known as shear stress damping factor. The flow resistance partitioning indicates that only a portion of total flow energy actually contributes to the bedload transport, while the rest is lost to overcome the additional resistance due to bedforms, MRE, LWD and others.

The simulations' results show a power-law relationship between relative flow resistance and channel regime slope, namely channels with gentler slopes develop lower flow resistance, while they develop larger flow resistance for steep channels. R1 regime channels with a constant feeding rate (e.g. $Q_b = 5.0 \text{ kg/s}$) have caused a slight shift in relationship between flow resistance and channel regime slope, namely for a given relative flow resistance, channels maintained relatively larger slopes, because part of the erosion capacity of flow is used to transport the given sediments.

R1 regime channel resembles a natural condition with abundant of sediment supply from upstream or side slopes. The regime GSD of channel bed is therefore strongly influenced by the GSD of sediment supply from upstream. However, in case of R regime channels, with a constrained sediment supply condition, channel bed sediments coarsen intensively. The coarsening or buildup of an armouring layer occurs as a result of selective transport, where finer particles are transport downstream and larger particles of lower mobility remains on the channel bed. The effect of GSD is shown to be predominantly due to the mobility parameter. Coarse GSD required lower flow resistance to achieve a certain channel regime slope compared to finer GSD, mainly because coarse GSD has smaller mobility and therefore are difficult to be eroded. Thus, it can be inferred that coarser GSD contributes more to the total flow resistance compared to finer GSD. More importantly, the flow resistance variation with channel regime slope is well reflected by channel regime bedforms development that shows plane-bed to riffle-pool bedforms for gentle slopes and step-pool to cascade bedforms for steep channel slopes. The regime channel plan-form is shown to develop meandering, erosion at

inflow and deposition at outflow and a mixture of both in the course of achieving regime status. The similar trend of relative flow resistance variation with channel regime slope and development of larger bedforms for steep slopes are consistently observed for all used GSD, bedload feeding rate, and slope combinations cases. The regime channel simulations for combined channel cases show that the whole channel system develops toward achieving a single slope, namely the initial steeper stretches flattens and the gentler stretches steepens. This process relaxes the initially given sharp slope changes between two adjacent stretches. The relative resistance variation with channel stretch regime slopes for channel slope combination cases follows closely the results from single channel slopes.

The flow resistance and channel regime slope relationship from the regime channel simulations are shown to be in good agreement with some field investigations such as direct measurement of flow resistance or their back calculated values from measured bedload transport in some steep rivers and streams. The validity of this approach is tested on two examples of IRS (Maidan and Shakar-Dara rivers in Kabul River basin, Afghanistan) with known boundary conditions and bed evolution. The flow resistance achieved from model calibration follows similar power-law relationship obtained from the regime channel simulations.

As an alternative approach, large flow resistance sources such as MRE and their arrangement in step-pool or cascade bedforms on steep riverbeds are dealt as rigid, immobile geometrical shapes in the regime channel simulations. MRE are quasi-randomly distributed over the entire channel bed as non-erodible trapezoidal shapes. MRE impose two distinct effects (i) they strongly changes the flow characteristics around them and (ii) they reduces the total exposed channel bed area to erosion. The hydraulic simulation of channels with MRE revealed that at lower slopes, the effect of reduced channel bed area to erosion is more dominant, because the bed shear stress actually increases in micro-channels around MRE compared to a plane-bed channel. However, in the case of steeper bed slopes, MRE protects the channel bed both in terms of reducing the exposed area and the shear stress in micro-channel regions around MRE.

The regime channel simulation with MRE show that initially by increasing the MRE concentration, larger channel slopes can be stabilised to achieve their regime state. However, after reaching a certain concentration values; further increases in MRE may not necessary stabilise larger channel slopes. The relationship between MRE concentrations and channel regime slopes follow a logarithmic-law with a horizontal asymptote. Similar results are also reported from flume experiments that the ratio of drag to total shear stress increases rapidly when the MRE are sufficiently distant. As the concentration of MRE increases, the ratio of drag to total shear stress first reach an asymptote and then decreases. The increase in drag shear stress as a result of MRE concentrations implies lower effective shear stress at the bed for sediment entrainment. Because the drag shear stress may not

contribute to the sediment transport, thus the bed erosion is reduced and channel slope stabilises. The effect of GSD indicate that for a given MRE concentration, larger regime channels can be achieved by coarser GSD, mainly due to the lower mobility of coarser GSD.

MRE arrangements as cascades are built in the model as non-erodible elements across the channel width in a predefined step-distance. Therefore, the channels develop a certain step-depth to achieve a regime status. The initially plane-bed of channels undergo large erosion right downstream and deposition in the upstream side of the rigid elements evolving a cascade bedforms. The results show a power-law relationship between channel regime slope and the ratio of step-length L_D to step-depth D_B also known as step-pool dimensions $\lambda = L_D/D_B$. The results obtained are in good agreement with field measurement of naturally occurring and artificially built step-pools dimension λ relationship with channel slope. Similar to regime channel simulations, MRE cascades develops larger step-depth D_B for finer GSD, mainly because of larger mobility of finer GSD. A constant sediment feeding rate reveals two distinct behaviours (i) at gentler slopes, step-depth D_B is strongly decreased and (ii) at steeper slopes, the difference in developed step-depths D_B between zero sediment feeding and a feeding rate of $Q_b = 5.0 \text{ kg/s}$ diminishes.

The main assumption for the regime channel simulation that at steeper slopes, larger flow resistance predominantly in form of bedforms develop could be well verified. Steeper channel slopes did produce larger bedforms compared to gentler slopes. Therefore, the main challenge in approximating the flow resistance in the modelling of bedload transport can be overcome using the measured IRS slope. Rough channel geometry, channel slopes, GSD of bed sediments and flow discharge are sufficient data for estimating the bedload transport in IRS. The larger flow resistance for steeper stretches of a river channel basically damps the pure hydraulically simulated energy gradient and hence avoids overestimation of bedload transport. Regime channel simulation results can be further improved if additional information such as bedforms, channel plan-form or spatial distribution of GSD for surface layer is available.

Using MRE and their arrangement in cascade bedforms as one sources of flow resistance require more detailed information about their size, distribution and mobility. Such information can only be made available after conducting a field investigation including measuring the channel bed geometry. Obtaining detailed riverbed information requires resources and time, which is hardly available for remote sites of mountainous IRS. In summary, the important findings of the regime channel simulation approach for estimating relative flow resistance and bedload transport are:

1. The relative flow resistance exhibits a power-law relationship with channel regime slope for all initial channel geometries (i.e. fixed-and extended widths and slope combinations), GSD and channels with and without sediment

- feeding.
2. Flow resistance variations with regime channel slope are well reproduced in form of bedforms, namely step-pools to cascades for steeper slopes and plane to riffle-pool bed developed for gentler channel slopes.
 3. MRE concentration on the channel bed initially led to stabilising channels' slopes up to a certain value, followed by an asymptotic behaviour, where further increase in MRE did not necessary led to further stabilisation.
 4. Arrangement of MRE in cascades exhibited a power-law relationship between step-pool dimension and channel regime slope that closely agrees with field observations of step-pool rivers and streams.
 5. Application of regime channel approach on case the studies of Maidan and Shakar-Dara rivers revealed that the power-law relationship between relative flow resistance and channel stretch slopes may vary from the academic channel cases, mainly due to difference in their boundary condition.

7.2. Outlook

One main assumption in this research work is the regime state of IRS, which implies that the regime channel slope does not significantly change during a bankfull flow. The regime state may be disrupted by an extreme flow event before a new regime state is established. In the regime channel approach, it is assumed that IRS receives sufficient bed forming flow during the wet season for bed building processes and bedforms generation. In mountainous regions, IRS experiences regular flow season with sufficient bed forming flow due to the rain and snowmelt in early spring and summer months. However, One may argue that some IRS in arid lowland regions have strong sporadic flow events as response to sudden precipitation and may not be in regime state, because the flow duration is not long enough for development of regime bed morphology. Therefore, it is required to validate the regime channel approach on IRS with sporadic flow events located in lowland regions to address the influence, the flow intermittency, flow magnitude and duration may have on the channel regime resistance development.

The regime simulations revealed that the numerically given large flow resistance values are reproduced in form of large bedforms for steep channels. In nature, flow resistance may be present in different forms such as MRE, coarse GSD, riverbed clogging, grains interlocking and in other site-specific forms. The contribution of each mentioned parameters require extensive flume and field investigations in order to determine the role of each flow resistance forms. The main assumption for the regime channel approach that relative flow resistance increases with increasing channel regime slope requires more evidence from fields, which is yet lacking.

Future studies may focus on the form (e.g. bedforms, MRE, and LWD) and their share in total different flow resistance at different regime channel slopes.

MRE and their arrangement in step-pool or cascade bedforms are the main flow resistance and riverbed erosion protection source in most of mountainous IRS, which are largely ignored in morphological modelling, due to the lack of information about them. IRS geometry is obtained from measured cross-sections and often MRE are not included in the measurement. Recent advancement in the river mapping technology such as Unmanned Aerial Vehicle (UAV) make it possible to capture high resolution and detailed river geometry by which the locations, size and distribution of MRE may be well detected. Thus implementation of MRE in real-life examples of river morphological modelling can help river scientists outline the major challenges and difficulties arise with modelling complex natural river geometries.

More research can be conducted to develop modelling techniques dealing with abrupt changes in geometry caused by MRE in order to accurately reproduce the effect of MRE under submerged and protruding water depths. The simulation of MRE channel shows that excessive erosion around MRE may eventually lead to unrealistically skinny elements, which in turn cause simulation instability. Therefore, modelling techniques can be improved to deal with the issue of MRE deformation when an intensive erosion around them occur in order to keep the size of MRE in the range of those naturally occurring in the rivers and streams and avoid simulation instability.

Bibliography

- [1] J. Aberle. "Spatially Averaged Near-Bed Flow Field over Rough Armor Layers." In: *River Flow*. 2006, pp. 153–162.
- [2] J Aberle and K Koll. "Double-Averaged Flow Field over Static Armor Layers." In: *Proceedings of the International Conference on Fluvial Hydraulics River Flow 2004, Vol. 1, Edited by M. Greco et Al.* Balkema, Brookfield, Vt: CRC Press, 2004, pp. 225–233.
- [3] J Aberle and G. M Smart. "The Influence of Roughness Structure on Flow Resistance on Steep Slopes." In: *Journal of Hydraulic Research Vol. 41, No. 3* (2003), pp. 259–269. ISSN: 0022-1686. DOI: 10.1080/00221680309499971.
- [4] A. D. Abrahams, G. Li, and J. F. Atkinson. "Step-Pool Streams: Adjustment to Maximum Flow Resistance." en. In: *Water Resources Research* 31.10 (Oct. 1995), pp. 2593–2602. ISSN: 1944-7973. DOI: 10.1029/95WR01957.
- [5] P. Ackers and W. R. White. "SEDIMENT TRANSPORT: NEW APPROACH AND ANALYSIS." In: *Journal of the Hydraulics Division* 99.hy11 (Nov. 1973).
- [6] P. Ackers. "Experiments on Small Streams in Alluvium." eng. In: *Journal of the Hydraulics Division* 90.4 (1964), pp. 1–37.
- [7] J. Aguirre-Pe. "Incipient Erosion in High Gradient Open Channel Flow with Artificial Roughness Elements." In: *Proc. 16th Congr. Int. Assoc. Hydraul. Res. San Paulo Brazil 2* (1975), pp. 137–180.
- [8] J. Almedeij and P. Diplas. "Bed Load Sediment Transport in Ephemeral and Perennial Gravel Bed Streams." en. In: *Eos, Transactions American Geophysical Union* 86.44 (Nov. 2005), pp. 429–434. ISSN: 2324-9250. DOI: 10.1029/2005E0440002.
- [9] J. H. Almedeij. "Bedload Transport in Gravel-Bed Streams under a Wide Range of Shields Stresses." PhD thesis. 2002.
- [10] E. D Andrews. "EFFECTIVE AND BANKFULL DISCHARGES OF STREAMS IN THE YAMPA RIVER BASIN, COLORADO AND WYOMING." In: *Journal of Hydrology*, 46 (1980), pp. 311–330.
- [11] A. Armanini. "Non-Uniform Sediment Transport: Dynamics of the Active Layer." In: *Journal of Hydraulic Research* 33.5 (Sept. 1995), pp. 611–622. ISSN: 0022-1686. DOI: 10.1080/00221689509498560.
- [12] A. Armanini and G. Silvio. "A One-Dimensional Model for the Transport of a Sediment Mixture in Non-Equilibrium Conditions." In: (1988). DOI: 10.1080/00221688809499212.

- [13] D. B. Arscott, S. Larned, M. R. Scarsbrook, and P. Lambert. "Aquatic Invertebrate Community Structure along an Intermittence Gradient: Selwyn River, New Zealand." In: *Journal of the North American Benthological Society* 29.2 (Mar. 2010), pp. 530–545. ISSN: 0887-3593. DOI: 10.1899/08-124.1.
- [14] A. H Arthington, J. M Bernardo, and M Ilheu. "TEMPORARY RIVERS: LINKING ECOHYDROLOGY, ECOLOGICAL QUALITY AND RECONCILIATION ECOLOGY." In: *River Research Application*; 30 (2014), pp. 1209–1215. DOI: 10.1002/rra.2831.
- [15] K. Ashida and M. Bayazit. "Initiation of Motion and Roughness of Flows in Steep Channels." In: *Proceedings of the 15th Congress of the International Association for Hydraulic Research*. Vol. 1. 1973, pp. 475–484.
- [16] R. A. Bagnold. "An Empirical Correlation of Bedload Transport Rates in Flumes and Natural Rivers." en. In: *Proc. R. Soc. Lond. A* 372.1751 (Oct. 1980), pp. 453–473. ISSN: 0080-4630, 2053-9169. DOI: 10.1098/rspa.1980.0122.
- [17] R. A. Bagnold. *An Approach to the Sediment Transport Problem from General Physics*. en. U.S. Government Printing Office, 1966.
- [18] R. A. Bagnold. "The Flow of Cohesionless Grains in Fluids." In: *Philosophical Transactions of the Royal Society of London A: Mathematical, Physical and Engineering Sciences* 249.964 (1956), pp. 235–297.
- [19] W Bartnik. "Determination Of The Critical Conditions Of Incipient Motion Of Bed Load In Mountain Rivers." In: *Fluvial Hydraulics of Mountain Regions, Lect. Notes Earth Sci., Vol. 37, Edited by A. Armanini, and G. Di Silvio*. Springer, Berlin, Heidelberg, 1991, pp. 83–88.
- [20] J. C Bathurst. "Flow Resistance Estimation in Mountain Rivers." In: *Journal of Hydraulic Engineering*, 111(4) (1985), pp. 625–643.
- [21] J. C. Bathurst. "Flow Resistance through the Channel Network." In: *Channel Network Hydrology* (1993), pp. 69–98.
- [22] J. C. Bathurst, H. H. Cao, and W. H. Graf. "Hydraulics and Sediment Transport in a Steep Flume. Data from the EPFL Study, Report 64." In: *Inst. of Hydrol., Wallingford, Oxon, England* (1984).
- [23] J. C. Bathurst, W. H. Graf, and H. H. Cao. "Bed Load Discharge Equations for Steep Mountain Rivers." In: *Sediment Transport in Gravel-Bed Rivers*. John Wiley and Sons New York. 1987. p 453-491, 8 fig, 5 tab, 55 ref. (1987).
- [24] J. C. Bathurst. "At-a-Site Variation and Minimum Flow Resistance for Mountain Rivers." In: *Journal of Hydrology* 269 (2002), pp. 11–26.
- [25] M Bayazit. "Free Surface Flow In A Channel Of Large Relative Roughness." In: *Journal of Hydraulic Research*, 14:2 (1976), pp. 115–126. ISSN: 1814-2079. DOI: 10.1080/00221687609499676.

- [26] J. P. Benstead and D. S. Leigh. "An Expanded Role for River Networks." In: *Nature Geoscience* 5.10 (Oct. 2012), pp. 678–679. ISSN: 1752-0894, 1752-0908. DOI: 10.1038/ngeo1593.
- [27] R. L. Beschta and W. L. Jackson. "The Intrusion of Fine Sediments into a Stable Gravel Bed." In: *Journal of the Fisheries Research Board of Canada* 36.2 (Feb. 1979), pp. 204–210. ISSN: 0015-296X. DOI: 10.1139/f79-030.
- [28] R. Bhamjee, J. B. Lindsay, and J. Cockburn. "Monitoring Ephemeral Headwater Streams: A Paired-Sensor Approach." en. In: *Hydrological Processes* 30.6 (Mar. 2016), pp. 888–898. ISSN: 1099-1085. DOI: 10.1002/hyp.10677.
- [29] P. Billi. "Morphology and Sediment Dynamics of Ephemeral Stream Terminal Distributary Systems in the Kobo Basin (Northern Welo, Ethiopia)." In: *Geomorphology. Drylands: Linking Landscape Processes to Sedimentary Environments* 85.1 (Mar. 2007), pp. 98–113. ISSN: 0169-555X. DOI: 10.1016/j.geomorph.2006.03.012.
- [30] A. P. Blaschke, K.-h. Steiner, R. Schmalfluss, D. Gutknecht, and D. Sengschmitt. *Clogging Processes in Hyporheic Interstices of an Impounded River the Danube at Vienna Austria*. 2003.
- [31] T. Blench. *Regime Behaviour of Canals and Rivers*. London: Butterworths Scientific Publications, 1957. 138 pp.
- [32] A. J. Boulton and P. S. Lake. "The Ecology of Two Intermittent Streams in Victoria, Australia. I. Multivariate Analyses of Physicochemical Features." en. In: *Freshwater Biology* 24.1 (Aug. 1990), pp. 123–141. ISSN: 1365-2427. DOI: 10.1111/j.1365-2427.1990.tb00313.x.
- [33] A. J. Boulton, R. J. Rolls, K. L. Jaeger, and T. Datry. "Hydrological Connectivity In Intermittent Rivers And Ephemeral Streams." In: *Intermittent Rivers and Ephemeral Streams Ecology and Management*. 1st Edition. Elsevier, 2017.
- [34] A. Boulton, M. Brock, B. Robson, D. Ryder, J. Chambers, and J. Davis. *Australian Freshwater Ecology: Processes and Management*. English. 2 edition. Chichester, West Sussex: Wiley-Blackwell, May 2014. ISBN: 978-1-118-56823-1.
- [35] A. J. Boulton and W. D. Williams. "Aquatic Biota." en. In: Royal Society of South Australia, 1996.
- [36] D. I. Bray. "Estimating Average Velocity in Gravel-Bed Rivers." eng. In: *Journal of the Hydraulics Division* 105.9 (1979), pp. 1103–1122.
- [37] A. C. Brayshaw, L. E. Frostick, and I. Reid. "The Hydrodynamics of Particle Clusters and Sediment Entrapment in Coarse Alluvial Channels." en. In: *Sedimentology* 30.1 (Feb. 1983), pp. 137–143. ISSN: 1365-3091. DOI: 10.1111/j.1365-3091.1983.tb00656.x.
- [38] J. S. Bridge. "A Revised Model for Water Flow, Sediment Transport, Bed Topography and Grain Size Sorting in Natural River Bends." In: *Water Resources Research* 28.4 (1992), pp. 999–1013. ISSN: 1944-7973. DOI: 10.1029/91WR03088.

- [39] J. M. Buffington and D. Tonina. "Hyporheic Exchange in Mountain Rivers II: Effects of Channel Morphology on Mechanics, Scales, and Rates of Exchange." en. In: *Geography Compass* 3.3 (May 2009), pp. 1038–1062. ISSN: 17498198, 17498198. DOI: 10.1111/j.1749-8198.2009.00225.x.
- [40] G. Buss, Z Cai, B Cardenas, J Fleckenstein, D Hannah, K Heppell, P Hulme, T Ibrahim, D Kaeser, S Krause, D Lawler, D Lerner, J Mant, I Malcolm, G Old, G Parkin, R Pickup, G Pinay, J Porter, G Rhodes, A Richie, J Riley, A Robertson, D Sear, B Shields, J Smith, J Tellam, and P Wood. *The Hyporheic Handbook*. English. OCLC: 465371854. Bristol: Environment Agency, 2009. ISBN: 978-1-84911-131-7.
- [41] T. C. Byrd, D. J. Furbish, and J. Warburton. "ESTIMATING DEPTH-AVERAGED VELOCITIES IN ROUGH CHANNELS." In: *Earth Surf. Process. Landforms* 25 (2000), pp. 167–173.
- [42] L. Campbell, I. McEwan, V. Nikora, D. Pokrajac, M. Gallagher, and C. Manes. "Bed-Load Effects on Hydrodynamics of Rough-Bed Open-Channel Flows." In: *Journal of Hydraulic Engineering* 131.7 (2005), pp. 576–585.
- [43] F. Canovaro, E. Paris, and L. Solari. "Effects of Macro-Scale Bed Roughness Geometry on Flow Resistance." en. In: *Water Resources Research* 43.10 (Oct. 2007), W10414. ISSN: 1944-7973. DOI: 10.1029/2006WR005727.
- [44] F. Canovaro, E. Paris, and L. Solari. "Influence of Macro-Roughness Arrangement on Flow Resistance." In: *River Flow, Napples* (2004), pp. 287–293.
- [45] F. Canovaro and L. Solari. "Dissipative Analogies between a Schematic Macro-Roughness Arrangement and Step-Pool Morphology." en. In: *Earth Surface Processes and Landforms* 32.11 (Oct. 2007), pp. 1628–1640. ISSN: 1096-9837. DOI: 10.1002/esp.1590.
- [46] Z. Cao, G. Pender, and J. Meng. "Explicit Formulation of the Shields Diagram for Incipient Motion of Sediment." In: *Journal of Hydraulic Engineering* 132.10 (2006), pp. 1097–1099.
- [47] M. B. Cardenas. "A Model for Lateral Hyporheic Flow Based on Valley Slope and Channel Sinuosity: TECHNICAL NOTE." en. In: *Water Resources Research* 45.1 (Jan. 2009). ISSN: 00431397. DOI: 10.1029/2008WR007442.
- [48] F. G. Carollo, Ferro Vito, and Termini Donatella. "Analyzing Turbulence Intensity in Gravel Bed Channels." In: *Journal of Hydraulic Engineering* 131.12 (Dec. 2005), pp. 1050–1061. DOI: 10.1061/(ASCE)0733-9429(2005)131:12(1050).
- [49] M. A. Carson and M. J. Kirkby. *Hillslope Form and Process*. en. Cambridge University Press, June 1972. ISBN: 978-0-521-08234-1.
- [50] M. J. Cartigny, D. Ventra, G. Postma, and J. H. Den Berg. "Morphodynamics and Sedimentary Structures of Bedforms under Supercritical-Flow Conditions: New Insights from Flume Experiments." In: *Sedimentology* 61.3 (2013), pp. 712–748. ISSN: 0037-0746. DOI: 10.1111/sed.12076.

- [51] N. Chahinian, M.-G. Tournoud, J.-L. Perrin, and B. Picot. "Flow and Nutrient Transport in Intermittent Rivers: A Modelling Case-Study on the Vène River Using SWAT 2005." In: *Hydrological Sciences Journal* 56.2 (Mar. 2011), pp. 268–287. ISSN: 0262-6667. DOI: 10.1080/02626667.2011.559328.
- [52] T. P. Chapin, A. S. Todd, and M. P. Zeigler. "Robust, Low-Cost Data Loggers for Stream Temperature, Flow Intermittency, and Relative Conductivity Monitoring." en. In: *Water Resources Research* 50.8 (Aug. 2014), pp. 6542–6548. ISSN: 1944-7973. DOI: 10.1002/2013WR015158.
- [53] S. M. Chartrand, M. Jellinek, P. J. Whiting, and J. Stamm. "Geometric Scaling of Step-Pools in Mountain Streams: Observations and Implications." In: *Geomorphology* 129.1 (June 2011), pp. 141–151. ISSN: 0169-555X. DOI: 10.1016/j.geomorph.2011.01.020.
- [54] S. M. Chartrand and P. J. Whiting. "Alluvial Architecture in Headwater Streams with Special Emphasis on Step-Pool Topography." In: *Earth Surface Processes and Landforms* 25.6 (June 2000), pp. 583–600. ISSN: 1096-9837. DOI: 10.1002/1096-9837(200006)25:6<583::AID-ESP92>3.0.CO;2-3.
- [55] M. Chiari and D. Rickenmann. "Back-Calculation of Bedload Transport in Steep Channels with a Numerical Model." In: *Earth Surface Processes and Landforms* 36.6 (2010), pp. 805–815. ISSN: 1096-9837. DOI: 10.1002/esp.2108.
- [56] M. Chiari and D. Rickenmann. "Back-Calculation of Bedload Transport in Steep Channels with a Numerical Model." en. In: *Earth Surface Processes and Landforms* 36.6 (May 2011), pp. 805–815. ISSN: 1096-9837. DOI: 10.1002/esp.2108.
- [57] Y.-M. Chiew and G. Parker. "Incipient Sediment Motion on Non-Horizontal Slopes." en. In: *Journal of Hydraulic Research* 32.5 (Sept. 1994), pp. 649–660. ISSN: 0022-1686, 1814-2079. DOI: 10.1080/00221689409498706.
- [58] A. Chin. "The Morphologic Structure of Step-Pools in Mountain Streams." In: *Geomorphology* 27.3 (Mar. 1, 1999), pp. 191–204. ISSN: 0169-555X. DOI: 10.1016/S0169-555X(98)00083-X.
- [59] A. Chin and J. D. Phillips. "The Self-Organization of Step-Pools in Mountain Streams." In: *Geomorphology. Mountain Rivers II: Channel Processes* 83.3 (Jan. 2007), pp. 346–358. ISSN: 0169-555X. DOI: 10.1016/j.geomorph.2006.02.021.
- [60] N. L. Coleman and C. V. Alonso. "Two-Dimensional Channel Flows over Rough Surfaces." In: *Journal of Hydraulic Engineering*, 109(2): (1983), pp. 175–188.
- [61] F. Comiti, L. Mao, A. Wilcox, E. E. Wohl, and M. A. Lenzi. "Field-Derived Relationships for Flow Velocity and Resistance in High-Gradient Streams." In: *Journal of Hydrology* 340 (2007), pp. 48–62. DOI: 10.1016/j.jhydro1.2007.03.021.
- [62] F. Comiti, A. Andreoli, and M. A. Lenzi. "Morphological Effects of Local Scouring in Step-Pool Streams." In: *Earth Surface Processes and Landforms* 30.12 (2005), pp. 1567–1581. ISSN: 1096-9837. DOI: 10.1002/esp.1217.

- [63] J. Constantz, D. Stonestorm, A. E. Stewart, R. Niswonger, and T. R. Smith. "Analysis of Streambed Temperatures in Ephemeral Channels to Determine Streamflow Frequency and Duration." en. In: *Water Resources Research* 37.2 (Feb. 2001), pp. 317–328. ISSN: 1944-7973. DOI: 10.1029/2000WR900271.
- [64] R. U. Cooke, A. Warren, and A. S. Goudie. *Desert Geomorphology*. en. CRC Press, 1993. ISBN: 978-0-203-02059-3.
- [65] J. R. Cooper, J. Aberle, K. Koll, and S. J. Tait. "Influence of Relative Submergence on Spatial Variance and Form-Induced Stress of Gravel-Bed Flows." en. In: *Water Resources Research* 49.9 (Sept. 2013), pp. 5765–5777. ISSN: 1944-7973. DOI: 10.1002/wrcr.20464.
- [66] J. F. Costelloe, R. B. Grayson, and T. A. McMahon. "Modelling Stream Flow for Use in Ecological Studies in a Large, Arid Zone River, Central Australia." en. In: *Hydrological Processes* 19.6 (Apr. 2005), pp. 1165–1183. ISSN: 1099-1085. DOI: 10.1002/hyp.5558.
- [67] K. H Costigan, M. D Daniels, and W. K Dodds. "Fundamental Spatial and Temporal Disconnections in the Hydrology of an Intermittent Prairie Headwater Network." In: *Journal of Hydrology* 522 (2015), pp. 305–316.
- [68] K. H Costigan, K. L Jaeger, C. W Goss, K. M Fritz, and P. C Goebel. "Understanding Controls on Flow Permanence in Intermittent Rivers to Aid Ecological Research: Integrating Meteorology, Geology and Land Cover." In: *Ecohydrol.* 9, (2016), pp. 1141–1153. DOI: 10.1002/eco.1712.
- [69] K. H Costigan, M. J Kennard, C Leigh, E. Sauquet, T. Datry, and A. J. Boulton. "Flow Regimes In Intermittent Rivers And Ephemeral Streams." In: *Intermittent Rivers and Ephemeral Streams Ecology and Management*. 1st Edition. Elsevier, 2017.
- [70] Y. Cui, C. Paola, and G. Parker. "Numerical Simulation of Aggradation and Downstream Fining." In: *Journal of Hydraulic Research* 34.2 (Mar. 1996), pp. 185–204. ISSN: 0022-1686. DOI: 10.1080/00221689609498496.
- [71] J. H. Curran and E. E. Wohl. "Large Woody Debris and Flow Resistance in Step-Pool Channels, Cascade Range, Washington." In: *Geomorphology. Interactions between Wood and Channel Forms and Processes* 51.1 (Mar. 20, 2003), pp. 141–157. ISSN: 0169-555X. DOI: 10.1016/S0169-555X(02)00333-1.
- [72] A. Dai, T. Qian, K. E. Trenberth, and J. D. Milliman. "Changes in Continental Freshwater Discharge from 1948 to 2004." en. In: *Journal of Climate* 22.10 (May 2009), pp. 2773–2792. ISSN: 0894-8755, 1520-0442. DOI: 10.1175/2008JCLI2592.1.
- [73] A. Dai, K. E. Trenberth, and T. Qian. "A Global Dataset of Palmer Drought Severity Index for 1870–2002: Relationship with Soil Moisture and Effects of Surface Warming." In: *Journal of Hydrometeorology* 5.6 (Dec. 2004), pp. 1117–1130. ISSN: 1525-755X. DOI: 10.1175/JHM-386.1.

- [74] T. Datry. "Benthic and Hyporheic Invertebrate Assemblages along a Flow Intermittence Gradient: Effects of Duration of Dry Events." en. In: *Freshwater Biology* 57.3 (Mar. 2012), pp. 563–574. ISSN: 1365-2427. DOI: 10.1111/j.1365-2427.2011.02725.x.
- [75] T. Datry, N. Bonada, and A. J. Boulton. "General Introduction." en. In: *Intermittent Rivers and Ephemeral Streams Ecology and Management*. 1st Edition. Academic Press, 2017. ISBN: 978-0-12-803904-5.
- [76] T. Datry, R Corti, A Foulquier, D Von Schiller, and K. Tockner. "One for All, All for One: A Global River Research Network." In: *EOS Earth & Space Science News, American Geophysical Union*, 97 (15) (2016), pp. 13–15. DOI: 10.1029/2016E0053587.
- [77] T. Datry, S. T Larned, and K. Tockner. "Intermittent Rivers: A Challenge for Freshwater Ecology." In: *BioScience Vol. 64(3)*, (2014), pp. 229–235. DOI: 10.1093/biosci/bit027.
- [78] G. C. L. David. "Characterizing Flow Resistance in High Gradient Mountain Streams, Fraser Experimental Forest, Colorado." Thesis. Colorado State University Libraries, 2011.
- [79] J. A. Day. "Environmental Correlates of Aquatic Faunal Distribution in the Namib Desert." In: *Namib ecology* 25 (1990), pp. 99–107.
- [80] T. Demir. "Downstream Changes in Bed Material Size and Shape Characteristics in a Small Upland Stream: Cwm Treweryn, in South Wales." In: *Yerbilimleri Dergisi* 5.28 (2003), pp. 33–47.
- [81] M. Detert and V. Weitbrecht. "User Guide to Gravelometric Image Analysis by BASEGRAIN." In: (Jan. 2013).
- [82] S. Dey, S. Sarkar, and L. Solari. "Near-Bed Turbulence Characteristics at the Entrainment Threshold of Sediment Beds." In: *Journal of Hydraulic Engineering* 137.9 (Sept. 2011), pp. 945–958. DOI: 10.1061/(ASCE)HY.1943-7900.0000396.
- [83] R. Di Felice. "Liquid Fluidisation of Binary-Solid Mixtures." PhD thesis. University College London (University of London), 1988.
- [84] S. Dinar, D. Katz, L. De Stefano, and B. Blankespoor. "Climate Change, Conflict, and Cooperation: Global Analysis of the Effectiveness of International River Treaties in Addressing Water Variability." In: *Political Geography* 45 (Mar. 2015), pp. 55–66. ISSN: 0962-6298. DOI: 10.1016/j.polgeo.2014.08.003.
- [85] P. Diplas, J. Almedeij, and C. L. Dancey. "Do Perennial and Ephemeral Streams Represent Parts of the Same Continuum?" In: (2006).
- [86] A. Dittrich and K. Koll. "Velocity Field and Resistance of Flow over Rough Surfaces with Large and Small Relative Submergence." In: *International Journal of Sediment Research* 12.3 (1997), pp. 21–33.

- [87] P. Döll and H. M. Schmied. "How Is the Impact of Climate Change on River Flow Regimes Related to the Impact on Mean Annual Runoff? A Global-Scale Analysis." In: *Environmental Research Letters* 7.1 (Mar. 2012), p. 014037. ISSN: 1748-9326. DOI: 10.1088/1748-9326/7/1/014037.
- [88] B. C. Eaton, R. G. Millar, and S. Davidson. "Channel Patterns: Braided, Anabranching, and Single-Thread." In: *Geomorphology* 120.3 (Aug. 2010), pp. 353–364. ISSN: 0169-555X. DOI: 10.1016/j.geomorph.2010.04.010.
- [89] H. A. Einstein. *The Bed-Load Function for Sediment Transportation in Open Channel Flows*. Vol. 1026. US Department of Agriculture Washington DC, 1950.
- [90] F. Engelund. "FLOW AND BED TOPOGRAPHY IN CHANNEL BENDS." In: *Journal of the Hydraulics Division* 100.Proc. Paper 10963 (Nov. 1974).
- [91] F. Engelund and E. Hansen. "A Monograph on Sediment Transport in Alluvial Streams." In: *Technical University of Denmark Osteroldgade 10, Copenhagen K.* (1967).
- [92] FAO-Aquastat. *AQUASTAT Database. Food and Agriculture Organization of the United Nations (FAO)*. http://www.fao.org/nr/water/aquastat/About_us/index.stm. 2016.
- [93] H. D. Farias, M. T. Pilan, M. T. Mattar, and F. J. Pece. "Regime Width of Alluvial Channels: Conciliation of Several Approaches." In: *Proceedings of the ICHE Conference, Cottbus, Germany*. 1998.
- [94] R. Ferguson. "Flow Resistance Equations for Gravel- and Boulder-Bed Streams." In: *Water Resources Research*, Vol. 43, W05427 (2007). DOI: 10.1029/2006WR005422.
- [95] V. Ferro. "Friction Factor for Gravel-Bed Channel with High Boulder Concentration." In: *Journal of Hydraulic Engineering* 125.7 (July 1, 1999), pp. 771–778. DOI: 10.1061/(ASCE)0733-9429(1999)125:7(771).
- [96] S. G. Fisher, L. J. Gray, N. B. Grimm, and D. E. Busch. "Temporal Succession in a Desert Stream Ecosystem Following Flash Flooding." en. In: *Ecological Monographs* 52.1 (Feb. 1982), pp. 93–110. ISSN: 1557-7015. DOI: 10.2307/2937346.
- [97] K. M. Fritz, E. Hagenbuch, E. D'Amico, M. Reif, P. J. Wigington, S. G. Leibowitz, R. L. Comeleo, J. L. Ebersole, and T.-L. Nadeau. "Comparing the Extent and Permanence of Headwater Streams From Two Field Surveys to Values From Hydrographic Databases and Maps." en. In: *JAWRA Journal of the American Water Resources Association* 49.4 (Aug. 2013), pp. 867–882. ISSN: 1752-1688. DOI: 10.1111/jawr.12040.
- [98] L. E. Frostick and I. Reid. "Sorting Mechanisms in Coarse-Grained Alluvial Sediments: Fresh Evidence from a Basalt Plateau Gravel, Kenya." en. In: *Journal of the Geological Society* 137.4 (July 1980), pp. 431–441. ISSN: 0016-7649, 2041-479X. DOI: 10.1144/gsjgs.137.4.0431.

- [99] F. Gallart, N. Cid, J. Latron, P. Llorens, N. Bonada, J. Jeuffroy, S.-M. Jiménez-Argudo, R.-M. Vega, C. Solà, M. Soria, M. Bardina, A.-J. Hernández-Casahuga, A. Fidalgo, T. Estrela, A. Munné, and N. Prat. "TREHS: An Open-Access Software Tool for Investigating and Evaluating Temporary River Regimes as a First Step for Their Ecological Status Assessment." en. In: *Science of The Total Environment* 607-608 (Dec. 2017), pp. 519–540. ISSN: 00489697. DOI: 10.1016/j.scitotenv.2017.06.209.
- [100] P. W. Gassman, M. R. Reyes, C. H. Green, and J. G. Arnold. "The Soil and Water Assessment Tool: Historical Development, Applications, and Future Research Directions." en. In: *Transactions of the ASABE* 50.4 (2007), pp. 1211–1250. ISSN: 2151-0040. DOI: 10.13031/2013.23637.
- [101] A. C. Gellis, M. J. Pavich, P. R. Bierman, E. M. Clapp, A. Ellevein, and S. Aby. "Modern Sediment Yield Compared to Geologic Rates of Sediment Production in a Semi-Arid Basin, New Mexico: Assessing the Human Impact." en. In: *Earth Surface Processes and Landforms* 29.11 (Oct. 2004), pp. 1359–1372. ISSN: 1096-9837. DOI: 10.1002/esp.1098.
- [102] J. Gessler. "Friction Factor of Armored River Beds." In: *Journal of Hydraulic Engineering* 116.4 (1990), pp. 531–542.
- [103] T Ghilardi. "Sediment Transport and Flow Conditions in Steep Rivers with Large Immobile Boulders." PhD thesis. ÉCOLE POLYTECHNIQUE FÉDÉRALE DE LAUSANNE, 2014.
- [104] T Ghilardi, M. J Franca, and A. J Schleiss. "Sediment Transport in Steep Channels with Large Roughness Elements." In: *Proceedings of River Flow 2014. No. EPFL-CONF-202023. CRC Press/Balkema*. 2014, pp. 899–907.
- [105] T. Ghilardi and A. J. Schleiss. "Steep Flume Experiments with Large Immobile Boulders and Wide Grain Size Distribution as Encountered in Alpine Torrents." In: (2012).
- [106] L. A. Giménez-Curto and M. A. C. Lera. "Oscillating Turbulent Flow over Very Rough Surfaces." en. In: *Journal of Geophysical Research: Oceans* 101.C9 (Sept. 1996), pp. 20745–20758. ISSN: 2156-2202. DOI: 10.1029/96JC01824.
- [107] P. H Gleick. "Global Freshwater Resources: Soft-Path Solutions for the 21st Century." In: *Science* 302 (2003), pp. 1524–1528.
- [108] S. E. Godsey and J. W. Kirchner. "Dynamic, Discontinuous Stream Networks: Hydrologically Driven Variations in Active Drainage Density, Flowing Channels and Stream Order." en. In: *Hydrological Processes* 28.23 (Nov. 2014), pp. 5791–5803. ISSN: 1099-1085. DOI: 10.1002/hyp.10310.
- [109] N. D. Gordon. *Stream Hydrology: An Introduction for Ecologists*. en. John Wiley and Sons, June 2004. ISBN: 978-0-470-84357-4.
- [110] D Gore, G Brierley, J Pickard, and J Jansen. "Anatomy of a Floodout in Semi-Arid Eastern Australia." In: *Geomorphologie Supplementary Issues* 122 (2000), pp. 113–139.

- [111] W. H. Graf. "Flow Resistance Over A Gravel Bed: Its Consequence On Initial Sediment Movement." In: *Fluvial Hydraulics of Mountain Regions, Lect. Notes Earth Sci., Vol. 37, Edited by A. Armanini, and G. Di Silvio*. Springer, Berlin, Heidelberg, 1991, pp. 17–32.
- [112] W. L. Graf. "Channel Instability in a Braided, Sand Bed River." en. In: *Water Resources Research* 17.4 (Aug. 1981), pp. 1087–1094. ISSN: 1944-7973. DOI: 10.1029/WR017i004p01087.
- [113] W. L. Graf. *Fluvial Processes in Dryland Rivers*. Ed. by D. Barsch, I. Douglas, F. Joly, M. Marcus, and B. Messerli. Vol. 3. Springer Series in Physical Environment. Berlin, Heidelberg: Springer Berlin Heidelberg, 1988. ISBN: 978-3-642-83050-1 978-3-642-83048-8. DOI: 10.1007/978-3-642-83048-8.
- [114] G. E. Grant, F. J. Swanson, and M. G. Wolman. "Pattern and Origin of Stepped-Bed Morphology in High-Gradient Streams, Western Cascades, Oregon." In: *Geol. Soc. Am. Bull., Vol. 102* (1990), pp. 340–352.
- [115] A. J. Grass. "Structural Features of Turbulent Flow over Smooth and Rough Boundaries." en. In: *Journal of Fluid Mechanics* 50.2 (Nov. 1971), pp. 233–255. ISSN: 1469-7645, 0022-1120. DOI: 10.1017/S0022112071002556.
- [116] T. Grischek and R. Bartak. "Riverbed Clogging and Sustainability of Riverbank Filtration." en. In: *Water* 8.12 (Dec. 2016), p. 604. DOI: 10.3390/w8120604.
- [117] B. Gungle. *Timing and Duration of Flow in Ephemeral Streams of the Sierra Vista Subwatershed of the Upper San Pedro Basin, Cochise County, Southeastern Arizona*. USGS Numbered Series 2005-5190. 2007, p. 50.
- [118] A. Günter. "Die Kritische Mittlere Sohlenschubspannung Bei Geschiebe-Mischungen Unter Berücksichtigung Der Deckschichtbildung Und Der Turbulenzbedingten Sohlenschubspannungsschwankungen." PhD thesis. Zürich: EIDGENÖSSISCHEN TECHNISCHEN HOCHSCHULE ZÜRICH, 1971.
- [119] T. Hafner. "Uferrückbau und eigendynamische Gewässerentwicklung: Aspekte der Modellierung und Abschätzungsmöglichkeiten in der Praxis." Zugl.: München, Techn. Univ., Diss., 2008. PhD thesis. 2008.
- [120] W. F. Hansen. "Identifying Stream Types and Management Implications." In: *Forest Ecology and Management*. Special Issue: THE SCIENCE OF MANAGING FORESTS TO SUSTAIN 143.1 (Apr. 2001), pp. 39–46. ISSN: 0378-1127. DOI: 10.1016/S0378-1127(00)00503-X.
- [121] M. Hartwig and D. Borchardt. "Alteration of Key Hyporheic Functions through Biological and Physical Clogging along a Nutrient and Fine-Sediment Gradient." en. In: *Ecohydrology* 8.5 (July 2015), pp. 961–975. ISSN: 1936-0592. DOI: 10.1002/eco.1571.

- [122] M. A. Hassan. "Characteristics of Gravel Bars in Ephemeral Streams." In: *Journal of Sedimentary Research* 75.1 (2005), pp. 29–42. ISSN: 1527-1404. DOI: Wilcock, P. R., and Kenworthy, S. T., 2002, A two-fraction model for the transport of sand / gravel mixtures: *Water Resources Research*, v. 38, 10.1029/2001WR000684..
- [123] M. A. Hassan, R. Egozi, and G. Parker. "Experiments on the effect of hydrograph characteristics on vertical grain sorting in gravel bed rivers." English (US). In: *Water Resources Research* 42.9 (Sept. 2006). ISSN: 0043-1397. DOI: 10.1029/2005WR004707.
- [124] M. A. Hassan and I. Reid. "The Influence of Microform Bed Roughness Elements on Flow and Sediment Transport in Gravel Bed Rivers." en. In: *Earth Surface Processes and Landforms* 15.8 (Dec. 1990), pp. 739–750. ISSN: 1096-9837. DOI: 10.1002/esp.3290150807.
- [125] T. Hayashi. "Alluvial bedforms of small scale and roughness." Japanese. In: *Doboku Gakkai Ronbunshu* 1989.411 (1989), pp. 1–12.
- [126] J Hazelton, S Roylance, W Brown, T Lancaster, H Shovic, T Mack, K Vining, and A Vecchia. *Southeast Afghanistan Water Resources Assessment*. 2009.
- [127] R. D. Hey. "Flow Resistance in Gravel-Bed Rivers." eng. In: *Journal of the Hydraulics Division* 105.4 (1979), pp. 365–379.
- [128] J. L. Higson and M. B. Singer. "The Impact of the Streamflow Hydrograph on Sediment Supply from Terrace Erosion." In: *Geomorphology* 248.Supplement C (Nov. 2015), pp. 475–488. ISSN: 0169-555X. DOI: 10.1016/j.geomorph.2015.07.037.
- [129] K. M. Hill and D. Tan. "Granular Flows Applied to Gravel-Bed Rivers." en. In: *Gravel-Bed Rivers*. Ed. by D. Tsutsumi and J. B. Laronne. John Wiley & Sons, Ltd, 2017, pp. 73–95. ISBN: 978-1-118-97143-7. DOI: 10.1002/9781118971437.ch3.
- [130] J. O. Hinze. *Turbulence*. en. McGraw-Hill, 1975. ISBN: 978-0-07-029037-2.
- [131] M. Hirano. "RIVER-BED DEGRADATION WITH ARMORING." en. In: *Proceedings of the Japan Society of Civil Engineers* 1971.195 (Nov. 1971), pp. 55–65. ISSN: 0385-5392, 1884-4936. DOI: 10.2208/jscej1969.1971.195_55.
- [132] J. Hooke. "Coarse Sediment Connectivity in River Channel Systems: A Conceptual Framework and Methodology." In: *Geomorphology* 56.1 (Nov. 2003), pp. 79–94. ISSN: 0169-555X. DOI: 10.1016/S0169-555X(03)00047-3.
- [133] H. Q. Huang, C. Deng, G. C. Nanson, B. Fan, X. Liu, T. Liu, and Y. Ma. "A Test of Equilibrium Theory and a Demonstration of Its Practical Application for Predicting the Morphodynamics of the Yangtze River." In: *Earth Surface Processes and Landforms* 39.5 (2014), pp. 669–675. ISSN: 1096-9837. DOI: 10.1002/esp.3522.
- [134] R. P. Hunziker. "Fraktionsweiser Geschiebetransport." PhD Thesis. ETH Zurich, 1995.
- [135] S. Ikeda. "Prediction of Alternate Bar Wavelength and Height." In: *Journal of Hydraulic Engineering* 110.4 (Apr. 1984), pp. 371–386. ISSN: 0733-9429, 1943-7900. DOI: 10.1061/(ASCE)0733-9429(1984)110:4(371).

- [136] C. C. Inglis. *Behaviour and Control of Rivers and Canals (with the Aid of Models), Part I*. 1949.
- [137] IPCC. *Introduction*. In: *Climate Change 2013: The Physical Science Basis. Contribution of Working Group I to the Fifth Assessment Report of the Intergovernmental Panel on Climate Change* [Stocker, T.F., D. Qin, G.-K. Plattner, M. Tignor, S.K. Allen, J. Boschung, A. Nauels, Y. Xia, V. Bex and P.M. Midgley (Eds.)] Cambridge University Press, 2013 b.
- [138] IPCC. *Observations: Atmosphere and Surface*. In: *Climate Change 2013: The Physical Science Basis. Contribution of Working Group I to the Fifth Assessment Report of the Intergovernmental Panel on Climate Change* [Stocker, T.F., D. Qin, G.-K. Plattner, M. Tignor, S.K. Allen, J. Boschung, A. Nauels, Y. Xia, V. Bex and P.M. Midgley (Eds.)]. Cambridge University Press, 2013 a.
- [139] IPCC. *Observations: Cryosphere*. In: *Climate Change 2013: The Physical Science Basis. Contribution of Working Group I to the Fifth Assessment Report of the Intergovernmental Panel on Climate Change* [Stocker, T.F., D. Qin, G.-K. Plattner, M. Tignor, S.K. Allen, J. Boschung, A. Nauels, Y. Xia, V. Bex and P.M. Midgley (Eds.)]. Cambridge University Press, 2013.
- [140] K. M. Ivkovic, B. F. W. Croke, and R. A. Kelly. "Overcoming the Challenges of Using a Rainfall–Runoff Model to Estimate the Impacts of Groundwater Extraction on Low Flows in an Ephemeral Stream." en. In: *Hydrology Research* 45.1 (Feb. 2014), pp. 58–72. ISSN: 0029-1277, 2224-7955. DOI: 10.2166/nh.2013.204.
- [141] P. J. Jacobson, K. M. Jacobson, P. L. Angermeier, and D. S. Cherry. "Variation in Material Transport and Water Chemistry along a Large Ephemeral River in the Namib Desert." en. In: *Freshwater Biology* 44.3 (July 2000), pp. 481–491. ISSN: 1365-2427. DOI: 10.1046/j.1365-2427.2000.00604.x.
- [142] K. L. Jaeger and J. D. Olden. "Electrical Resistance Sensor Arrays as a Means to Quantify Longitudinal Connectivity of Rivers." en. In: *River Research and Applications* 28.10 (Dec. 2012), pp. 1843–1852. ISSN: 1535-1467. DOI: 10.1002/rra.1554.
- [143] K. L. Jaeger, N. A. Sutfin, S. Tooth, K. Michaelides, and M. Singer. "Geomorphology and Sediment Regimes of Intermittent Rivers and Ephemeral Streams." In: *Intermittent Rivers and Ephemeral Streams Ecology and Management*. 1st Edition. Elsevier, 2017.
- [144] K. L. Jaeger, J. D. Olden, and N. A. Pelland. "Climate Change Poised to Threaten Hydrologic Connectivity and Endemic Fishes in Dryland Streams." en. In: *Proceedings of the National Academy of Sciences* 111.38 (Sept. 2014), pp. 13894–13899. ISSN: 0027-8424, 1091-6490. DOI: 10.1073/pnas.1320890111.
- [145] R. D. Jarret. "Hydrologic and Hydraulic Research in Mountain Rivers." In: *Water Res. Bull. WARBAQ*, 26 (3). 1990, pp. 419–429.

- [146] I. Joshi, W. Dai, A. Bilal, A. R. Upreti, and Z. He. "Evaluation and Comparison of Extremal Hypothesis-Based Regime Methods." In: *Water* 10.3 (3 Mar. 2018), p. 271. DOI: 10.3390/w10030271.
- [147] G. Katul, P. Wiberg, J. Albertson, and G. Hornberger. "A Mixing Layer Theory for Flow Resistance in Shallow Streams: MIXING LAYER THEORY FOR FLOW RESISTANCE." en. In: *Water Resources Research* 38.11 (Nov. 2002), pp. 32–1–32–8. ISSN: 00431397. DOI: 10.1029/2001WR000817.
- [148] G. H. Keulegan. "LAWS OF TURBULENT FLOW IN OPEN CHANNELS." In: *Journal of Research, National Bureau of Standards, Vol. 121* (1938), pp. 707–741.
- [149] M King and B Sturtewagen. *Making the Most of Afghanistan's River Basins: Opportunities for Regional Cooperation*. 2010.
- [150] M. S. Kirkgöz. "Turbulent Velocity Profiles for Smooth and Rough Open Channel Flow." In: *Journal of Hydraulic Engineering* 115 (1989), pp. 1543–1561.
- [151] B. Kironoto and W. Graf. *Turbulence Characteristics in Rough Uniform Open-Channel Flow*. Vol. 112. Dec. 1994. DOI: 10.1680/iwtme.1995.28114.
- [152] A. Klaphake and W. Scheumann. *Politische Antworten Auf Die Globale Wasserkrise: Trends Und Konflikte*. Bundeszentrale für politische Bildung, 2001.
- [153] R. Klar. *Langzeitsimulation des Geschiebetransports in alpinen Tälern: Weiterentwicklung von Methoden zur Modellierung der langfristigen Sohllagenentwicklung und zur Ermittlung von Hochwassergefahren in inneralpinen Tälern*. ger. 1. Auflage. Forum Umwelttechnik und Wasserbau Band 24. Innsbruck: Innsbruck University Press, 2016. ISBN: 978-3-903122-66-6.
- [154] A. D Knight and G. C. Nanson. "Distinctiveness, Diversity and Uniqueness in Arid Zone River Systems." en. In: *Arid Zone Geomorphology: Process, Form and Change in Drylands*. Ed. by D. S. G. Thomas. Third Edition. Chichester, UK: John Wiley & Sons, Ltd, 1997, pp. 269–300. ISBN: 978-0-470-71077-7. DOI: 10.1002/9780470710777.ch12.
- [155] K Koll. "Feststofftransport Und Geschwindigkeitsverteilung in Raugerinnen." PhD thesis. Karlsruhe, Germany: Universität Fridericiana zu Karlsruhe (TH), 2002.
- [156] K Koll. "Parameterisation of the Vertical Velocity Profile in the Wall Region over Rough Surfaces." en. In: *River Flow 2006, Two Volume Set: Proceedings of the International Conference on Fluvial Hydraulics, Lisbon, Portugal, 6-8 September 2006*. CRC Press, Sept. 2006, pp. 163–172. ISBN: 978-1-4398-3386-5.
- [157] U. C Kothyari and R. K. Jain. "Influence of Cohesion on the Incipient Motion Condition of Sediment Mixtures." In: *Water Resources Research, Vol. 44, W04410* (2008). DOI: 10.1029/2007WR006326.
- [158] R. A. Kuhnle. *Fractional Transport Rates of Bedload on Goodwin Creek, Dynamics of Gravel-Bed Rivers* P. Billi, RD Hey, CR Thorne, P. Tacconi, 141–155. John Wiley, New York, 1992.

- [159] G Lacey. "Stable Channels in Alluvium (Includes Appendices)." In: *Minutes of the Proceedings of the Institution of Civil Engineers* 229.1930 (Jan. 1930), pp. 259–292. DOI: 10.1680/imotp.1930.15592.
- [160] P. S. Lake. "Ecological Effects of Perturbation by Drought in Flowing Waters." en. In: *Freshwater Biology* 48.7 (July 2003), pp. 1161–1172. ISSN: 1365-2427. DOI: 10.1046/j.1365-2427.2003.01086.x.
- [161] S. Lake, N. Bond, and P. Reich. "Floods Down Rivers: From Damaging to Replenishing Forces." In: *Advances in Ecological Research*. Floods in an Arid Continent 39 (Jan. 2006), pp. 41–62. ISSN: 0065-2504. DOI: 10.1016/S0065-2504(06)39003-4.
- [162] M. P Lamb, W. E Dietrich, and J. G Venditti. "Is the Critical Shields Stress for Incipient Sediment Motion Dependent on Channel-Bed Slope?" In: *Journal of Geophysical Research*, Vol. 113, f02008 (2008). DOI: 10.1029/2007JF000831.
- [163] M. P. Lamb, F. Brun, and B. M. Fuller. "Hydrodynamics of Steep Streams with Planar Coarse-Grained Beds: Turbulence, Flow Resistance, and Implications for Sediment Transport: HYDRODYNAMICS OF STEEP STREAMS." en. In: *Water Resources Research* 53.3 (Mar. 2017), pp. 2240–2263. ISSN: 00431397. DOI: 10.1002/2016WR019579.
- [164] J. Lange. "Dynamics of Transmission Losses in a Large Arid Stream Channel." In: *Journal of Hydrology* 306 (2005), pp. 112–126. DOI: 10.1016/j.jhydrol.2004.09.016.
- [165] S. T Larned, T. Datry, D. B Arscott, and K. Tockner. "Emerging Concepts in Temporary-River Ecology." In: *Freshwater Biology* 55, (2010), pp. 717–738. DOI: 10.1111/j.1365-2427.2009.02322.x.
- [166] S. T. Larned, J. Schmidt, T. Datry, C. P. Konrad, J. K. Dumas, and J. C. Diettrich. "Longitudinal River Ecohydrology: Flow Variation down the Lengths of Alluvial Rivers." en. In: *Ecohydrology* 4.4 (July 2011), pp. 532–548. ISSN: 1936-0592. DOI: 10.1002/eco.126.
- [167] J. B. Laronne, J. Lekach, H. Cohen, and J. Gray. "Experimental Drainage Basins in Israel." In: *AGU Fall Meeting Abstracts* 51 (Dec. 2002).
- [168] J. B. Laronne, I. Reid, Y. Yitshak, and L. E. Frostick. *Recording Bedload Discharge in a Semiarid Channel, Nahal Yatir, Israel*. Vol. 210. International Association of Hydrological Sciences Publication, 1992.
- [169] J. B. Laronne, I. Reid, Y. Yitshak, and L. E. Frostick. "The Non-Layering of Gravel Streambeds under Ephemeral Flood Regimes." In: *Journal of Hydrology* 159.1-4 (1994), pp. 353–363.
- [170] J. B. Laronne and L. Reid. "Very High Rates of Bedload Sediment Transport by Ephemeral Desert Rivers." en. In: *Nature* 366.6451 (Nov. 1993), pp. 148–150. ISSN: 0028-0836. DOI: 10.1038/366148a0.

- [171] J. B. Laronne and Y. Shlomi. "Depositional Character and Preservation Potential of Coarse-Grained Sediments Deposited by Flood Events in Hyper-Arid Braided Channels in the Rift Valley, Arava, Israel." In: *Sedimentary Geology*. Drylands 195.1 (Feb. 2007), pp. 21–37. ISSN: 0037-0738. DOI: 10.1016/j.sedgeo.2006.07.008.
- [172] D. S. L. Lawrence. "Hydraulic Resistance in Overland Flow during Partial and Marginal Surface Inundation: Experimental Observations and Modeling." en. In: *Water Resources Research* 36.8 (Aug. 2000), pp. 2381–2393. ISSN: 1944-7973. DOI: 10.1029/2000WR900095.
- [173] D. S. L. Lawrence. "Macroscale Surface Roughness and Frictional Resistance in Overland Flow." en. In: *Earth Surface Processes and Landforms* 22.4 (Apr. 1997), pp. 365–382. ISSN: 1096-9837. DOI: 10.1002/(SICI)1096-9837(199704)22:4<365::AID-ESP693>3.0.CO;2-6.
- [174] A. J. Lee and R. I. Ferguson. "Velocity and Flow Resistance in Step-Pool Streams." In: *Geomorphology* 46.1 (July 2002), pp. 59–71. ISSN: 0169-555X. DOI: 10.1016/S0169-555X(02)00054-5.
- [175] M. Lenzi, L. Mao, and F. Comiti. "When Does Bedload Transport Begin in Steep Boulder-Bed Streams?" en. In: *Hydrological Processes* 20.16 (Oct. 2006), pp. 3517–3533. ISSN: 1099-1085. DOI: 10.1002/hyp.6168.
- [176] M. A. Lenzi. "Step-Pool Evolution in the Rio Cordon, Northeastern Italy." In: *Earth Surface Processes and Landforms* 26.9 (Aug. 1, 2001), pp. 991–1008. ISSN: 1096-9837. DOI: 10.1002/esp.239.
- [177] L. B. Leopold and W. W. Emmett. "Bedload Measurements, East Fork River, Wyoming." en. In: *Proceedings of the National Academy of Sciences* 73.4 (Apr. 1976), pp. 1000–1004. ISSN: 0027-8424, 1091-6490. DOI: 10.1073/pnas.73.4.1000.
- [178] L. B. Leopold and M. G. Wolman. *River Channel Patterns: Braided, Meandering and Straight*. 1957.
- [179] L. B. Leopold, W. W. Emmett, and R. M. Myrick. *Channel and Hillslope Processes in a Semiarid Area, New Mexico*. Vol. 352. US Government Printing Office, 1966.
- [180] L. B. Leopold and T. Maddock. *The Hydraulic Geometry of Stream Channels and Some Physiographic Implications*. Vol. 252. US Government Printing Office, 1953.
- [181] T. E. Lisle. "Sediment Transport and Resulting Deposition in Spawning Gravels, North Coastal California." en. In: *Water Resources Research* 25.6 (June 1989), pp. 1303–1319. ISSN: 1944-7973. DOI: 10.1029/WR025i006p01303.
- [182] W. C. Little and P. G. Mayer. "The Role of Sediment Gradation of Channel Armouring." In: *Publ. ERC-0672, Ga. Inst. of Technol., Atlanta* (1972), p. 104.
- [183] W. H. Lowe, K. H. Nislow, and G. E. Likens. "Forest Structure and Stream Salamander Diets: Implications for Terrestrial-Aquatic Connectivity." In: *Verhandlungen der Internationalen Vereinigung für Theoretische und Angewandte Limnologie* 29 (2005), pp. 279–286.

- [184] W. H. Lowe and G. E. Likens. "Moving Headwater Streams to the Head of the Class." In: *BioScience* 55.3 (2005), pp. 196–197. ISSN: 0006-3568. DOI: 10.1641/0006-3568(2005)055[0196:MHSTTH]2.0.CO;2.
- [185] J. A. Mabbutt. *Desert Landforms*. Canberra : Australian National University Press, 1977.
- [186] W. A. MacFarlane and E. Wohl. "Influence of Step Composition on Step Geometry and Flow Resistance in Step-Pool Streams of the Washington Cascades." In: *Water Resources Research* 39.2 (Feb. 1, 2003). ISSN: 1944-7973. DOI: 10.1029/2001WR001238.
- [187] C. Manes, D. Pokrajac, I. McEwan, and V. Nikora. "Turbulence Structure of Open Channel Flows over Permeable and Impermeable Beds: A Comparative Study." In: *Physics of Fluids* 21.12 (Dec. 2009), p. 125109. ISSN: 1070-6631. DOI: 10.1063/1.3276292.
- [188] L. Mao, G. P. Uyttendaele, A. Iroumé, and M. A. Lenzi. "Field Based Analysis of Sediment Entrainment in Two High Gradient Streams Located in Alpine and Andine Environments." In: *Geomorphology* 93.3 (Jan. 2008), pp. 368–383. ISSN: 0169-555X. DOI: 10.1016/j.geomorph.2007.03.008.
- [189] W. J. Matthews. "North American Prairie Streams as Systems for Ecological Study." In: *Journal of the North American Benthological Society* 7.4 (Dec. 1988), pp. 387–409. ISSN: 0887-3593. DOI: 10.2307/1467298.
- [190] O. T McDonough, J. D Hosen, and M. A Palmer. "Temporary Streams: The Hydrology, Geography and Ecology of Non Perennially Flowing Waters." In: *River Ecosystems: Dynamics, Management and Conservation*. Publisher: Nova Science Publishers, Inc., Editors: H.S. Elliot, L.E. Martin. 2011, pp. 259–289.
- [191] C. Mendoza-Lera and M. Mutz. "Microbial Activity and Sediment Disturbance Modulate the Vertical Water Flux in Sandy Sediments." In: *Freshwater Science* 32.1 (Mar. 2013), pp. 26–38. ISSN: 2161-9549. DOI: 10.1899/11-165.1.
- [192] F Métivier, P Meunier, M Moreira, A Crave, C Chaduteau, B Ye, and G Liu. "Transport Dynamics and Morphology of a High Mountain Stream during the Peak Flow Season: The Ürümqi River (Chinese Tian Shan)." In: *Second International Conference on Fluvial Hydraulics - RIVER FLOW*. 2004.
- [193] M. Mett. "Determination of Discharge Information for Arid Areas with Ephemeral Flow with the Help of Remote Sensing Techniques." PhD thesis. Innsbruck, Austria: Innsbruck, 2016.
- [194] A. Meyer and E. I. Meyer. "Discharge Regime and the Effect of Drying on Macroinvertebrate Communities in a Temporary Karst Stream in East Westphalia (Germany)." In: *Aquatic Sciences* 62.3 (Oct. 2000), pp. 216–231. ISSN: 1015-1621, 1420-9055. DOI: 10.1007/PL00001333.
- [195] J. L. Meyer and J. B. Wallace. "Lost Linkages and Lotic Ecology: Rediscovering Small Streams." In: *Ecology: Achievement and challenge* 295317 (2001).

- [196] E Meyer-Peter and R Müller. "Formulas for Bed-Load Transport." In: *Paper Presented at 2nd Meeting, Int. Assoc. for Hydroaul. Environ. Eng. and Res., Madrid*. 1948.
- [197] K. Michaelides and G. J. Martin. "Sediment Transport by Runoff on Debris-Mantled Dryland Hillslopes." en. In: *Journal of Geophysical Research: Earth Surface* 117.F3 (Sept. 2012), F03014. ISSN: 2156-2202. DOI: 10.1029/2012JF002415.
- [198] K. Michaelides and M. B. Singer. "Impact of Coarse Sediment Supply from Hillslopes to the Channel in Runoff-Dominated, Dryland Fluvial Systems." en. In: *Journal of Geophysical Research: Earth Surface* 119.6 (June 2014), 2013JF002959. ISSN: 2169-9011. DOI: 10.1002/2013JF002959.
- [199] R. T. Milhous. "Sediment Transport in a Gravel-Bottomed Stream." PhD Thesis. 1973.
- [200] Millennium Ecosystem Assessment. *Ecosystems and Human Well-Being: Current State & Trends Assessment*. 2005.
- [201] M. C. Miller, I. N. McCAYE, and P. D. Komar. "Threshold of Sediment Motion under Unidirectional Currents." en. In: *Sedimentology* 24.4 (Aug. 1977), pp. 507–527. ISSN: 1365-3091. DOI: 10.1111/j.1365-3091.1977.tb00136.x.
- [202] R. L. Miller and R. J. Byrne. "The Angle of Repose for a Single Grain on a Fixed Rough Bed." en. In: *Sedimentology* 6.4 (July 1966), pp. 303–314. ISSN: 1365-3091. DOI: 10.1111/j.1365-3091.1966.tb01897.x.
- [203] P. C. D. Milly, J. Betancourt, M. Falkenmark, R. M. Hirsch, Z. W. Kundzewicz, D. P. Lettenmaier, and R. J. Stouffer. "Stationarity Is Dead: Whither Water Management?" en. In: *Science* 319.5863 (Feb. 2008), pp. 573–574. ISSN: 0036-8075, 1095-9203. DOI: 10.1126/science.1151915.
- [204] T. Mizuyama. "Bedload Transport in Steep Channels." PhD thesis. Kyoto, Japan: Kyoto, 1977.
- [205] S. H. Mohajeri, S. Grizzi, M. Righetti, G. P. Romano, and V. Nikora. "The Structure of Gravel-Bed Flow with Intermediate Submergence: A Laboratory Study." en. In: *Water Resources Research* 51.11 (Nov. 2015), pp. 9232–9255. ISSN: 1944-7973. DOI: 10.1002/2015WR017272.
- [206] E. Morin, T. Grodek, O. Dahan, G. Benito, C. Kulls, Y. Jacoby, G. V. Langenhove, M. Seely, and Y. Enzel. "Flood Routing and Alluvial Aquifer Recharge along the Ephemeral Arid Kuiseb River, Namibia." In: *Journal of Hydrology* 368.1 (Apr. 2009), pp. 262–275. ISSN: 0022-1694. DOI: 10.1016/j.jhydrol.2009.02.015.
- [207] H. M. Morris. "Flow in Rough Conduits. ASCE Transactions, Vol. 120, Paper No. 2745." In: *ASME*. Vol. 120. 1955, pp. 373–410.
- [208] E. R. Mueller, J. Pitlick, and Nelson. "Variation in the Reference Shields Stress for Bed Load Transport in Gravel-Bed Streams and Rivers." In: *Water Resources Research*, Vol. 41, W04006 (2005). DOI: 10.1029/2004WR003692.

- [209] R. Müller. "Theoretische Grundlagen Der Fluss-Und Wildbachverbauungen." PhD Thesis. ETH Zurich, 1943.
- [210] R. J. Naiman, H. Décamps, M. E. McClain, and G. E. Likens. "Riparia: Ecology, Conservation, and Management of Streamside Communities." In: *Riparia: Ecology, Conservation, and Management of Streamside Communities*. Burlington: Academic Press, 2005, pp. 1–18. ISBN: 978-0-12-663315-3. DOI: 10.1016/B978-012663315-3/50002-2.
- [211] H Nakagawa, T Tsujimoto, and Y Shimizu. "Turbulent Flow with Small Relative Submergence." In: *Fluvial Hydraulics of Mountain Regions, Lect. Notes Earth Sci., Vol. 37, Edited by A. Armanini, and G. Di Silvio*. Springer, Berlin, Heidelberg, 1991, pp. 33–44.
- [212] C. R. Neill. "Mean-Velocity Criterion for Scour of Coarse Uniform Bed-Material." In: (1967).
- [213] I. Nezu and H. Nakagawa. "Turbulence in Open-Channel Flows, International Association for Hydraulic Research." In: *Balkema, Rotterdam* (1993).
- [214] I. K. Nikitin. "Turbulent Channel Flow and Processes in the Near-Bed Region." In: *Ukraine Acad. Sci., Kiev, Ukraine (in Russian)* (1963).
- [215] V. Nikora, D. Goring, I. McEwan, and G. Griffiths. "Spatially Averaged Open-Channel Flow over Rough Bed." In: *Journal of Hydraulic Engineering* 127.2 (2001), pp. 123–133.
- [216] V. I. Nikora, D. G. Goring, and B. J. F. Biggs. "On Gravel-Bed Roughness Characterization." en. In: *Water Resources Research* 34.3 (Mar. 1998), pp. 517–527. ISSN: 1944-7973. DOI: 10.1029/97WR02886.
- [217] V. I. Nikora, K. Koll, S. R. Mclean, A. Ditrich, and J. Aberle. "Zero-Plane Displacement for Rough-Bed Open-Channel Flows." English. In: *Fluvial Hydraulics River Flow 2002* (2002).
- [218] V. I. Nikora and S. R. Mclean. "Environmental Flows over Rough Beds: A Spatial Averaging Approach." In: (2001).
- [219] M Nitsche, D Rickenmann, J. M Turowski, A Badoux, and J. W Kirchner. "Evaluation of Bedload Transport Predictions Using Flow Resistance Equations to Account for Macro-Roughness in Steep Mountain Streams." In: *Water Resources Research, Vol. 47, W08513* (2011). DOI: 10.1029/2011WR010645.
- [220] J. D. Nowinski, M. B. Cardenas, and A. F. Lightbody. "Evolution of Hydraulic Conductivity in the Floodplain of a Meandering River Due to Hyporheic Transport of Fine Materials." en. In: *Geophysical Research Letters* 38.1 (Jan. 2011), p. L01401. ISSN: 1944-8007. DOI: 10.1029/2010GL045819.
- [221] M. Nujić, I. f. W. u. U. mbH Hydrotec, and Z. P. A. Hunziker. "Benutzerhandbuch Hydro_AS-2D Version 4.0, 2D-Strömungsmodell Feur Die Wasserwirtschaftliche Praxis." In: *Aachen. Google Scholar* (2015), p. 58.

- [222] M. Nujić, I. f. W. u. U. mbH Hydrotec, and Z. P. A. Hunziker. "Benutzerhandbuch HYDRO_FT-2D, Erweiterung Zu HYDRO_AS-2D Zur Simulation Des Stofftransports." In: *Aachen. Google Scholar* (2015), p. 44.
- [223] T. Okazaki, Y. Gonda, Y. Nishii, and H. Kawabe. "Characteristics of Step-Pool Morphology in the Mountain Streams of Japan." In: (2006), p. 12.
- [224] K. W Olesen. "BED TOPOGRAPHY IN SHALLOW RIVER BENDS." PhD thesis. Delft, The Netherlands: Technical University of Delft, 1987.
- [225] E. M. O'Loughlin and V. S. S Annambhotla. "Flow Phenomena Near Rough Boundaries." In: *Journal of Hydraulic Research*, 7:2 (1969), pp. 231–250. doi: 10.1080/00221686909500265.
- [226] J Oosterkamp. *Observations from the Air, the Foot of Spin Ghar, Field Report*. Tech. rep. LGCD Jalalabad, 2009.
- [227] S. Pagliara and P. Chiavaccini. "Energy Dissipation on Block Ramps." In: *Journal of Hydraulic Engineering* 132.1 (2006), pp. 41–48.
- [228] M. A. Palmer, C. A. Reidy Liermann, C. Nilsson, M. Flörke, J. Alcamo, P. S. Lake, and N. Bond. "Climate Change and the World's River Basins: Anticipating Management Options." en. In: *Frontiers in Ecology and the Environment* 6.2 (Mar. 2008), pp. 81–89. ISSN: 1540-9309. doi: 10.1890/060148.
- [229] S. M. Palt. "Sedimenttransportprozesse im Himalaya-Karakorum und ihre Bedeutung für Wasserkraftanlagen [online]." In: (2001).
- [230] I. Panagiotopoulos, G. Voulgaris, and M. B. Collins. "The Influence of Clay on the Threshold of Movement of Fine Sandy Beds." In: *Coastal Engineering* 32.1 (Oct. 1997), pp. 19–43. ISSN: 0378-3839. doi: 10.1016/S0378-3839(97)00013-6.
- [231] A. T. Papanicolaou and A. G. Tsakiris. "Boulder Effects on Turbulence and Bedload Transport." In: *Gravel-Bed Rivers: Process and Disasters* (2017), p. 33.
- [232] A. N. Papanicolaou, C. M. Kramer, A. G. Tsakiris, T. Stoesser, S. Bomminayuni, and Z. Chen. "Effects of a Fully Submerged Boulder within a Boulder Array on the Mean and Turbulent Flow Fields: Implications to Bedload Transport." en. In: *Acta Geophysica* 60.6 (Dec. 2012), pp. 1502–1546. ISSN: 1895-6572, 1895-7455. doi: 10.2478/s11600-012-0044-6.
- [233] C. Parker, N. J. Clifford, and C. R. Thorne. "Understanding the Influence of Slope on the Threshold of Coarse Grain Motion: Revisiting Critical Stream Power." In: *Geomorphology* 126.1 (Mar. 2011), pp. 51–65. ISSN: 0169-555X. doi: 10.1016/j.geomorph.2010.10.027.
- [234] G. Parker. "TRANSPORT OF GRAVEL AND SEDIMENT MIXTURES." In: *Sedimentation Engineering Processes, Measurements, Modeling, and Practice*. ASCE Manuals and Reports on Engineering Practice No. 110, (eds) M. Garcia. 2008, pp. 165–243. ISBN: 978-0-7844-7128-9.

- [235] G. Parker, S. Dhamotharan, and H. Stefan. "Model Experiments on Mobile, Paved Gravel Bed Streams." en. In: *Water Resources Research* 18.5 (Oct. 1982), pp. 1395–1408. ISSN: 1944-7973. DOI: 10.1029/WR018i005p01395.
- [236] G. C. Pazis and W. H. Graf. "Weak Sediment Transport." eng. In: *Journal of the Hydraulics Division* 103.7 (1977), pp. 799–802.
- [237] B. C. Phillips and A. J. Sutherland. "Spatial Lag Effects in Bed Load Sediment Transport." In: *Journal of Hydraulic Research* 27.1 (Jan. 1989), pp. 115–133. ISSN: 0022-1686. DOI: 10.1080/00221688909499247.
- [238] G. Piqué, D. Vericat, S. Sabater, and R. J. Batalla. "Effects of Biofilm on River-Bed Scour." In: *Science of The Total Environment* 572.Supplement C (Dec. 2016), pp. 1033–1046. ISSN: 0048-9697. DOI: 10.1016/j.scitotenv.2016.08.009.
- [239] O. Pironneau. *Finite Element Methods for Fluids*. Chichester; New York; Paris: Wiley ; Masson, 1989. ISBN: 978-0-471-92255-1 978-2-225-81863-9.
- [240] D. M. Powell. "Chapter 12: Dryland Rivers: Processes and Forms." en. In: *Geomorphology of Desert Environments*. Ed. by A. J. Parsons and A. D. Abrahams. Dordrecht: Springer Netherlands, 2009. ISBN: 978-1-4020-5718-2 978-1-4020-5719-9. DOI: 10.1007/978-1-4020-5719-9.
- [241] D. M. Powell. "Patterns and Processes of Sediment Sorting in Gravel-Bed Rivers." In: *Progress in Physical Geography* 22,1 (1988), pp. 1–32.
- [242] D. M. Powell, J. B. Laronne, I. Reid, and R. Barzilai. "The Bed Morphology of Upland Single-Thread Channels in Semi-Arid Environments: Evidence of Repeating Bedforms and Their Wider Implications for Gravel-Bed Rivers." en. In: *Earth Surface Processes and Landforms* 37.7 (June 2012), pp. 741–753. ISSN: 1096-9837. DOI: 10.1002/esp.3199.
- [243] D. M. Powell, I. Reid, J. B. Laronne, and L. Frostick. "Bed Load as a Component of Sediment Yield from a Semiarid Watershed of the Northern Negev." In: *Erosion and Sediment Yield: Global and Regional Perspectives (Proceedings of the Exeter Symposium, July 1996)*. IAHS Publ. No. 236, 1996. 1996, pp. 389–397.
- [244] C. Pringle. "What Is Hydrologic Connectivity and Why Is It Ecologically Important?" en. In: *Hydrological Processes* 17.13 (Sept. 2003), pp. 2685–2689. ISSN: 1099-1085. DOI: 10.1002/hyp.5145.
- [245] J. Pu, J. Wei, and Y. Huang. "Velocity Distribution and 3D Turbulence Characteristic Analysis for Flow over Water-Worked Rough Bed." en. In: *Water* 9.9 (Sept. 2017), p. 668. ISSN: 2073-4441. DOI: 10.3390/w9090668.
- [246] M. R. Raupach, R. A. Antonia, and S. Rajagopalan. "Rough-Wall Turbulent Boundary Layers." In: *Appl. Mech. Rev* 44.1 (1991), pp. 1–25.
- [247] M. R. Raupach, A. S. Thom, and I. Edwards. "A Wind-Tunnel Study of Turbulent Flow Close to Regularly Arrayed Rough Surfaces." In: *Boundary-Layer Meteorology* 18.4 (1980), pp. 373–397.

- [248] P. A Raymond, J Hartmann, R Lauerwald, S Sobek, C McDonald, M Hoover, D Butman, R Striegl, E Mayorga, C Humborg, P Kortelainen, H Dürr, M Meybeck, P Ciais, and P Guth. "Global Carbon Dioxide Emissions from Inland Waters." In: *Nature*, 503 (2013), pp. 335–359. DOI: 10.1038/nature12760.
- [249] D. E. Reid and E. J. Hickin. "Flow Resistance in Steep Mountain Streams." In: *Earth Surface Processes and Landforms* 33.14 (June 13, 2008), pp. 2211–2240. ISSN: 01979337. DOI: 10.1002/esp.1682.
- [250] I. Reid, J. T. Layman, and L. E. Frostick. "The Continuous Measurement Of Bedload Discharge." In: *Journal of Hydraulic Research* 18.3 (July 1980), pp. 243–249. ISSN: 0022-1686. DOI: 10.1080/00221688009499550.
- [251] I. Reid and L. E. Frostick. "Channel Form, Flows and Sediments of Endogenous Ephemeral Rivers in Deserts." en. In: *Arid Zone Geomorphology: Process, Form and Change in Drylands*. Ed. by D. S. G. Thomas. Third Edition. Chichester, UK: John Wiley & Sons, Ltd, 2011, pp. 301–332. ISBN: 978-0-470-71077-7. DOI: 10.1002/9780470710777.ch13.
- [252] I. Reid and J. B. Laronne. "Bed Load Sediment Transport in an Ephemeral Stream and a Comparison with Seasonal and Perennial Counterparts." en. In: *Water Resources Research* 31.3 (Mar. 1995), pp. 773–781. ISSN: 1944-7973. DOI: 10.1029/94WR02233.
- [253] L. V. Reynolds, P. B. Shafroth, and N. LeRoy Poff. "Modeled Intermittency Risk for Small Streams in the Upper Colorado River Basin under Climate Change." In: *Journal of Hydrology* 523 (Apr. 2015), pp. 768–780. ISSN: 0022-1694. DOI: 10.1016/j.jhydrol.2015.02.025.
- [254] D. Rickenmann. "An Alternative Equation for Mean Flow Velocity for Gravel Bed Rivers and Mountain Torrents." In: G.V. Cotroneo & R.R. Rumer (Eds), *Proceedings ASCE 1994 National Conference on Hydraulic Engineering, Vol. 1*. Buffalo N.Y., USA, 1994, pp. 672–676.
- [255] D. Rickenmann. "Fliessgeschwindigkeit Wildbächen Und Gebirgsflüssen Rickenmann-1996_Fliessgeschwindigkeit.Pdf." In: *Wasser, Energie, Luft-eau, Energi, Air*, 88. Jahrgang, Heft 11/12, Ch5401 Baden (1996).
- [256] D. Rickenmann and A. Recking. "Evaluation of Flow Resistance in Gravel-Bed Rivers through a Large Field Data Set." In: *Water Resources Research*, Vol. 47, W07538 (2011). DOI: 10.1029/2010WR009793.
- [257] C. T. Robinson, D. Tonolla, B. Imhof, R. Vukelic, and U. Uehlinger. "Flow Intermittency, Physico-Chemistry and Function of Headwater Streams in an Alpine Glacial Catchment." en. In: *Aquatic Sciences* 78.2 (Apr. 2016), pp. 327–341. ISSN: 1015-1621, 1420-9055. DOI: 10.1007/s00027-015-0434-3.

- [258] R. J. Rolls, C. Leigh, and F. Sheldon. "Mechanistic Effects of Low-Flow Hydrology on Riverine Ecosystems: Ecological Principles and Consequences of Alteration." In: *Freshwater Science* 31.4 (Dec. 2012), pp. 1163–1186. ISSN: 2161-9549. DOI: 10.1899/12-002.1.
- [259] D. L. Rosgen. *Applied River Morphology*. Wildland Hydrology, 1996. ISBN: 978-0-9653289-0-6.
- [260] A. G. Roy, T. Buffin-Bélanger, H. Lamarre, and A. D. Kirkbride. "Size, Shape and Dynamics of Large-Scale Turbulent Flow Structures in a Gravel-Bed River." en. In: *Journal of Fluid Mechanics* 500 (Jan. 2004), pp. 1–27. ISSN: 1469-7645, 0022-1120. DOI: 10.1017/S0022112003006396.
- [261] I. L. Rozovskii. *Flow of Water in Bends of Open Channels*. At head of title: Academy of Sciences of the Ukrainian SSR. Institute of Hydrology and Hydraulic Engineering Added t.p. in Russian: Dvizhenie vody. Kiev, Washington, D.C., available from the Office of Technical Services, U.S. Dept. of Commerce, 1961]: Academy of Sciences of the Ukrainian SSR, Israel Program for Scientific Translations, 1957.
- [262] N Sadid, S Haun, and S Wieprecht. "An Overview of Hydro-Sedimentological Characteristics of Intermittent Rivers in Kabul Region of Kabul River Basin." English. In: *Wieprecht et Al. (Eds). River Sedimentation: Proceedings of the 13th International Symposium on River Sedimentation, ISRS*. OCLC: 965356245. Stuttgart, Germany: Taylor & Francis Group, London, 2016, pp. 85–91. ISBN: 978-1-317-22531-7.
- [263] N. Sadid, S. Haun, and S. Wieprecht. "An Overview of Hydro-Sedimentological Characteristics of Intermittent Rivers in Kabul Region of Kabul River Basin." In: *International Journal of River Basin Management* 0.0 (Apr. 2017), pp. 1–13. ISSN: 1571-5124. DOI: 10.1080/15715124.2017.1321004.
- [264] P. J. Sandercock and J. M. Hooke. "Vegetation Effects on Sediment Connectivity and Processes in an Ephemeral Channel in SE Spain." In: *Journal of Arid Environments* 75.3 (Mar. 2011), pp. 239–254. ISSN: 0140-1963. DOI: 10.1016/j.jaridenv.2010.10.005.
- [265] P. Sandercock, J. Hooke, and J. Mant. "Vegetation in Dryland River Channels and Its Interaction with Fluvial Processes." en. In: *Progress in Physical Geography* 31.2 (Apr. 2007), pp. 107–129. ISSN: 0309-1333. DOI: 10.1177/0309133307076106.
- [266] R. Sando and K. W. Blasch. "Predicting Alpine Headwater Stream Intermittency: A Case Study in the Northern Rocky Mountains." In: *Ecohydrology & Hydrobiology* 15.2 (June 2015), pp. 68–80. ISSN: 1642-3593. DOI: 10.1016/j.ecohyd.2015.04.002.
- [267] U. Schälchli. "The Clogging of Coarse Gravel River Beds by Fine Sediment." In: *Hydrobiologia* 235/236 : 189-197 (1992).
- [268] A. P. Schick, J. Lekach, and M. A. Hassan. "Vertical Exchange of Coarse Bedload in Desert Streams." en. In: *Geological Society, London, Special Publications* 35.1 (Jan. 1987), pp. 7–16. ISSN: 0305-8719, 2041-4927. DOI: 10.1144/GSL.SP.1987.035.01.02.

- [269] H Schlichting. *Boundary-Layer Theory*. 6th ed. New York: McGraw-Hill, 1968.
- [270] M. Schmautz. "Eigendynamische Aufweitung in einer geraden Gewässerstrecke: Entwicklung und Untersuchungen an einem numerischen Modell." ger. PhD thesis. 2003.
- [271] H. Schmidt. "Microbial Stabilization of Lotic Fine Sediments." PhD thesis. Stuttgart, Germany: University of Stuttgart, 2017.
- [272] A. Schneider, A. Jost, C. Coulon, M. Silvestre, S. Théry, and A. Ducharne. "Global-Scale River Network Extraction Based on High-Resolution Topography and Constrained by Lithology, Climate, Slope, and Observed Drainage Density." In: *Geophysical Research Letters* 44.6 (2017), pp. 2773–2781. ISSN: 1944-8007. DOI: 10.1002/2016GL071844.
- [273] F. Schöberl. "Zur Frage Der Gefällsausbildung Beim Selbststabilisierungsprozess von Erodierenden Fluss-Strecken." PhD thesis. Innsbruck, 1979.
- [274] J. Schubert. "Hydraulic Aspects of Riverbank Filtration—Field Studies." In: *Journal of Hydrology* 266.3 (2002), pp. 145–161.
- [275] S. A Schumm. "River Adjustment to Altered Hydrologic Regimen_Murrumbidgee River and Paleochannels, Australia." In: *U.S. Geol. Surv. Prof. Pap.* (1968), p. 598.
- [276] S. A. Schumm. *The Fluvial System*. en. Blackburn Press, 1977. ISBN: 978-1-930665-79-8.
- [277] M. Shanafield and P. G. Cook. "Transmission Losses, Infiltration and Groundwater Recharge through Ephemeral and Intermittent Streambeds: A Review of Applied Methods." en. In: *Journal of Hydrology* 511 (Apr. 2014), pp. 518–529. ISSN: 00221694. DOI: 10.1016/j.jhydrol.2014.01.068.
- [278] P. A. Shaw and R. G. Bryant. "Pans, Playas and Salt Lakes." In: *Arid Zone Geomorphology*. Ed. by D. S. G. Thomas. Chichester, UK: John Wiley & Sons, Ltd, Mar. 2011, pp. 373–401. ISBN: 978-0-470-71077-7 978-0-470-51908-0. DOI: 10.1002/9780470710777.ch15.
- [279] S. B. Shaw. "Investigating the Linkage between Streamflow Recession Rates and Channel Network Contraction in a Mesoscale Catchment in New York State." en. In: *Hydrological Processes* 30.3 (Jan. 2016), pp. 479–492. ISSN: 1099-1085. DOI: 10.1002/hyp.10626.
- [280] F. Sheldon, S. E. Bunn, J. M. Hughes, A. H. Arthington, S. R. Balcombe, and C. S. Fellows. "Ecological Roles and Threats to Aquatic Refugia in Arid Landscapes: Dryland River Waterholes." en. In: *Marine and Freshwater Research* 61.8 (2010), p. 885. ISSN: 1323-1650. DOI: 10.1071/MF09239.
- [281] A Shields. "Anwendung Der Ähnlichkeitsmechanik Und Der Turbulenzforschung Auf Die Geschiebebewegung." In: *Mitt, der Preuss. Versuchsanst. für Wasserbau und Schiffbau, Heft 26, Berlin, Germany* (1936).

- [282] A. Shvidchenko and G. Pender. "Macroturbulent Structure of Open-channel Flow over Gravel Beds." In: *Water Resources Research* 37.3 (Mar. 2001), pp. 709–719. ISSN: 0043-1397. DOI: 10.1029/2000WR900280.
- [283] A. B. Shvidchenko and G. Pender. "Flume Study of the Effect of Relative Depth on the Incipient Motion of Coarse Uniform Sediments." en. In: *Water Resources Research* 36.2 (Feb. 2000), pp. 619–628. ISSN: 1944-7973. DOI: 10.1029/1999WR900312.
- [284] M. B. Singer and K. Michaelides. "How Is Topographic Simplicity Maintained in Ephemeral Dryland Channels?" In: *Geology* 42.12 (Dec. 2014), pp. 1091–1094. ISSN: 0091-7613. DOI: 10.1130/G36267.1.
- [285] U. K. Singh, Z. Ahmad, and A. Kumar. "Incipient Motion for Gravel Particles in Cohesive Mixture of Clay-Silt-Gravel." In: *Proceedings of the 13th International Symposium on River Sedimentation*. Stuttgart, Germany: CRC Press, 2016, pp. 96–96. ISBN: ISBN: 978-1-138-02945-3.
- [286] G. M. Smart, M. J. Duncan, and J. M. Walsh. "Relatively Rough Flow Resistance Equations." In: *Journal of Hydraulic Engineering* 128.6 (2002), pp. 568–578.
- [287] T. H. Snelder, T. Datry, N. Lamouroux, S. T. Larned, E. Sauquet, H. Pella, and C. Catalogne. "Regionalization of Patterns of Flow Intermittence from Gauging Station Records." en. In: *Hydrology and Earth System Sciences* 17.7 (July 2013), pp. 2685–2699. ISSN: 1607-7938. DOI: 10.5194/hess-17-2685-2013.
- [288] M. Sophocleous. "Interactions between Groundwater and Surface Water: The State of the Science." en. In: *Hydrogeology Journal* 10.1 (Feb. 2002), pp. 52–67. ISSN: 1431-2174, 1435-0157. DOI: 10.1007/s10040-001-0170-8.
- [289] J. B. Southard and L. A. Boguchwal. "Bed Configuration in Steady Unidirectional Water Flows; Part 2, Synthesis of Flume Data." In: *Journal of Sedimentary Research* 60.5 (Sept. 1, 1990), pp. 658–679. ISSN: 1527-1404. DOI: 10.1306/212F9241-2B24-11D7-8648000102C1865D.
- [290] M. Spannring. "Die Wirkung von Buhnen Auf Strömung Und Sohle Eines Flie\s Sgewässers: Parameterstudie an Einem Numerischen Modell." PhD Thesis. Lehrstuhl für Wasserbau und Wasserwirtschaft, 1999.
- [291] J. A. Stanford and J. V. Ward. "An Ecosystem Perspective of Alluvial Rivers: Connectivity and the Hyporheic Corridor." en. In: *Journal of the North American Benthological Society* 12.1 (Mar. 1993), pp. 48–60. ISSN: 0887-3593, 1937-237X. DOI: 10.2307/1467685.
- [292] E. H. Stanley, S. G. Fisher, and N. B. Grimm. "Ecosystem Expansion and Contraction in Streams." In: *BioScience* 47.7 (1997), pp. 427–435. ISSN: 0006-3568. DOI: 10.2307/1313058.
- [293] A. L. Steward, D. Von Schiller, K. Tockner, J. C. Marshall, and S. E. Bunn. "When the River Runs Dry: Human and Ecological Values of Dry Riverbeds." In: *Front Ecol Environ*; 10(4) (2012), pp. 202–209. DOI: 10.1890/110136.

- [294] T. Stoesser, W. Rodi, and G. H. Jirka. "Large-Eddy Simulation of Flow over Rough Channel Beds." In: *Proc., Int. Conf. on Fluvial Hydraulics, River Flow 2004*. Taylor & Francis Group, London, 2004, pp. 265–270.
- [295] Y. Storz-Peretz and J. B. Laronne. "The Morpho-textural Signature of Large Bed-forms in Ephemeral Gravel-bed Channels of Various Planforms." en. In: *Hydrological Processes* 32.5 (Feb. 2018), pp. 617–635. ISSN: 1099-1085. DOI: 10.1002/hyp.11437.
- [296] J. W Stringer and C Perkins. *Kentucky Forest Practice Guidelines for Water Quality Management*. 2001.
- [297] C.-C. Su, J.-Y. Lu, and J.-H. Hong. "A Field Investigation of the Sediment Transport Characteristics of a High Sediment Load Intermittent River in Taiwan." In: *Hydrol. Process.* 27, (2013), pp. 4043–4056. DOI: 10.1002/hyp.9517.
- [298] N. A Sutfin, J. R Shaw, E. E Wohl, and D. J Cooper. "A Geomorphic Classification of Ephemeral Channels in a Mountainous, Arid Region, Southwestern Arizona, USA." In: *Geomorphology* 221 (2014), pp. 164–175.
- [299] K. Suzuki and A. Hano. "Grain Size Change of Bed Surface Layer and Sediment Discharge of an Equilibrium River Bed." In: *Mitteilungen der Versuchsanstalt fur Wasserbau, Hydrologie und Glaziologie an der Eidgenossischen Technischen Hochschule Zurich* 117 (1992), pp. 151–156.
- [300] A. Talmon, N. Struiksma, and M. Van Mierlo. "Laboratory Measurements of the Direction of Sediment Transport on Transverse Alluvial-Bed Slopes." In: *Journal of Hydraulic Research* 33.4 (July 1995), pp. 495–517. ISSN: 0022-1686. DOI: 10.1080/00221689509498657.
- [301] S. K. Thappeta, S. M. Bhallamudi, P. Fiener, and B. Narasimhan. "Resistance in Steep Open Channels Due to Randomly Distributed Macroroughness Elements at Large Froude Numbers." In: *Journal of Hydrologic Engineering* 22.12 (Dec. 2017), p. 04017052. ISSN: 1084-0699, 1943-5584. DOI: 10.1061/(ASCE)HE.1943-5584.0001587.
- [302] V. Thomas and J. Warner. "Hydropolitics in the Harirud/Tejen River Basin: Afghanistan as Hydro-Hegemon?" In: *Water International* 40.4 (June 2015), pp. 593–613. ISSN: 0250-8060. DOI: 10.1080/02508060.2015.1059164.
- [303] S. M Thompson and P. L Campbell. "Hydraulics of A Large Channel Paved With Boulders." In: *Journal of Hydraulic Research*, 7:4 (1979), pp. 341–354. DOI: 10.1080/00221687909499577.
- [304] J. B. Thornes. "Channel Changes in Ephemeral Streams: Observations, Problems and Models." In: *River channel changes* (1977), pp. 317–335.
- [305] S. Tooth. "9.31 Dryland Fluvial Environments: Assessing Distinctiveness and Diversity from a Global Perspective." en. In: *Treatise on Geomorphology*. Elsevier, 2013, pp. 612–644. ISBN: 978-0-08-088522-3. DOI: 10.1016/B978-0-12-374739-6.00257-8.

- [306] S. D Tooth. "Floodouts in Central Australia." In: *A. J. Miller and A. Gupta, Eds., Varieties of Fluvial Form*. Chichester: Wiley & Sons, 1999 a, pp. 219–247.
- [307] S. Tooth. "Downstream Changes in Dryland River Channels: The Northern Plains of Arid Central Australia." In: *Geomorphology* 34.1 (Aug. 2000), pp. 33–54. ISSN: 0169-555X. DOI: 10.1016/S0169-555X(99)00130-0.
- [308] S. Tooth and G. C. Nanson. "Anabranching Rivers on the Northern Plains of Arid Central Australia." In: *Geomorphology* 29.3 (1999), pp. 211–233.
- [309] S. Tooth and G. C. Nanson. "Distinctiveness and Diversity of Arid Zone River Systems." en. In: *Arid Zone Geomorphology*. Ed. by D. S. G. Thomas. John Wiley & Sons, Ltd, 2011, pp. 269–300. ISBN: 978-0-470-71077-7. DOI: 10.1002/9780470710777.ch12.
- [310] S. Tooth and G. C. Nanson. "Equilibrium and Nonequilibrium Conditions in Dryland Rivers." In: *Physical Geography* 21.3 (2000), pp. 183–211.
- [311] T. Tsujimoto. "Bed Load Transport In Steep Channels." In: *Fluvial Hydraulics of Mountain Regions, Lect. Notes Earth Sci., Vol. 37, Edited by A. Armanini, and G. Di Silvio*. Springer, Berlin, Heidelberg, 1991, pp. 89–102.
- [312] C. Ulrich, S. S. Hubbard, J. Florsheim, D. Rosenberry, S. Borglin, M. Trotta, and D. Seymour. "Riverbed Clogging Associated with a California Riverbank Filtration System: An Assessment of Mechanisms and Monitoring Approaches." In: *Journal of Hydrology* 529.Part 3 (Oct. 2015), pp. 1740–1753. ISSN: 0022-1694. DOI: 10.1016/j.jhydrol.2015.08.012.
- [313] UNDESA Population Division. *World Population Prospects: The 2015 Revision, Volume I: Comprehensive Tables (ST/ESA/SER.A/379)*. 2015.
- [314] L. C. Van Rijn. *Principles of Sediment Transport in Rivers, Estuaries and Coastal Seas. 1: Principles of Sediment Transport in Rivers, Estuaries and Coastal Seas*. eng. OCLC: 832662677. Amsterdam: Aqua Publications, 1993. ISBN: 978-90-800356-2-1.
- [315] H. van Steijn. "Debris-Flow Magnitude—Frequency Relationships for Mountainous Regions of Central and Northwest Europe." In: *Geomorphology* 15.3-4 (1996), pp. 259–273.
- [316] G. Verstraeten, J. Poesen, K. Gillijns, and G. Govers. "The Use of Riparian Vegetated Filter Strips to Reduce River Sediment Loads: An Overestimated Control Measure?" In: *Hydrological Processes* 20.20 (Apr. 2006), pp. 4259–4267. ISSN: 0885-6087. DOI: 10.1002/hyp.6155.
- [317] C. J. Vörösmarty, P. Green, J. Salisbury, and R. B. Lammers. "Global Water Resources: Vulnerability from Climate Change and Population Growth." en. In: *Science* 289.5477 (July 2000), pp. 284–288. ISSN: 0036-8075, 1095-9203. DOI: 10.1126/science.289.5477.284.

- [318] R. V. Vorste, R. Corti, A. Sagouis, and T. Datry. "Invertebrate Communities in Gravel-Bed, Braided Rivers Are Highly Resilient to Flow Intermittence." In: *Freshwater Science* 35.1 (Jan. 2016), pp. 164–177. ISSN: 2161-9549. DOI: 10.1086/683274.
- [319] P. L. Wiberg and J. D. Smith. "Calculations of the Critical Shear Stress for Motion of Uniform and Heterogeneous Sediments." en. In: *Water Resources Research* 23.8 (1987 b), pp. 1471–1480. ISSN: 1944-7973. DOI: 10.1029/WR023i008p01471.
- [320] D. D. Williams. *The Biology of Temporary Waters*. Oxford, New York: Oxford University Press, Dec. 2005. ISBN: 978-0-19-852812-8.
- [321] T. C. Winter, J Harvey, O. L. Franke, and W. M. Alley. *Ground Water and Surface Water: A Single Resource*. U.S. Geological Survey Circular 1139. Denver, Colo: U.S. Geological Survey, 1998. ISBN: 978-0-607-89339-7.
- [322] E. E Wohl and D. M Thompson. "VELOCITY CHARACTERISTICS ALONG A SMALL STEP-POOL CHANNEL." In: *Earth Surf. Process. Landforms* 25 (2000), pp. 353–367.
- [323] E. Wohl, S. Madsen, and L. MacDonald. "Characteristics of Log and Clast Bed-Steps in Step-Pool Streams of Northwestern Montana, USA." In: *Geomorphology* 20.1-2 (Sept. 1997), pp. 1–10. ISSN: 0169555X. DOI: 10.1016/S0169-555X(97)00021-4.
- [324] E. E. Wohl and H. Ikeda. "The Effect of Roughness Configuration on Velocity Profiles in an Artificial Channel." en. In: *Earth Surface Processes and Landforms* 23.2 (Feb. 1998), pp. 159–169. ISSN: 1096-9837. DOI: 10.1002/(SICI)1096-9837(199802)23:2<159::AID-ESP829>3.0.CO;2-P.
- [325] E. E. Wohl and P. P. Pearthree. "Debris Flows as Geomorphic Agents in the Huachuca Mountains of Southeastern Arizona." In: *Geomorphology* 4.3 (Oct. 1991), pp. 273–292. ISSN: 0169-555X. DOI: 10.1016/0169-555X(91)90010-8.
- [326] A. T. Wolf. "Conflict and Cooperation along International Waterways." In: *Water Policy* 1.2 (Apr. 1998), pp. 251–265. ISSN: 1366-7017. DOI: 10.1016/S1366-7017(98)00019-1.
- [327] A. T. Wolf. "The Transboundary Freshwater Dispute Database Project." en. In: *Water International* 24.2 (June 1999), pp. 160–163. ISSN: 0250-8060, 1941-1707. DOI: 10.1080/02508069908692153.
- [328] M. G. Wolman and R. Gerson. "Relative Scales of Time and Effectiveness of Climate in Watershed Geomorphology." en. In: *Earth Surface Processes* 3.2 (Apr. 1978), pp. 189–208. ISSN: 1931-8065. DOI: 10.1002/esp.3290030207.
- [329] M. G. Wolman and J. P Miller. "Magnitude and Frequency of Forces in Geomorphic Processes." In: *Journal of Geology* 68 (1960), pp. 54–74.

- [330] K. B. Woodward, C. S. Fellows, S. M. Mitrovic, and F. Sheldon. "Patterns and Bioavailability of Soil Nutrients and Carbon across a Gradient of Inundation Frequencies in a Lowland River Channel, Murray–Darling Basin, Australia." In: *Agriculture, Ecosystems & Environment* 205.Supplement C (July 2015), pp. 1–8. ISSN: 0167-8809. DOI: 10.1016/j.agee.2015.02.019.
- [331] M. S. Yalin and A. M. Da Silva. "On the Computation of Equilibrium Channels in Cohesionless Alluvium." In: *JOURNAL OF HYDROSCIENCE AND HYDRAULIC ENGINEERING* 15.2 (1997), pp. 1–14. ISSN: 0912-2508.
- [332] M. S. Yalin and A. M. Da Silva. "On the Determination of Regime Channels in Cohesionless Alluvium." In: *General Lecture, Proc. Conf. on Management of Landscapes Disturbed by Channel Incision*, SSY Wang, EJ Langendoen, FD Shields Jr. Eds., CCHE, University of Mississippi. 1997, pp. 77–86.
- [333] M. S. Yalin and A. M. Da Silva. "Regime Channels in Cohesionless Alluvium." en. In: *Journal of Hydraulic Research* 37.6 (Nov. 1999), pp. 725–742. ISSN: 0022-1686, 1814-2079. DOI: 10.1080/00221689909498508.
- [334] M. S. Yalin. *River Mechanics*. 1st ed. Oxford ; New York: Pergamon Press, 1992. ISBN: 978-0-08-040190-4.
- [335] M. S. Yalin and A. M. da Silva. *Fluvial Processes*. 5B 1905. Delft: IAHR, International Association for Hydraulic Research, 2001. ISBN: 90-805649-2-3.
- [336] M. S. Yalin and E. Karahan. "Inception of Sediment Transport." eng. In: *Journal of the Hydraulics Division* 105.11 (1979), pp. 1433–1443.
- [337] C. T. Yang and C. C. S. Song. "Theory of Minimum Rate of Energy Dissipation." In: *Journal of the Hydraulics Division, American Society of Civil Engineers*. Vol. 105. 1979.
- [338] C. T. Yang. "Minimum Unit Stream Power and Fluvial Hydraulics." eng. In: *Journal of the Hydraulics Division* 102.7 (1976), pp. 919–934.
- [339] S. Yochum. "FLOW RESISTANCE ESTIMATION IN HIGH-GRADIENT STREAMS." In: 2010, p. 12.
- [340] A. Yörük. "Unsicherheiten bei der hydrodynamischen Modellierung von Überschwemmungsgebieten." PhD thesis. 2008.
- [341] U. Zanke. *On the Influence of Turbulence on the Initiation of Sediment Motion*. Vol. 18. Jan. 2003.
- [342] A. Zimmermann, M. Church, and M. A. Hassan. "Step-Pool Stability: Testing the Jammed State Hypothesis." en. In: *Journal of Geophysical Research: Earth Surface* 115.F2 (June 2010), F02008. ISSN: 2156-2202. DOI: 10.1029/2009JF001365.
- [343] A. Zimmermann and M. Church. "Channel Morphology, Gradient Profiles and Bed Stresses during Flood in a Step–Pool Channel." In: *Geomorphology* 40.3 (Oct. 1, 2001), pp. 311–327. ISSN: 0169-555X. DOI: 10.1016/S0169-555X(01)00057-5.

- [344] C. Zimmermann and E. Naudascher. "Sohlausbildung Und Sedimentbewegung in Kruemmungen Alluvialer Gerinne." In: *Wasserwirtschaft* 69.4 (1979), pp. 110–117. ISSN: 0043-0978.

A. Appendix A

A.1. Initial and boundary conditions in Hydro_FT-2D

Initial and boundary conditions for Hydro_FT-2D can be assigned through the Surface-water Modelling System (SMS) tool. Inflow and outflow boundaries are defined using node strings connecting at least two adjacent nodes or one element. Once node strings are set, the rest of the boundary nodes are automatically considered as the no-flow boundary. The no-flow boundary is implemented in the model such that the transverse component of flow velocity to this boundary at each no-flow boundary node is set to zero and thus the flow velocity parallel to the no-flow boundary is ensured. This condition is also called a slip-velocity boundary condition, in which the tangential shear stress is not considered. At open boundaries, Hydro_FT-2D offers the following options for defining the initial and boundary conditions (Nujić et al. 2015b):

- Inflow boundary condition can be defined by hydrographs of flow discharges in m^3/s ; time in seconds s and the flow directions in degrees $^\circ$ at the boundary nodes can also be given.
- Likewise, the sediment transport rates in kg/s , the percentage of each grain class p_i in % can be defined as a function of time in seconds s to provide the sediment feeding rates as an inflow boundary condition.
- The inflow boundary condition can also be connected to the outflow, which resembles a recirculation of flow and sediment in a flume experiment. Additionally, the inflow can also be connected to another control-section that can be set by a node string at any interesting location. In such a condition, in addition to the inflow data, the sediment transport rates through this control-section can also be given to the inflow. The user can decide what percentage of the total sediment transport rates from a predefined control-section should be recirculated to the inflow as a function of time.
- At the outflow, boundary conditions can be defined by a rating curve or (h-q)-relation and energy gradient in per mill unit. The rating curve is given in flow discharge m^3/s and water level (m.a.sl) or any other elevation reference. The rating curve can be defined for outflow cross-section or flow over a weir, where its crown coefficient can also be given in the model.

- As an initial hydraulic boundary condition, water depth and flow velocity can be defined for each node for the whole mesh and then exported as an ASCII file to the Data-in (AS) folder. These initial values for water depth (Wtiefe_0.dat) and velocity (Geschw_0.dat) can be given either arbitrarily or the result of a simulation to generate an initial condition.
- Initial condition for a morphological simulation may consist percentage of grain classes p_i for all three layers, namely surface or active layer AS, subsurface layer US and base layer GS. The p_i values are given for each node of the mesh and are exported to specific files generated by Hydro_FT-2D. The files for grain classes are designated by (FA_al-i.dat), (FA_ul-i.dat), (FA_bl-i.dat), where i stands for the grain class (i.e. class 1, 2, 3 ... 12) for active, subsurface and base layers respectively. The sum of the p_i values for all grain classes must equal unity.
- The maximum thickness of the bed that is set as erodible can also be defined by setting the value of the node for the whole mesh except for the outflow boundary nodes, which are set by the program as non-erodible. The nodes' values can then be exported to a designated file (DZG_Layer-1.dat).
- Similarly, specific areas of the mesh can be defined by zones number for sediment feeding or sediment withdrawal (extraction). The sediment is manually fed at a specific rate or sediment is withdrawn at a particular rate or when a pre-defined horizon is exceeded, the deposited sediment is automatically removed. The zones of sediment feeding or withdrawal can be defined through SMS and exported to the files designated as (Verklapp-in.de) and (Bagger-in.de) respectively. The sediment extraction or sediment input rates are defined in separate files designated as (Bagger.inp) and (Verklapp.inp).

A.1.1. Model parameters

Model parameters for Hydro_FT-2D can be set through SMS pre and post-processing tool. Some selected model parameters used are listed in table A.1 and A.2 for hydraulic and morphologic parts of the simulations respectively.

Table A.1.: Some selected parameters for hydraulic calculations by Hydro_FT-2D

Parameters	Descriptions	Values used
Time interval Q_Strg	Defines the time in seconds s, at which the inflow hydrograph is read, and the results for outflows from model outflow and any control section is registered in the output file.	10
Time interval SMS	Defines the time in seconds s at which the 2D data (i.e. velocity components, water depth, bed evolution, bedload transport rates and others) are written in the output file.	50000
Hmin	Indicates the minimum water depth in m in a node to be considered as wet and included in the calculations	0.01
VELMAX	Maximum allowable velocity in m/s. If velocity at a node exceeds this limit, the program assumes a reduced velocity of magnitude (VELMAX) for this node.	6.0
CMUVISC	The coefficient for determination of eddy viscosity	0.6
SFC	The parameter for acceleration of simulation. This parameter may influence the results and even cause instability if used for highly variable hydrographs. A value of unity means no acceleration of the simulation.	1.0

Some parameters are selected for morphological simulations using Hhydro_FT-2D is listed in table A.2.

Table A.2.: Some selected parameters used for morphologic simulations by Hydro_FT-2D

Parameters	Descriptions	Methods / values used
Roughness critical shear stresses (Rauheits ermittlung)	<p>Four options are available for defining roughness and critical shear stress in Hydro_FT-2D</p> <ol style="list-style-type: none"> 1. Both roughness and critical shear stress parameters are treated as constant and defined via SMS-menu. In this option, $\tau_c^* = \tau_{ce}^*$ and total roughness k_{st} and grain roughness k'_{st} are invariable with time 2. Critical shear stress $\tau_c^* = \tau_{ce}^*$ is calculated using Yalin and da Silva (2001) equation 4.50, and total roughness k_{st} and grain roughness k'_{st} are invariable with time 3. Critical shear stress is defined as a constant value in SMS, while the total roughness k_{st}, and grain roughness k'_{st} are defined as a function of time using Yalin and da Silva (2001) equation 3.64. 4. Both critical shear stress $\tau_c^* = \tau_{ce}^*$ and roughness $k_{st}; k'_{st}$ are calculated using Yalin and da Silva (2001) equations 	(1)
Bedload transport equation (Stofftransport formel)	In Hydro_FT-2D, three sediment transport equation is implemented. The Engelund and Hansen (1967), Ackers and White (1973) and modified by Hunziker (1995) version of Meyer-Peter and Müller (1948) equation for fractional sediment transport simulations.	MPM
Shear stress fluctuations (Schubspannungs schwankungen)	If checked, considers the shear stress fluctuations for calculation of dimensionless shear stress as suggested by Pazis and Graf (1977) for the so-called weak sediment transport	Checked

<p>Loading Law: C_ALaeng 1 C_Alaeng 2</p>	<p>Loading law concept is implemented with MPM formula to consider the effect of the spatial lag where sediment transport requires to reach its full capacity as observed by Phillips and Sutherland (1989); Spannring (1999). According to Nujić et al. (2015), if $\alpha_L = 0$ and $L_{50} = 0$ are selected, the program runs two times faster</p> $\frac{\partial(q_b^*)}{\partial t} + \frac{\partial(q_b^* \cos \alpha)}{\partial x} + \frac{\partial(q_b^* \sin \alpha)}{\partial y} = -\frac{1}{L_S} (q_b^* - q_b)$ $L_S = \alpha_L (\tau_{dms}^* - \tau_{cm}^*) D_{ms} + L_{S0} .$	<p>4000</p>
<p>Critical shear stress, Theta_cr (MPM)</p>	<p>The critical shear stress for initiation of motion τ_{ce}^*.</p>	<p>0.05</p>
<p>Pre-Factor for MPM equation (SCF_Formel)</p>	<p>The pre-factor is used to modify the mobility parameter in MPM bedload transport equation (4.42) $k_F \cdot 8$</p>	<p>1.0</p>
<p>Secondary current coefficient (A_r Kruemmungs koeff.)</p>	<p>This coefficient is used to change the influence of secondary current on the channel bends by:</p> $\tan \delta_{Sec} = \frac{\tau_{Sec}}{\tau_{\Gamma}} \cong \frac{\tau_{Sec}}{\tau_0} = -A_{Sec} \frac{h}{R_{Sec}}$ <p>δ_{Sec} angle deviation from flow direction, τ_{Γ}, and τ_{Sec} are shear stresses in flow and secondary current directions, A_{Sec} secondary current factor varies (7-12), R_{Sec} radius of bend calculated locally, and h is water depth.</p>	<p>10</p>
<p>pal and pul</p>	<p>Parameters for steering the thickness of active and subsurface layers.</p>	<p>pal=1 pul=4</p>
<p>Number of grain size classes (NF)</p>	<p>Hydro_FT-2D allows up to 12 number of size classes.</p>	<p>12</p>
<p>Di,m</p>	<p>Mean grain diameter of the grain class in mm.</p>	

B. Appendix B

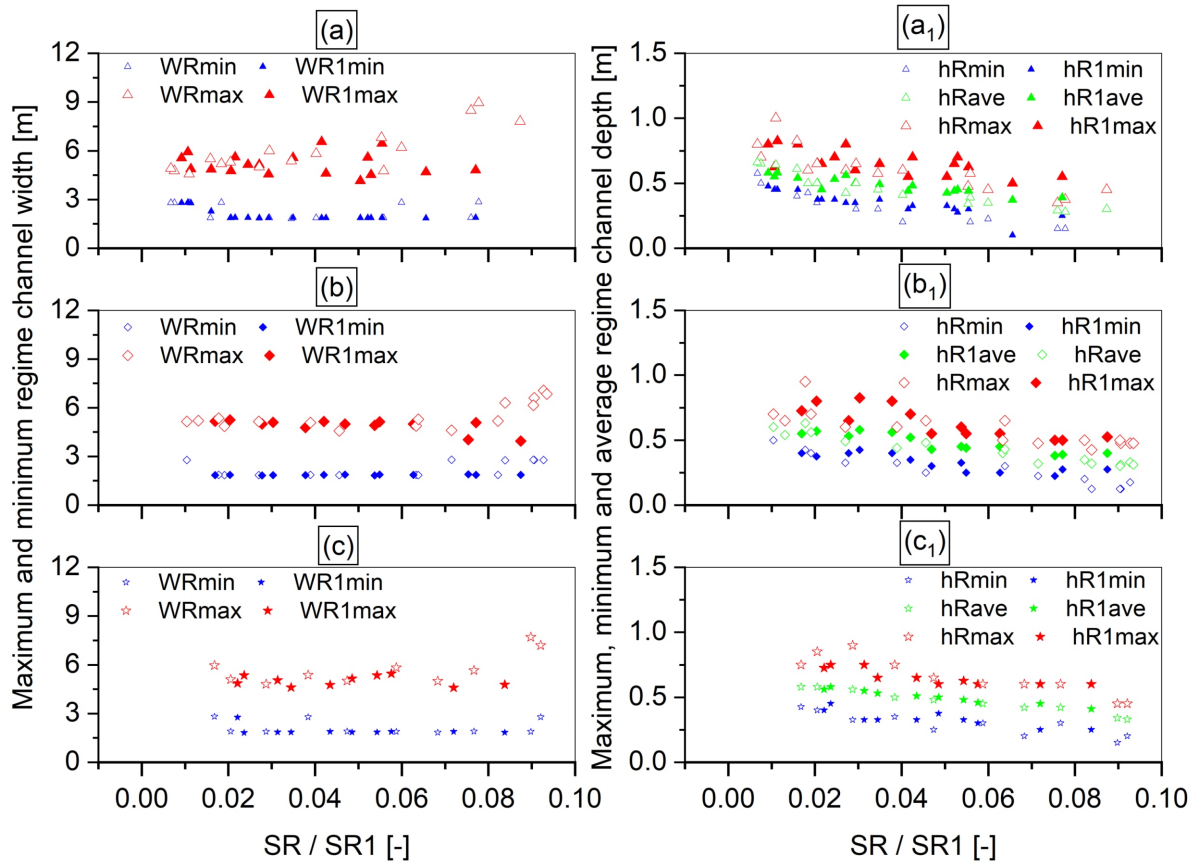


Figure B.1.: Maximum and minimum regime channel width and depth variations with channel regime slope respectively for (a) and (a₁) $D_{mo} = 28.4 \text{ mm}$, (b) and (b₁) $D_{mo} = 47.3 \text{ mm}$, (c) and (c₁) $D_{mo} = 66.3 \text{ mm}$ for fixed-width channels

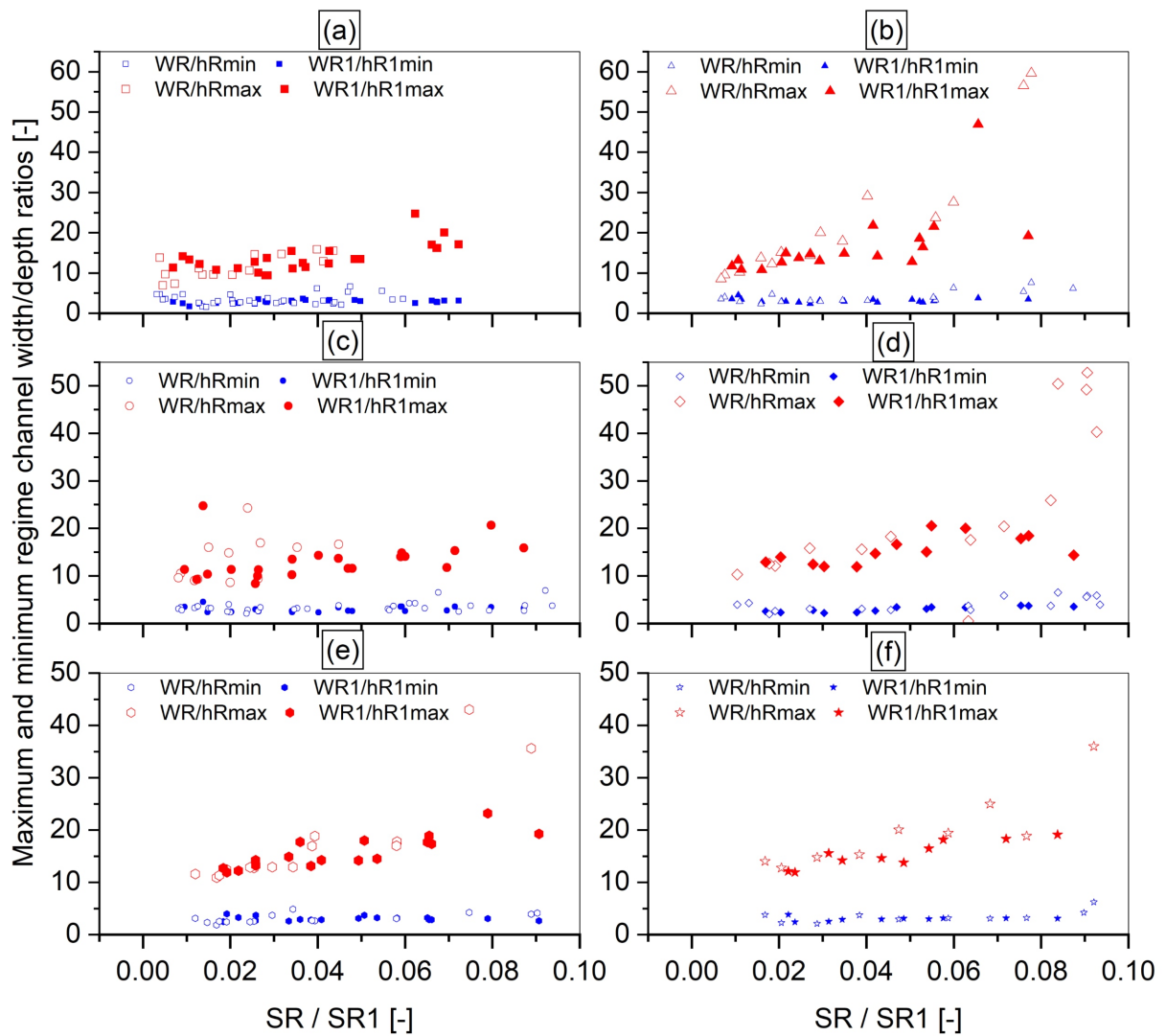


Figure B.2.: Maximum and minimum regime channel width to depth variations with channel regime slope for D_{mo} values of (a) 19.0 mm (b) 28.4 mm (c) 38.0 mm (d) 47.3 mm (e) 57.0 mm and (f) 66.3 mm for fixed-width channels

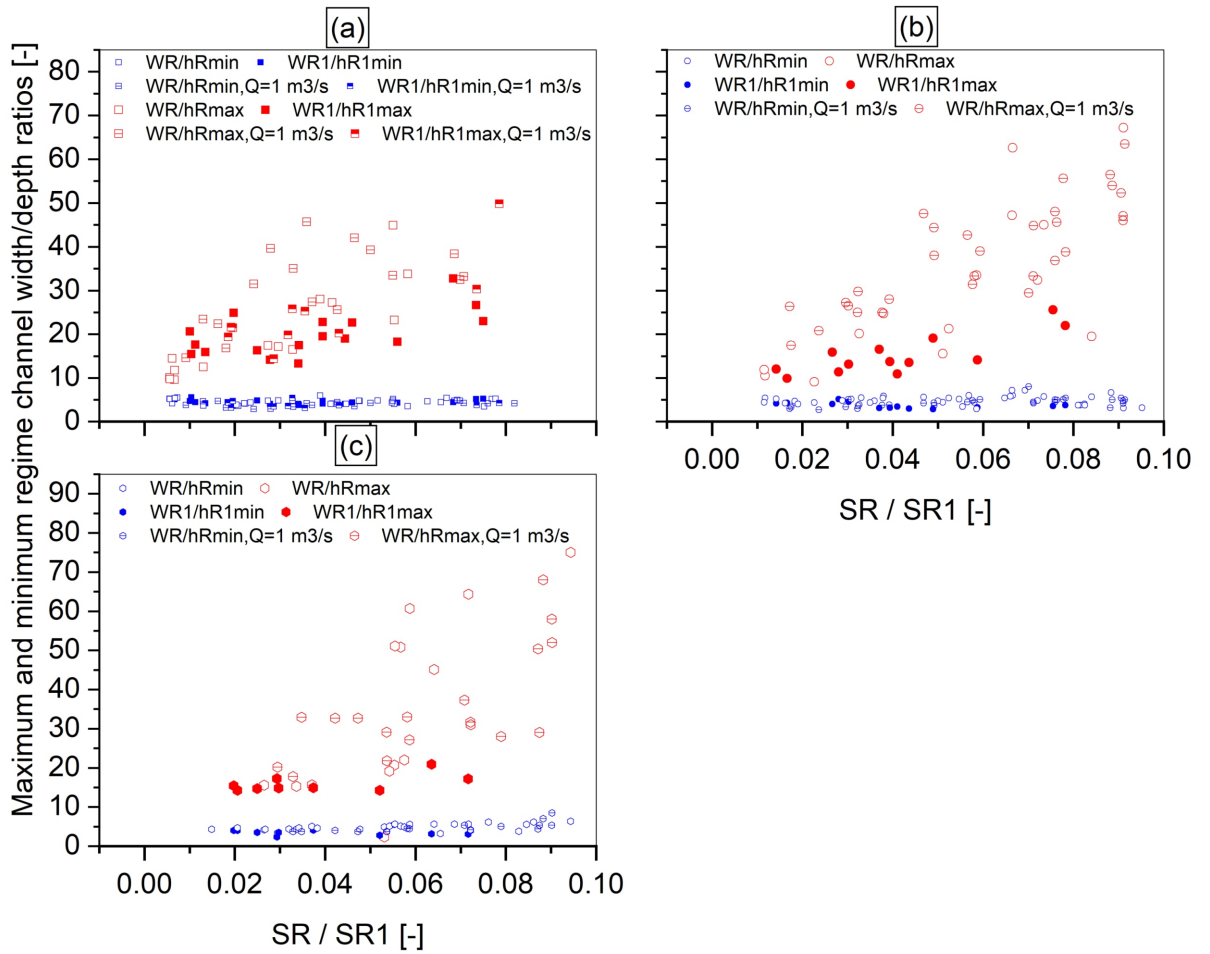


Figure B.3.: Maximum and minimum regime channel width to depth variations with channel regime slope for D_{m0} values of (a) 19.0 mm (b) 38.0 mm (c) 57.0 mm for fixed-width channels

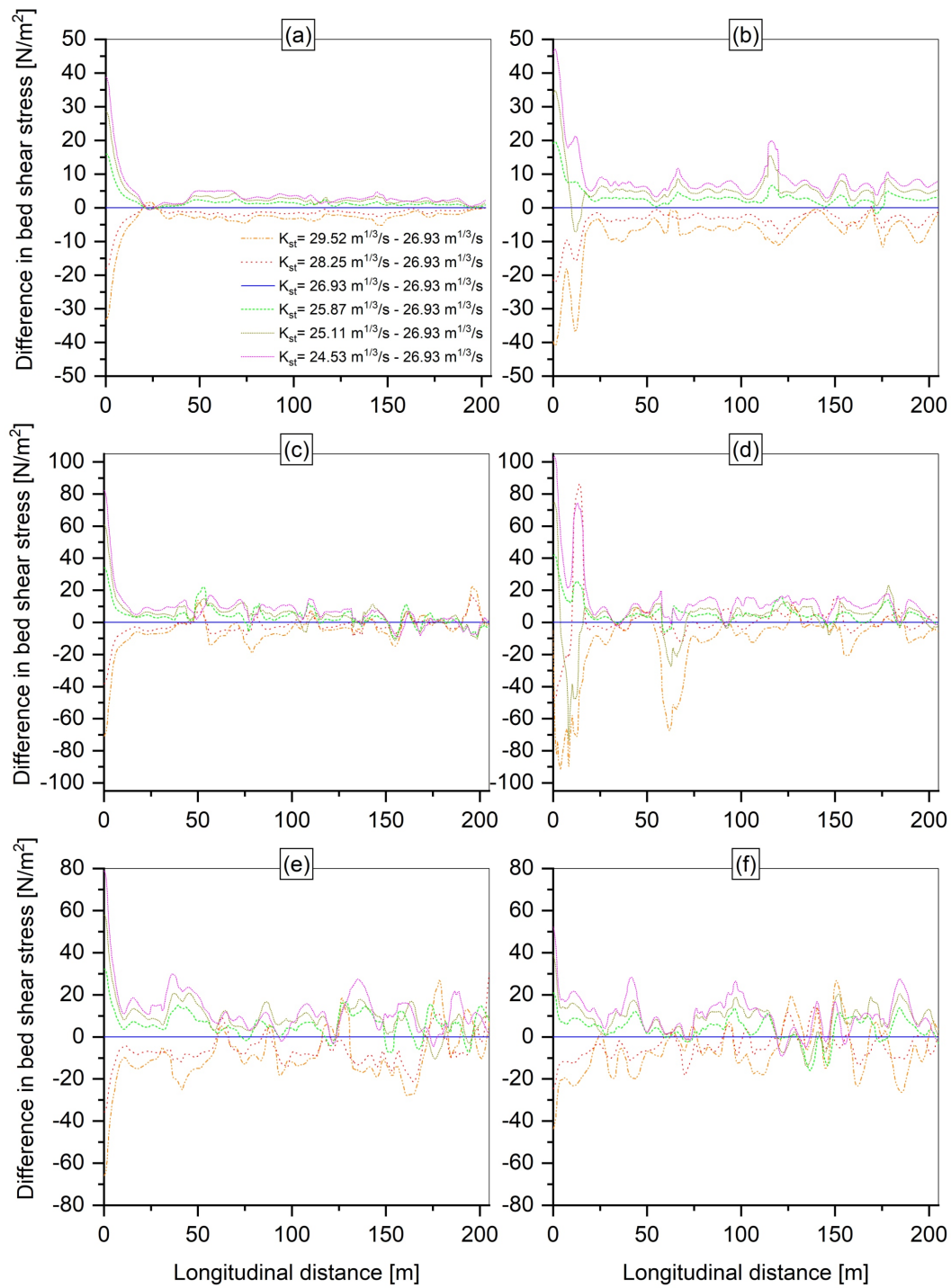


Figure B.4.: Difference in the bed shear stress arising from total roughness with respect to a reference roughness for channel regime slopes (a) 0.7% (b) 2.5% (c) 4.5% (d) 6.6% (e) 8.3% (f) 9.35%

C. Appendix C

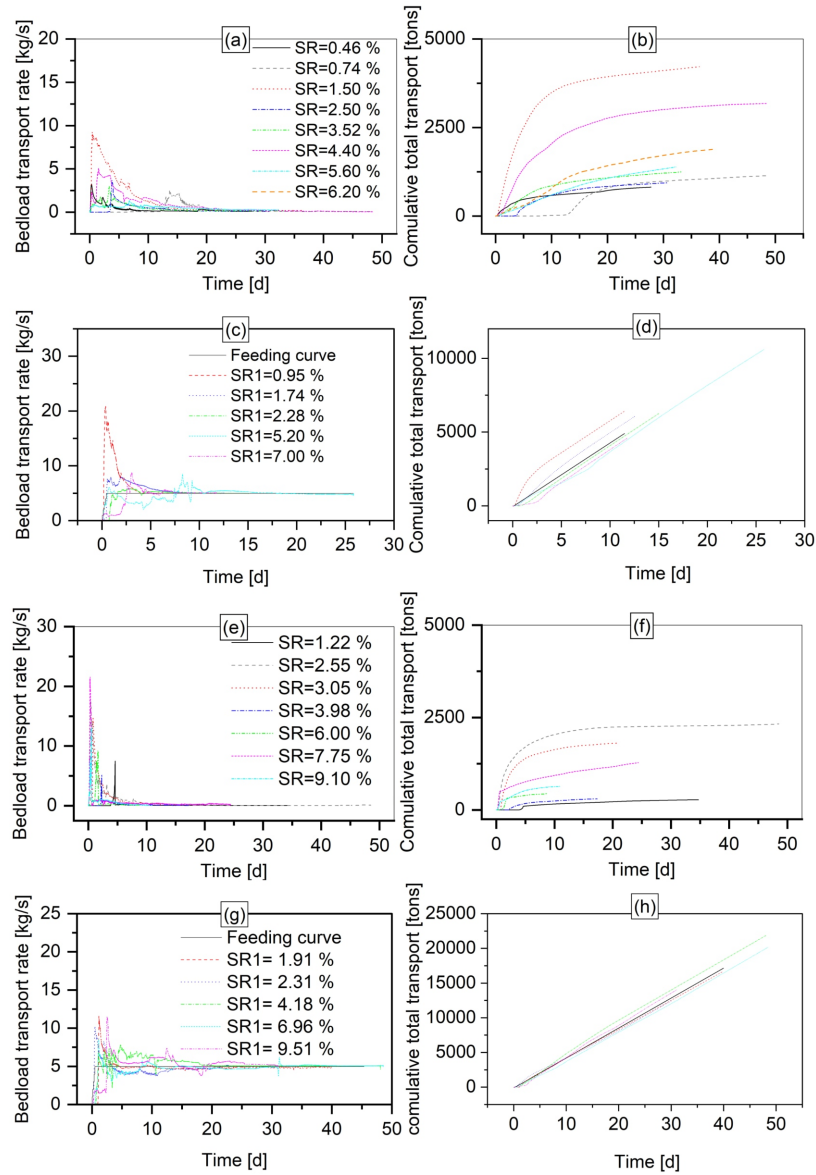


Figure C.1.: Bedload transport and their cumulative total transport variation over time at models' outflow for D_{m0} values 19.0 mm and 57.0 mm respectively in (a) (b) (c) (d) and (e) (f) (g) (h) for fixed-width channels

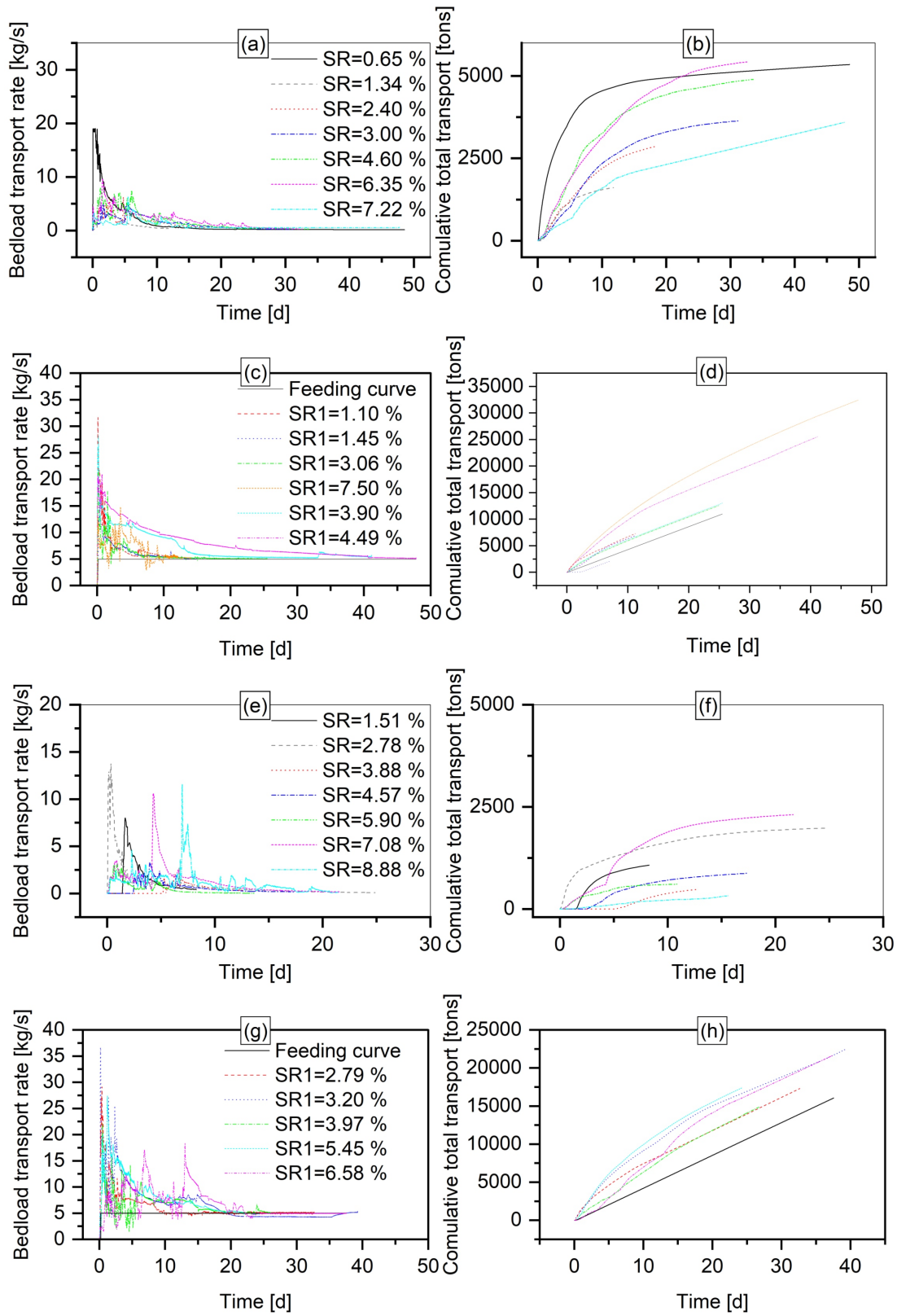


Figure C.2.: Bedload transport and their cumulative total transport variation over time at models' outflow for D_{mo} values 19.0 mm and 57.0 mm respectively in (a) (b) (c) (d) and (e) (f) (g) (h) for extended-width channels

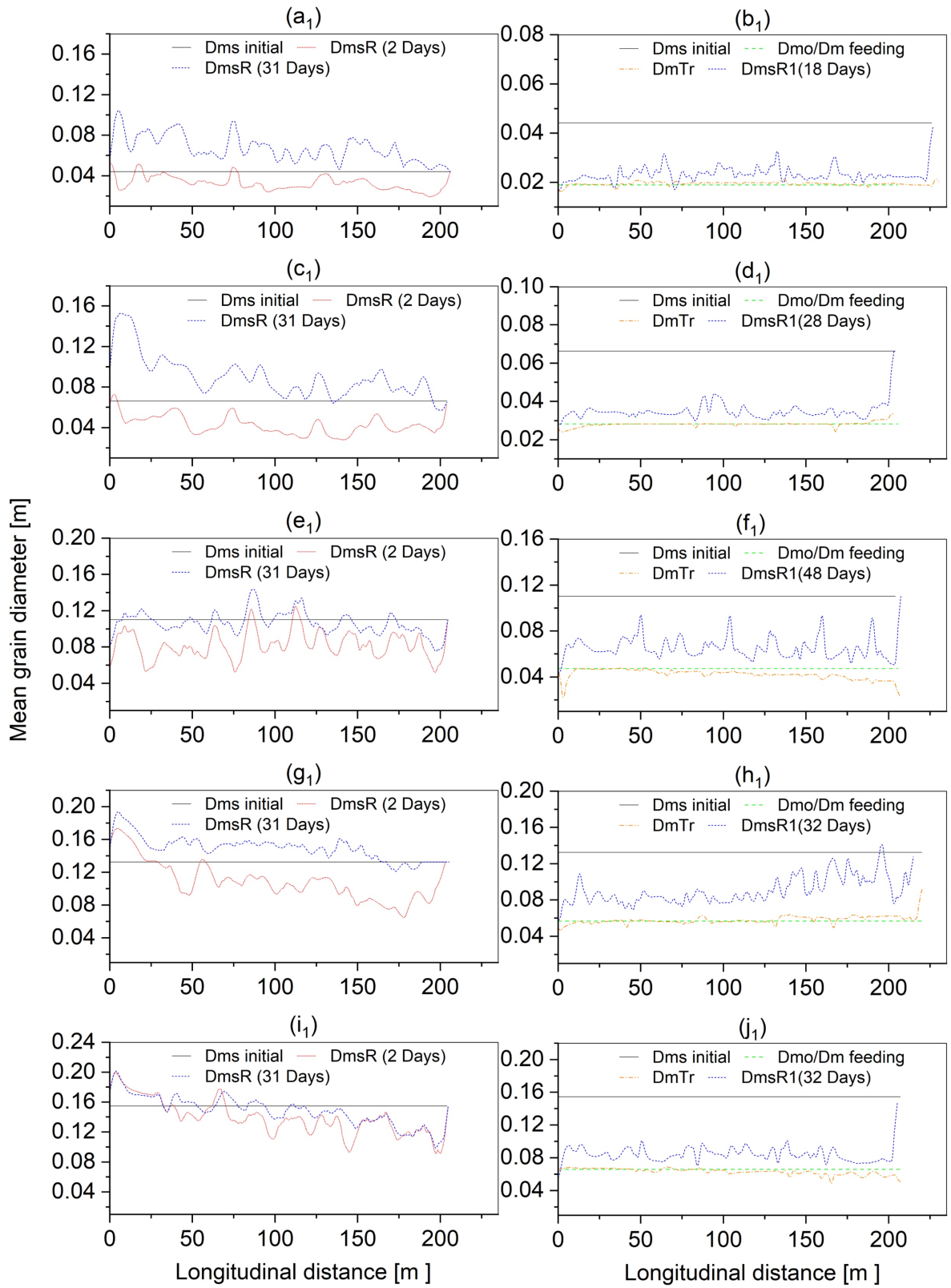


Figure C.3.: GSD at initial and regime state respectively for R and $R1$ regime channels for for D_{mo} values (a1), (b1) 19.0 mm (c1), (d1) 28.4 mm (e1), (f1) 47.3 mm (g1), (h1) 57.0 mm and (i1), (j1) 66.3 mm

D. Appendix D

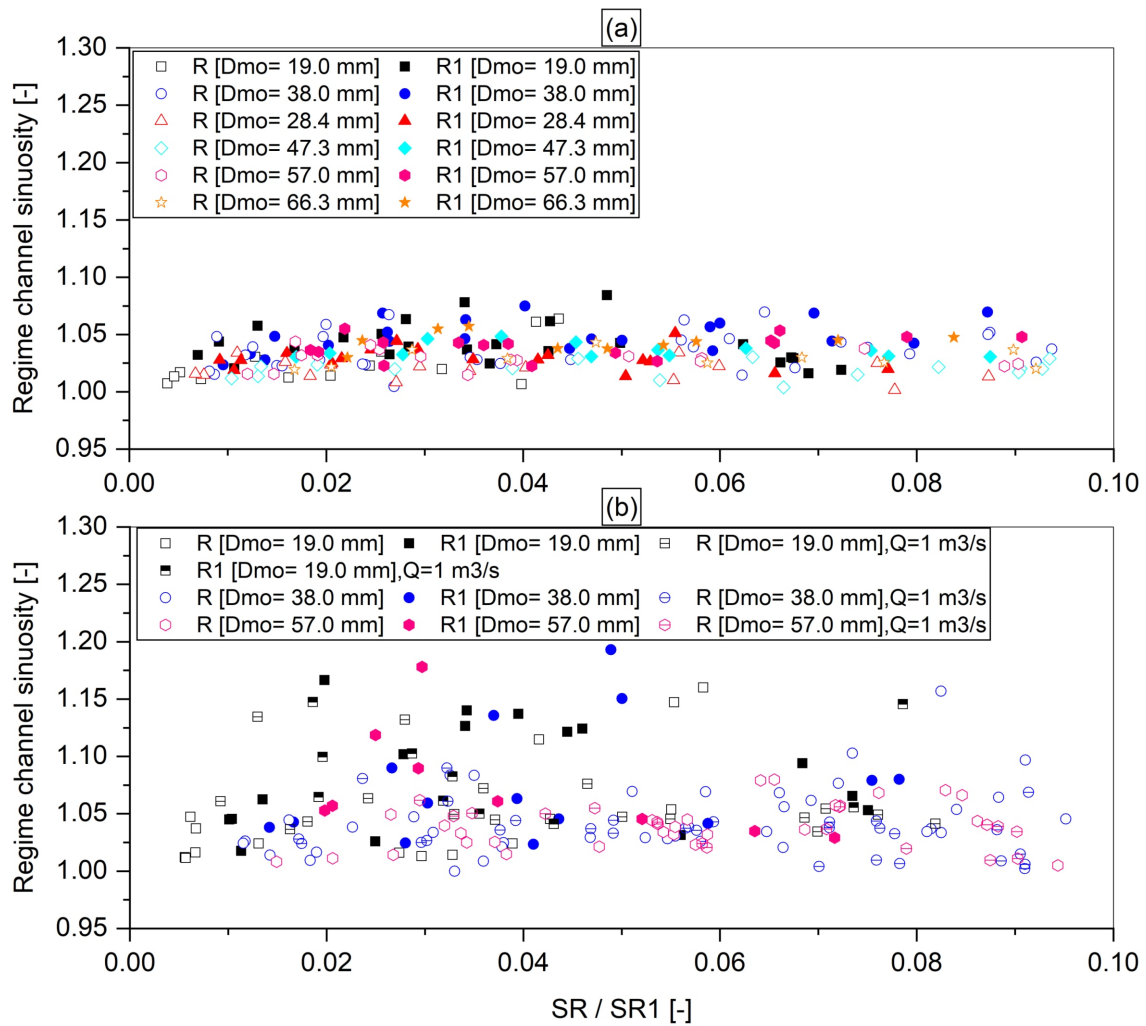


Figure D.1.: Regime channel sinuosity for all tested GSD in (a) *R* regime channel (b) *R1* regime channel

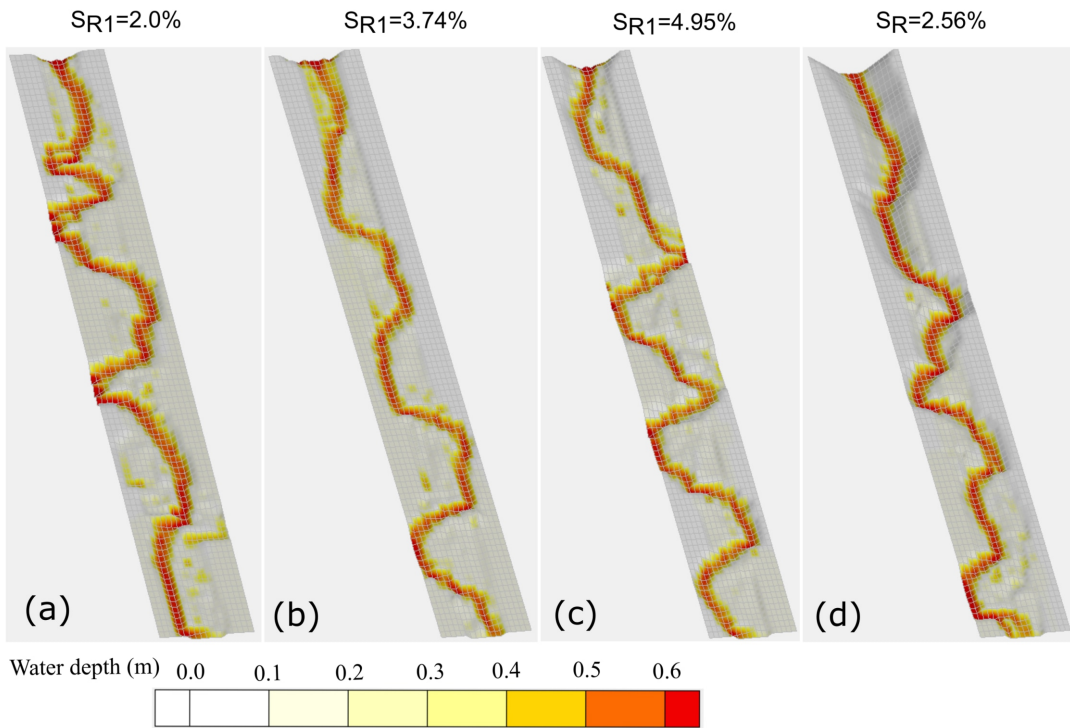


Figure D.2.: Plan-form development for R_1 channels are shown for some selected channel regime slopes

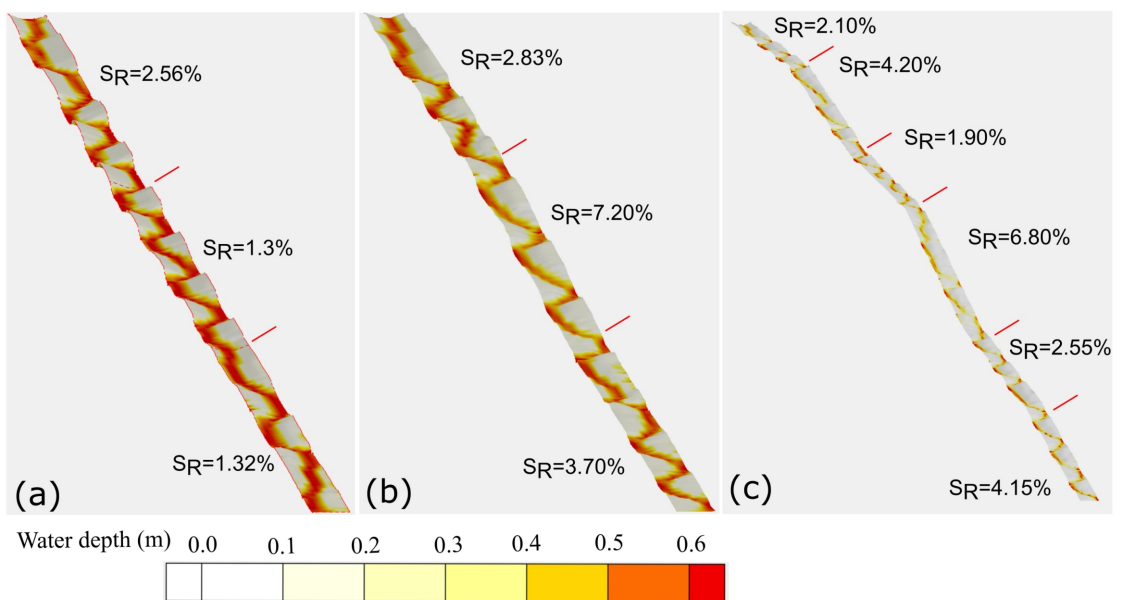


Figure D.3.: Plan-form development for three examples of slope combination cases 1, 2 and 3 respectively in (a), (b), and (c)

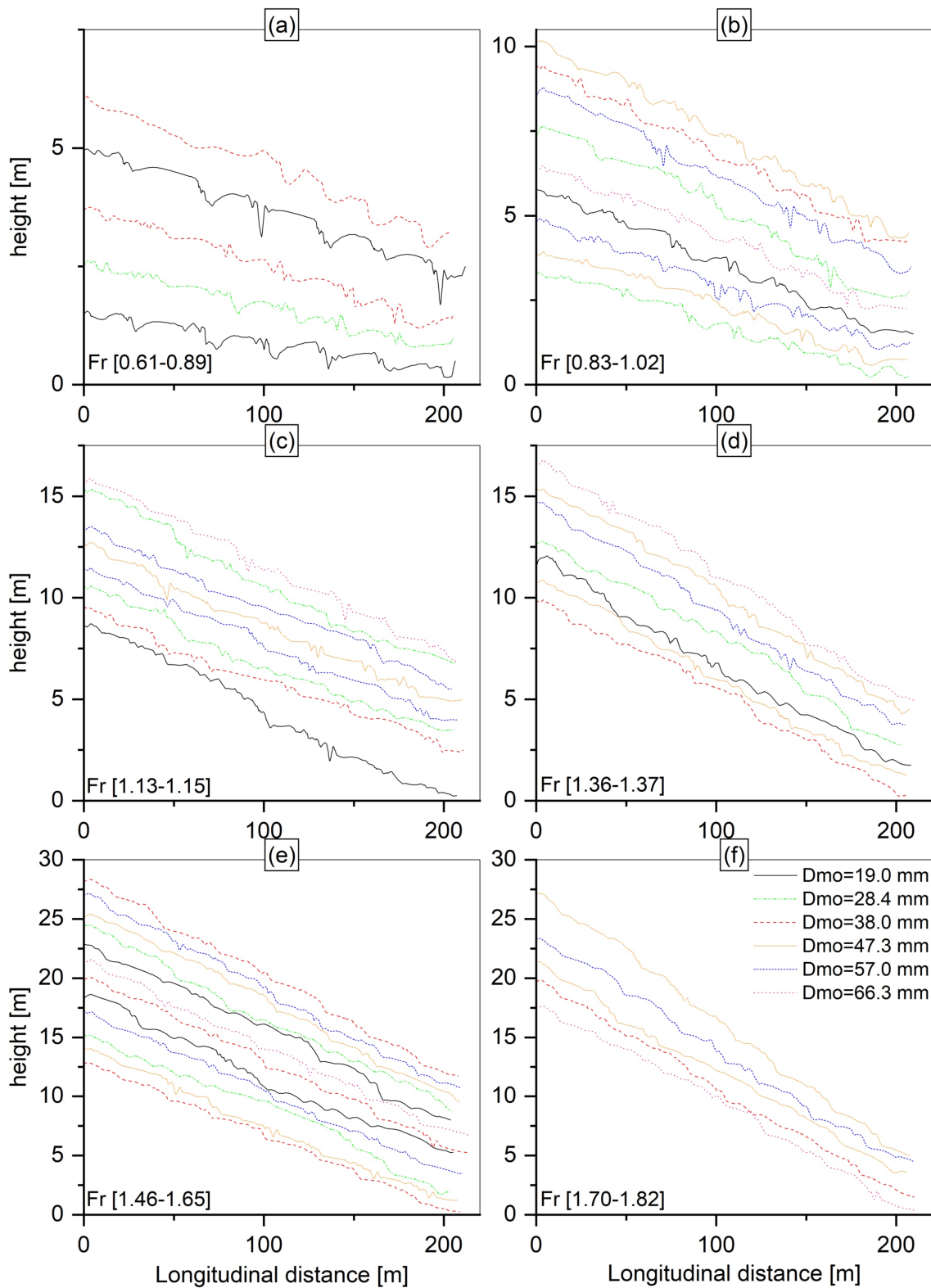


Figure D.4.: Longitudinal profiles for R1 fixed-width channels for regime slopes (a) 0.0-1.5% (b) 1.5-3.0% (c) 3.0-4.5% (d) 4.5-6.0% (e) 6.0-8.0% (f) 8.0-10.0%

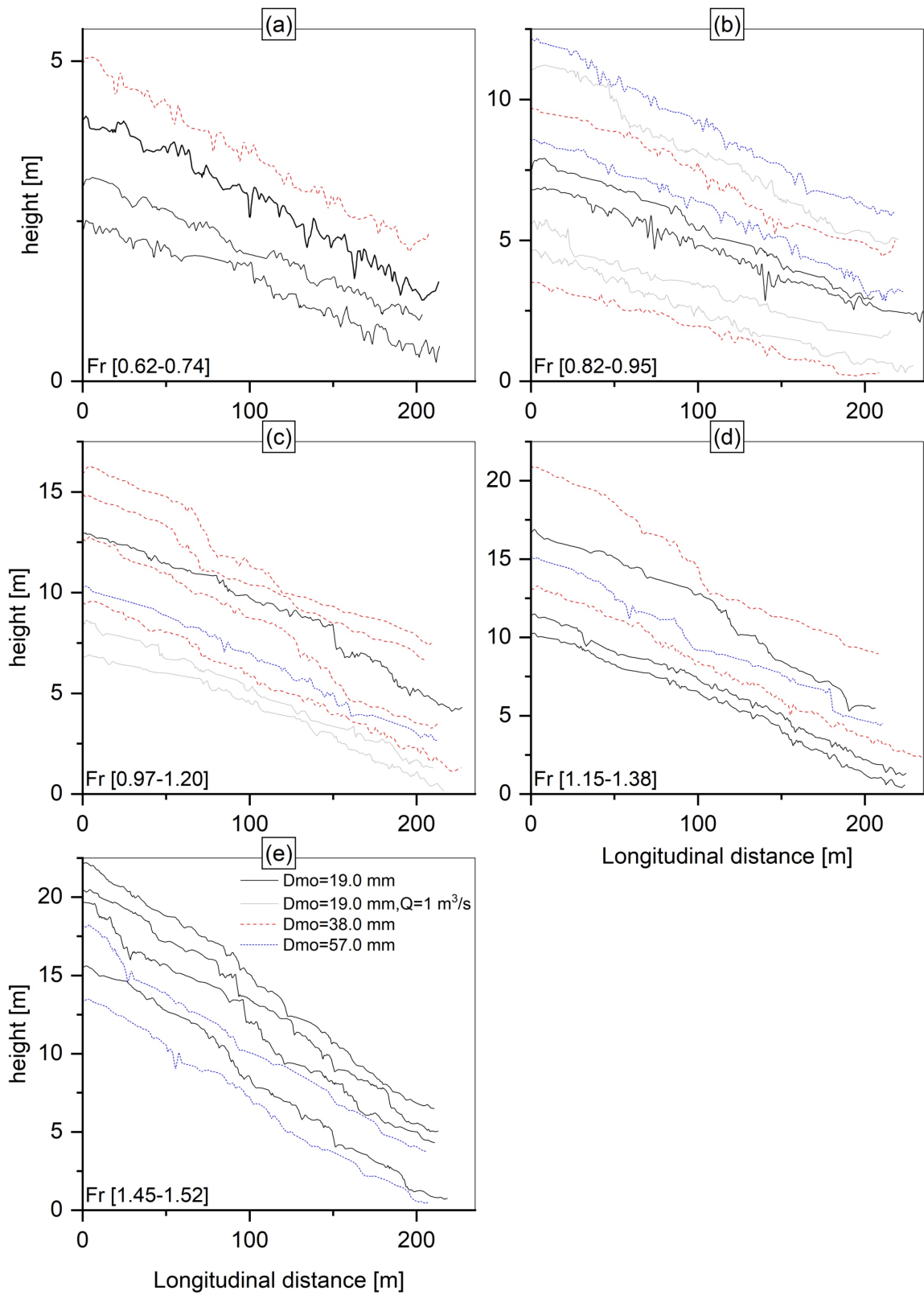


Figure D.5.: Longitudinal profiles for R1 extended-width channels for regime slopes (a) 0.0-1.5% (b) 1.5-3.0% (c) 3.0-4.5% (d) 4.5-6.0% (e) 6.0-8.0%

E. Appendix E

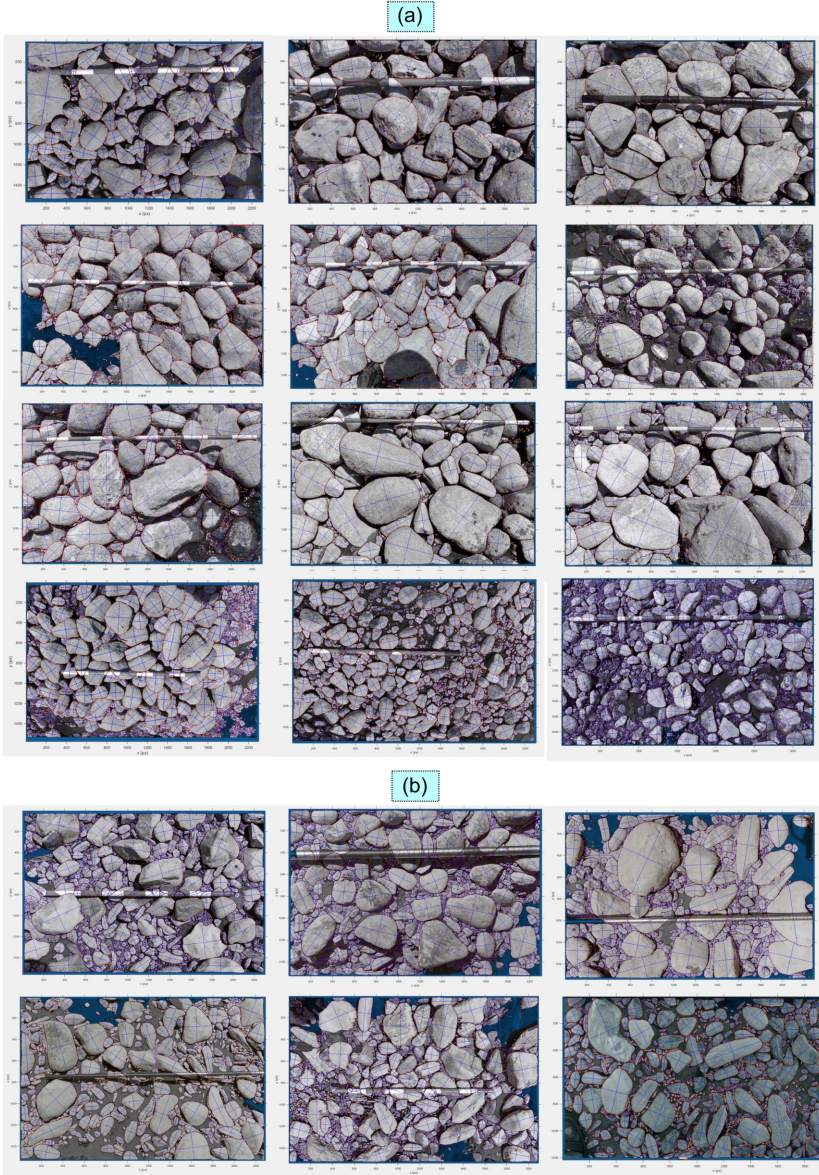


Figure E.1.: Photogrammetric analysis tool (Basegrain) of samples from (a) Shakar-Dara River (b) Maidan River

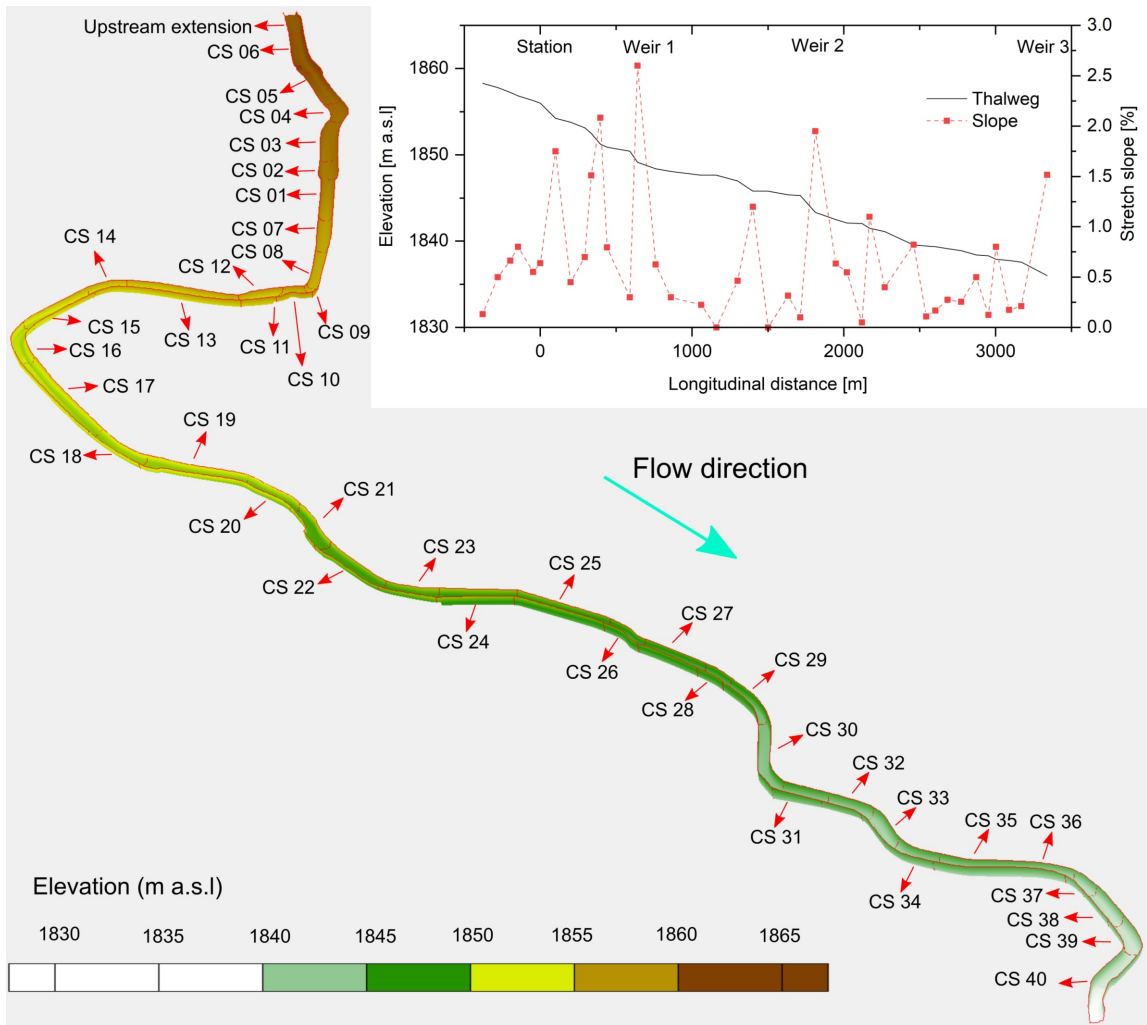


Figure E.2.: Plan-form development for R1 channels are shown for some selected channel regime slopes

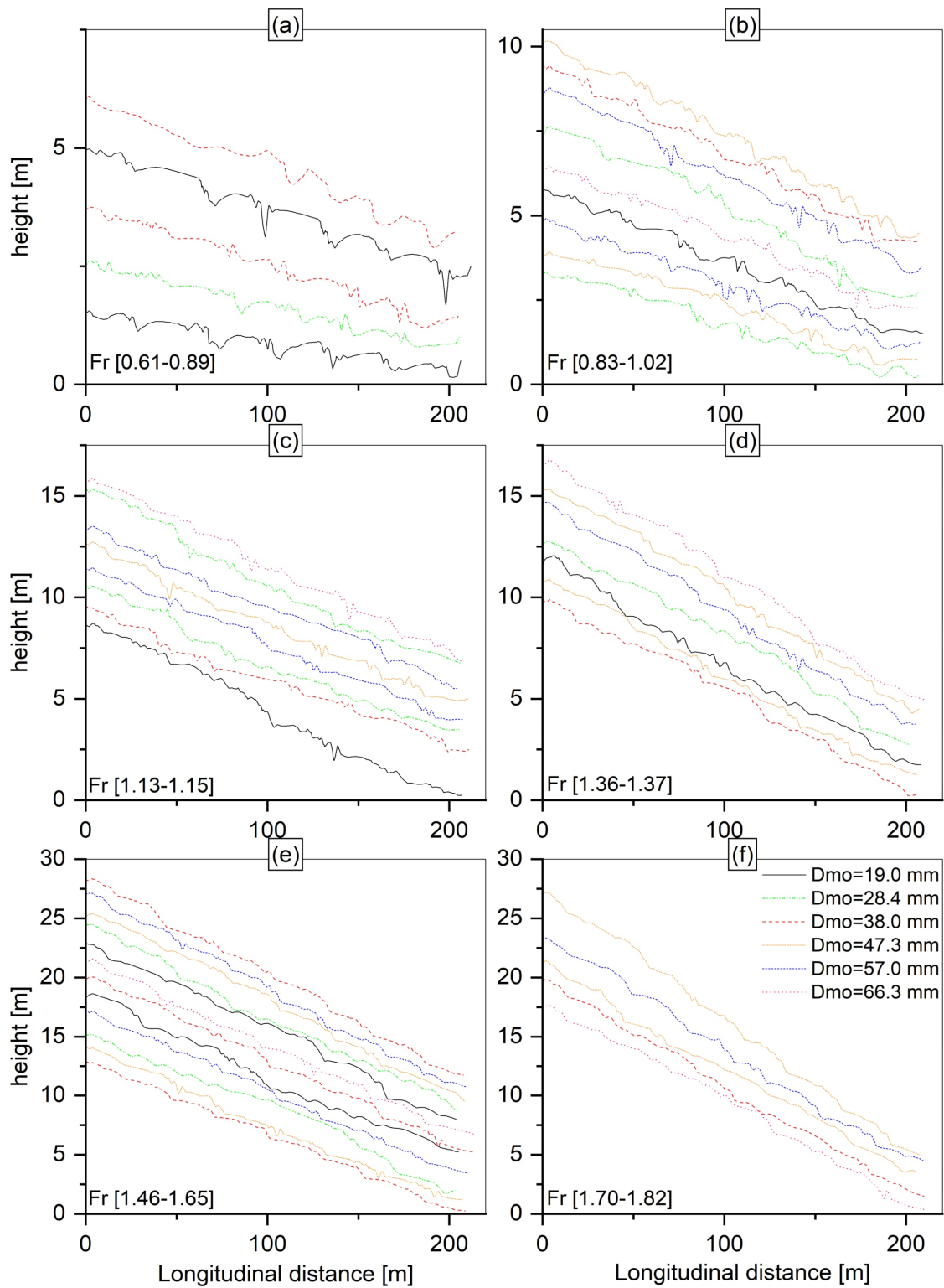


Figure E.3.: Longitudinal profiles for R1 fixed-width channels for regime slopes (a) 0.0-1.5% (b) 1.5-3.0% (c) 3.0-4.5% (d) 4.5-6.0% (e) 6.0-8.0% (f) 8.0-10.0%

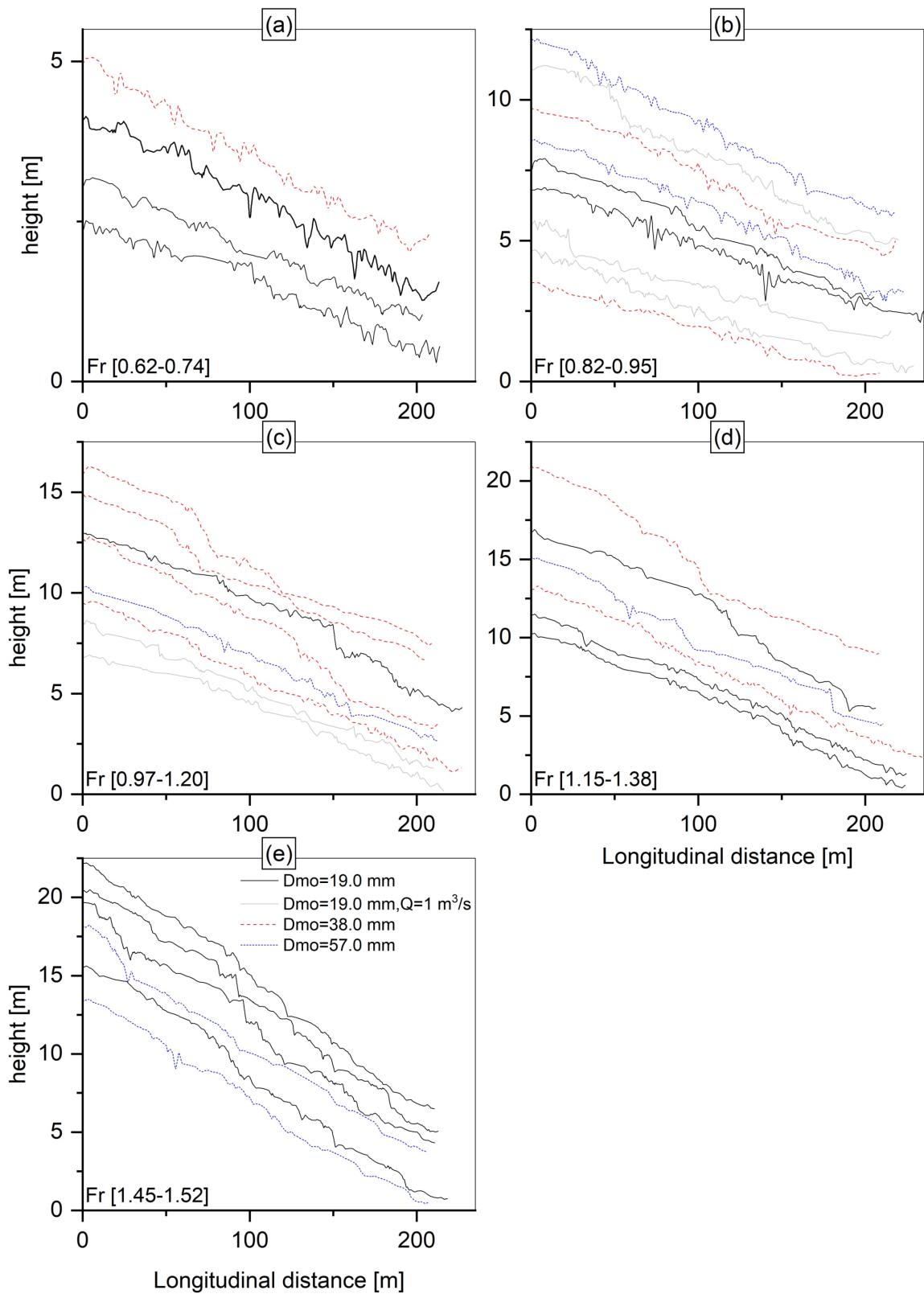
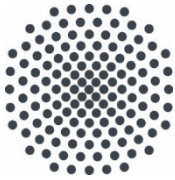


Figure E.4.: Longitudinal profiles for R1 extended-width channels for regime slopes (a) 0.0-1.5% (b) 1.5-3.0% (c) 3.0-4.5% (d) 4.5-6.0% (e) 6.0-8.0%



**Institut für Wasser- und
Umweltsystemmodellierung
Universität Stuttgart**

Pfaffenwaldring 61
70569 Stuttgart (Vaihingen)
Telefon (0711) 685 - 60156
Telefax (0711) 685 - 51073
E-Mail: iws@iws.uni-stuttgart.de
<http://www.iws.uni-stuttgart.de>

Direktoren

Prof. Dr. rer. nat. Dr.-Ing. András Bárdossy
Prof. Dr.-Ing. Rainer Helmig
Prof. Dr.-Ing. Wolfgang Nowak
Prof. Dr.-Ing. Silke Wieprecht

Emeriti

Prof. Dr.-Ing. habil. Dr.-Ing. E.h. Jürgen Giesecke
Prof. Dr.h.c. Dr.-Ing. E.h. Helmut Kobus, PhD

**Lehrstuhl für Wasserbau und
Wassermengenwirtschaft**

Leiterin: Prof. Dr.-Ing. Silke Wieprecht
Stellv.: Dr.-Ing. Kristina Terheiden
Versuchsanstalt für Wasserbau
Leiter: Stefan Haun, PhD

**Lehrstuhl für Hydromechanik
und Hydrosystemmodellierung**

Leiter: Prof. Dr.-Ing. Rainer Helmig
Stellv.: apl. Prof. Dr.-Ing. Holger Class

Lehrstuhl für Hydrologie und Geohydrologie

Leiter: Prof. Dr. rer. nat. Dr.-Ing. András Bárdossy
Stellv.: Dr. rer. nat. Jochen Seidel
Hydrogeophysik der Vadosen Zone
(mit Forschungszentrum Jülich)
Leiter: Prof. Dr. J.A. Sander Huisman

**Lehrstuhl für Stochastische Simulation und
Sicherheitsforschung für Hydrosysteme**

Leiter: Prof. Dr.-Ing. Wolfgang Nowak
Stellv.: apl. Prof. Dr.-Ing. Sergey Oladyskhin

**VEGAS, Versuchseinrichtung zur
Grundwasser- und Altlastensanierung**

Leiter: Dr.-Ing. Simon Kleinknecht
PD Dr.-Ing. Claus Haslauer

Verzeichnis der Mitteilungshefte

- 1 Röhnisch, Arthur: *Die Bemühungen um eine Wasserbauliche Versuchsanstalt an der Technischen Hochschule Stuttgart*, und Fattah Abouleid, Abdel: *Beitrag zur Berechnung einer in lockeren Sand gerammten, zweifach verankerten Spundwand*, 1963
- 2 Marotz, Günter: *Beitrag zur Frage der Standfestigkeit von dichten Asphaltbelägen im Großwasserbau*, 1964
- 3 Gurr, Siegfried: *Beitrag zur Berechnung zusammengesetzter ebener Flächentragwerke unter besonderer Berücksichtigung ebener Stauwände, mit Hilfe von Randwert- und Lastwertmatrizen*, 1965
- 4 Plica, Peter: *Ein Beitrag zur Anwendung von Schalenkonstruktionen im Stahlwasserbau*, und Petrikat, Kurt: *Möglichkeiten und Grenzen des wasserbaulichen Versuchswesens*, 1966

- 5 Plate, Erich: *Beitrag zur Bestimmung der Windgeschwindigkeitsverteilung in der durch eine Wand gestörten bodennahen Luftschicht*, und Röhnisch, Arthur; Marotz, Günter: *Neue Baustoffe und Bauausführungen für den Schutz der Böschungen und der Sohle von Kanälen, Flüssen und Häfen; Gesteungskosten und jeweilige Vorteile*, sowie Unny, T.E.: *Schwingungsuntersuchungen am Kegelstrahlschieber*, 1967
- 6 Seiler, Erich: *Die Ermittlung des Anlagenwertes der bundeseigenen Binnenschiffahrtsstraßen und Talsperren und des Anteils der Binnenschifffahrt an diesem Wert*, 1967
- 7 *Sonderheft anlässlich des 65. Geburtstages von Prof. Arthur Röhnisch mit Beiträgen von* Benk, Dieter; Breitling, J.; Gurr, Siegfried; Haberhauer, Robert; Honekamp, Hermann; Kuz, Klaus Dieter; Marotz, Günter; Mayer-Vorfelder, Hans-Jörg; Miller, Rudolf; Plate, Erich J.; Radomski, Helge; Schwarz, Helmut; Vollmer, Ernst; Wildenhahn, Eberhard; 1967
- 8 Jumikis, Alfred: *Beitrag zur experimentellen Untersuchung des Wassernachschubs in einem gefrierenden Boden und die Beurteilung der Ergebnisse*, 1968
- 9 Marotz, Günter: *Technische Grundlagen einer Wasserspeicherung im natürlichen Untergrund*, 1968
- 10 Radomski, Helge: *Untersuchungen über den Einfluß der Querschnittsform wellenförmiger Spundwände auf die statischen und rammtechnischen Eigenschaften*, 1968
- 11 Schwarz, Helmut: *Die Grenztragfähigkeit des Baugrundes bei Einwirkung vertikal gezogener Ankerplatten als zweidimensionales Bruchproblem*, 1969
- 12 Erbel, Klaus: *Ein Beitrag zur Untersuchung der Metamorphose von Mittelgebirgsschneedecken unter besonderer Berücksichtigung eines Verfahrens zur Bestimmung der thermischen Schneequalität*, 1969
- 13 Westhaus, Karl-Heinz: *Der Strukturwandel in der Binnenschifffahrt und sein Einfluß auf den Ausbau der Binnenschiffskanäle*, 1969
- 14 Mayer-Vorfelder, Hans-Jörg: *Ein Beitrag zur Berechnung des Erdwiderstandes unter Ansatz der logarithmischen Spirale als Gleitflächenfunktion*, 1970
- 15 Schulz, Manfred: *Berechnung des räumlichen Erddruckes auf die Wandung kreiszylindrischer Körper*, 1970
- 16 Mobasseri, Manoutschehr: *Die Rippenstützmauer. Konstruktion und Grenzen ihrer Standsicherheit*, 1970
- 17 Benk, Dieter: *Ein Beitrag zum Betrieb und zur Bemessung von Hochwasserrückhaltebecken*, 1970
- 18 Gàl, Attila: *Bestimmung der mitschwingenden Wassermasse bei überströmten Fischbauchklappen mit kreiszylindrischem Staublech*, 1971, vergriffen
- 19 Kuz, Klaus Dieter: *Ein Beitrag zur Frage des Einsetzens von Kavitationserscheinungen in einer Düsenströmung bei Berücksichtigung der im Wasser gelösten Gase*, 1971, vergriffen
- 20 Schaak, Hartmut: *Verteilleitungen von Wasserkraftanlagen*, 1971
- 21 *Sonderheft zur Eröffnung der neuen Versuchsanstalt des Instituts für Wasserbau der Universität Stuttgart mit Beiträgen von* Brombach, Hansjörg; Dirksen, Wolfram; Gàl, Attila; Gerlach, Reinhard; Giesecke, Jürgen; Holthoff, Franz-Josef; Kuz, Klaus Dieter; Marotz, Günter; Minor, Hans-Erwin; Petrikat, Kurt; Röhnisch, Arthur; Rueff, Helge; Schwarz, Helmut; Vollmer, Ernst; Wildenhahn, Eberhard; 1972
- 22 Wang, Chung-su: *Ein Beitrag zur Berechnung der Schwingungen an Kegelstrahlschiebern*, 1972
- 23 Mayer-Vorfelder, Hans-Jörg: *Erdwiderstandsbeiwerte nach dem Ohde-Variationsverfahren*, 1972
- 24 Minor, Hans-Erwin: *Beitrag zur Bestimmung der Schwingungsanfachungsfunktionen überströmter Stauklappen*, 1972, vergriffen

- 25 Brombach, Hansjörg: *Untersuchung strömungsmechanischer Elemente (Fluidik) und die Möglichkeit der Anwendung von Wirbelkammerelementen im Wasserbau*, 1972, vergriffen
- 26 Wildenhahn, Eberhard: *Beitrag zur Berechnung von Horizontalfilterbrunnen*, 1972
- 27 Steinlein, Helmut: *Die Eliminierung der Schwebstoffe aus Flußwasser zum Zweck der unterirdischen Wasserspeicherung, gezeigt am Beispiel der Iller*, 1972
- 28 Holthoff, Franz Josef: *Die Überwindung großer Hubhöhen in der Binnenschifffahrt durch Schwimmerhebwerke*, 1973
- 29 Röder, Karl: *Einwirkungen aus Baugrundbewegungen auf trog- und kastenförmige Konstruktionen des Wasser- und Tunnelbaues*, 1973
- 30 Kretschmer, Heinz: *Die Bemessung von Bogenstaumauern in Abhängigkeit von der Talform*, 1973
- 31 Honekamp, Hermann: *Beitrag zur Berechnung der Montage von Unterwasserpipelines*, 1973
- 32 Giesecke, Jürgen: *Die Wirbelkammertriode als neuartiges Steuerorgan im Wasserbau*, und Brombach, Hansjörg: *Entwicklung, Bauformen, Wirkungsweise und Steuereigenschaften von Wirbelkammerverstärkern*, 1974
- 33 Rueff, Helge: *Untersuchung der schwingungserregenden Kräfte an zwei hintereinander angeordneten Tiefschützen unter besonderer Berücksichtigung von Kavitation*, 1974
- 34 Röhnisch, Arthur: *Einpreßversuche mit Zementmörtel für Spannbeton - Vergleich der Ergebnisse von Modellversuchen mit Ausführungen in Hüllwellrohren*, 1975
- 35 *Sonderheft anlässlich des 65. Geburtstages von Prof. Dr.-Ing. Kurt Petrikat mit Beiträgen von:* Brombach, Hansjörg; Erbel, Klaus; Flinspach, Dieter; Fischer jr., Richard; Gàl, Attila; Gerlach, Reinhard; Giesecke, Jürgen; Haberhauer, Robert; Hafner Edzard; Hausenblas, Bernhard; Horlacher, Hans-Burkhard; Hutarew, Andreas; Knoll, Manfred; Krummet, Ralph; Marotz, Günter; Merkle, Theodor; Miller, Christoph; Minor, Hans-Erwin; Neumayer, Hans; Rao, Syamala; Rath, Paul; Rueff, Helge; Ruppert, Jürgen; Schwarz, Wolfgang; Topal-Gökceli, Mehmet; Vollmer, Ernst; Wang, Chung-su; Weber, Hans-Georg; 1975
- 36 Berger, Jochum: *Beitrag zur Berechnung des Spannungszustandes in rotationssymmetrisch belasteten Kugelschalen veränderlicher Wandstärke unter Gas- und Flüssigkeitsdruck durch Integration schwach singulärer Differentialgleichungen*, 1975
- 37 Dirksen, Wolfram: *Berechnung instationärer Abflußvorgänge in gestauten Gerinnen mittels Differenzenverfahren und die Anwendung auf Hochwasserrückhaltebecken*, 1976
- 38 Horlacher, Hans-Burkhard: *Berechnung instationärer Temperatur- und Wärmespannungsfelder in langen mehrschichtigen Hohlzylindern*, 1976
- 39 Hafner, Edzard: *Untersuchung der hydrodynamischen Kräfte auf Baukörper im Tiefwasserbereich des Meeres*, 1977, ISBN 3-921694-39-6
- 40 Ruppert, Jürgen: *Über den Axialwirbelkammerverstärker für den Einsatz im Wasserbau*, 1977, ISBN 3-921694-40-X
- 41 Hutarew, Andreas: *Beitrag zur Beeinflußbarkeit des Sauerstoffgehalts in Fließgewässern an Abstürzen und Wehren*, 1977, ISBN 3-921694-41-8, vergriffen
- 42 Miller, Christoph: *Ein Beitrag zur Bestimmung der schwingungserregenden Kräfte an unterströmten Wehren*, 1977, ISBN 3-921694-42-6
- 43 Schwarz, Wolfgang: *Druckstoßberechnung unter Berücksichtigung der Radial- und Längsverschiebungen der Rohrwandung*, 1978, ISBN 3-921694-43-4
- 44 Kinzelbach, Wolfgang: *Numerische Untersuchungen über den optimalen Einsatz variabler Kühlsysteme einer Kraftwerkskette am Beispiel Oberrhein*, 1978, ISBN 3-921694-44-2
- 45 Barczewski, Baldur: *Neue Meßmethoden für Wasser-Luftgemische und deren Anwendung auf zweiphasige Auftriebsstrahlen*, 1979, ISBN 3-921694-45-0

- 46 Neumayer, Hans: *Untersuchung der Strömungsvorgänge in radialen Wirbelkammerverstärkern*, 1979, ISBN 3-921694-46-9
- 47 Elalfy, Youssef-Elhassan: *Untersuchung der Strömungsvorgänge in Wirbelkammerdiolen und -drosseln*, 1979, ISBN 3-921694-47-7
- 48 Brombach, Hansjörg: *Automatisierung der Bewirtschaftung von Wasserspeichern*, 1981, ISBN 3-921694-48-5
- 49 Geldner, Peter: *Deterministische und stochastische Methoden zur Bestimmung der Selbstdichtung von Gewässern*, 1981, ISBN 3-921694-49-3, vergriffen
- 50 Mehlhorn, Hans: *Temperaturveränderungen im Grundwasser durch Brauchwassereingleitungen*, 1982, ISBN 3-921694-50-7, vergriffen
- 51 Hafner, Edzard: *Rohrleitungen und Behälter im Meer*, 1983, ISBN 3-921694-51-5
- 52 Rinnert, Bernd: *Hydrodynamische Dispersion in porösen Medien: Einfluß von Dichteunterschieden auf die Vertikalvermischung in horizontaler Strömung*, 1983, ISBN 3-921694-52-3, vergriffen
- 53 Lindner, Wulf: *Steuerung von Grundwasserentnahmen unter Einhaltung ökologischer Kriterien*, 1983, ISBN 3-921694-53-1, vergriffen
- 54 Herr, Michael; Herzer, Jörg; Kinzelbach, Wolfgang; Kobus, Helmut; Rinnert, Bernd: *Methoden zur rechnerischen Erfassung und hydraulischen Sanierung von Grundwasserkontaminationen*, 1983, ISBN 3-921694-54-X
- 55 Schmitt, Paul: *Wege zur Automatisierung der Niederschlagsermittlung*, 1984, ISBN 3-921694-55-8, vergriffen
- 56 Müller, Peter: *Transport und selektive Sedimentation von Schwebstoffen bei gestautem Abfluß*, 1985, ISBN 3-921694-56-6
- 57 El-Qawasmeh, Fuad: *Möglichkeiten und Grenzen der Tropfbewässerung unter besonderer Berücksichtigung der Verstopfungsanfälligkeit der Tropfelemente*, 1985, ISBN 3-921694-57-4, vergriffen
- 58 Kirchenbaur, Klaus: *Mikroprozessorgesteuerte Erfassung instationärer Druckfelder am Beispiel seegangsbelasteter Baukörper*, 1985, ISBN 3-921694-58-2
- 59 Kobus, Helmut (Hrsg.): *Modellierung des großräumigen Wärme- und Schadstofftransports im Grundwasser*, Tätigkeitsbericht 1984/85 (DFG-Forschergruppe an den Universitäten Hohenheim, Karlsruhe und Stuttgart), 1985, ISBN 3-921694-59-0, vergriffen
- 60 Spitz, Karlheinz: *Dispersion in porösen Medien: Einfluß von Inhomogenitäten und Dichteunterschieden*, 1985, ISBN 3-921694-60-4, vergriffen
- 61 Kobus, Helmut: *An Introduction to Air-Water Flows in Hydraulics*, 1985, ISBN 3-921694-61-2
- 62 Kaleris, Vassilios: *Erfassung des Austausches von Oberflächen- und Grundwasser in horizontalebene Grundwassermodellen*, 1986, ISBN 3-921694-62-0
- 63 Herr, Michael: *Grundlagen der hydraulischen Sanierung verunreinigter Porengrundwasserleiter*, 1987, ISBN 3-921694-63-9
- 64 Marx, Walter: *Berechnung von Temperatur und Spannung in Massenbeton infolge Hydratation*, 1987, ISBN 3-921694-64-7
- 65 Koschitzky, Hans-Peter: *Dimensionierungskonzept für Sohlbelüfter in Schußrinnen zur Vermeidung von Kavitationsschäden*, 1987, ISBN 3-921694-65-5
- 66 Kobus, Helmut (Hrsg.): *Modellierung des großräumigen Wärme- und Schadstofftransports im Grundwasser*, Tätigkeitsbericht 1986/87 (DFG-Forschergruppe an den Universitäten Hohenheim, Karlsruhe und Stuttgart) 1987, ISBN 3-921694-66-3
- 67 Söll, Thomas: *Berechnungsverfahren zur Abschätzung anthropogener Temperaturanomalien im Grundwasser*, 1988, ISBN 3-921694-67-1
- 68 Dittrich, Andreas; Westrich, Bernd: *Bodenseeufererosion, Bestandsaufnahme und Bewertung*, 1988, ISBN 3-921694-68-X, vergriffen

- 69 Huwe, Bernd; van der Ploeg, Rienk R.: *Modelle zur Simulation des Stickstoffhaushaltes von Standorten mit unterschiedlicher landwirtschaftlicher Nutzung*, 1988, ISBN 3-921694-69-8, vergriffen
- 70 Stephan, Karl: *Integration elliptischer Funktionen*, 1988, ISBN 3-921694-70-1
- 71 Kobus, Helmut; Zilliox, Lothaire (Hrsg.): *Nitratbelastung des Grundwassers, Auswirkungen der Landwirtschaft auf die Grundwasser- und Rohwasserbeschaffenheit und Maßnahmen zum Schutz des Grundwassers*. Vorträge des deutsch-französischen Kolloquiums am 6. Oktober 1988, Universitäten Stuttgart und Louis Pasteur Strasbourg (Vorträge in deutsch oder französisch, Kurzfassungen zweisprachig), 1988, ISBN 3-921694-71-X
- 72 Soyeaux, Renald: *Unterströmung von Stauanlagen auf klüftigem Untergrund unter Berücksichtigung laminarer und turbulenter Fließzustände*, 1991, ISBN 3-921694-72-8
- 73 Kohane, Roberto: *Berechnungsmethoden für Hochwasserabfluß in Fließgewässern mit überströmten Vorländern*, 1991, ISBN 3-921694-73-6
- 74 Hassinger, Reinhard: *Beitrag zur Hydraulik und Bemessung von Blocksteinrampen in flexibler Bauweise*, 1991, ISBN 3-921694-74-4, vergriffen
- 75 Schäfer, Gerhard: *Einfluß von Schichtenstrukturen und lokalen Einlagerungen auf die Längsdispersion in Porengrundwasserleitern*, 1991, ISBN 3-921694-75-2
- 76 Giesecke, Jürgen: *Vorträge, Wasserwirtschaft in stark besiedelten Regionen; Umweltforschung mit Schwerpunkt Wasserwirtschaft*, 1991, ISBN 3-921694-76-0
- 77 Huwe, Bernd: *Deterministische und stochastische Ansätze zur Modellierung des Stickstoffhaushalts landwirtschaftlich genutzter Flächen auf unterschiedlichem Skalenniveau*, 1992, ISBN 3-921694-77-9, vergriffen
- 78 Rommel, Michael: *Verwendung von Kluffdaten zur realitätsnahen Generierung von Kluffnetzen mit anschließender laminar-turbulenter Strömungsberechnung*, 1993, ISBN 3-92 1694-78-7
- 79 Marschall, Paul: *Die Ermittlung lokaler Stofffrachten im Grundwasser mit Hilfe von Einbohrloch-Meßverfahren*, 1993, ISBN 3-921694-79-5, vergriffen
- 80 Ptak, Thomas: *Stofftransport in heterogenen Porenaquiferen: Felduntersuchungen und stochastische Modellierung*, 1993, ISBN 3-921694-80-9, vergriffen
- 81 Haakh, Frieder: *Transientes Strömungsverhalten in Wirbelkammern*, 1993, ISBN 3-921694-81-7
- 82 Kobus, Helmut; Cirpka, Olaf; Barczewski, Baldur; Koschitzky, Hans-Peter: *Versuchseinrichtung zur Grundwasser- und Altlastensanierung VEGAS, Konzeption und Programmrahmen*, 1993, ISBN 3-921694-82-5
- 83 Zang, Weidong: *Optimaler Echtzeit-Betrieb eines Speichers mit aktueller Abflußregenerierung*, 1994, ISBN 3-921694-83-3, vergriffen
- 84 Franke, Hans-Jörg: *Stochastische Modellierung eines flächenhaften Stoffeintrages und Transports in Grundwasser am Beispiel der Pflanzenschutzmittelproblematik*, 1995, ISBN 3-921694-84-1
- 85 Lang, Ulrich: *Simulation regionaler Strömungs- und Transportvorgänge in Karstaquiferen mit Hilfe des Doppelkontinuum-Ansatzes: Methodenentwicklung und Parameteridentifikation*, 1995, ISBN 3-921694-85-X, vergriffen
- 86 Helmig, Rainer: *Einführung in die Numerischen Methoden der Hydromechanik*, 1996, ISBN 3-921694-86-8, vergriffen
- 87 Cirpka, Olaf: *CONTRACT: A Numerical Tool for Contaminant Transport and Chemical Transformations - Theory and Program Documentation -*, 1996, ISBN 3-921694-87-6
- 88 Haberlandt, Uwe: *Stochastische Synthese und Regionalisierung des Niederschlages für Schmutzfrachtberechnungen*, 1996, ISBN 3-921694-88-4
- 89 Croisé, Jean: *Extraktion von flüchtigen Chemikalien aus natürlichen Lockergesteinen mittels erzwungener Luftströmung*, 1996, ISBN 3-921694-89-2, vergriffen

- 90 Jorde, Klaus: *Ökologisch begründete, dynamische Mindestwasserregelungen bei Ausleitungskraftwerken*, 1997, ISBN 3-921694-90-6, vergriffen
- 91 Helmig, Rainer: *Gekoppelte Strömungs- und Transportprozesse im Untergrund - Ein Beitrag zur Hydrosystemmodellierung-*, 1998, ISBN 3-921694-91-4, vergriffen
- 92 Emmert, Martin: *Numerische Modellierung nichtisothermer Gas-Wasser Systeme in porösen Medien*, 1997, ISBN 3-921694-92-2
- 93 Kern, Ulrich: *Transport von Schweb- und Schadstoffen in staugeregelten Fließgewässern am Beispiel des Neckars*, 1997, ISBN 3-921694-93-0, vergriffen
- 94 Förster, Georg: *Druckstoßdämpfung durch große Luftblasen in Hochpunkten von Rohrleitungen 1997*, ISBN 3-921694-94-9
- 95 Cirpka, Olaf: *Numerische Methoden zur Simulation des reaktiven Mehrkomponententransports im Grundwasser*, 1997, ISBN 3-921694-95-7, vergriffen
- 96 Färber, Arne: *Wärmetransport in der ungesättigten Bodenzone: Entwicklung einer thermischen In-situ-Sanierungstechnologie*, 1997, ISBN 3-921694-96-5
- 97 Betz, Christoph: *Wasserdampfdestillation von Schadstoffen im porösen Medium: Entwicklung einer thermischen In-situ-Sanierungstechnologie*, 1998, SBN 3-921694-97-3
- 98 Xu, Yichun: *Numerical Modeling of Suspended Sediment Transport in Rivers*, 1998, ISBN 3-921694-98-1, vergriffen
- 99 Wüst, Wolfgang: *Geochemische Untersuchungen zur Sanierung CKW-kontaminierter Aquifere mit Fe(0)-Reaktionswänden*, 2000, ISBN 3-933761-02-2
- 100 Sheta, Hussam: *Simulation von Mehrphasenvorgängen in porösen Medien unter Einbeziehung von Hysterese-Effekten*, 2000, ISBN 3-933761-03-4
- 101 Ayros, Edwin: *Regionalisierung extremer Abflüsse auf der Grundlage statistischer Verfahren*, 2000, ISBN 3-933761-04-2, vergriffen
- 102 Huber, Ralf: *Compositional Multiphase Flow and Transport in Heterogeneous Porous Media*, 2000, ISBN 3-933761-05-0
- 103 Braun, Christopherus: *Ein Upscaling-Verfahren für Mehrphasenströmungen in porösen Medien*, 2000, ISBN 3-933761-06-9
- 104 Hofmann, Bernd: *Entwicklung eines rechnergestützten Managementsystems zur Beurteilung von Grundwasserschadensfällen*, 2000, ISBN 3-933761-07-7
- 105 Class, Holger: *Theorie und numerische Modellierung nichtisothermer Mehrphasenprozesse in NAPL-kontaminierten porösen Medien*, 2001, ISBN 3-933761-08-5
- 106 Schmidt, Reinhard: *Wasserdampf- und Heißluftinjektion zur thermischen Sanierung kontaminierter Standorte*, 2001, ISBN 3-933761-09-3
- 107 Josef, Reinhold: *Schadstoffextraktion mit hydraulischen Sanierungsverfahren unter Anwendung von grenzflächenaktiven Stoffen*, 2001, ISBN 3-933761-10-7
- 108 Schneider, Matthias: *Habitat- und Abflussmodellierung für Fließgewässer mit unscharfen Berechnungsansätzen*, 2001, ISBN 3-933761-11-5
- 109 Rathgeb, Andreas: *Hydrodynamische Bemessungsgrundlagen für Lockerdeckwerke an überströmbaren Erddämmen*, 2001, ISBN 3-933761-12-3
- 110 Lang, Stefan: *Parallele numerische Simulation instationärer Probleme mit adaptiven Methoden auf unstrukturierten Gittern*, 2001, ISBN 3-933761-13-1
- 111 Appt, Jochen; Stumpp Simone: *Die Bodensee-Messkampagne 2001, IWS/CWR Lake Constance Measurement Program 2001*, 2002, ISBN 3-933761-14-X
- 112 Heimerl, Stephan: *Systematische Beurteilung von Wasserkraftprojekten*, 2002, ISBN 3-933761-15-8, vergriffen
- 113 Iqbal, Amin: *On the Management and Salinity Control of Drip Irrigation*, 2002, ISBN 3-933761-16-6
- 114 Silberhorn-Hemminger, Annette: *Modellierung von Kluftaquifersystemen: Geostatistische Analyse und deterministisch-stochastische Kluftgenerierung*, 2002, ISBN 3-933761-17-4

- 115 Winkler, Angela: *Prozesse des Wärme- und Stofftransports bei der In-situ-Sanierung mit festen Wärmequellen*, 2003, ISBN 3-933761-18-2
- 116 Marx, Walter: *Wasserkraft, Bewässerung, Umwelt - Planungs- und Bewertungsschwerpunkte der Wasserbewirtschaftung*, 2003, ISBN 3-933761-19-0
- 117 Hinkelmann, Reinhard: *Efficient Numerical Methods and Information-Processing Techniques in Environment Water*, 2003, ISBN 3-933761-20-4
- 118 Samaniego-Eguiguren, Luis Eduardo: *Hydrological Consequences of Land Use / Land Cover and Climatic Changes in Mesoscale Catchments*, 2003, ISBN 3-933761-21-2
- 119 Neunhäuserer, Lina: *Diskretisierungsansätze zur Modellierung von Strömungs- und Transportprozessen in geklüftet-porösen Medien*, 2003, ISBN 3-933761-22-0
- 120 Paul, Maren: *Simulation of Two-Phase Flow in Heterogeneous Porous Media with Adaptive Methods*, 2003, ISBN 3-933761-23-9
- 121 Ehret, Uwe: *Rainfall and Flood Nowcasting in Small Catchments using Weather Radar*, 2003, ISBN 3-933761-24-7
- 122 Haag, Ingo: *Der Sauerstoffhaushalt staugeregelter Flüsse am Beispiel des Neckars - Analysen, Experimente, Simulationen -*, 2003, ISBN 3-933761-25-5
- 123 Appt, Jochen: *Analysis of Basin-Scale Internal Waves in Upper Lake Constance*, 2003, ISBN 3-933761-26-3
- 124 Hrsg.: Schrenk, Volker; Batereau, Katrin; Barczewski, Baldur; Weber, Karolin und Koschitzky, Hans-Peter: *Symposium Ressource Fläche und VEGAS - Statuskolloquium 2003, 30. September und 1. Oktober 2003*, 2003, ISBN 3-933761-27-1
- 125 Omar Khalil Ouda: *Optimisation of Agricultural Water Use: A Decision Support System for the Gaza Strip*, 2003, ISBN 3-933761-28-0
- 126 Batereau, Katrin: *Sensorbasierte Bodenluftmessung zur Vor-Ort-Erkundung von Schadensherden im Untergrund*, 2004, ISBN 3-933761-29-8
- 127 Witt, Oliver: *Erosionsstabilität von Gewässersedimenten mit Auswirkung auf den Stofftransport bei Hochwasser am Beispiel ausgewählter Stauhaltungen des Oberrheins*, 2004, ISBN 3-933761-30-1
- 128 Jakobs, Hartmut: *Simulation nicht-isothermer Gas-Wasser-Prozesse in komplexen Kluft-Matrix-Systemen*, 2004, ISBN 3-933761-31-X
- 129 Li, Chen-Chien: *Deterministisch-stochastisches Berechnungskonzept zur Beurteilung der Auswirkungen erosiver Hochwasserereignisse in Flusstauhaltungen*, 2004, ISBN 3-933761-32-8
- 130 Reichenberger, Volker; Helmig, Rainer; Jakobs, Hartmut; Bastian, Peter; Niessner, Jennifer: *Complex Gas-Water Processes in Discrete Fracture-Matrix Systems: Up-scaling, Mass-Conservative Discretization and Efficient Multilevel Solution*, 2004, ISBN 3-933761-33-6
- 131 Hrsg.: Barczewski, Baldur; Koschitzky, Hans-Peter; Weber, Karolin; Wege, Ralf: *VEGAS - Statuskolloquium 2004*, Tagungsband zur Veranstaltung am 05. Oktober 2004 an der Universität Stuttgart, Campus Stuttgart-Vaihingen, 2004, ISBN 3-933761-34-4
- 132 Asie, Kemal Jabir: *Finite Volume Models for Multiphase Multicomponent Flow through Porous Media*. 2005, ISBN 3-933761-35-2
- 133 Jacob, George: *Development of a 2-D Numerical Module for Particulate Contaminant Transport in Flood Retention Reservoirs and Impounded Rivers*, 2004, ISBN 3-933761-36-0
- 134 Nowak, Wolfgang: *Geostatistical Methods for the Identification of Flow and Transport Parameters in the Subsurface*, 2005, ISBN 3-933761-37-9
- 135 Süß, Mia: *Analysis of the influence of structures and boundaries on flow and transport processes in fractured porous media*, 2005, ISBN 3-933761-38-7
- 136 Jose, Surabhin Chackiath: *Experimental Investigations on Longitudinal Dispersive Mixing in Heterogeneous Aquifers*, 2005, ISBN: 3-933761-39-5

- 137 Filiz, Fulya: *Linking Large-Scale Meteorological Conditions to Floods in Mesoscale Catchments*, 2005, ISBN 3-933761-40-9
- 138 Qin, Minghao: *Wirklichkeitsnahe und recheneffiziente Ermittlung von Temperatur und Spannungen bei großen RCC-Staumauern*, 2005, ISBN 3-933761-41-7
- 139 Kobayashi, Kenichiro: *Optimization Methods for Multiphase Systems in the Subsurface - Application to Methane Migration in Coal Mining Areas*, 2005, ISBN 3-933761-42-5
- 140 Rahman, Md. Arifur: *Experimental Investigations on Transverse Dispersive Mixing in Heterogeneous Porous Media*, 2005, ISBN 3-933761-43-3
- 141 Schrenk, Volker: *Ökobilanzen zur Bewertung von Altlastensanierungsmaßnahmen*, 2005, ISBN 3-933761-44-1
- 142 Hundecha, Hirpa Yeshewatesfa: *Regionalization of Parameters of a Conceptual Rainfall-Runoff Model*, 2005, ISBN: 3-933761-45-X
- 143 Wege, Ralf: *Untersuchungs- und Überwachungsmethoden für die Beurteilung natürlicher Selbstreinigungsprozesse im Grundwasser*, 2005, ISBN 3-933761-46-8
- 144 Breiting, Thomas: *Techniken und Methoden der Hydroinformatik - Modellierung von komplexen Hydrosystemen im Untergrund*, 2006, ISBN 3-933761-47-6
- 145 Hrsg.: Braun, Jürgen; Koschitzky, Hans-Peter; Müller, Martin: *Ressource Untergrund: 10 Jahre VEGAS: Forschung und Technologieentwicklung zum Schutz von Grundwasser und Boden*, Tagungsband zur Veranstaltung am 28. und 29. September 2005 an der Universität Stuttgart, Campus Stuttgart-Vaihingen, 2005, ISBN 3-933761-48-4
- 146 Rojanschi, Vlad: *Abflusskonzentration in mesoskaligen Einzugsgebieten unter Berücksichtigung des Sickerraumes*, 2006, ISBN 3-933761-49-2
- 147 Winkler, Nina Simone: *Optimierung der Steuerung von Hochwasserrückhaltebeckensystemen*, 2006, ISBN 3-933761-50-6
- 148 Wolf, Jens: *Räumlich differenzierte Modellierung der Grundwasserströmung alluvialer Aquifere für mesoskalige Einzugsgebiete*, 2006, ISBN: 3-933761-51-4
- 149 Kohler, Beate: *Externe Effekte der Laufwasserkraftnutzung*, 2006, ISBN 3-933761-52-2
- 150 Hrsg.: Braun, Jürgen; Koschitzky, Hans-Peter; Stuhmann, Matthias: *VEGAS-Statuskolloquium 2006*, Tagungsband zur Veranstaltung am 28. September 2006 an der Universität Stuttgart, Campus Stuttgart-Vaihingen, 2006, ISBN 3-933761-53-0
- 151 Niessner, Jennifer: *Multi-Scale Modeling of Multi-Phase - Multi-Component Processes in Heterogeneous Porous Media*, 2006, ISBN 3-933761-54-9
- 152 Fischer, Markus: *Beanspruchung eingeeerdeter Rohrleitungen infolge Austrocknung bindiger Böden*, 2006, ISBN 3-933761-55-7
- 153 Schneck, Alexander: *Optimierung der Grundwasserbewirtschaftung unter Berücksichtigung der Belange der Wasserversorgung, der Landwirtschaft und des Naturschutzes*, 2006, ISBN 3-933761-56-5
- 154 Das, Tapash: *The Impact of Spatial Variability of Precipitation on the Predictive Uncertainty of Hydrological Models*, 2006, ISBN 3-33761-57-3
- 155 Bielinski, Andreas: *Numerical Simulation of CO₂ sequestration in geological formations*, 2007, ISBN 3-933761-58-1
- 156 Mödinger, Jens: *Entwicklung eines Bewertungs- und Entscheidungsunterstützungssystems für eine nachhaltige regionale Grundwasserbewirtschaftung*, 2006, ISBN 3-933761-60-3
- 157 Manthey, Sabine: *Two-phase flow processes with dynamic effects in porous media - parameter estimation and simulation*, 2007, ISBN 3-933761-61-1
- 158 Pozos Estrada, Oscar: *Investigation on the Effects of Entrained Air in Pipelines*, 2007, ISBN 3-933761-62-X
- 159 Ochs, Steffen Oliver: *Steam injection into saturated porous media – process analysis including experimental and numerical investigations*, 2007, ISBN 3-933761-63-8

- 160 Marx, Andreas: *Einsatz gekoppelter Modelle und Wetterradar zur Abschätzung von Niederschlagsintensitäten und zur Abflussvorhersage*, 2007, ISBN 3-933761-64-6
- 161 Hartmann, Gabriele Maria: *Investigation of Evapotranspiration Concepts in Hydrological Modelling for Climate Change Impact Assessment*, 2007, ISBN 3-933761-65-4
- 162 Kebede Gurmessa, Tesfaye: *Numerical Investigation on Flow and Transport Characteristics to Improve Long-Term Simulation of Reservoir Sedimentation*, 2007, ISBN 3-933761-66-2
- 163 Trifković, Aleksandar: *Multi-objective and Risk-based Modelling Methodology for Planning, Design and Operation of Water Supply Systems*, 2007, ISBN 3-933761-67-0
- 164 Götzinger, Jens: *Distributed Conceptual Hydrological Modelling - Simulation of Climate, Land Use Change Impact and Uncertainty Analysis*, 2007, ISBN 3-933761-68-9
- 165 Hrsg.: Braun, Jürgen; Koschitzky, Hans-Peter; Stuhmann, Matthias: *VEGAS – Kolloquium 2007*, Tagungsband zur Veranstaltung am 26. September 2007 an der Universität Stuttgart, Campus Stuttgart-Vaihingen, 2007, ISBN 3-933761-69-7
- 166 Freeman, Beau: *Modernization Criteria Assessment for Water Resources Planning; Klamath Irrigation Project, U.S.*, 2008, ISBN 3-933761-70-0
- 167 Dreher, Thomas: *Selektive Sedimentation von Feinstschwebstoffen in Wechselwirkung mit wandnahen turbulenten Strömungsbedingungen*, 2008, ISBN 3-933761-71-9
- 168 Yang, Wei: *Discrete-Continuous Downscaling Model for Generating Daily Precipitation Time Series*, 2008, ISBN 3-933761-72-7
- 169 Kopecki, Ianina: *Calculational Approach to FST-Hemispheres for Multiparametrical Benthos Habitat Modelling*, 2008, ISBN 3-933761-73-5
- 170 Brommundt, Jürgen: *Stochastische Generierung räumlich zusammenhängender Niederschlagszeitreihen*, 2008, ISBN 3-933761-74-3
- 171 Papafotiou, Alexandros: *Numerical Investigations of the Role of Hysteresis in Heterogeneous Two-Phase Flow Systems*, 2008, ISBN 3-933761-75-1
- 172 He, Yi: *Application of a Non-Parametric Classification Scheme to Catchment Hydrology*, 2008, ISBN 978-3-933761-76-7
- 173 Wagner, Sven: *Water Balance in a Poorly Gauged Basin in West Africa Using Atmospheric Modelling and Remote Sensing Information*, 2008, ISBN 978-3-933761-77-4
- 174 Hrsg.: Braun, Jürgen; Koschitzky, Hans-Peter; Stuhmann, Matthias; Schrenk, Volker: *VEGAS-Kolloquium 2008 Ressource Fläche III*, Tagungsband zur Veranstaltung am 01. Oktober 2008 an der Universität Stuttgart, Campus Stuttgart-Vaihingen, 2008, ISBN 978-3-933761-78-1
- 175 Patil, Sachin: *Regionalization of an Event Based Nash Cascade Model for Flood Predictions in Ungauged Basins*, 2008, ISBN 978-3-933761-79-8
- 176 Assteerawatt, Anongnart: *Flow and Transport Modelling of Fractured Aquifers based on a Geostatistical Approach*, 2008, ISBN 978-3-933761-80-4
- 177 Karnahl, Joachim Alexander: *2D numerische Modellierung von multifraktionalem Schwebstoff- und Schadstofftransport in Flüssen*, 2008, ISBN 978-3-933761-81-1
- 178 Hiester, Uwe: *Technologieentwicklung zur In-situ-Sanierung der ungesättigten Bodenzone mit festen Wärmequellen*, 2009, ISBN 978-3-933761-82-8
- 179 Laux, Patrick: *Statistical Modeling of Precipitation for Agricultural Planning in the Volta Basin of West Africa*, 2009, ISBN 978-3-933761-83-5
- 180 Ehsan, Saqib: *Evaluation of Life Safety Risks Related to Severe Flooding*, 2009, ISBN 978-3-933761-84-2
- 181 Prohaska, Sandra: *Development and Application of a 1D Multi-Strip Fine Sediment Transport Model for Regulated Rivers*, 2009, ISBN 978-3-933761-85-9
- 182 Kopp, Andreas: *Evaluation of CO₂ Injection Processes in Geological Formations for Site Screening*, 2009, ISBN 978-3-933761-86-6
- 183 Ebigbo, Anozie: *Modelling of biofilm growth and its influence on CO₂ and water (two-phase) flow in porous media*, 2009, ISBN 978-3-933761-87-3

- 184 Freiboth, Sandra: *A phenomenological model for the numerical simulation of multiphase multicomponent processes considering structural alterations of porous media*, 2009, ISBN 978-3-933761-88-0
- 185 Zöllner, Frank: *Implementierung und Anwendung netzfreier Methoden im Konstruktiven Wasserbau und in der Hydromechanik*, 2009, ISBN 978-3-933761-89-7
- 186 Vasin, Milos: *Influence of the soil structure and property contrast on flow and transport in the unsaturated zone*, 2010, ISBN 978-3-933761-90-3
- 187 Li, Jing: *Application of Copulas as a New Geostatistical Tool*, 2010, ISBN 978-3-933761-91-0
- 188 AghaKouchak, Amir: *Simulation of Remotely Sensed Rainfall Fields Using Copulas*, 2010, ISBN 978-3-933761-92-7
- 189 Thapa, Pawan Kumar: *Physically-based spatially distributed rainfall runoff modelling for soil erosion estimation*, 2010, ISBN 978-3-933761-93-4
- 190 Wurms, Sven: *Numerische Modellierung der Sedimentationsprozesse in Retentionsanlagen zur Steuerung von Stoffströmen bei extremen Hochwasserabflussereignissen*, 2011, ISBN 978-3-933761-94-1
- 191 Merkel, Uwe: *Unsicherheitsanalyse hydraulischer Einwirkungen auf Hochwasserschutzdeiche und Steigerung der Leistungsfähigkeit durch adaptive Strömungsmodellierung*, 2011, ISBN 978-3-933761-95-8
- 192 Fritz, Jochen: *A Decoupled Model for Compositional Non-Isothermal Multiphase Flow in Porous Media and Multiphysics Approaches for Two-Phase Flow*, 2010, ISBN 978-3-933761-96-5
- 193 Weber, Karolin (Hrsg.): *12. Treffen junger WissenschaftlerInnen an Wasserbauinstituten*, 2010, ISBN 978-3-933761-97-2
- 194 Bliedernicht, Jan-Geert: *Probability Forecasts of Daily Areal Precipitation for Small River Basins*, 2011, ISBN 978-3-933761-98-9
- 195 Hrsg.: Koschitzky, Hans-Peter; Braun, Jürgen: *VEGAS-Kolloquium 2010 In-situ-Sanie- rung - Stand und Entwicklung Nano und ISCO -, Tagungsband zur Veranstaltung am 07. Oktober 2010 an der Universität Stuttgart, Campus Stuttgart-Vaihingen*, 2010, ISBN 978-3-933761-99-6
- 196 Gafurov, Abror: *Water Balance Modeling Using Remote Sensing Information - Focus on Central Asia*, 2010, ISBN 978-3-942036-00-9
- 197 Mackenberg, Sylvia: *Die Quellstärke in der Sickerwasserprognose: Möglichkeiten und Grenzen von Labor- und Freilanduntersuchungen*, 2010, ISBN 978-3-942036-01-6
- 198 Singh, Shailesh Kumar: *Robust Parameter Estimation in Gauged and Ungauged Basins*, 2010, ISBN 978-3-942036-02-3
- 199 Doğan, Mehmet Onur: *Coupling of porous media flow with pipe flow*, 2011, ISBN 978-3-942036-03-0
- 200 Liu, Min: *Study of Topographic Effects on Hydrological Patterns and the Implication on Hydrological Modeling and Data Interpolation*, 2011, ISBN 978-3-942036-04-7
- 201 Geleta, Habtamu Itefa: *Watershed Sediment Yield Modeling for Data Scarce Areas*, 2011, ISBN 978-3-942036-05-4
- 202 Franke, Jörg: *Einfluss der Überwachung auf die Versagenswahrscheinlichkeit von Stau- stufen*, 2011, ISBN 978-3-942036-06-1
- 203 Bakimchandra, Oinam: *Integrated Fuzzy-GIS approach for assessing regional soil ero- sion risks*, 2011, ISBN 978-3-942036-07-8
- 204 Alam, Muhammad Mahboob: *Statistical Downscaling of Extremes of Precipitation in Mesoscale Catchments from Different RCMs and Their Effects on Local Hydrology*, 2011, ISBN 978-3-942036-08-5

- 205 Hrsg.: Koschitzky, Hans-Peter; Braun, Jürgen: *VEGAS-Kolloquium 2011 Flache Geothermie - Perspektiven und Risiken*, Tagungsband zur Veranstaltung am 06. Oktober 2011 an der Universität Stuttgart, Campus Stuttgart-Vaihingen, 2011, ISBN 978-3-933761-09-2
- 206 Haslauer, Claus: *Analysis of Real-World Spatial Dependence of Subsurface Hydraulic Properties Using Copulas with a Focus on Solute Transport Behaviour*, 2011, ISBN 978-3-942036-10-8
- 207 Dung, Nguyen Viet: *Multi-objective automatic calibration of hydrodynamic models – development of the concept and an application in the Mekong Delta*, 2011, ISBN 978-3-942036-11-5
- 208 Hung, Nguyen Nghia: *Sediment dynamics in the floodplain of the Mekong Delta, Vietnam*, 2011, ISBN 978-3-942036-12-2
- 209 Kuhlmann, Anna: *Influence of soil structure and root water uptake on flow in the unsaturated zone*, 2012, ISBN 978-3-942036-13-9
- 210 Tuhtan, Jeffrey Andrew: *Including the Second Law Inequality in Aquatic Ecodynamics: A Modeling Approach for Alpine Rivers Impacted by Hydropeaking*, 2012, ISBN 978-3-942036-14-6
- 211 Tolossa, Habtamu: *Sediment Transport Computation Using a Data-Driven Adaptive Neuro-Fuzzy Modelling Approach*, 2012, ISBN 978-3-942036-15-3
- 212 Tatomir, Alexandru-Bodgan: *From Discrete to Continuum Concepts of Flow in Fractured Porous Media*, 2012, ISBN 978-3-942036-16-0
- 213 Erbertseder, Karin: *A Multi-Scale Model for Describing Cancer-Therapeutic Transport in the Human Lung*, 2012, ISBN 978-3-942036-17-7
- 214 Noack, Markus: *Modelling Approach for Interstitial Sediment Dynamics and Reproduction of Gravel Spawning Fish*, 2012, ISBN 978-3-942036-18-4
- 215 De Boer, Cjstmir Volkert: *Transport of Nano Sized Zero Valent Iron Colloids during Injection into the Subsurface*, 2012, ISBN 978-3-942036-19-1
- 216 Pfaff, Thomas: *Processing and Analysis of Weather Radar Data for Use in Hydrology*, 2013, ISBN 978-3-942036-20-7
- 217 Lebreuz, Hans-Henning: *Addressing the Input Uncertainty for Hydrological Modeling by a New Geostatistical Method*, 2013, ISBN 978-3-942036-21-4
- 218 Darcis, Melanie Yvonne: *Coupling Models of Different Complexity for the Simulation of CO₂ Storage in Deep Saline Aquifers*, 2013, ISBN 978-3-942036-22-1
- 219 Beck, Ferdinand: *Generation of Spatially Correlated Synthetic Rainfall Time Series in High Temporal Resolution - A Data Driven Approach*, 2013, ISBN 978-3-942036-23-8
- 220 Guthke, Philipp: *Non-multi-Gaussian spatial structures: Process-driven natural genesis, manifestation, modeling approaches, and influences on dependent processes*, 2013, ISBN 978-3-942036-24-5
- 221 Walter, Lena: *Uncertainty studies and risk assessment for CO₂ storage in geological formations*, 2013, ISBN 978-3-942036-25-2
- 222 Wolff, Markus: *Multi-scale modeling of two-phase flow in porous media including capillary pressure effects*, 2013, ISBN 978-3-942036-26-9
- 223 Mosthaf, Klaus Roland: *Modeling and analysis of coupled porous-medium and free flow with application to evaporation processes*, 2014, ISBN 978-3-942036-27-6
- 224 Leube, Philipp Christoph: *Methods for Physically-Based Model Reduction in Time: Analysis, Comparison of Methods and Application*, 2013, ISBN 978-3-942036-28-3
- 225 Rodríguez Fernández, Jhan Ignacio: *High Order Interactions among environmental variables: Diagnostics and initial steps towards modeling*, 2013, ISBN 978-3-942036-29-0
- 226 Eder, Maria Magdalena: *Climate Sensitivity of a Large Lake*, 2013, ISBN 978-3-942036-30-6

- 227 Greiner, Philipp: *Alkoholinjektion zur In-situ-Sanierung von CKW Schadensherden in Grundwasserleitern: Charakterisierung der relevanten Prozesse auf unterschiedlichen Skalen*, 2014, ISBN 978-3-942036-31-3
- 228 Lauser, Andreas: *Theory and Numerical Applications of Compositional Multi-Phase Flow in Porous Media*, 2014, ISBN 978-3-942036-32-0
- 229 Enzenhöfer, Rainer: *Risk Quantification and Management in Water Production and Supply Systems*, 2014, ISBN 978-3-942036-33-7
- 230 Faigle, Benjamin: *Adaptive modelling of compositional multi-phase flow with capillary pressure*, 2014, ISBN 978-3-942036-34-4
- 231 Oladyshkin, Sergey: *Efficient modeling of environmental systems in the face of complexity and uncertainty*, 2014, ISBN 978-3-942036-35-1
- 232 Sugimoto, Takayuki: *Copula based Stochastic Analysis of Discharge Time Series*, 2014, ISBN 978-3-942036-36-8
- 233 Koch, Jonas: *Simulation, Identification and Characterization of Contaminant Source Architectures in the Subsurface*, 2014, ISBN 978-3-942036-37-5
- 234 Zhang, Jin: *Investigations on Urban River Regulation and Ecological Rehabilitation Measures, Case of Shenzhen in China*, 2014, ISBN 978-3-942036-38-2
- 235 Siebel, Rüdiger: *Experimentelle Untersuchungen zur hydrodynamischen Belastung und Standsicherheit von Deckwerken an überströmbaren Erddämmen*, 2014, ISBN 978-3-942036-39-9
- 236 Baber, Katherina: *Coupling free flow and flow in porous media in biological and technical applications: From a simple to a complex interface description*, 2014, ISBN 978-3-942036-40-5
- 237 Nuske, Klaus Philipp: *Beyond Local Equilibrium — Relaxing local equilibrium assumptions in multiphase flow in porous media*, 2014, ISBN 978-3-942036-41-2
- 238 Geiges, Andreas: *Efficient concepts for optimal experimental design in nonlinear environmental systems*, 2014, ISBN 978-3-942036-42-9
- 239 Schwenck, Nicolas: *An XFEM-Based Model for Fluid Flow in Fractured Porous Media*, 2014, ISBN 978-3-942036-43-6
- 240 Chamorro Chávez, Alejandro: *Stochastic and hydrological modelling for climate change prediction in the Lima region, Peru*, 2015, ISBN 978-3-942036-44-3
- 241 Yulizar: *Investigation of Changes in Hydro-Meteorological Time Series Using a Depth-Based Approach*, 2015, ISBN 978-3-942036-45-0
- 242 Kretschmer, Nicole: *Impacts of the existing water allocation scheme on the Limarí watershed – Chile, an integrative approach*, 2015, ISBN 978-3-942036-46-7
- 243 Kramer, Matthias: *Luftbedarf von Freistrahlturbinen im Gegendruckbetrieb*, 2015, ISBN 978-3-942036-47-4
- 244 Hommel, Johannes: *Modeling biogeochemical and mass transport processes in the subsurface: Investigation of microbially induced calcite precipitation*, 2016, ISBN 978-3-942036-48-1
- 245 Germer, Kai: *Wasserinfiltration in die ungesättigte Zone eines makroporösen Hanges und deren Einfluss auf die Hangstabilität*, 2016, ISBN 978-3-942036-49-8
- 246 Hörning, Sebastian: *Process-oriented modeling of spatial random fields using copulas*, 2016, ISBN 978-3-942036-50-4
- 247 Jambhekar, Vishal: *Numerical modeling and analysis of evaporative salinization in a coupled free-flow porous-media system*, 2016, ISBN 978-3-942036-51-1
- 248 Huang, Yingchun: *Study on the spatial and temporal transferability of conceptual hydrological models*, 2016, ISBN 978-3-942036-52-8
- 249 Kleinknecht, Simon Matthias: *Migration and retention of a heavy NAPL vapor and remediation of the unsaturated zone*, 2016, ISBN 978-3-942036-53-5

- 250 Kwakye, Stephen Oppong: *Study on the effects of climate change on the hydrology of the West African sub-region*, 2016, ISBN 978-3-942036-54-2
- 251 Kissinger, Alexander: *Basin-Scale Site Screening and Investigation of Possible Impacts of CO₂ Storage on Subsurface Hydrosystems*, 2016, ISBN 978-3-942036-55-9
- 252 Müller, Thomas: *Generation of a Realistic Temporal Structure of Synthetic Precipitation Time Series for Sewer Applications*, 2017, ISBN 978-3-942036-56-6
- 253 Grüninger, Christoph: *Numerical Coupling of Navier-Stokes and Darcy Flow for Soil-Water Evaporation*, 2017, ISBN 978-3-942036-57-3
- 254 Suroso: *Asymmetric Dependence Based Spatial Copula Models: Empirical Investigations and Consequences on Precipitation Fields*, 2017, ISBN 978-3-942036-58-0
- 255 Müller, Thomas; Mosthaf, Tobias; Gunzenhauser, Sarah; Seidel, Jochen; Bárdossy, András: *Grundlagenbericht Niederschlags-Simulator (NiedSim3)*, 2017, ISBN 978-3-942036-59-7
- 256 Mosthaf, Tobias: *New Concepts for Regionalizing Temporal Distributions of Precipitation and for its Application in Spatial Rainfall Simulation*, 2017, ISBN 978-3-942036-60-3
- 257 Fenrich, Eva Katrin: *Entwicklung eines ökologisch-ökonomischen Vernetzungsmodells für Wasserkraftanlagen und Mehrzweckspeicher*, 2018, ISBN 978-3-942036-61-0
- 258 Schmidt, Holger: *Microbial stabilization of lotic fine sediments*, 2018, ISBN 978-3-942036-62-7
- 259 Fetzer, Thomas: *Coupled Free and Porous-Medium Flow Processes Affected by Turbulence and Roughness – Models, Concepts and Analysis*, 2018, ISBN 978-3-942036-63-4
- 260 Schröder, Hans Christoph: *Large-scale High Head Pico Hydropower Potential Assessment*, 2018, ISBN 978-3-942036-64-1
- 261 Bode, Felix: *Early-Warning Monitoring Systems for Improved Drinking Water Resource Protection*, 2018, ISBN 978-3-942036-65-8
- 262 Gebler, Tobias: *Statistische Auswertung von simulierten Talsperrenüberwachungsdaten zur Identifikation von Schadensprozessen an Gewichtsstaumauern*, 2018, ISBN 978-3-942036-66-5
- 263 Harten, Matthias von: *Analyse des Zuppinger-Wasserrades – Hydraulische Optimierungen unter Berücksichtigung ökologischer Aspekte*, 2018, ISBN 978-3-942036-67-2
- 264 Yan, Jieru: *Nonlinear estimation of short time precipitation using weather radar and surface observations*, 2018, ISBN 978-3-942036-68-9
- 265 Beck, Martin: *Conceptual approaches for the analysis of coupled hydraulic and geomechanical processes*, 2019, ISBN 978-3-942036-69-6
- 266 Haas, Jannik: *Optimal planning of hydropower and energy storage technologies for fully renewable power systems*, 2019, ISBN 978-3-942036-70-2
- 267 Schneider, Martin: *Nonlinear Finite Volume Schemes for Complex Flow Processes and Challenging Grids*, 2019, ISBN 978-3-942036-71-9
- 268 Most, Sebastian Christopher: *Analysis and Simulation of Anomalous Transport in Porous Media*, 2019, ISBN 978-3-942036-72-6
- 269 Buchta, Rocco: *Entwicklung eines Ziel- und Bewertungssystems zur Schaffung nachhaltiger naturnaher Strukturen in großen sandgeprägten Flüssen des norddeutschen Tieflandes*, 2019, ISBN 978-3-942036-73-3
- 270 Thom, Moritz: *Towards a Better Understanding of the Biostabilization Mechanisms of Sediment Beds*, 2019, ISBN 978-3-942036-74-0
- 271 Stolz, Daniel: *Die Nullspannungstemperatur in Gewichtsstaumauern unter Berücksichtigung der Festigkeitsentwicklung des Betons*, 2019, ISBN 978-3-942036-75-7
- 272 Rodriguez Pretelin, Abelardo: *Integrating transient flow conditions into groundwater well protection*, 2020, ISBN: 978-3-942036-76-4

- 273 Weishaupt, Kilian: *Model Concepts for Coupling Free Flow with Porous Medium Flow at the Pore-Network Scale: From Single-Phase Flow to Compositional Non-Isothermal Two-Phase Flow*, 2020, ISBN: 978-3-942036-77-1
- 274 Koch, Timo: *Mixed-dimension models for flow and transport processes in porous media with embedded tubular network systems*, 2020, ISBN: 978-3-942036-78-8
- 275 Gläser, Dennis: *Discrete fracture modeling of multi-phase flow and deformation in fractured poroelastic media*, 2020, ISBN: 978-3-942036-79-5
- 276 Seitz, Lydia: *Development of new methods to apply a multi-parameter approach – A first step towards the determination of colmation*, 2020, ISBN: 978-3-942036-80-1
- 277 Ebrahim Bakhshipour, Amin: *Optimizing hybrid decentralized systems for sustainable ur-ban drainage infrastructures planning*, 2021, ISBN: 978-3-942036-81-8
- 278 Seitz, Gabriele: *Modeling Fixed-Bed Reactors for Thermochemical Heat Storage with the Reaction System $\text{CaO}/\text{Ca}(\text{OH})_2$* , 2021, ISBN: 978-3-942036-82-5
- 279 Emmert, Simon: *Developing and Calibrating a Numerical Model for Microbially Enhanced Coal-Bed Methane Production*, 2021, ISBN: 978-3-942036-83-2
- 280 Heck, Katharina Klara: *Modelling and analysis of multicomponent transport at the interface between free- and porous-medium flow - influenced by radiation and roughness*, 2021, ISBN: 978-3-942036-84-9
- 281 Ackermann, Sina: *A multi-scale approach for drop/porous-medium interaction*, 2021, ISBN: 978-3-942036-85-6
- 282 Beckers, Felix: *Investigations on Functional Relationships between Cohesive Sediment Erosion and Sediment Characteristics*, 2021, ISBN: 978-3-942036-86-3
- 283 Schlabing, Dirk: *Generating Weather for Climate Impact Assessment on Lakes*, 2021, ISBN: 978-3-942036-87-0
- 284 Becker, Beatrix: *Efficient multiscale multiphysics models accounting for reversible flow at various subsurface energy storage sites*, 2021, ISBN: 978-3-942036-88-7
- 285 Reuschen, Sebastian: *Bayesian Inversion and Model Selection of Heterogeneities in Geo-statistical Subsurface Modeling*, 2021, ISBN: 978-3-942036-89-4
- 286 Michalkowski, Cynthia: *Modeling water transport at the interface between porous GDL and gas distributor of a PEM fuel cell cathode*, 2022, ISBN: 978-3-942036-90-0
- 287 Koca, Kaan: *Advanced experimental methods for investigating flow-biofilm-sediment interactions*, 2022, ISBN: 978-3-942036-91-7
- 288 Modiri, Ehsan: *Clustering simultaneous occurrences of extreme floods in the Neckar catchment*, 2022, ISBN: 978-3-942036-92-4
- 289 Mayar, Mohammad Assem: *High-resolution spatio-temporal measurements of the colmation phenomenon under laboratory conditions*, 2022, ISBN: 978-3-942036-93-1
- 290 Schäfer Rodrigues Silva, Aline: *Quantifying and Visualizing Model Similarities for Multi-Model Methods*, 2022, ISBN: 978-3-942036-94-8
- 291 Moreno Leiva, Simón: *Optimal planning of water and renewable energy systems for copper production processes with sector coupling and demand flexibility*, 2022, ISBN 978-3-942036-95-5
- 292 Schönau, Steffen: *Modellierung von Bodenerosion und Sedimentausttrag bei Hochwasserereignissen am Beispiel des Einzugsgebiets der Rems*, 2022, ISBN 978-3-942036-96-2
- 293 Glatz, Kumiko: *Upscaling of Nanoparticle Transport in Porous Media*, 2022, ISBN 978-3-942036-97-9
- 294 Pavía Santolamazza, Daniela: *Event-based flood estimation using a random forest algorithm for the regionalization in small catchments*, 2022, ISBN 978-3-942036-98-6
- 295 Haun, Stefan: *Advanced Methods for a Sustainable Sediment Management of Reservoirs*, 2022, ISBN 978-3-942036-99-3

- 296 Herma, Felix: *Data Processing and Model Choice for Flood Prediction*, 2022, ISBN 978-3-910293-00-7
- 297 Weinhardt, Felix: *Porosity and permeability alterations in processes of biomineralization in porous media - microfluidic investigations and their interpretation*, 2022, ISBN 978-3-910293-01-4
- 298 Sadid, Najibullah: *Bedload Transport Estimation in Mountainous Intermittent Rivers and Streams*, 2023, ISBN 978-3-910293-02-1

Die Mitteilungshefte ab der Nr. 134 (Jg. 2005) stehen als pdf-Datei über die Homepage des Instituts: www.iws.uni-stuttgart.de zur Verfügung.